UNIVERSITY OF BELGRADE

FACULTY OF CIVIL ENGINEERING

Veljko B. Pujević

NUMERICAL MODELING OF THE VEGETATION AND ATMOSPHERE EFFECT ON THE BEHAVIOUR OF CIVIL INFRASTRUCTURE EMBANKMENTS

Doctoral Dissertation

Belgrade, 2021

UNIVERZITET U BEOGRADU

GRAĐEVINSKI FAKULTET

Veljko B. Pujević

NUMERIČKO MODELIRANJE UTICAJA VEGETACIJE I ATMOSFERE NA PONAŠANJE NASIPA GRADJEVINSKE INFRASTRUKTURE

doktorska disertacija

Beograd, 2021

Veljko B. Pujević

Numerical Modeling of the Vegetation and Atmosphere Effect on the Behaviour of Civil Infrastructure Embankments

Advisor:

Prof. Dr. Mirjana Vukićević
University of Belgrade, Faculty of Civil Engineering

Committee:

Prof. Dr. Mirjana Vukićević
University of Belgrade, Faculty of Civil Engineering

Prof. Dr. Lidija Zdravković
Imperial College London, Faculty of Engineering, Department of Civil and Environmental Engineering

Assist. Prof. Dr. Sanja Jocković
University of Belgrade, Faculty of Civil Engineering

PhD thesis defense date:

_____

This thesis is dedicated to my parents, Marina and Branislav Pujević, for their endless love, support and encouragement throughout my life journey and whose good examples have taught me to work hard for the things I strive to achieve

"One of the great challenges in life
is knowing enough to think you're right
but not enough to know you're wrong"

— Neil deGrasse Tyson

Numerical Modeling of the Vegetation and Atmosphere Effect on the Behaviour of Civil Infrastructure Embankments

Abstract

The soil-vegetation-atmosphere interaction is a dynamic process, which governs the continuous change of soil hydrological conditions. These changes directly affect the seasonal and long-term performance of infrastructure cut and embankment slopes. It has been established that the combined effect of vegetation and precipitation induces seasonal cycles of shrinkage and swelling, which give rise to serviceability issues and consequential high maintenance costs.

Numerous researchers attempted to incorporate the effect of the soil-vegetation-atmosphere system interaction in the analysis of boundary value problems. The goal was to improve the understanding of the effects of this complex interaction on the hydro-mechanical response of infrastructure embankments. However, the proposed approaches were unable to quantitatively reproduce the observed hydraulic behaviour.

Within the framework of the present thesis, a different approach is proposed. It is based on the fully coupled flow-deformation analysis, combined with unsaturated soil mechanics theory and sophisticated climatic boundary conditions, implemented within the ICFEP numerical code. Two types of unsaturated constitutive models were applied, elasto-plastic unsaturated Mohr-Coulomb type model and advanced BBM model. The instrumented railway embankment located in the UK, suffering from poor track ride quality related to the presence of vegetation on the slopes, is used for validation purposes. The comparative analysis suggests that proposed models are plausible representative of reality.

Subsequently, a comprehensive parametric analysis is conducted. The results indicate that unsaturated hydraulic properties of clay fill represent the key factors governing the embankment response to seasonal wetting-drying patterns.

Keywords: embankment, clay fill, ash, unsaturated soils, vegetation, precipitation, soil-atmosphere interaction, serviceability, slope stability

Scientific Field: Civil Engineering
Scientific Subfield: Geotechnical Engineering

Numeričko modeliranje uticaja vegetacije i atmosfere na ponašanje nasipa gradjevinske infrastrukture

Rezime

Interakcija između atmosfere, vegetacije i tla je dinamičan proces koji je direktno odgovoran za kontinuiranu promenu stanja vode u tlu. Ove promene imaju značajan, često nepovoljan uticaj kako na sezonsko, tako i na dugoročno ponašanje brojnih geotehničkih zemljanih konstrukcija, kao što su nasipi i useci. Praksa je utvrdila da je delovanjem vegetacije i atmosfere posebno ugrožena upotrebljivost infrastrukturnih nasipa izgrađenih od glinovitih materijala, što se ogleda u značajnom porastu nepredviđenih troškova održavanja.

Brojni su pokušaji da se efekat predmetne interakcije implementira u analizi graničnih problema kako bi se unapredilo razumevanja njenog uticaja na hidro-mehaničko ponašanje infrastrukturnih nasipa. Medjutim, numeričke prognoze dosadašnjih proračunskih pristupa nisu bile konzistentne sa in-situ merenjima.

U okviru ove disertacije predložen je drugačiji pristup koji se zasniva na spregnutoj filtraciono-defromacionoj analizi uz primenu hidrauličkih i mehaničkih konstitutivnih modela za nezasićene geomaterijale u kombinaciji sa sofisticiranim klimatskim graničnim uslovima. Razmatrana su dva nezasićena konstitutivna modela (BBM i nezasićeni Mohr-Coulom) različitog stepena složenosti. Numeričke analize sprovedene su u programu ICFEP. Visoka pozdanost predloženog pristupa verifikovana je uporednom analizom sa rezultatima terenskog osmatranja eksperimentalne deonice železničkog nasipa na jugu Engleske koji je podložan prekomernim cikličnim deformacijama bubrenja i skupljanja prouzrokovanih delovanjem vegetacije.

U nastavku, sprovedena je detaljna parametarska analiza koja je kao ključne faktore koji kontrolišu sezonske-ciklične varijacije pornih pritisaka i deformacija identifikovala nezasićene hidrauličke karakteristike glinovite ispune.

Ključne reči: nasip, glinovita ispuna, pepeo, nezasićeni geomaterijali, vegetacija, presipitacija, interakcija sistema tlo-atmosfera

Naučna oblast: Gradjevinarstvo
Uža naučna oblast: Gradjevinska geotehnika

Table of Contents

List of Figures

List of Tables

Chapter 1: Introduction

1.1 General

Approximately 5,000 km of embankment has been supporting the UK's railway infrastructure for more than 100 years. Failures and in particular serviceability issues of these ageing embankments affect track alignment, causing train speed restrictions, which lead to delay and disruption to rail services. Network Rail estimates that train delays arising from poor earthwork performance was 400,000 minutes over the period 2000-2003 at a cost of £26 million (Scott, Loveridge & O'Brien, 2007; Glendinning *et al.*, 2009). Additional financial expenditures come from expensive releveling and remedial works. Majority of these delays were located in southern England, particularly in the region of London clay basin. Additionally, based on geological mapping it was identified that these geotechnical issues were mainly located in areas of high-plasticity clays, which were the primary construction material for earthworks (O'Brien, 2013). Vast majority of the UK's railway embankments were constructed at the turn of the 19th and the 20th centuries employing techniques which differ significantly from modern day construction methods. Soils from surrounding cut areas were tipped on the ground surface to their full height without any kind of prior preparation of ground area and with little or no mechanical compaction (Skempton, 1996).

In order to establish the causes of performance problems, geotechnical field forensic investigations on instrumented embankments were carried out (Loveridge *et al.*, 2010; Smethurst, Clarke & Powrie, 2012). Analyses of the long-term monitoring data have indicated that observed deformations and delayed failures are triggered mainly by seasonal and persistent influence of climate variations and particularly by the type and spatial distribution of vegetation. These generate exchanges of water between the topsoil and the atmosphere, through processes such as rainfall infiltration, water evaporation from the soil pores and transpiration through vegetation, which, combined are referred to as slope–vegetation-atmosphere (SVA) interaction (Elia *et al.*, 2017).

The change in soil hydrological conditions caused by the soil-vegetation-atmosphere interaction consists of the soil moisture content and pore water pressure variations. It is generally known that the magnitude and variation of pore water pressures (pwp's) is the key parameter affecting the long-term performance of infrastructure cut and embankment slopes. Pore water pressures directly influence the effective stress state and in turn, the soil shear strength and volumetric behaviour.

Monotonic variations of pwp's are intrinsic to consolidation/swelling processes which took place upon construction/excavation in low permeability soils. On the other hand, seasonal non-monotonic complex variations in pwp's are direct consequence of slope–vegetation-atmosphere interaction. The ability of vegetation to transpire, remove water from the soil varies seasonally. During the summer drier months, when the plant water demand and the solar radiation are the greatest, the rate of moisture extraction from the soil is at its peak and exceeds the infiltration. During the winter months when the vegetation go dormant and solar radiation is reduced, evapotranspiration processes are diminished or ceased, allowing rainfall to infiltrate and wet the soil. These opposite processes cause cycles of drying and wetting, and associated pore water pressure variations within the soil. Seasonal cyclic changes of effective stresses consistent with pwp variations are equivalent to successive loading-unloading paths. Therefore in embankments constructed of clay having a high volume change potential, these are accompanied by corresponding cycles of soil shrinkage and swelling (Smethurst *et al.*, 2015; Loveridge *et al.*, 2010). Due to the irregular distribution of vegetation along the embankment length as well as variations in vegetation species, sizes and densities related to water demands, together with intrinsic heterogeneity of the clay fill, alternating volumetric deformations are nonuniform, both in longitudinal and lateral direction, thereby inducing excessive differential movements of the track and consequently poor ride quality. These are characterized as serviceability limit states (SLS) and are

most frequent during late summer/early autumn, when the effects of desiccation on high-plasticity clay fills are most significant.

Beside serviceability issues which are typically inherent to densely vegetated slopes, stability problems are mainly associated with modestly vegetated slopes and in particular with vegetation clearance (Glendinning *et al.*, 2009). There are multiple benefits associated with the vegetation presence on the engineering and natural slopes. Vegetation contributes to weak soil stabilisation through combination of effects, which include: dissipation of excess pore pressures, weight of the plants especially heavy trees may enhance stability in case of adequate positioning on the slope, mechanical root reinforcement of the soil, and most importantly generation of matric suctions, negative tensile pore water pressures, which significantly increase soil shear strength (Greenwood, Norris & Wint, 2004; O'Brien, 2007). The mature trees on the embankment slopes are able to develop very large and persistent soil suctions deeper within the root zone during the summer drier periods (Biddle, 1998), which could significantly exceed the total stress due to the weight of the embankment. Field measurements have showed that tree-induced suctions are maintained during the wet winter season because rainfall infiltration from the ground surface is not capable of penetrating deeper than 2-3 m into soil mass, which is insufficient for rewetting of this persistently dry zone (Loveridge *et al.*, 2010). In over-steep embankments, or embankments weakened by strain softening and vulnerable to progressive failure, these persistent suctions may be crucial in preventing deep-seated instability (O'Brien, 2007; Glendinning *et al.*, 2009; Loveridge *et al.*, 2010).

From the previous discussion, it can be seen that the influence of mature vegetation is concurrently hazardous and beneficial. High water demand trees have detrimental impact on serviceability by affecting line and level of railway track, but at the same time help maintain slope stability through persistent soil suctions. Infrastructure owners must manage slope vegetation, including mature trees, to reduce the influence on track movement without compromising embankment stability. The role of vegetation management on existing infrastructure slopes is therefore to maximise the beneficial actions while minimising the detrimental ones (Glendinning *et al.*, 2009).

Even though this issue was somewhat recognized by the geotechnical engineering community, until recently it did not receive required attention from researchers. This was primarily due to the lack of adequate tools that would enable both experimental and numerical treatment of this complex multidisciplinary problem. That is further complicated by the fact that embankments are intrinsically unsaturated and the behaviour of unsaturated geomaterials is incomparably more complex than the behaviour of saturated materials. Recent rapid development of technology and numerical methods, provided possibilities for this dynamic interaction between soil, vegetation and the atmosphere to be more thoroughly studied.

Numerous researchers attempted to incorporate the effect of the soil-vegetation-atmosphere system interaction in the analysis of boundary problems. Simplified approaches involve the prescription of successive summer and winter pore water pressure profiles, which are selected to match the respective field measurements (Russell *et al.*, 2000; Kovacevic, Potts & Vaughan, 2001; Nyambayo, Potts & Addenbrooke, 2004; O'Brien, Ellis & Russell, 2004; Lees, 2013). This modelling principle is essentially erroneous because what is actually sought are pwp variations in response to the combined effect of precipitation and evapotranspiration. An alternative approach based on two independent analysis brought significant improvement in conceptual modelling of the SVA interaction. Authors (Rouainia *et al.*, 2009; Davies, 2011; Rahardjo, Satyanaga & Leong, 2012) employed hydrological software to calculate the pwp variation from meteorological, vegetation and permeability data and afterwards exported the predicted pwps in another numerical code to evaluate mechanical behaviour. Despite obvious advantages, the main drawback of such staggered approach lies in the fact that hydro-mechanical coupling is only partially captured, preventing realistic displacement predictions. Beside these coupled and loosely coupled analysis some numerical groups (Smethurst, Clarke & Powrie,

2012; Briggs, Smethurst & Powrie, 2014; Briggs *et al.*, 2016), were exploring the extent to which pure hydraulic models, incorporating unsaturated water flow and sophisticated hydraulic boundary conditions, were able to reproduce the observed behaviour of clay fill embankments in relation to SVA interaction. Reported results revealed that proposed approach was capable of qualitatively capturing the observed hydraulic behaviour patterns, but the maximum pwp values and their seasonal variations were excessively overpredicted (more than 10 times).

The assessment of the slope displacements resulting from the slope–vegetation-atmosphere interaction is crucial for the evaluation of the serviceability of structures interacting with slopes, like rail tracks and requires the performance of fully coupled numerical analyses (O. C. Zienkiewicz *et al.*, 1999; Potts & Zdravković, 1999, 2001). Within the framework of present thesis, such fully coupled flow-deformation approach was combined with partially saturated soil mechanics theory in an attempt to gain broader insight into processes governing the complex interaction. Magnolia Road Project is used as a case study for this investigation. It is an example of an embankment that was suffering from poor track ride quality and a high rate of maintenance due to movements associated with the presence of vegetation on the slopes of the embankment (Arup Geotechnics, 2007). This dissertation explains the role of vegetation and precipitation on the performance of unsaturated "dumped" clay fill embankments, through the numerical simulations and interpretation of monitoring data from aforementioned instrumented embankment.

1.2 Scope of the Research – Objectives

The scope of the research presented in this thesis is divided into two parts. The first part is predominantly focused on broadening the knowledge of other scientific disciplines relevant to the research topic. The second part deals with capabilities of ICFEP numerical code in modelling the impact of SVA on unsaturated embankment slopes.

The aims of the dissertation thesis can be summarised as follows:

- the first part refers to furthering, via a literature review, the current understanding of the fundamental principles and processes constituting the soil-vegetation-atmosphere system interaction, in particular mechanism of water uptake by roots and methods of evapotranspiration estimation that can be adopted for use in geotechnical engineering.

- the second part of the research goals refers to the application of acquired multidisciplinary knowledge together with the existing ICFEP (Imperial College Finite Element Program) capabilities in the numerical study of the behaviour of experimental embankment, suffering from the effects of SVA interaction. The central objective is the evaluation of quantitative predictions of the proposed modelling strategy incorporating fully coupled partially saturated flow-deformation behaviour and advanced climatic/vegetation boundary conditions. The additional task is to suggest causes of differences between results of proposed modelling approach and alternative ones found in literature, as well as to provide possible explanations for discrepancies compared to field data.

- the third part aims to provide some practical guidelines regarding vegetation management relevant to performance of infrastructural embankments, via extensive parametric study. This includes the identification of key parameters governing the behaviour of dumped clay fill embankment prior to and following vegetation removal. Another goal is to enhance the understanding of the effects of certain pertinent factors on the hydro-mechanical behaviour of unsaturated clay materials subjected to "atmospheric actions".

In addition to the defined goals, it was reckoned that current study, involving high quality pore suction, deformation, vegetation and meteorological monitoring data, combined with unsaturated hydro-mechanical models, could serve as a good basis for validation of the root water uptake model implemented into the ICFEP by (Nyambayo, 2004).

1.3 Thesis Layout

The outline of this dissertation thesis is provided in the following paragraphs:

Chapter 2 of the thesis is focused mainly on the literature review of essential constituents governing soil-vegetation-atmosphere system interaction. The fundamental principle of soil water balance is presented, with particular emphasis on evapotranspiration process and different methods available for estimating its potential rates. Afterwards, a review of models that can account for the uptake of water by plant roots is provided. At the end of the chapter, an overview of numerical strategies for modelling the SVA interaction, together with corresponding application examples from literature is given.

Chapter 3 provides a state of knowledge about the behaviour of unsaturated soil materials. In the introductory section, subsurface water distribution is explained. Subsequently, the fundamentals of partially saturated soil behaviour, including capillary mechanisms, water retention behaviour, and mechanical aspects, highlighting in particular complex volumetric response, are reviewed. Finally, existing ICFEP tools for the modelling of unsaturated soil behaviour are introduced. Firstly, the coupled unsaturated formulation is examined. Afterwards, two distinct types of partially saturated constitutive models, the evaluation of which with respect to SVA interaction represents one of the main goals of the thesis, are presented in detail. Following this, comprehensive description of precipitation and vegetation hydraulic boundary conditions, which are of key relevance to the numerical simulations undertaken in this thesis, is provided.

Chapter 4 presents the results of the Magnolia road case study. It is a heavily instrumented railway embankment in the south-east of England, suffering from serviceability issues related to SVA interaction. An outline of site properties and field measurements, with emphasis placed on interpretation of data from the vegetation effect perspective, is given. Thereafter, the created numerical model, with a sequence of performed analysis stages and selected parameters values are systematically elaborated. Additionally, calibration of key parameters is thoroughly explained. Finally, the model predictions are presented and comparisons with field data are made.

Chapter 5 presents the results of parametric study. It investigates the effects of various parameters involved in the soil-vegetation-atmosphere interaction relevant to embankment performance. Besides, it provides explanations of improvements, in terms of more reliable quantitative predictions, of proposed numerical model versus existing ones.

Chapter 6 summarises the work carried out in this thesis and presents the main conclusions of the study. Suggestions for further research are also provided.

Chapter 2: Review of Soil-Vegetation-Atmosphere System Interaction Components in Relation to Infrastructure Embankments

2.1 Introduction

The vast majority of the UK rail network have been constructed in the 19th century, more than 100 years ago. The techniques used back then, do not comply with modern geotechnical engineering codes of practice. Detailed explanations and illustrations of construction process are provided in the paper by (Skempton, 1996). Similarly to present practice, embankments were formed from excavated materials from nearby areas of cut, but without any specification requirements regarding the fill properties. Another contrast lies in the fact that materials were tipped in one layer to the full height of embankment with little or no mechanical compaction applied. As a result, excessive post-construction settlements and slope collapses occurred, delaying the opening of the railways. To keep the alignment of the track, readily available granular fill, such as locomotive ash or track ballast, were topped up.

These uncompacted clay fills are often known as 'dumped' clay fills (Vaughan, Kovacevic & Potts, 2004). Figure 2.1 schematically illustrates the differences between modern properly compacted clay fill embankments and historic dumped clay fill embankments. Later ones are pronouncedly heterogeneous, characterized by presence of relic shear surfaces, pockets of high permeability sand lenses and leftovers of topsoil and alluvium along the base of the embankment. These remnant alluvium deposits are consequence of a lack of proper preparation of the foundation subgrade.

The structure of the dumped clay fill is, as described above, quite different to the modern clay fills and also to the original parent clay. The conceptual model for the dumped clay fill, as proposed by (O'Brien, Ellis & Russell, 2004), is illustrated in Figure 2.2. The micro-fabric is comprised of clods of the parent material typically 50 to 300 mm diameter, surrounded by a softened matrix. The matrix has been found to include sand and silt sized particles, which may have been introduced during the construction process. It was found that the clods of parent material govern the compressibility and shear modulus of the soil, while the matrix controls the permeability and shear strength. Additionally, (Biddle, 1998) suggested that the matrix, due to its particular features, represents a suitable medium for growth of plant and tree roots.

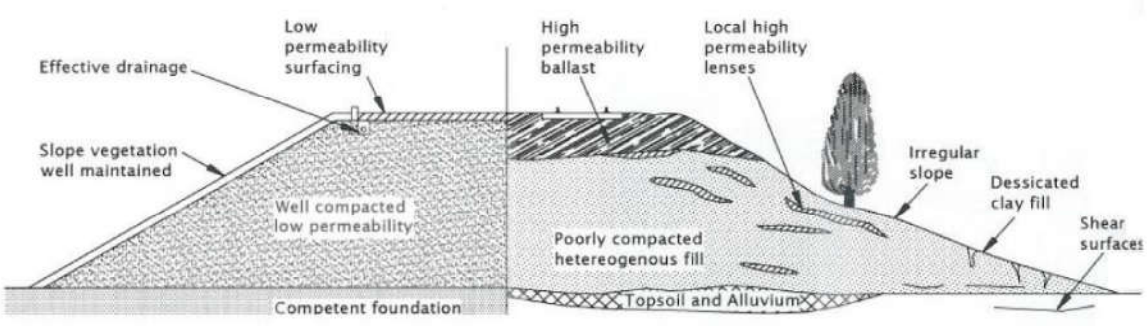

Figure 2.1 Cross-section configuration of modern vs historical rail embankment after (O'Brien, 2007)

The overall shape of these embankments can be quite variable. Some embankments have retained a relatively steep uniform slope, whereas others have a 'coat-hanger' appearance with an oversteepened upper slope and a shallower lower slope. This distinct shape is established in response to long-term variations in the pore water pressures. Perennial seasonal pwp cycles are the driving force behind the ratcheting-type deformation mechanism, which accumulation lead to a 'coat-hanger' shape.

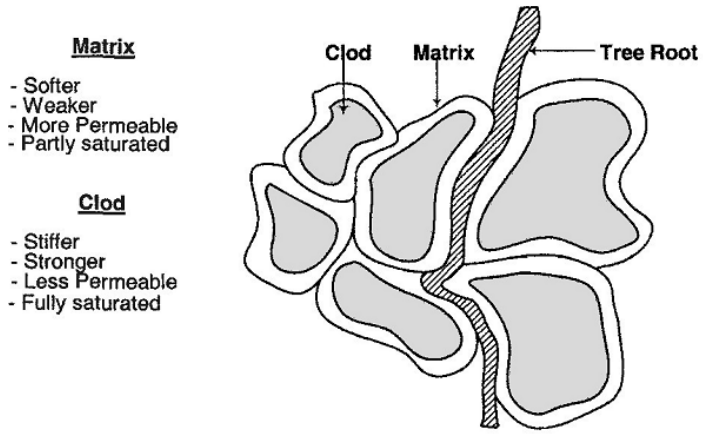

Figure 2.2 Conceptual model of dumped clay fill structure (O'Brien, Ellis & Russell, 2004)

Seasonal changes in pore water pressure and soil moisture content profiles, originate from the variable meteorological settings and vegetation effects. This continuous modification of the ground surface water regime is known as the soil-vegetation-atmosphere interaction. The influence of this interaction has been significant in the serviceability and stability of common geotechnical engineering projects, such as embankments and cut slopes. Pore water pressure changes within a slope related to climatic perturbations and tree root water uptake, have been shown to be able to induce soil erosion, shrinkage–swelling and cracking, thus leading to a potential reduction of the available soil strength with depth.

Numerous observations of damage to structures and infrastructure interacting with slope displacements, related to the slope–vegetation-atmosphere interaction, are reported in the literature. For artificial soil slopes, made of partially saturated soils, specifically for road and railway infrastructure embankments, movements associated with variations in the soil degree of saturation due to the soil–atmosphere interaction have been widely observed to jeopardize the serviceability and safety of the infrastructure (Elia *et al.*, 2017). In the UK, respective interaction is the main source of railway track distortions, resulting in speed restrictions and delays for passengers, leading to increasing frequency of costly track maintenance for infrastructure owners like LUL and Network Rail (Andrei, 2000)(Scott, Loveridge & O'Brien, 2007).

2.2 Soil Water Balance Theory

The dynamic nature of the hydrological cycle is continuously affecting the soil water conditions, inducing constant variations in soil moisture content and corresponding pore water pressure.

It is a common practice in geotechnical design to utilize the information about the short-term soil water conditions, gathered by conventional geotechnical site investigations. However, following this approach, dynamic and constantly changing interaction is neglected, which can have detrimental implications to geotechnical engineering projects (Blight, 2003).

Surface unsaturated zone above the ground water table, known as *vadose zone,* represents dynamic interface of the soil through which exchange of water between the earth and the atmosphere is taking place. The behaviour of soils in the vadose zone is closely related to the water balance between the earth and the atmosphere. Soil water balance was originally the field of interest and research of soil scientists, agronomists and hydrologists before (Blight, 1997) introduced it to the geotechnical engineering community, emphasizing its importance for the understanding of the various processes taking place in the unsaturated zone.

According to (Hillel, 1982), the term water balance is used to express the application of the statement of energy conservation to part of the hydrological cycle. The equation consists of the algebraic sum of water fluxes entering and exiting a specific volume during a defined time interval (Novák, 2012). According to the theory of mass conservation (Blight, 1997), the soil water balance can be expressed as follows:

Water input into the soil = Water output + Water stored within

Where:
Water input = Infiltration = Precipitation(P) – Interception (I_{nt}) – Surface runoff (R_{off})
Water output = Evapotranspiration (ET) + Ground water table recharge (R_{ech})
Water stored = Change in water stored in the soil(ΔS)

Therefore, the equation for the soil water balance can expressed in the following form:

$$P - I_{nt} - R_{off} = ET + R_{ech} + \Delta S$$

A more generalized form of the soil water balance equation, involving additional components, is given in the paper by (Fatahi, Khabbaz & Indraratna, 2014). Beside already mentioned ones, which are relevant for local scale geotechnical boundary value problems, the newly incorporated ones include: supplemental irrigation rate and lateral ground water inflow, as water input components, and drainage rate, percolation rate and lateral ground water outflow, as water output components.

$$I_T(t) + SI(t) + F_I(t) = E(t) + T(t) + D(t) + P(t) + F_O(t) + \Delta S(t)$$

When modelling the soil-vegetation-atmosphere interaction, it is necessary to evaluate all components constituting the soil water balance. The inflow part of the equation consists of precipitation that falls on and enters the soil surface. The amount of rainwater that can infiltrate the soil depends on the relationship between the rainfall intensity and infiltration rate. Precipitation rate exceeding infiltration rate will result in ponding on the ground surface. Depending on the geomorphology of the catchment area, ponded water can flow out (surface run-off) or be removed by soil evaporation (Novák, 2012). There are many watershed models capable of modelling run-off. The techniques used by these models vary from using simple empirical relations to complex physically based governing equations. However, since this flow occurs outside of the analysis domain and rarely impacts ground water regime, run-off was not explicitly modelled within this research study.

The existence of a vegetative cover hinders rainwater to reach the soil surface. In that case, a fraction of the precipitation will be intercepted by plant leaves and stems (vegetation canopy). The vegetation canopy is able to store a certain amount of water and later this water will be returned to the atmosphere through the process of evaporation. The water that is intercepted and then evaporated is referred as the interception loss. This loss depends heavily on the type and stage of vegetation development, together with precipitation intensity and duration. Several models are available in the literature for the estimation of interception loss (Rutter *et al.*, 1971; Gash, 1979). However, due to complexity and lack of field data for derivation of model parameters, this component of soil water balance will be either neglected or approximately assessed in present thesis.

According to (Novák, 2012), evapotranspiration component governs the outflow part of the soil water balance equation and will be discussed in more detail in the next section. The author also states that the groundwater recharge component can be ignored in cases where the phreatic surface lies at depth greater than 2m from the ground surface. In his work (Blight, 2003) argues that transpiration is component of greatest uncertainty in soil water balance equation, mostly because of numerous factors it depends on. The aforementioned processes that constitute the water cycle are schematically illustrated in the Figure 2.3.

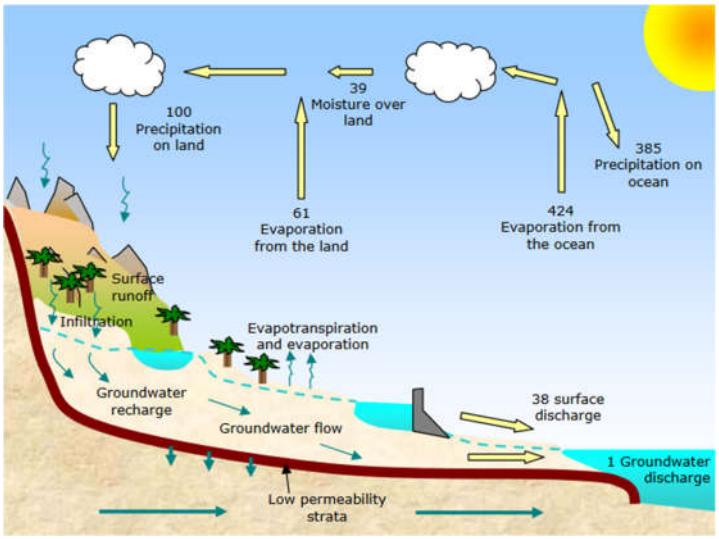

Figure 2.3 Water cycle components

2.3 Evapotranspiration Process

The term evapotranspiration encompasses two separate processes, evaporation and transpiration. Transpiration represents the process by which plants remove water from the soil and release it to the atmosphere. Evaporation, on the other hand, defines direct transfer from the evaporating surfaces to the atmosphere. These surfaces can be the soil, the water table or plant surfaces intercepting water. Both processes take place at the same time, which constitutes their distinction particularly difficult (Allen *et al.*, 1998).

In the process of evaporation, water is returned to the atmosphere through phase transition from the liquid into the gaseous phase. Water in the gaseous state is termed water vapor. In order for the water molecules to leave the water surface an energy is required, the amount of which will dictate the rate of evaporation. Therefore, evaporation acts as a link between the energy and water transport processes. The energy balance is applied close or at the level of the evaporating surface, where the vertical fluxes of water and energy remain practically unchanged. The surface energy balance equation, as described by (Bowen, 1926) is given below:

$$R = L \cdot E + H + G$$

Where:

R the net radiation at the reference level (W/m^2);
L the latent heat of evaporation ($L=2.45 \cdot 10^6$ J/kg at T=20°C);
E the water vapor flux (evapotranspiration) ($kg/m^2 \cdot s$);
H the convective heat flux from evaporating surface to the atmosphere causing changes in air temperature (W/m^2);
G the soil heat flux causing changes in the soil temperature (W/m^2);

As stated by (Allen *et al.*, 1998) solar radiation and ambient air temperature are the primary sources of the energy required for a water molecule to vaporize. In cases of unlimited water and energy supply the soil evaporation is driven by the vapor pressure gradient (the difference between the water vapor pressure at the surface and the surrounding atmosphere), which in turn is dependent only on the meteorological conditions. In this situation, the resulting rate corresponds to the potential (maximum) evaporation rate. The progressive saturation of the surrounding air will gradually limit the evaporation rate, unless the saturated air is replaced by dry air. This signifies the importance of assessing air humidity and wind speed (and turbulence) when estimating the evaporation process. In the case where

the evaporating surface is soil, additional parameters such as the shading of the crop canopy, as well as soil water content and permeability also affect the rate of evaporation (Allen *et al.*, 1998). In the book by (Linsley, Kohler & Paulhus, 1982) it is stated that the rate of evaporation from a saturated soil surface is approximately equal to rate of evaporation from an adjacent water surface, assuming equal temperature.

Transpiration is the principle mechanism by which precipitation on land areas is returned back to the atmosphere. Transpiration is the process of water movement through a plant and its evaporation from aerial parts, such as leaves, stems and flowers. Only a small amount (around 1-2%) of that water is used by plants to synthesize sugars necessary for growth and metabolism. The remainder 97–99% is lost by transpiration. Transpiration occurs through substomatal cavities, openings in the leaf interior (see Figure 2.4). The transport of water from the roots to the leaves is driven by the combination of capillary action and potential energy gradients, with the later one being more superior. Evaporation of water from the plant leaves creates a potential energy decrease, which results in water being drawn up the vascular system of the plant. Movement of water along the vascular system generates a reduction in pressure head at the root level, thereby triggering the flow of water from the surrounding soil towards the roots. The plants are able to control this process using guard cells. Guard cells surround the stomata and control opening/closing mechanism, and therefore the magnitude of the hydraulic gradients within the plant. Transpiration could actually be thought of as a necessary "cost" associated with the opening of the stomata to allow the diffusion of carbon dioxide gas from the air for photosynthesis.

Transpiration, similarly to direct evaporation, also depends on energy supply, radiation, air humidity, air temperature and wind speed (Allen *et al.*, 1998). Additionally, plant properties itself play a major role in transpiration process, governing the rates of outflow moisture fluxes. These include properties above the ground level, such as size and number of leaf stomata, their function and leaf area, as well as below ground level, such as root depth, root distribution, soil water potential, moisture content and permeability.

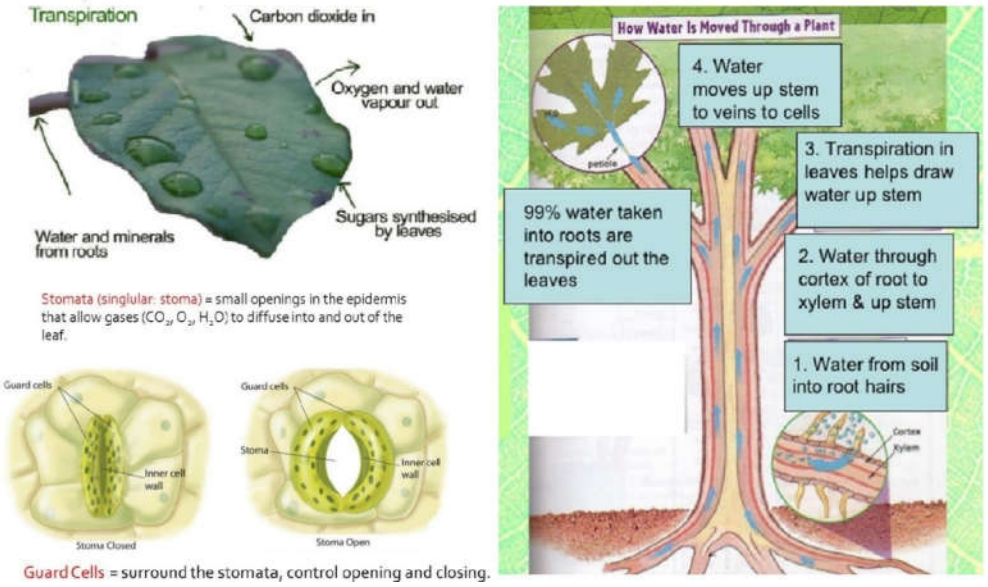

Figure 2.4 Transpiration process – gas exchange trough stomata

2.4 Methods for the Estimation of Evapotranspiration

A vast variety of methods regarding the estimation of evapotranspiration and its components (evaporation, transpiration) have been published in the literature, as it is a subject that has received

major attention in the fields of hydrology, agronomy and soil science. Methods of evapotranspiration estimation can be divided into two broad categories, mainly methods of measurement or calculation.

The first group of methods is based on direct measurement of evapotranspiration through the use of lysimeter, an isolated vessel filled with soil, in which plant can be cultivated. Such procedures are rarely if ever used in practice, mainly due to unreliable data they provide (Novák, 2012), and in particular excessive costs of their construction and operation (Allen *et al.*, 1998).

On the other hand, numerous calculation methods for assessment of evapotranspiration has been developed, primarily for the purpose of agricultural water management. These methods generally differ in the principles they are based on, input data requirements and the type of the evaporating surface they are referring to. Noteworthy methods include: soil water balance method, energy balance method, combination method and empirical methods. From these, combination method is generally accepted by codes of practices and guidelines, including Food and Agriculture Organization.

2.4.1 FAO Penman-Monteith Combination Method

Combination method by (Penman, 1946), is derived combining energy balance equation at the evaporating surface level with equations describing the vertical steady flux of heat and water vapor above the evaporating surface. The evaporation estimated by this method represents the potential one, as it is assumed that supply of water is unlimited (Novák, 2012). Method input parameters are common meteorological variables, such as air temperature, humidity, atmospheric pressure, sunshine duration and wind speed.

First attempts to expand the use of Penman's equation to vegetative surfaces, involved the introduction of so-called surface resistance factors. These factors include the combined resistance of vapor flow through stomata openings, total leaf area and soil surface (Allen *et al.*, 1998). The most popular equation of the combination method that incorporates both aerodynamic and surface resistance factors is the Penman-Monteith equation presented below:

$$LET = \frac{\Delta(R_n - G) + \rho_a c_p \dfrac{(u_{sat} - u_a)}{r_a}}{\Delta + \gamma\left(1 + \dfrac{r_s}{r_a}\right)}$$

Where:

Δ the gradient of the relationship between saturation water vapor pressure and temperature;
ρ_α the mean air density at constant pressure;
c_p the specific air heat;
u_{sat}, u_α the saturated and actual water vapor pressure respectively;
γ the psychrometric constant;
r_s, r_α the surface and aerodynamic resistance factors respectively (see Figure 2.5);

The rest of the parameters originate from the energy balance equation. If the resistances r_s and r_α of a specific crop are known, then the Penman-Monteith equation can provide the crop evapotranspiration, as the rest of the required parameters can be measured from meteorological data (Allen *et al.*, 1998). However, the estimation of crop specific parameters, such as the surface resistance factor, is rather cumbersome, which makes the use of the Penman-Monteith method in its original form complicated.

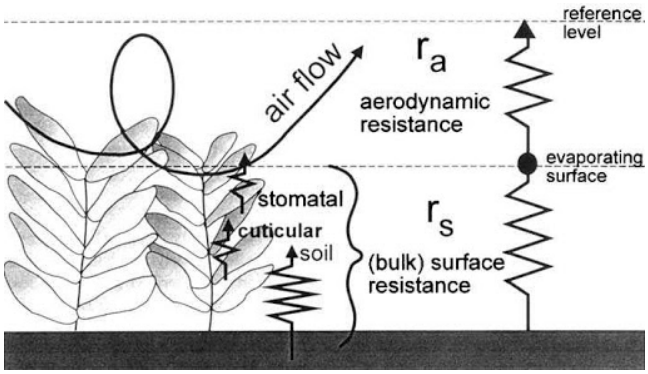

Figure 2.5 Surface (bulk) and aerodynamic resistances for water vapor flow

To overcome these difficulties, the concept of reference surface is introduced. The idea is basically to calculate the evapotranspiration of a reference surface and to relate it to a specific plant by using the appropriate crop (plant) coefficients.

One such procedure, termed crop evapotranspiration ET_0, is proposed by the Food and Agriculture Organization (FAO) of the United Nations. It is intended for the estimation of reference and crop evapotranspiration, taking into account the effect of climate and crop characteristics. The basic idea behind the crop factor approach is that meteorological factors are separated from crop factors, i.e. it is assumed that ET_0 depends on meteorological factors only (see Figure 2.6).

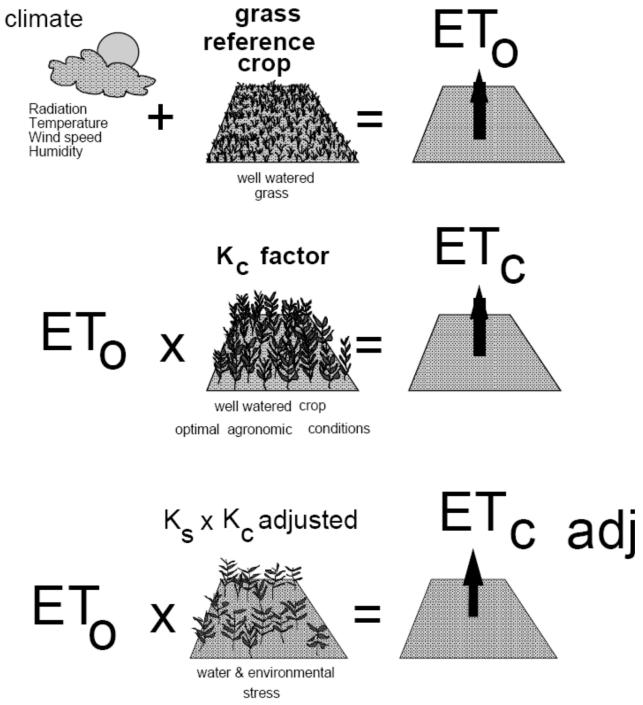

Figure 2.6 FAO semi-empirical procedure for evaluating crop evapotranspiration under standard and non-standard conditions

The FAO procedure distinguishes between reference crop evapotranspiration ET_0, crop evapotranspiration under standard conditions ET_c, and crop evapotranspiration under nonstandard conditions ET_{c_adj}. ET_0 is a climatic parameter expressing the evaporation power of the atmosphere. ET_c refers to the evapotranspiration from large fields under optimum agronomical and soil water

conditions. Therefore, it could be said that ET_c corresponds to potential evapotranspiration. ET_{c_adj} cover nonstandard conditions including water and salinity stress, effects of pests, disease, sparse vegetation and low fertility. This reduces evapotranspiration rate is obtained by introduction of adequate adjustment factors.

Method adopted by FAO for calculation of reference evapotranspiration ET_0, is Penman-Monteith combination method. The reference surface defined by FAO represents an idealized grass surface, with assumed height of 0.12 m, a surface resistance factor of 70 s/m and a reflection coefficient (albedo) of 0.23 (see Figure 2.7). The reference surface closely resembles an extensive surface of green, well-watered grass of uniform height, actively growing and completely shading the ground.

The FAO Penman-Monteith equation for the reference evapotranspiration calculation is as follows:

$$ET_o = \frac{0.408\Delta(R_n - G) + \gamma \frac{900}{T+273} \vartheta_2 (u_{sat} - u_a)}{\Delta + \gamma(1 + 0.34 v_2)}$$

Where:

Δ	gradient of the relationship between saturation vapor pressure and temperature;
R_n	net radiation – difference between the incoming net shortwave R_{ns} and outgoing net longwave radiation R_{nl}
G	soil heat flux (assuming that soil temperature follows air temperature)
γ	psychrometric constant
T	mean air temperature (°C) (obtained from the maximum and minimum air temperature, measured at 2 m height)
v_2	mean wind velocity, measure at 2 m height
u_{sat}, u_a	saturation and actual water vapor pressure

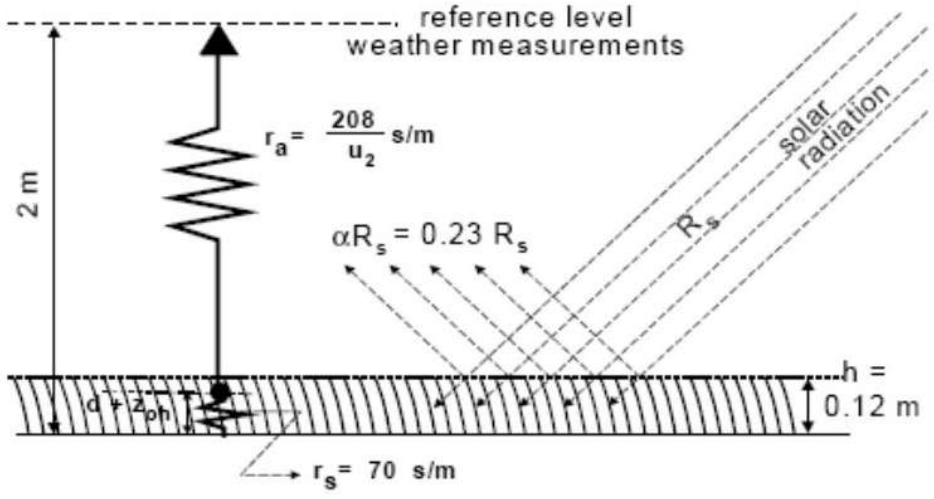

Figure 2.7 The characteristics of hypothetical reference crop

The FAO Penman-Monteith method requires data concerning the site location (altitude, latitude), and meteorological variables (solar radiation, air temperature, humidity and wind velocity). The recommended equation can be used to calculate evapotranspiration for daily, weekly, ten-daily and monthly periods. A great advantage of the FAO Penman-Monteith method is that it includes various relationships and correlations that can account for missing climatic data. Reasonable estimates of evapotranspiration can be derived even for cases where only the maximum and minimum air

temperature is available (Allen *et al.*, 1998). The relationships required for obtaining the listed parameters, specifically for the case of limited climatic data, are provided in Appendix A of this thesis, and in the FAO Irrigation and Drainage Paper No. 56.

The crop (plant) evapotranspiration ET_c differs distinctly from the reference evapotranspiration ET_0. The sources of difference are numerous, including ground cover, canopy properties and aerodynamic resistance of the crop. All these differences are integrated into the so-called crop coefficient K_c, which essentially is a plant-specific parameter. In the crop coefficient approach, crop evapotranspiration ET_c is calculated by multiplying ET_0 by K_c (see Figure 2.6).

Two approaches, regarding the determination of the crop coefficient K_c are available: the single and the dual crop coefficient approach. In the single crop coefficient approach, the difference in evapotranspiration between the cropped and reference grass is combined into one single coefficient K_c. In the dual crop coefficient approach, the crop coefficient is split into two factors describing separately the differences in evaporation and transpiration between the crop and reference surface, $K_c=K_{cb}+K_e$. In the latter case, the basal crop coefficient K_{cb} accounts for plant transpiration, whereas K_e for evaporation from the soil surface. The approach to follow should be selected as a function of the purpose of the calculation, the time step considered, the level of accuracy required and the availability of climatic data. It is recommended that the single crop coefficient approach for assessment of ET_c is more suitable for solution of typical irrigation problems, when weekly or longer time steps are considered and when limited climatic data are available. On the other hand, the dual crop coefficient approach is employed for real-time irrigation planning or for research on the daily variations of soil water balance and requires more tedious calculations.

As the crop develops, the ground cover, crop height and the leaf area change. Due to differences in evapotranspiration during the various growth stages, the K_c for a given crop will vary over the growing period. The growing period can be divided into four distinct growth stages: initial, crop development, mid-season and late season. The changing characteristics of the crop over the growing season also affect the K_c coefficient, which is depicted in the Figure 2.8, along with the main influencing factors.

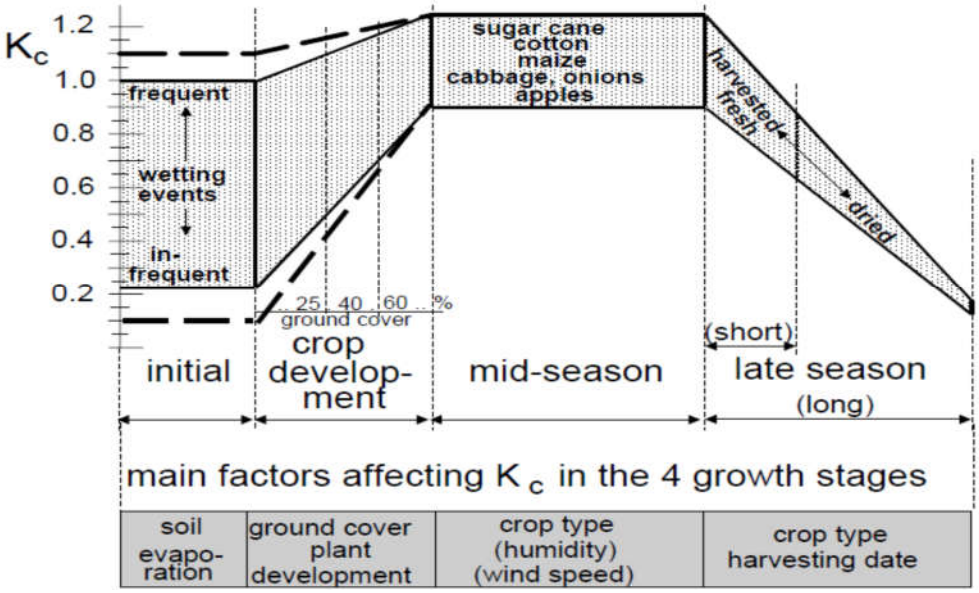

Figure 2.8 Typical variation of the crop coefficient Kc during the growing period (Allen et al., 1998)

The initial stage covers the period from planting day to approximately 10% ground cover. During this period, the leaf area of the crop is low and soil evaporation is dominant one of the two water extraction processes. During this period, $K_{c,ini}$ is influenced by the frequency and magnitude of the wetting events, as evaporation increases when the soil is wet and decreases when conditions are dry.

The crop development stage corresponds to the period between 10% ground cover and full ground cover. During this period, transpiration steadily increases and starts to govern the evapotranspiration process, as the increased ground shading, due to crop development, confines the evaporation process.

The mid-season stage is usually the longest of the growing period and covers the transition from full ground cover to the start of maturity. During this period the value of K_c ($K_{c,mid}$) reaches its peak and remains constant for most growing conditions.

The late season stage covers the period from the start of maturity to harvest or full senescence, where the calculation procedure of K_c and ET_c usually ends. For perennial vegetation, which can grow during a whole calendar year, the planting and termination dates coincide. The value of K_c ($K_{c,end}$) depends on whether the crop is allowed to dry out in the field and on irrigation practices.

Representative values for the length of the aforementioned stages and their respective coefficients Kc, concerning various types of crops, are provided in tabulated form by (Allen *et al.*, 1998).

The FAO Penman-Monteith method (Allen *et al.*, 1998) also involves numerous procedures that account for the calculation of crop evapotranspiration under field conditions that significantly differ from the standard ones. The calculated ET_c is then modified with various adjustment factors to give $ET_{c,adj}$, which accounts for the reduced evapotranspiration rate. Specifically, the influence of soil water stress is taken into consideration by incorporating a water stress coefficient K_s that decreases the crop coefficient K_c.

2.4.2 Empirical Methods

Estimations of evapotranspiration can also be made by means of empirical relationships. Many equations have been proposed over the years to allow the calculation of potential evapotranspiration when limited climatic data are available, thus overcoming the need for non-standard meteorological data input. The fact that these empirical correlations are commonly related to some specific environmental conditions, constrains theirs's wider application.

Empirical equations can be categorized according to the set of data they are based on. (Xu & Singh, 2002) state that empirical equations can be divided in three groups: mass-transfer based methods, radiation-based methods and temperature-based methods. In this research, reference will be made to a temperature-based method, as temperature data are considered to be the most easily accessible.

One of the most popular empirical methods is the one proposed by (Thornthwaite, 1948). The method is intended for the calculation of monthly potential evapotranspiration, based on positive average air temperatures for the months under consideration. The equation is given in the following form:

$$E_p = 1.6\left(\frac{10T_m}{I}\right)^a$$

Where:

T_m the monthly average air temperature (°C);
I the heat index, calculated from monthly indices;
a the exponent α, function of the heat index

$$I = \sum_{j=1}^{12} i_j$$

$$i_j = (\frac{T_j}{5})^{1.514}$$

$$a = (0.0675 \times I^3 - 7.71 \times I^2 + 1792 \times I + 49239) \times 10^{-5}$$

Thornthwaite's equation might be unsuitable for application in arid or semi-arid regions, as it was originally developed for the humid conditions of north-east North America (Blight, 1997). (McKenney & Rosenberg, 1993) stated that Thornthwaite's equation significantly underestimates potential evapotranspiration and that the results are particularly sensitive to changes in temperature.

2.5 Modelling of Vegetation - Root Water Uptake Models

The hydrological interface between the plant's root system and the soil is a boundary of particular importance, through which most of the water flow to the atmosphere takes place. That is confirmed by the fact that in temperate climate the annual ratio of transpiration over evapotranspiration varies approximately from 0.6 to 0.8 (Novák, 2012). This means that the hydraulic link between soil domain and the atmosphere is established mainly through the root water uptake, which generates negative water fluxes. Besides, plant canopy (leaves and steams) protect the slope, by intercepting water and restricting the rainwater infiltration. For these reasons, it is essential to account for vegetation, when modelling slope–atmosphere interaction.

Estimation of the changes in soil water regime (including pore water pressures and moisture contents) affected by a vegetation cover requires either direct filed measurements or the use of mathematical models for the water uptake by plant roots. According to (Feddes, Bresler & Neuman, 1974), depending on the size of water movement zone of interest, several different scales for modelling water uptake by plant roots are available. These include microscopic, mesoscopic and the macroscopic scales, which all refer to local areas. For the geotechnical boundary value problems, meso and macro scale models are only relevant, since micro scale approach deals with plant roots at the tissue and cellular level. Mesoscopic models require very detailed information about plant, root (details of each single root are required) and soil features, as well as knowledge about mutual interaction of these components. Macroscopic models, on the other hand, treat the entire plant root system in an integrated, smeared sense. In other words, this means that both the soil and roots are assumed to be a continuous media. Hence, in the macroscopic approach, it is assumed that the entire root zone participates in the extraction of moisture from small differential volumes of the root zone at a certain rate.

The mesoscopic approach considers the radial flow of soil water towards a single individual root. This representative root is modelled as a linear narrow tube, having uniform thickness and absorptive properties, with constant sink along its length (Feddes & Raats, 2004). A set of these representative roots can then be used to describe a complete root system. In this method, the flow equation is solved, using cylindrical coordinates, for the distribution of pressure head, soil water content and water flux from the roots outwards (Feddes *et al.*, 2001). The main limitations preventing the implementation of mesoscopic models in geotechnical engineering practice lies in necessity of providing very detailed information about root and plant features, and the need for very fine element discretization to realistically simulate complex root system architecture. Usually, details about root geometry and soil heterogeneity are not readily available.

The macroscopic models constitute the majority of root water uptake models used to simulate water removal for hydrological purposes. In the macroscopic approach, the water extraction by roots is simulated by incorporating a sink term into the Richards water flow equation, derived by combination

of mass-balance equation and Darcy's constitutive law. The one-dimensional form of Richards equation (governing equation for water transport) accounting for root water uptake is given below:

$$c(h_w)\frac{\partial h_w}{\partial t} = \frac{\partial}{\partial z}\left(k(h_w)\frac{\partial h_w}{\partial z}\right) + \frac{\partial k(h_w)}{\partial z} - S(z,t)$$

Where:

h_w	the soil water potential expressed in terms of pressure head (m)
$c(h_w)$	the differential water capacity (m^{-1})
k	the hydraulic conductivity of soil (m/s)
$S(z,t)$	the sink term representing the root water uptake rate (m^3/m^3*s)

The function $S(z,t)$ can be defined as the volume of water drawn out by plant roots from a unit volume of soil per unit time (Novák, 2012). The summation of the water extraction rates along the root depth gives the transpiration rate:

$$T = \int_0^{z_{max}} S(z)dz$$

Numerous sink term functions have been proposed in the literature over the years, varying according to the principles and assumptions these are based on. According to (Gardner, 1964; Hillel, Talpaz & Van Keulen, 1976; Herkelrath, Miller & Gardner, 1977) rate of water uptake is proportional to the difference between potential energy of the water within plant tissue and that of a surrounding soil. (Feddes, Bresler & Neuman, 1974) suggest somewhat different perspective for root water uptake, assuming it to be proportional to the difference between the plant surface and the soil water potential. Although the above relationships are correct from a physiological point of view, they require parameters that are difficult to measure (Novák, 1987). Alternative approach for estimating the root water uptake rates, which is not supported by firm theoretical background, but pure empiricism, was proposed by (Molz & Remson, 1970; P. A. C. Raats, 1976). They have developed empirical correlations for the assessment of the sink term, based on the results from field measurements. The important finding of theirs work was the observation that root water uptake rate is decreasing with depth. The drawback of such empirical equations is the fact that they do not take account of environmental properties and specifically the effect of soil water content variation.

The methodology that over the years of research and application proved to be most viable and efficient was the one proposed by (Feddes, Kowalik & Zaradny, 1978). It is semi-empirical approach derived by combining empirical relationships with physically valid functions. It provides a link between the water uptake rate by plant roots, transpiration rate and properties of roots and soil. In theirs work (Feddes, Kowalik & Zaradny, 1978) sink term is related to pressure head, h, and the maximum water extraction rate, S_{max}, as follows:

$$S = \alpha(h) \times S_{max}$$

Where:

S	the actual water extraction rate
$\alpha(h)$	a dimensionless function depending on pressure head
S_{max}	the maximum (potential) water extraction rate, not limited by soil water content

The main advantage of such formulation is that the effect of soil moisture content is separated from function for the potential root water uptake rate S_{max}. The effect of soil water content variations on the actual water extraction rate are incorporated into the $\alpha(h)$ coefficient, which captures the forementioned effect indirectly via soil water potential changes. Moreover, as soil moisture content is not affecting S_{max}, the shape of its function will depend only on the root system properties, mainly

on the root depth. The summary of most representative semi-empirical relationships for the S_{max} function found in the literature are given in the Table 2.1.

Table 2.1 Review of potential water extraction rate functions

Author	Distribution	Function	Notes
(Feddes, Kowalik & Zaradny, 1978)	constant	$S_{max} = \frac{T_p}{z_{max}}$	T_p - maximum (potential) transpiration rate (m3/m2*s), not limited by soil water content z_{max} - the maximum root depth (m)
(Hoogland, Feddes & Belmans, 1981)	linear	$S_{max} = \alpha - b \cdot z_r$	α,b - empirical constants
(Prasad, 1988)	linear	$S_{max} = \alpha_j - b_j \cdot z_r$ $S_{max} = \frac{2T_p}{z_{max}}(1 - \frac{z_r}{z_{max}})$	for $z_r = z_{max} \rightarrow S_{max}=0$ $\alpha_j = \frac{2T_p}{z_{max}} \quad b_j = \frac{2T_p}{z_{max}^2}$
(Novák, 1987)	exponential	$S_{max} = S_{max}^{surf} \times e^{-p\left(\frac{z_r}{z_{max}}\right)}$ $S_{max} = T_p \frac{p \times e^{-p\left(\frac{z_r}{z_{max}}\right)}}{z_{max}[1 - e^{-p}]}$	S_{max}^{surf} - the maximum water uptake rate by roots close to the surface p - dimensionless empirical constant that determines the curvature of the exponential function (p=3.64 for maize root system)

Plots of the listed water uptake functions are illustrated in the Figure 2.9. The results from field experiments reported by (Gerwitz & Page, 1974), demonstrate that in the 70% of cases, distribution of water uptake rate resembles the exponential one. The measurements were conducted under conditions where the soil moisture content is not a limiting factor.

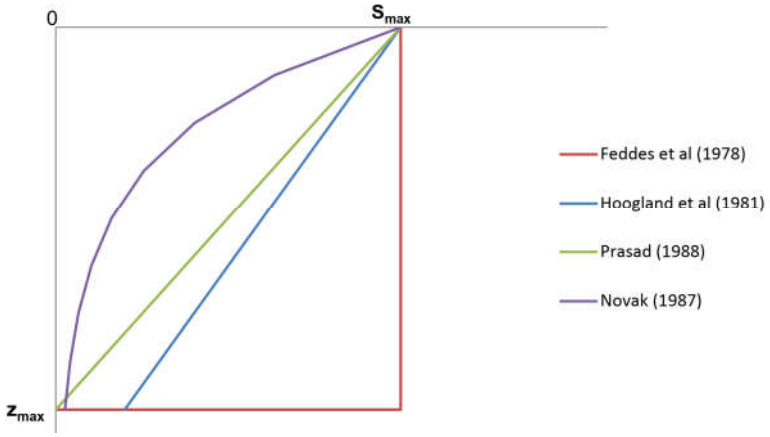

Figure 2.9 Schematic representation of various potential water uptake functions with depth

It should be noted that the presented functions represent maximum (potential) root water uptake rate, corresponding to conditions of unlimited supply of soil water. However, if transpiration is limited by soil moisture content, the S_{max} function must be modified by a function of soil water potential *α(h)*, as defined previously by equation of (Feddes, Kowalik & Zaradny, 1978). This modification considers the changes that occur in the distribution of water uptake along the plant roots due to insufficient water supply, therefore accounting for the effect of water stress.

The shape of one of the most commonly used reduction functions *α(h)*, recommended in the paper by (Feddes, Kowalik & Zaradny, 1978), is given in Figure 2.10. It is a piecewise function, which requires

four pressure head values (h_1, h_2, h_3 and h_4) for complete formulation. Between these values, α function varies linearly within range [0,1]. The h_1 value corresponds to the anaerobiosis point, when there is a lack of free oxygen. For pressure heads more positive than this value the actual water uptake is zero, as there is no air inside the porous space and therefore no plant transpiration occurs. The h_2 value marks the beginning of the anaerobic conditions. The h_3 value depends on the transpiration rate and thus it is considered to be species dependent. Finally, the h_4 value corresponds to the permanent wilting point, the conditions of maximum suction force that the plants can generate to absorb moisture from the soil.

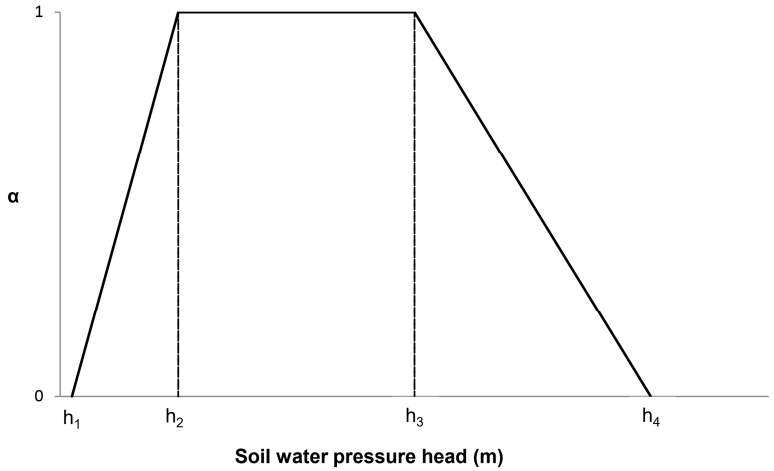

Figure 2.10 Dimensionless reduction coefficient as a function of soil water pressure head (Feddes, Kowalik & Zaradny, 1978)

The presented model, suggests that actual water uptake reduces when either too wet or too dry conditions exist in the soil, whereas it is equal to the potential water uptake for soil water pressure head values between h_2 and h_3. Typical values that have been published in the literature are $h_1 < -0.50$ cm, $-10 > h2 > -100$ cm and $h4 = -1.5*10^4$ cm (Novák, 2012).

Another factor that influence the root water uptake rate is the concentration of salts in soil water. One of the most popular reduction functions that account for salinity stress is the one proposed by (Maas & Hoffman, 1977), which is depicted in Figure 2.11 in terms of the electrical conductivity of soil water.

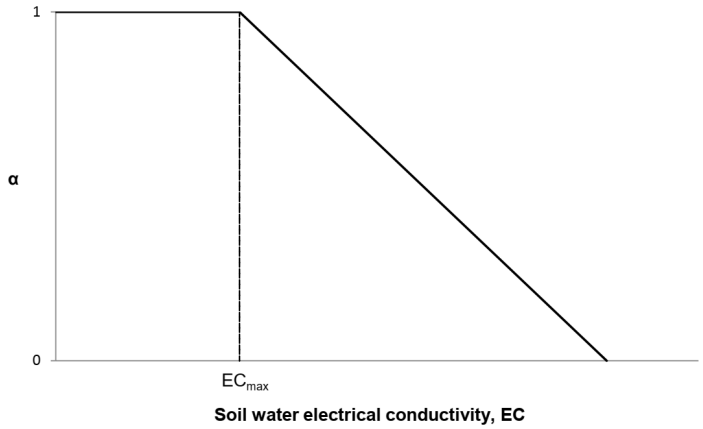

Figure 2.11 Dimensionless reduction coefficient as a function of soil water electrical conductivity (Maas & Hoffman, 1977)

In the literature numerous reduction functions have been published which combine the effects of water and salinity stress. However, it is reported by (Skaggs *et al.*, 2006), that the single equation approach for accounting for effects of water and salinity stress is unreliable. Additionally, they highlight the fact that it is not clear which one of the proposed root water uptake reduction functions is most suitable for problem under consideration.

The so far presented root water uptake functions are inherently one-dimensional, defined exclusively in terms of depth below ground surface (in terms of vertical coordinate z). Such an assumption may be valid where uniform vegetation cover exists but for isolated trees, water uptake is more complex. For spatial conditions corresponding to isolated trees, a simple extension of one-dimensional model is presented by (Rees & Ali, 2006). In proposed model, a linear distribution of root water uptake function is assumed in both vertical and radial directions away from tree.

Numerous enhancements of root water uptake functions, particularly with respect to plant root characteristics, have be introduced by (Fatahi, Khabbaz & Indraratna, 2009, 2014). In work by (Fatahi, Khabbaz & Indraratna, 2009), novel mathematical model for tree root water uptake distribution, incorporating root density function $G(\beta)$, has been developed.

$$S(x, y, z, t) = \alpha(h) \times G(\beta) \times F(T_p)$$

It is essentially 3-dimensional model, which treats root distribution effect $G(\beta)$ in a separate fashion, similarly to previously described $\alpha(h)$ function. The hyperbolic tangent function is assumed for $G(\beta)$, to match the fact that root water uptake must reach a limiting value when the density of tree root is such that water uptake approaches its physiological maximum.

The further improvement of their theoretical model consisted of capturing the evolution of shape and extent of the root system (Fatahi, Khabbaz & Indraratna, 2014). It was demonstrated by (Biddle, 1998), that root growth rates play an important role in water uptake patterns. To account for growth process root density function $G(\beta)$ was modified, in a way to be able to simulate the increase in the root zone size, as well as the time changes or the root length density. The initial root zone was assumed to have a conical shape as schematically illustrated in the Figure 2.12, with sigmoidal (single sine function) curves representing the expansion of the root zone dimensions $z_{max}(t)$ and $r_{max}(t)$. The same functional form was adopted for the description of the evolution of the maximum root length density $\beta_{max}(t)$.

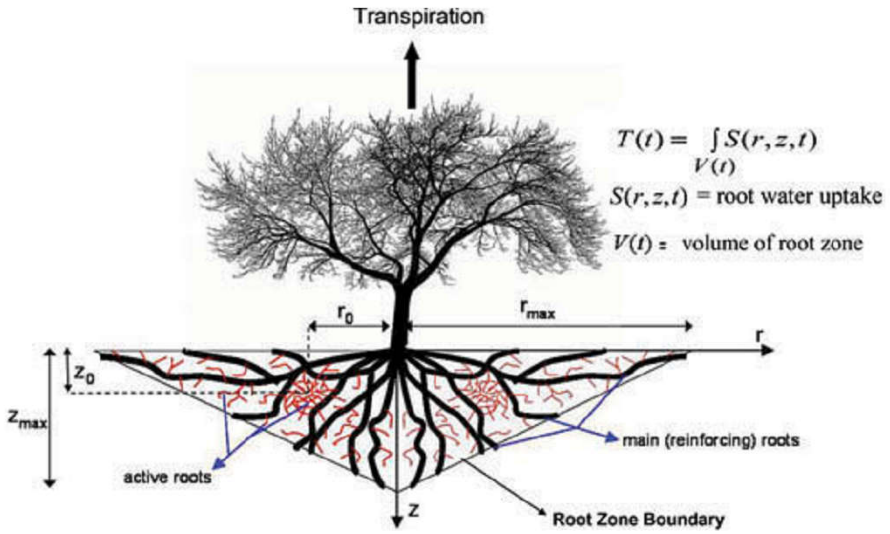

Figure 2.12 The assumed shape of the root zone after (Fatahi, Khabbaz & Indraratna, 2009, 2014)

Despite the great strides made in recent years, the modelling of such complex scenarios remains hampered by a lack of data to support in particular the inclusion of root characteristics and their time variations.

2.6 Possible Strategies for Modelling Soil-Vegetation-Atmosphere Interaction

It has long been recognized that ground water regime constitutes one of the main factors governing the behaviour of slopes. As was previously explained, the changes in ground water regime are direct consequence of the combined effect of rainfall and vegetation. Despite the acknowledgement of the great importance of soil-vegetation-atmosphere interaction on the performance of slopes, predicting this complex interaction is not straightforward. The difficulties lie in the dynamic nature of the boundary conditions and corresponding transient thermo-hydro-mechanical response of soils, which is coupled and highly nonlinear. Partial saturation of top soil layers (above the ground water table) adds to the complexity of the problem, rendering the use of numerical tools such as finite element method, necessity.

It should be noted that vast majority of the research published so far is related to stability issues of slopes induced by climatic perturbations. On the contrary, to date very little investigation has been carried out regarding the infrastructure serviceability problems connected to the slope-vegetation-atmosphere interaction. In the remainder of this section the review of available approaches and numerical tools for modelling the effects of the slope–atmosphere interaction on the thermal, hydraulic and mechanical state of the slope are discussed. The discussion will proceed from the simplest to the more advanced ones.

2.6.1 Hydraulic Modelling

The simplest approach includes uncoupled flow analysis, which simulates transient seepage in the slope, resulting from continuous flux boundary condition changes (i.e., infiltration, evaporation and transpiration). Within this uncoupled approach, only fluid flow continuity equations are considered, neglecting the effects of soil skeleton deformation and temperature variations. This purely hydraulic analysis is most commonly combined with limit equilibrium method, for the purpose of the assessment of slope stability. It provides the prediction of pore water pressures variations within a slope, in response to atmospheric conditions, which is subsequently used in stability evaluations, to derive the variation with time of the slope stability factor.

In most general form hydraulic models simulate flow of both fluid phases (water and air), within porous medium. In that case, additional constitutive relationships, beside Darcy's law, are introduced to capture the behaviour of gaseous phase. These include Fick's law to describe diffusion processes, Henry's law to describe dissolution of air in the water and psychrometric law to correlate suctions and relative humidities. However, in geotechnical engineering it is usual practice to disregard the gas balance (conservation of mass equation for the air phase), by assuming the air pressure to be constant and equal to the atmospheric. In that case model only simulates water mass balance equation. Further simplification can be introduced if water density is assumed to be constant, independent of the water pressure. This assumption converts the liquid mass-balance equation into a volume-balance equation of liquid water, which is commonly known as Richards' equation (Richards, 1931). Richards' equation represents governing differential equation for the flow through unsaturated porous medium and cause of that it is particularly suited for seepage analyses within vadose zone (region between ground surface and water table).

The primary input for fluid flow analysis are hydraulic properties of the soils. For the case of partially saturated fluid flow, two additional constitutive relationships are incorporated into Richards' equation. These are soil water retention curve (SWRC), which describes how the water content varies with the water stress (suction) and the hydraulic conductivity function, which specifies how the

hydraulic conductivity varies with the water stress (suction). For saturated case, only Darcy's constitutive equation, which links the water velocity to the hydraulic conductivity and the hydraulic gradient, is employed. It should be noted that despite the fact that Darcy's law was developed originally for saturated conditions, it was later proved that it holds for unsaturated state as well. More detailed review of SWRCs and hydraulic conductivity functions is provided in the next chapter, which deals in particular with unsaturated soil behaviour.

One of the first attempts to incorporate the use of root water uptake models in geotechnical engineering was conducted by (Tratch, Wilson & Fredlund, 1995). The authors acknowledged the importance of plant transpiration in the surface flow boundary condition and proposed a method of simulating the vegetation effects. They used SoilCover numerical code, a one-dimensional, transient, heat and mass transfer finite element model. For validation purposes a laboratory experiments were conducted. The experiments consisted of vegetated soil columns, which were allowed to desaturate in response to root water extraction. The moisture conditions, both surface and subsurface were continuously monitored, in order to establish the evapotranspiration rates and moisture profiles. The used numerical code already has had implemented scheme for calculating bare soil evaporation from an unsaturated soil surface. Plant transpiration was modelled by incorporating the sink term suggested by (Feddes, Kowalik & Zaradny, 1978) into the fluid flow equation and employing the potential soil water extraction rate function proposed by (Prasad, 1988).

The procedure based on the uncoupled hydraulic modelling was employed by (Briggs *et al.*, 2013; Briggs, Smethurst & Powrie, 2014; Briggs *et al.*, 2016), to examine the influence of climate and vegetation on clay fill railway embankments hydrology in UK.

The analyses have been conducted using the finite element software Vadose/W, which is capable of simulating both saturated and unsaturated water flow in response to an applied climatic boundary condition. The climate boundary condition requires as input daily meteorological data such as rainfall, air temperature, humidity, solar radiation and wind velocity. Particular feature of the model is that it separates two components of the evapotranspiration process. The ratio between the two evapotranspiration components is dependent upon the leaf area index, which represents the ratio of the surface area of the leaves to the soil surface area they cover. The water loss from the unsaturated soil surface due to evaporation is calculated using the Penman-Wilson equation (Wilson, 1990), whereas the root water uptake model proposed by (Prasad, 1988) is employed to account for the potential transpiration rate below the soil surface boundary condition. The actual transpiration rate is then calculated using the pore water suction dependent reduction function according to the recommendation by (Feddes, Kowalik & Zaradny, 1978). The relative balance of precipitation, evaporation and transpiration determines whether water infiltration or runoff will occur at the slope surface.

In paper by (Briggs *et al.*, 2013), the influence of clay fill and underlying foundation soil permeability on pore water pressure distributions within embankments for various winter weather scenarios was investigated. These analyses were conducted on one dimensional soil columns, the stratigraphy of which was chosen to represent a borehole (section) through the embankment. The authors decided to omit the ash layer overlying the surface clay fill from the analyses, as they considered it to be free draining. The groundwater table was selected to be at 2m depth below the foundation layer surface. The bottom and vertical boundaries of the mesh were assumed to be impermeable and the groundwater table was allowed to fluctuate in the vertical direction. The type of vegetation considered in the analyses was a vegetative cover consisting of grass and shrubs, with a maximum root depth of 0.9m. The geometry of the soil columns under examination as well as the values of permeability under consideration are illustrated in Figure 2.13_A. These three soil columns were subjected to extremely wet, intermediate and normal winter weather scenarios, after an initialisation period lasting 2 years. At the end of the initialisation period, the pore water pressure profiles were identical for all

3 soil columns. For all the analyses, the total time period under consideration was 4 years and daily time steps were used.

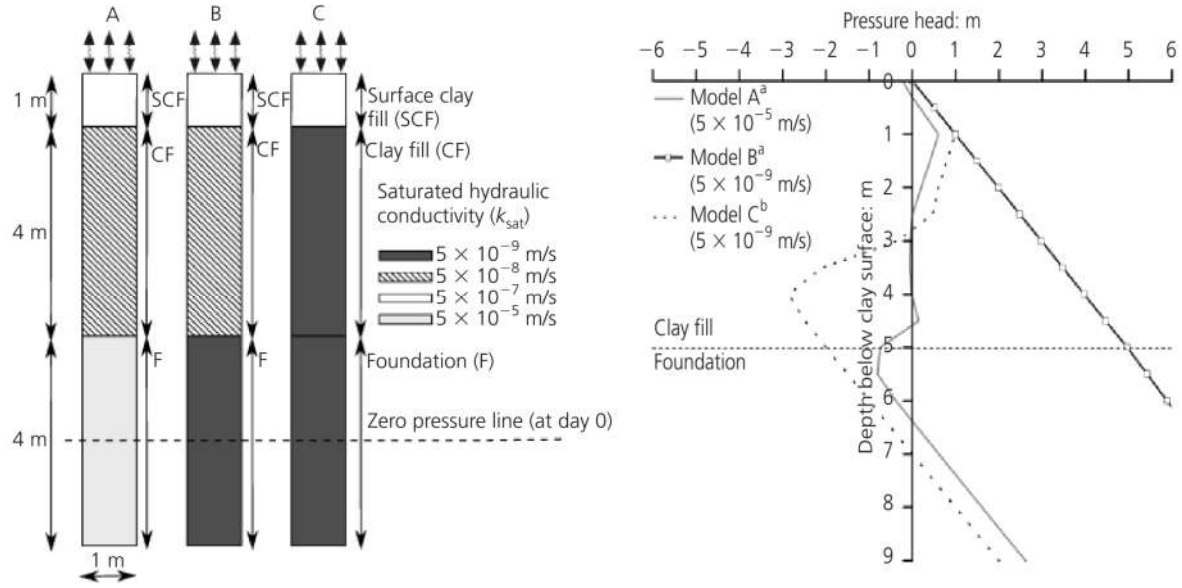

Figure 2.13 Geometry and stratigraphy of the soil columns (on the left), and predicted pressure head profiles for extreme wet winter scenario (on the right), after (Briggs et al., 2013)

The obtained results have demonstrated that the relative ratio of the saturated permeability of the clay fill and foundation soil layer has a significant effect on the winter pore water pressure profiles (see Figure 2.13_B). For the case of the extremely wet winter scenario (c. 1 in 100 years), under-drained pore pressure profiles were predicted for permeable foundation soil (chalk for instance). On the other hand, for embankments founded on London Clay (model B) pore pressure profiles close to hydrostatic with zero pressure line at the top of clay fill surface were calculated. However, it should be noted that this most critical situation was observed only in case where clay fill permeability was one order of magnitude greater than permeability of foundation soil, which is generally the case for the dumped clay fill embankments. In special case, when same permeabilities were attributed to both the clay fill and foundation layers, less water infiltration and therefore a less rapid response to the extreme rainfall event was observed. The clay fill was found to maintain suctions throughout the year, when the effect of intermediate or normal winter conditions were examined.

The influence of vegetation, particularly mature tree cover and tree removal, on the clay fill embankment hydrology is investigated by (Briggs, Smethurst & Powrie, 2014; Briggs *et al.*, 2016). Finite element analysis using the software Vadose/W have been conducted to explore the extent to which hydrological models with a climatic boundary condition and root water uptake function can provide useful comparisons with the field measurements. In both papers, monitoring results regarding the pore pressure distributions from an instrumented embankment at Hawkwell, on the Shenfield–Southend Victoria line, Essex, have been used for the numerical model validation purposes. The same data is used in the current thesis, as the basis for validation process. In the first paper published (Briggs, Smethurst & Powrie, 2014), the authors once again decided for one dimensional model, which has previously shown to be adequate (Briggs *et al.*, 2013), assuming uniformity in angle, permeability and vegetation along the slope. The soil column is representative of the borehole at the crest of the north embankment slope, comprising 1.1 m of ash and ballast overlying 3 m of clay fill, and 13 m of the London clay foundation soil at the bottom. The effect of mature trees, their subsequent removal and finally the re-establishment of shrubs and saplings was simulated by adjusting the depth of root water uptake (the program automatically calculates potential evapotranspiration based on the

meteorological data and plant species). The modelling results shown in Figure 2.14_A revealed that alterations in vegetation cover have profound influence on the embankment hydraulic regime. The clearance of the vegetation completely eliminates seasonal pore pressure fluctuations and shifts them towards the zero-pressure line. Although the predictions obtained were qualitatively in line with field hydrological measurements, quantitatively they were excessively inconsistent, overpredicting both the individual magnitudes and seasonal variations.

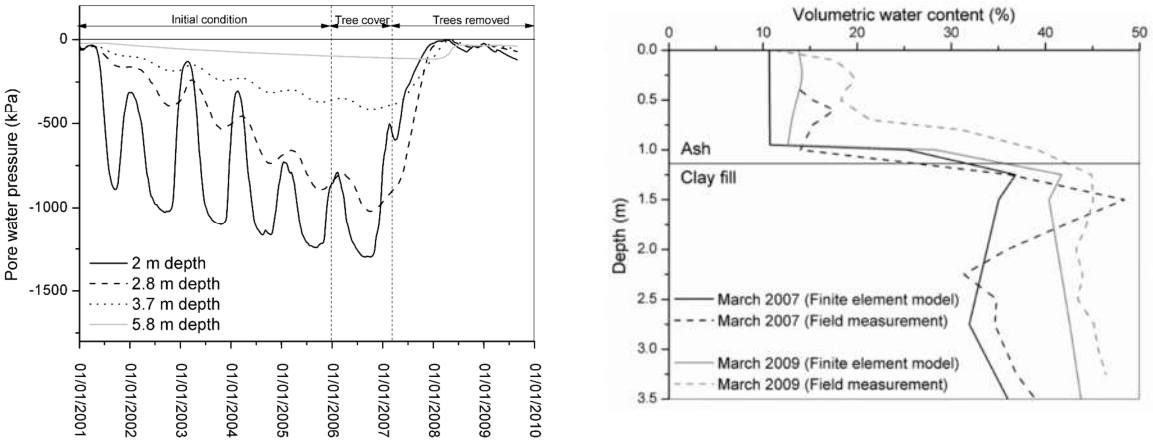

Figure 2.14 Predicted pore water pressure evolution (on the left) and volumetric water contents variations in response to vegetation cover changes (on the right), after (Briggs, Smethurst & Powrie, 2014)

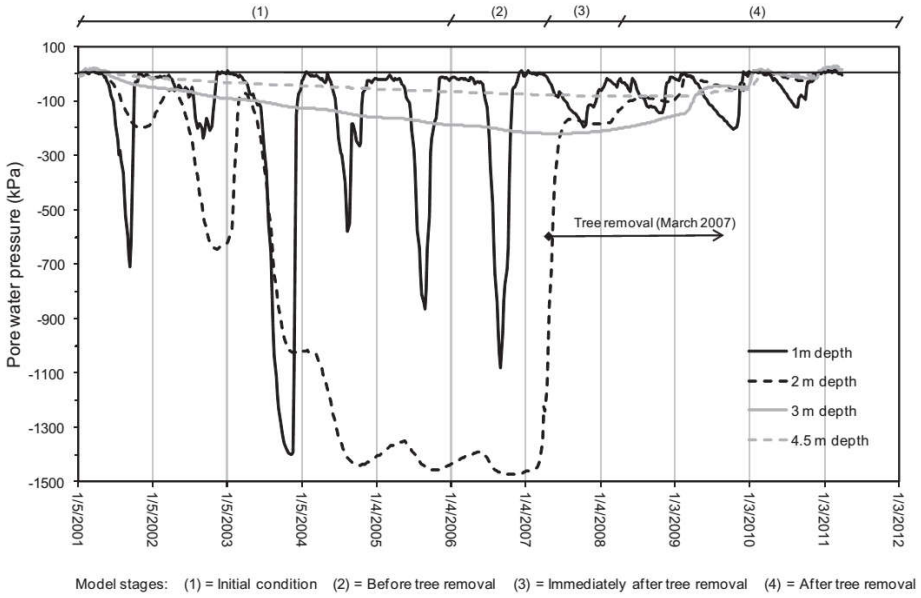

Figure 2.15 Midslope pore water pressure variation predicted by the finite element model after (Briggs et al., 2016)

As mentioned earlier, the Hawkwell case study was subsequently used once again (Briggs *et al.*, 2016), to examine the influence of vegetation cover on the hydrological conditions of the clay fill embankment. Within this more comprehensive investigation, two-dimensional finite element model was created, to enable more realistic simulations. In addition, two-dimensional analysis allows for more detailed elaboration of possible vegetation management strategies. The results demonstrated that, leaving trees over the lower 1/3 of the slope could be beneficial for both stability and serviceability of the embankment. In this way, persistent soil suctions are retained deep within the

root zone at the toe part of the slope, while at the same time magnitudes of the pore pressure fluctuations near the crest of the slope are reduced. Despite reasonable predictions regarding patterns of hydraulic behaviour, significant limitations in terms of quantitative simulation of pore pressures have still remained (see Figure 2.15).

2.6.2 Thermohydraulic Modelling

Thermohydraulic modelling represents an upgrade to pure hydraulic modelling. Beside mass balance equations for liquid and gas phases, energy balance equation (conservation of energy law) are introduced into formulation of governing differential equations. This allows the prediction of both liquid and gas pressure distributions, as well as temperature fields. The main advantage of this approach over the previous one lies in the fact that temperatures are known, which enables evapotranspiration rates to be derived from the numerical simulations, rather than being specified. Prerequisite is that all the climatic variables, together with the main characteristics of the vegetation are provided.

In defining the initial and boundary slope conditions, in addition to pore pressures, also temperature distribution needs to be prescribed. Furthermore, there is a demand for additional laboratory tests, in order to establish thermal conductivities and the volumetric heat capacities of slope materials. The required comprehensive characterization of the initial slope conditions along with unsaturated soil behaviour, renders this modelling approach still impractical.

2.6.3 Hydromechanical Modelling

The third and most utilised approach for modelling the effects of soil-vegetation-atmosphere interaction on the behaviour of slopes is based on the combining hydraulic and mechanical facets of behaviour. This is the only appropriate procedure when the soil deformations are of concern, which is the case when it is necessary to evaluate serviceability of structures interacting with slopes. For achieving full coupling of fluid flow and deformation, the equilibrium conditions and mass balance equations should be solved simultaneously. In addition to fully coupled hydro mechanical analysis, some researchers have been developing loosely coupled models (Rouainia *et al.*, 2009; Davies, 2011; Rutqvist *et al.*, 2002; Sun *et al.*, 2016a). A loosely coupled methodology consists essentially of conducting two independent analysis: one for the calculation of fluid flow and other for the calculation of soil skeleton deformation. This is also known as staggered approach, cause mass-balance (continuity equation) and momentum-balance (equilibrium equations) are not solved at the same time. At first, flow analysis is performed with suitable climatic and vegetation boundary conditions, and subsequently the computed surface pore water pressures are transferred to mechanical model. In addition, (Sun *et al.*, 2016b), used changes in porosity calculated by mechanical (actually hydro-mechanical computer code, but without sophisticated climatic boundary conditions), to update unsaturated hydraulic parameters for the next increment (time step) of uncoupled hydraulic simulations.

Some of the earliest attempts to encompass the effects of climate and vegetation on behaviour of earthworks was carried out by (Russell *et al.*, 2000; Kovacevic, Potts & Vaughan, 2001). The primary goal was to investigate the impact of the earth-vegetation-atmosphere interaction on the progressive failure mechanism of high-plasticity clay fill embankments. The procedure consisted of applying artificial winter and summer pore water pressure profiles (see Figure 2.16) and performing the coupled saturated flow-deformation analysis. These pore pressure profiles were selected to represent approximately those obtained by field measurements and observations, and were assigned cyclically over the time period under consideration. For each season (summer, winter), the pore water pressures were allowed to equilibrate (to reach steady-state conditions) before the pore water pressure profile of the next season was applied. The results highlighted that seasonal porewater pressures variations

driven by combined effect of vegetation and climate, could significantly weaken clay fill embankments, potentially leading to progressive failure.

In paper by (Nyambayo, Potts & Addenbrooke, 2004), authors argue about the correctness of a procedure where full dissipation of pore water pressures is allowed. They have stated that the obtained results are therefore independent of the true permeabilities of soil layers and that the depth of influence of surficial hydrological process propagates much deeper than occurs in the field. Rather, they recommended that consolidation process last no more than 6 months. The period of 6 months proved to be insufficient for the equilibrium to be attained, especially for less permeable conditions, thereby allowing the effects of permeabilities to be taken into account. The obtained results have shown that clay fill embankments of higher permeability ($1x10^{-7}$ - $1x10^{-8}$ m/sec) are more susceptible to progressive failure, as a result of larger seasonal pore water pressure variations. The lower permeability clay fill embankments ($1x10^{-9}$ m/sec) experienced smaller pore pressure changes, causing slower accumulation of deviatoric plastic strains, and were therefore able to stand-up for much longer time before failure.

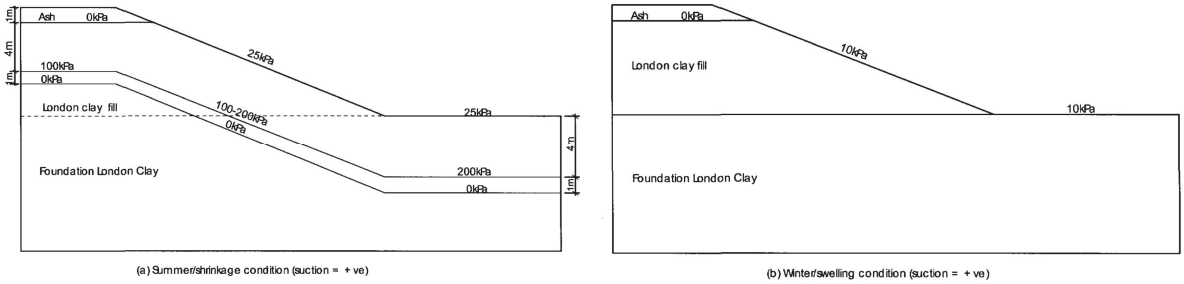

Figure 2.16 Summer and winter pore water pressure boundary conditions used to simulate seasonal effects of vegetation

Similar approach consisting of assigning pore suction cycles was employed by (Lees, 2013), for investigating deformations of Aldenham embankment dam. In order to simulate the effects of large trees in the vicinity of the embankment toe, authors adopted a suction zone 0.8 m below the ground surface, extending across an area encompassing approximately root zone of trees (Figure 2.17). The suction was switched between 50 kPa and 250 kPa every four weeks (a short interval was chosen to reduce analysis time), to reproduce tree induced winter/summer conditions. Field monitoring indicates that, as the fill material at the toe contracts due to the imposed suctions, the upper slope then slips downwards allowing a progressive failure mechanism to develop in the upper slope. This mechanism was recreated by the finite difference analysis.

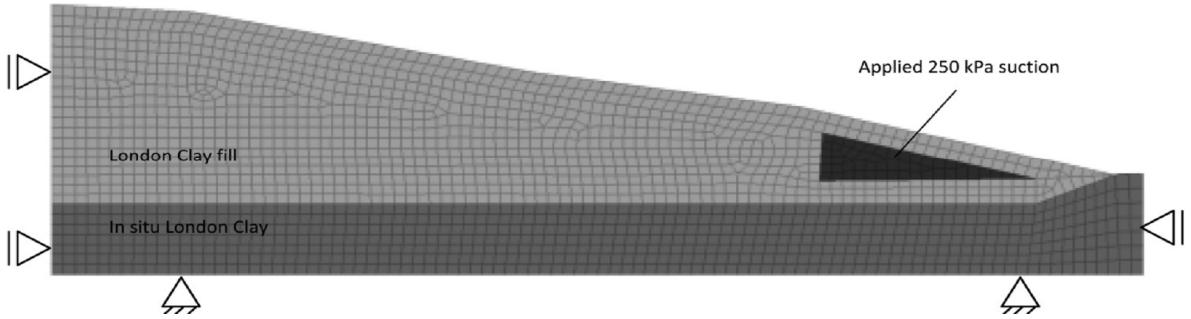

Figure 2.17 FLAC grid for the embankment dam with assigned suction zone representing trees (Lees, 2013)

However, the simulation of the soil-vegetation-atmosphere interaction by prescribing seasonal pore water pressure profiles results in an unrealistic representation of the continuous changes occurring in

the soil water balance and neglects the transient nature of the actual pore pressure profiles. Another implication of using a specified hydraulic boundary condition is that it might lead to water flow magnitudes that may not be achievable by vegetation during transpiration (Nyambayo & Potts, 2010).

Significant advances in the modelling of hydraulic boundary condition imposed by vegetation was brought about by (Rouainia *et al.*, 2009), which consisted of treating the pore pressures as unknowns, rather than prescribing them. The authors employed *Shetran* hydrological model, which is capable of predicting the daily pore pressure variation within a slope using as input: meteorological, soil and vegetation data. *Shetran* is capable of analysing both saturated and unsaturated fluid flow. The calculated surface pore water pressures were then transferred to the geotechnical model *Flac-tp*, in order to simulate the mechanical response of an embankment. The same method was used by (Davies *et al.*, 2014) to study the stability of a slope near Belfast. While *Shetran* captures the transient evolution of pore water pressures governed by soil water balance processes, the overall approach fails to effectively reproduce mechanical behaviour. Despite the *Flac-tp* is capable of simulating coupled behaviour, the predicted response is compromised by transferring only the surface pore water pressures, instead of the entire pore pressure profile.

In a work of (Nyambayo, 2004), it was suggested that a more realistic approach towards the soil-atmosphere modelling would be to use rainfall and evapotranspiration as input data in fully coupled analyses and to employ a root water uptake model (RWUM) to account for water loss due to transpiration. Such a model was incorporated into Imperial College Finite Element Program (ICFEP), by using the RWUM proposed by (Prasad, 1988) to account for potential soil water extraction rate corresponding to conditions of potential transpiration. The suction-dependent reduction function, suggested by (Feddes, Kowalik & Zaradny, 1978), was also implemented to account for the actual extraction rate. The potential water extraction rate function and the suction-dependent reduction function that have been incorporated into ICFEP are described in more detail and illustrated in the next chapter. Similarly to staggered approach of (Rouainia *et al.*, 2009; Davies *et al.*, 2014), the fact that pore water pressure profiles were allowed to be predicted, instead of prescribed, represents a significant improvement in modelling vegetation and climate effects on slope behaviour.

In his thesis (Nyambayo, 2004) undertook a series of fully coupled analyses, considering saturated water flow, on an embankment at Chattenden, Kent. The analyses were carried out parametrically to investigate the influence on the pore water pressure regime of various parameters, such as the maximum root depth, stiffness and the mass permeability of the clay fill. Moreover, the impact of a potential increase in permeability due to desiccation cracking was assessed. The results from the analyses validated the model, in terms of its capability to simulate the observed pattern of seasonal pore pressure changes within embankments. The most important conclusions from the analyses are reviewed in the subsequent paragraphs.

To quantify the effect of the maximum root depth r_{max}, values of 2, 2.5 and 3 m were considered. The results showed that shallower roots affect predominantly suctions closer to the ground surface, whereas deeper root systems are associated with higher suctions at deeper levels. Larger root depths are also linked to somewhat greater pore water pressure changes. The difference in the obtained pore water pressure profiles between the 3 root depths under consideration was found to be largest in the first years of the analysis and decreasing in later time steps. The analysis also showed that depth of influence, that is the maximum depth to which the pore water pressure variations propagate is independent of the r_{max}.

The additional analyses were performed to investigate the influence of the clay fill stiffness. The results demonstrated that stiffer clay fill materials yielded higher suctions at the end of summer and lower suctions at the end of winter, but in general it seemed that the overall effect of stiffness on the

failure mechanism was negligible. Similar conclusions with respect to the stiffness impact to progressive failure of clay fill embankments were drawn by (Kovacevic, Potts & Vaughan, 2001).

The influence of the permeability of clay fill material was investigated by using three values that differ from each other by an order of magnitude 10^{-7}, 10^{-8} and 10^{-9} m/s. Permeability was assumed to be isotropic but to vary in terms of mean effective stress according to a logarithmic law. Two higher permeabilities 10^{-7}, 10^{-8} m/s yielded similar pore water pressure profiles, characterized by larger seasonal variations. For the case of more impermeable clay fill, larger suctions were predicted during the summer period. Significant amount of these suctions, particularly in the root zone (at 2-3 m depth), was maintained during the following winter months. Besides, the effect of permeability increase due to desiccation cracking in the clay fill was also studied. A smeared crack permeability model was employed, which assumes that cracking commences when minimum principal stress σ_3 enters tensile domain. The logarithmic relationship between mass permeability and tensile minimum principal stress σ_3 is adopted, with the maximum ratios of cracked over intact mass permeability being equal to 10 and 100. The increase in permeability triggered by opening of cracks lead to more pronounced suction variations over the one winter/summer cycle, especially close to ground surface. Higher permeability of shallow slope portions proved to be beneficial for stability, allowing more water to infiltrate during rainfalls and therefore making water available for later evapotranspiration. Thus, the water extraction is restricted to surficial layers, thereby preventing deeper pore water pressure oscillations, which are responsible for large seasonal cyclic movements.

Chapter 3: Review of the Behaviour and ICFEP Numerical Tools for Unsaturated Soils

3.1 Introduction

The interaction between the soil and the atmosphere drives continuous movement of water in and out from the ground, affecting the distribution of subsurface water. In his book (Bear, 1972) proposed that soil profile can be divided into zones depending on the amount of water present within the pores of the soil. Schematic representation of the subsurface water distribution is illustrated in Figure 3.1.

It is common misperception that groundwater table represents 'free water surface' within the soil mass. Actually, groundwater table is the surface of zero pore water pressure (relative to atmospheric pressure). An alternative name for the zero-pore pressure line, widely found in the literature, is the phreatic surface. Below the groundwater table, soil is fully saturated and water is in a compression state. This is so-called groundwater zone or zone of saturation.

Zone above the ground water table is zone of aeration, comprised of unsaturated soils and is characterized by tensile (negative relative to atmospheric pressure) pore water stress. This unsaturated region also known as *vadose zone,* is further subdivided into three zones: capillary fringe, intermediate two-phase zone and soil-water zone (dry zone).

Capillary fringe is a quasi-saturated zone immediately above the phreatic surface, in which water is held under capillary action. Within the capillary fringe, the soil retains a high degree of saturation, usually in excess of 90% (Fredlund & Rahardjo, 1993). The height of this zone is dependent upon the pore size and distribution within the soil.

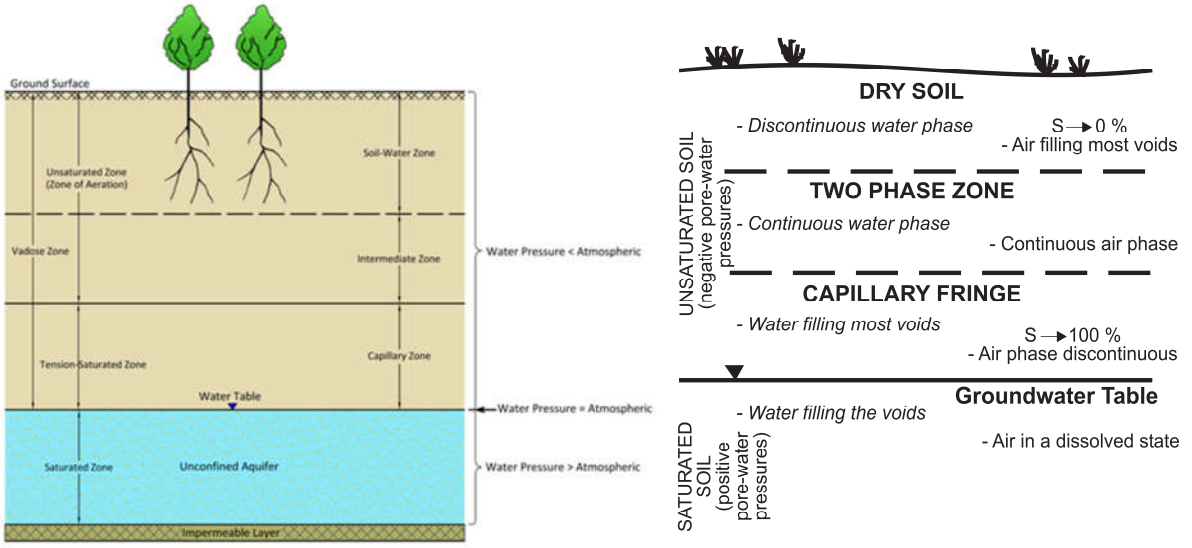

Figure 3.1 Hydrologic zones below the ground surface (on the left), after (Sanders, 1998), and after (Fredlund, 2000) (on the right)

Above this tension-saturated zone (Freeze & Cherry, 1979), lies the intermediate zone, characterized by the continuity of both fluid phases in the pore space. The corresponding water content is normally at or below the field capacity, which represents water content of the soil after all gravitational drainage has ceased. In this truly unsaturated zone, capillarity is dominant, but is not the only retention mechanism responsible for holding water. Other retention mechanisms could contribute, including

osmotic and electrostatic mechanisms. Despite moisture content being close to filed capacity, water may still flow through this zone under the influence of gravity.

Depending on the climatic region, at the top of the profile is either soil water zone (temperate region) or dry zone (arid region). This zone extends from the surface to below the root zone and is heavily influenced by ground surface conditions. Water moves down through the zone under gravitational forces and upwards due to surface evaporation and water uptake from plants and vegetation. This dynamic change of moisture has significant implications on pore water pressure profiles close to the ground surface, as illustrated in the Figure 3.2. The water content can range from fully saturated after heavy rainfall events, to almost hygroscopic after a prolonged dry period.

Position of water table relative to the ground surface and soil type controls the existence of the upper two zones. For example, in cases of shallow water tables the capillary fringe may rise up to the surface.

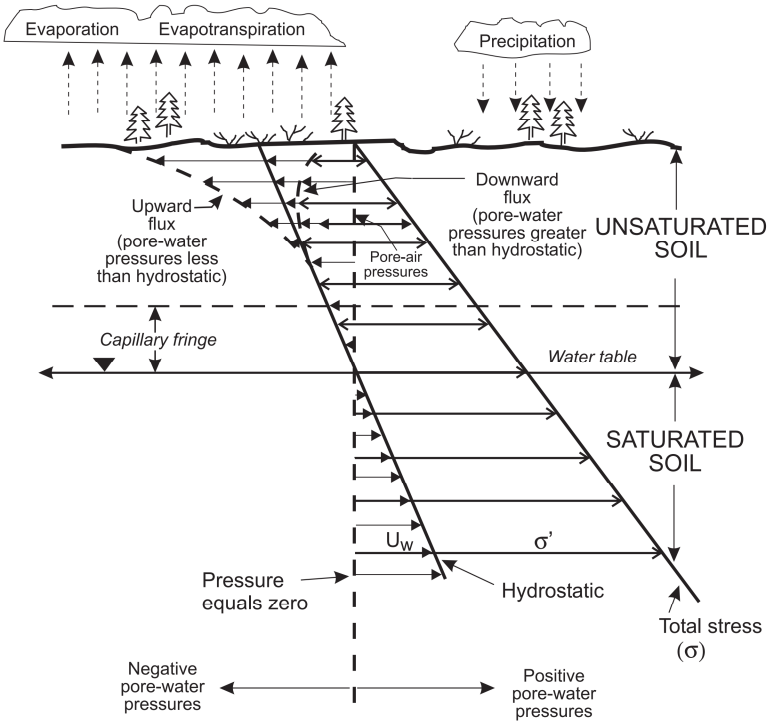

Figure 3.2 Pore water pressure distribution profile within unsaturated zone, after (Fredlund, 2000)

It is clear from the illustrated profiles that above groundwater table soils are inherently unsaturated, either truly (both fluid phases are continuous) or apparently (air phase in the form of occluded bubbles). Consequently, infrastructure earthwork slopes are mostly unsaturated, but depending on the type of earthwork and position of phreatic surface, could be idealized as saturated. That is the case with infrastructure cuttings, which are for the sake of simplification commonly modelled as saturated. This assumption is reasonable and justified by the fact that saturation states of cut materials are close to fully saturated conditions. On the contrary, infrastructure embankments would likely be partially saturated throughout the working life. The main reason lies in the fact that compacted fill materials, from which embankments are constructed, are by their nature truly unsaturated. This means that at the time of compaction embankments are essentially unsaturated, and usually remain such, unless adverse combination of environmental conditions alters the embankment hydraulic regime. Therefore, to study the effects of soil-atmosphere interaction on performance of infrastructure embankments, an understanding of how water flows within this unsaturated zone and also how the change in degree of saturation affects soil behaviour, is crucial.

3.2 Fundamentals of Unsaturated Soil Behaviour

Partially saturated soils distinct principally from fully saturated in that the void space within soil skeleton is concurrently occupied by two fluid phases, a liquid and a gaseous phase. The liquid phase contains water and dissolved air. On the other hand, in addition to dry air, the gas phase also includes water vapor. The schematic representation of the unsaturated soil is illustrated in Figure 3.3.

The common simplification introduced in modelling the behaviour of partially saturated soils consists of treating the water and air phases as immiscible, homogeneous fluids, characterized by separate pore pressures, namely pore water pressure p_w and pore air pressure p_a.

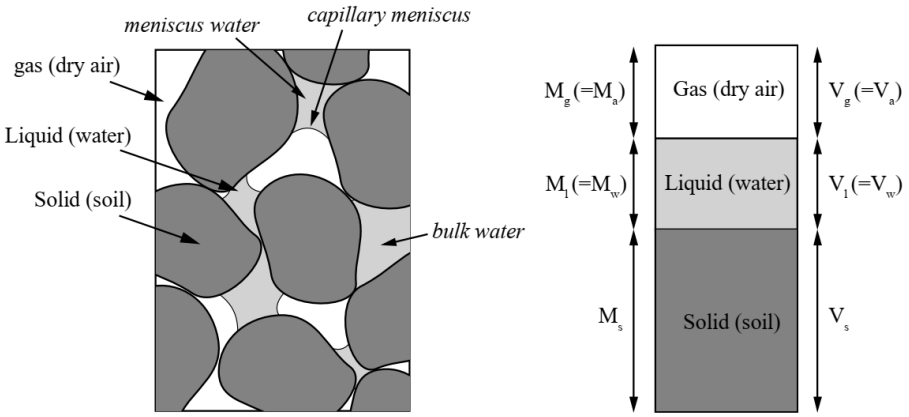

Figure 3.3 Representation of a partially saturated soil structure and three phase diagram

3.2.1 Capillary Effects

The interface between water and air is the surface of paramount importance, that directly governs the behaviour of unsaturated geomaterials. The free liquid surface in contact with air behaves as tensioned membrane. This phenomenon is known as the surface tension and stems from the imbalance of intermolecular Van der Waals force. Within the water medium the attractions between water molecules are effectively in equilibrium in all directions, which implies that the resultant force acting on the individual water molecule is zero. However, on the free water surface there are no neighbouring molecules above, and a resultant downward force is generated. In order for the water molecule to remain at the surface an additional energy is required. This energy is actually the surface tension. Although, the thickness of this water membrane is measured in nanometre units, its extreme tensile strength of around 20 MPa, allows for example some insects to walk on water.

The surface tension represents the first prerequisite for the establishment of capillary mechanisms. Another phenomenon that in combination with surface tension contributes to formation of capillary mechanism is the adhesive force between the water molecules and minerals of soil particles. The most common building mineral present in soil particles is silica (SiO_2). When the tensioned membrane-free water surface is in contact with solid surface made of silica (like glass for instance), it tend to curves due to the attractive forces between water and silica molecules. The curved water-air interface is known as meniscus. This is depicted in Figure 3.4, together with the water molecule conditions necessary to form the surface tension.

The capillary mechanism characterised by meniscus concave on the air side, allows the generation of matric suction. The matric suction represents the tensile pore water stress, that is negative relative to air (atmospheric) pressure.

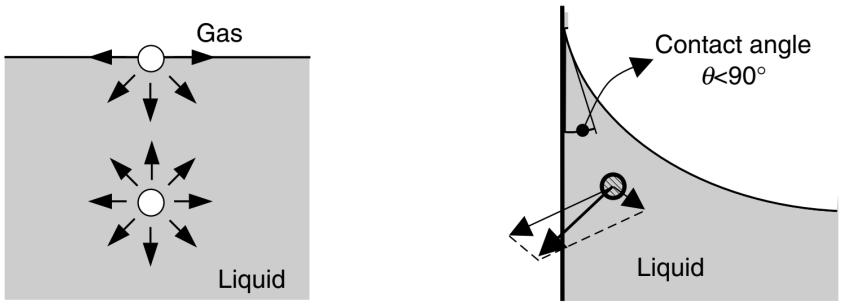

Figure 3.4 Surface tension phenomenon and formation of meniscus, after (Laloui, 2013)

To better understand the role that capillary actions have on the behaviour of partially saturated soils, the negative water stresses are studied further in a simple case of capillary tube. The Figure 3.5, illustrates the capillary tube of diameter *d*.

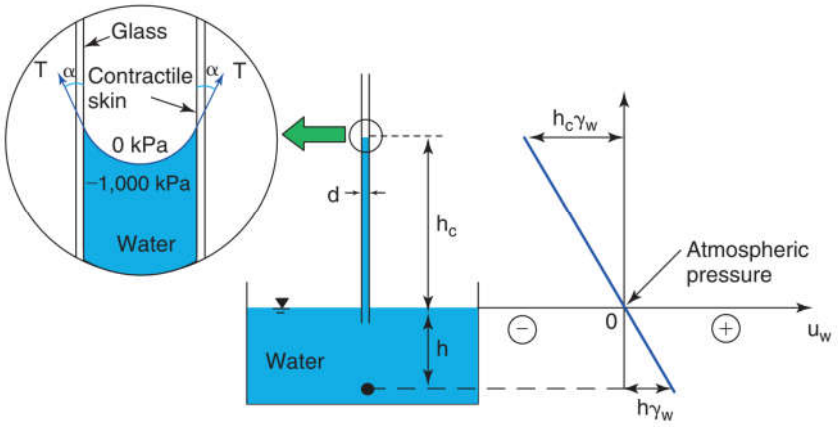

Figure 3.5 Capillary tube – negative water pressure generated by meniscus, after (Briaud, 2013)

The water stress behind the meniscus can be obtained by considering the vertical force equilibrium of the air–water interface. In the cases when contact angle is lower than 90°, the fluids pressure difference becomes negative, implying that the water stress is lower compared to air pressure.

$$u_w - u_a = -\frac{4T\cos\alpha}{d} = -\frac{2T}{R}$$

where u_w is water stress, u_a is atmospheric pressure, T is surface tension, α is the contact angle and R is interface curvature radius. The magnitude of surface tension is T = 73 mN/m, which is essentailly very small force, but which effects increase dramatically when dealing with small scales. For example if the pore size of the granular material is assumed to be of the order of one tenth of the corresponding average particle size, and for simplicity the contact angle α is assumed to be zero, the following relative gauge and absolute pressures are obtained for common soil types, Table 3.1.

Table 3.1 Gauge and absolute water pressures for basic soil types

	Sand	*Silt*	*Clay*
dgrain (mm)	2	0.075	0.002
dpore (mm)	0.2	0.0075	0.0002
uw-ua (kPa)	-1.4	-38	-1440
uw (kPa)	98.6	62	-1340

As can be seen from the Table 3.1, for very small pore sizes, for example intrinsic to clay soils, absolute water stress may be even negative, tensile, implying that water is being stretched in partially saturated geomaterials.

For real unsaturated particulate materials characterized by wide range of pore sizes, the water is localized at the interparticle contacts within the formed menisci for larger void spaces (meniscus water), as illustrated in Figure 3.6. At the same time smaller pores may be saturated (bulk water), Figure 3.7. Therefore, two types of interparticle contacts exist, namely meniscus contacts and saturated contacts (Laloui, 2013). The behaviour of saturated contacts within the unsaturated soils is identical to behaviour of fully saturated soils, in a sense that contact forces are influenced directly by external total load and by the pore-water pressure (Figure 3.7). On the other hand, in the case of meniscus contacts, the surface tension act as a glue, pulling the two particles towards each other, thereby generating an increase in normal component of interparticle force, without change in tangential one. The insensitivity of tangential interparticle force to changes in negative water stress in the case of meniscus contact is the principal thing that differs the two types of contacts. The additional normal componential interparticle force provides the stabilising effect and makes the dry unsaturated materials significantly stiffer and harder than corresponding saturated ones.

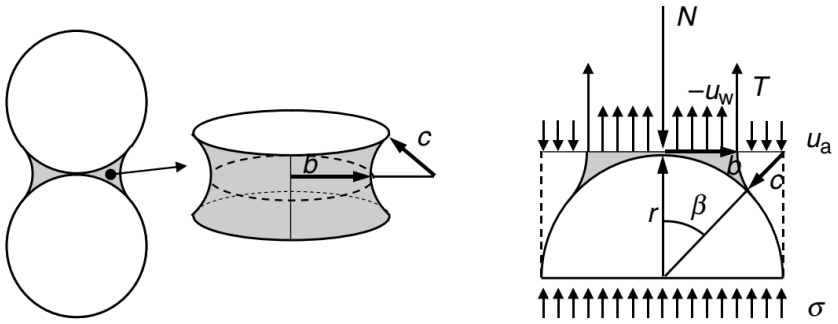

Figure 3.6 Equilibrium at the meniscus contact, after (Laloui, 2013)

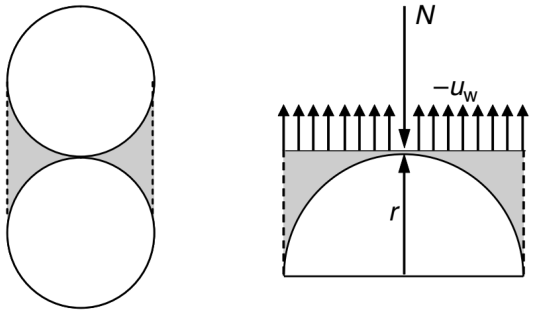

Figure 3.7 Equilibrium at the saturated contact, after (Laloui, 2013)

Writing the equilibrium of vertical forces that act upon the horizontal plane passing through the meniscus contact formed between two rigid spherical particles, as shown in Figure 3.6, gives the following relationship:

$$\frac{N}{A} = (\sigma - u_a) + \left[\frac{1}{A}\left(A_w + P_w \frac{cb}{b-c}\right)\right](u_a - u_w)$$

where *N/A* is the interparticle normal stress; σ is the total stress; A_w and P_w are the wetted area and wetted perimeter, and A is the total area.

If the shape of 3-dimensional meniscus surface is approximated to Plateau nodoid, with circular meridian curve, the radii *b* and *c* in the upper expression reduce to:

$$c = r\left(\frac{1}{\cos\beta} - 1\right) \qquad b = r\left(1 + \tan\beta - \frac{1}{\cos\beta}\right)$$

where, *r* is the particle radius and β is the angle defining the position of the meniscus junction.

If the second term of the equilibrium equation of vertical forces, which represents the normal component of interparticle force generated by the presence of meniscus, is plotted against suction (u_a - u_w) for different values of the particle radius *r*, the following relationships are obtained (Figure 3.8).

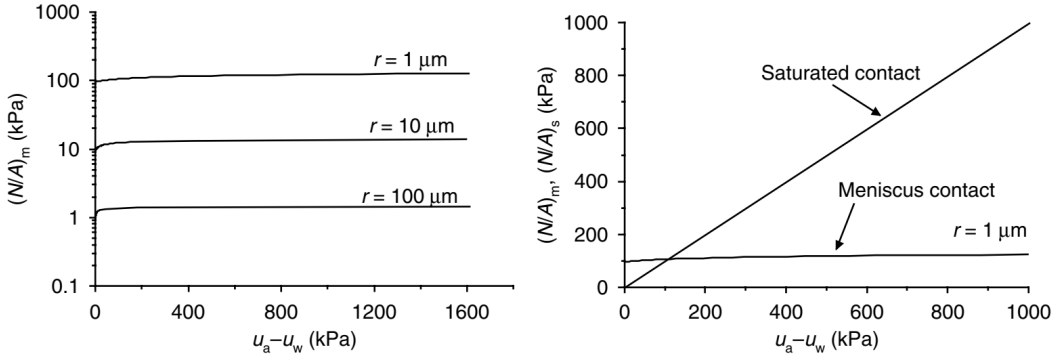

Figure 3.8 Relationship between interparticle stresses and suction generated by meniscus contact (on the left), and comparison with saturated contact (on the right), after (Laloui, 2013)

It can be seen that in the case of meniscus contact the normal interparticle forces are insensitive to the magnitude of water stress within meniscus, and depend exclusively on the particle size. On the other hand, in the case of saturated contacts, the normal intergranular force is linearly increasing with suction. This relation is obtained from the equilibrium condition of vertical forces acting on the saturated contact (Figure 3.7), which gives:

$$\frac{N}{A} = \sigma - u_w = \sigma + s$$

The derived relationship confirms that the saturated contact of sub-saturated regions of unsaturated soils behaves in the same manner as the fully satureated ones, as the normal interpartical stress reduces to effective stress.

The two relationships suggest that the magnitude of stabilising effects of the meniscus contacts depend only on the soil type (grain size distribution) and disappears entirely and instanteniously upon the wetting (loss of meniscus). In contrary, the stabilising effects of the saturated contacts vary gradually with the changes in soil suction (water content).

These micro hydro-mechanical phenomena in combination with retention behaviour, discussed in the next section, helps to explain numerous specific macroscale responses inherent to unsaturated geomaterials (like volumetric collapse upon wetting, nonlinear increase in shear strength).

3.2.2 Soil Retention Behaviour

The two main mechanisms that are responsible for the desaturation of the soil medium are evaporation from the bare soil surface and transpiration related to root water uptake. If it is assumed, for illustration purposes (Figure 3.9), that the soil medium is initially fully saturated, the desaturation process starts to remove the water from the soil, and as a response the capillary menisci are formed at the surface between ground water and the atmosphere. At that moment the pore water stress shifts from compressive to tensile region and the matric suctions starts to gradually increase (state *a1* on the Figure 3.9). Further reduction of the pore water pressure (suction increase) brings about the formation of air cavities, in particular in larger voids, which provide less resistance to water extraction, equivalently to larger diameter capillary tubes. The occurrence of air within the soil mass reduces the soil degree of saturation, and the state *a2* in Figure 3.9 is reached. This state is known as quasi-saturated, as the air phase is still discontinuous and present within the soil only in the form of occluded air bubbles and air cavities. Degree of saturation characterising the quasi-saturated conditions is in the range $S_r > 85$ %. The further desaturation will steadily increase the surface menisci's contact angle, up until the critical angle is reached. At that point the menisci recede into the soil, air enters the pore space and true unsaturated conditions are attained (state *a3*). They are characterised by the continuity in both fluid phases. A value of suction conventionally assumed to represent the commencement of the partially saturated region is referred as air-entry suction s_E, and is located at the intersection of the horizontal line corresponding to the $S_r = 100$ % and the straight-line tangent to the curve at the inflection point. The air-entry suction value varies in huge range from couple to hundreds of kPa depending on the soil type. Upon the further drying soil will pass through the states *b* and *c* (in Figure 3.9) until ultimately reach the so-called residual state, in which water phase is no longer continuous and remains isolated at the particles' contacts. The established relationship between the degree of saturation (or volumetric water content) and matric suction is referred as the soil water retention curve (SWRC).

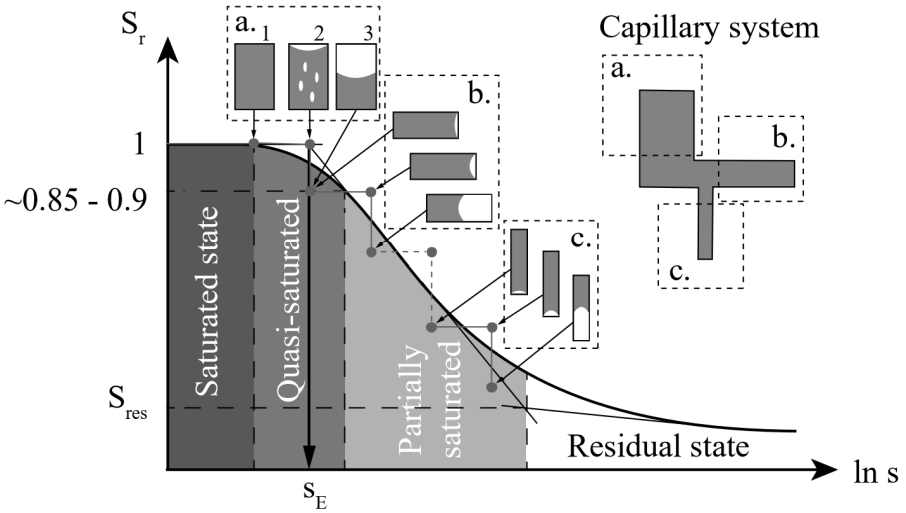

Figure 3.9 Soil water retention curve (SWRC) vs idealised capillary tubes system

For convenience of reference and ease of understanding the analogy is formed between the retention behaviour of the real geomaterial, defined by a continuous pore size distribution and a capillary tubes system with a finite number of different tube diameters. It can be seen that the SWRC for the capillary tube system has a stepwise shape, where as in the case of real soil with wide and continuous range of pore sizes is smooth.

The retention behaviour is generally not unique, but depends on several factors. The most important ones include the course of the process affecting the soil water conditions (drying/wetting) and the void ratio. Alternating drying and wetting paths produce hysteretic soil retention behaviour (Croney, 1952). The Figure 3.10 (left), illustrates the fundamental components of hysteretic SWR curve. The main drying and wetting curves represent the limiting boundaries, that encompass the possible retention states. Along the two primary curves the retention behaviour is irreversible (Wheeler, Sharma & Buisson, 2003). However, the seasonal wetting drying cycles induced by climatic and vegetation effects are such that the retention behaviour does not trace the main paths. Rather, the secondary-scanning paths are followed, which lie within the hysteretic domain, up until the main curves are reached. It is commonly assumed that the retention behaviour along scanning paths is reversible. The principal physical cause behind the hysteretic SWR behaviour is the so-called ink bottle effect (Laloui, 2013). It actually refers to geometric nonuniformity of the pores, which could be idealised by the capillary tube of changing diameter along its length, Figure 3.11. The drying process could be imagined as the lowering of the water level in the tube, which occurs without any obvious obstacles. However, if wetting is assumed as the rise of water, once the tube expansion is reached the capillary forces are unable to move up the water any further. Beside the ink bottle effect, other factors contribute to hysteretic response, like the pore fluid contact angle, entrapped air, and swelling, shrinking, or aging (Briaud, 2013).

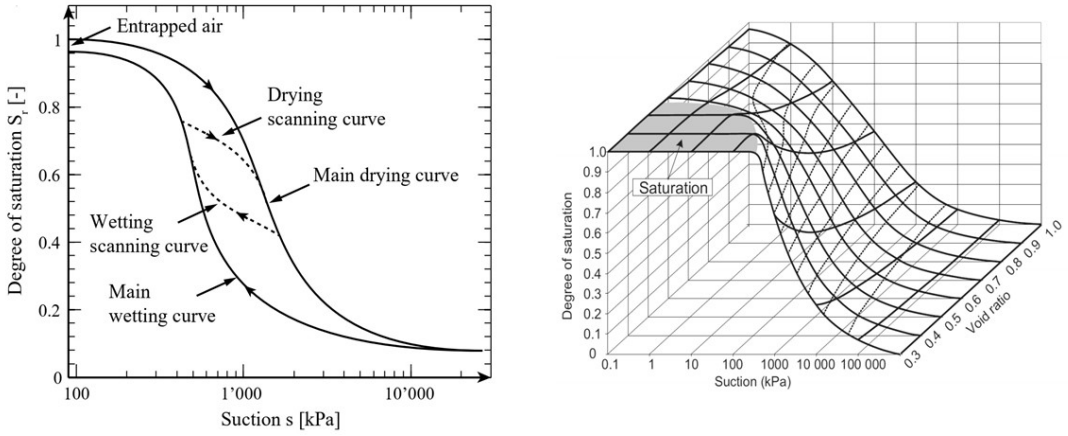

Figure 3.10 Hysteretic soil water retention behaviour (on the left side), and SWR surface in the s-v-S_r space

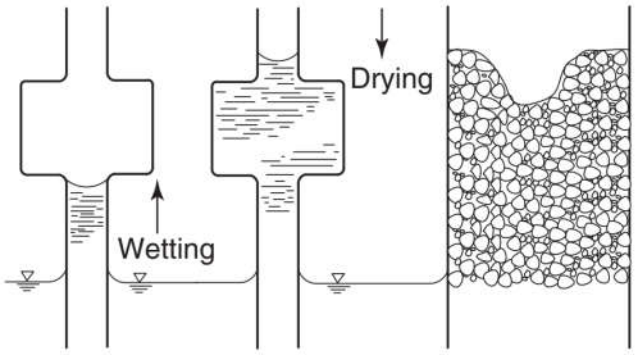

Figure 3.11 Ink bottle effect - geometric nonuniformity of the pores, after (Briaud, 2013)

Soil water retention behaviour, besides being hysteretic is also void ratio dependent, as is schematically illustrated in Figure 3.10 (on the right side). The changes in stresses, either net total stresses or suction, induce deformations of soil skeleton, with reflect to changes in volume of pores.

Bearing in mind that the degree of saturation is a function of volume of water and volume of voids $S_r = {}^{V_w}/_{V_v}$, it is clear the changes in void volume governed by stress changes, affect the magnitude of the degree of saturation, and consequently the SWR state. The changes in net total stress (and corresponding void ratio changes) shift the SWRC along the void ratio axis.

3.2.3 Volumetric Behaviour

The volumetric deformations of unsaturated soils are induced either by changes in net total stresses (external loads), or changes in matric suction. Two distinct types of volumetric behaviour of unsaturated soils have been widely identified (Fredlund & Morgenstern, 1976; Fredlund & Rahardjo, 1993). The first one refers to the dependence of the stiffness of soil structure on the magnitude of matric suction. It has been shown that the soils exhibit stiffer response at higher suction level, when subjected to isotropic net total stress changes (Wheeler & Sivakumar, 1995).

The second type of volumetric behaviour, intrinsic solely to truly unsaturated soils refers to the collapsible volumetric deformations. Depending on the confining stress level the soil material is exposed and the overconsolidation ratio, two different volumetric responses may be observed upon wetting (Figure 3.12). At low confining stresses the soil medium will swell, whereas at high stresses following initial swelling, very large volumetric strains, termed as collapse would occur (Laloui, 2013).

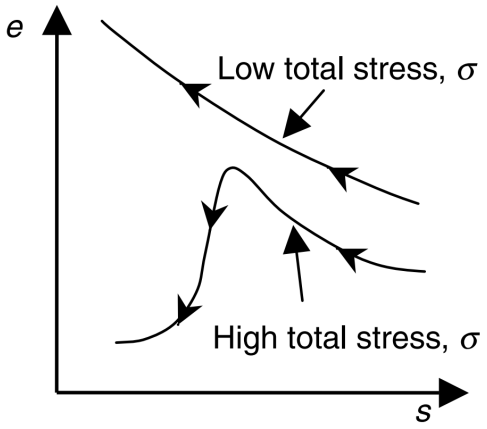

Figure 3.12 Volumetric response of unsaturated soil upon wetting

The observed odd behaviour could be explained by previously introduced micro hydro-mechanical phenomena, in particular meniscus and saturated interparticle contacts. The unsaturated soil medium could be imagined as being comprised of saturated sub-regions whose behaviour is governed by saturated contacts, and truly unsaturated regions in which water exists only at the interparticle contacts within the menisci. The wetting process reflects to the decrease in matric suction (see SWRC), which is equivalent to unloading effect. Therefore, the effective stresses in saturated subregions gradually reduce, thereby causing that zones to swell. At the same time the decrease in matric suction within menisci does not affect the normal component of the interparticle force (see Figure 3.8), so the overall volume increase is observed. However, wetting will gradually flood the menisci, which will progressively disappear. The loss of menisci causes instantaneous drop of additional normal interparticle force, which leads to the reduction of interparticle friction strength. In case soil medium is subjected to high confining stresses, the sudden loss of stabilising additional normal interparticle forces would result in slippage at the particle scale, causing an overall volumetric collapse.

3.3 Hydro-Mechanical Coupling for Unsaturated Soils

In a fully coupled flow-deformation analysis, the application of a stress will generate changes in volumetric water content. For the case of fully saturated soil, the void spaces are entirely filled with pore water. If it is assumed that both soil particles and water are incompressible, the application of stress will produce a change in the volume of soil water of equal magnitude to the change in volume of voids. In the unsaturated case, the pore fluid is composed of two phases, water and air. The air, whether in the form of occluded bubbles within the water phase, or as a continuous medium, is very compressible and can also flow. Therefore, the volumetric deformation of the pore voids will no longer be equal to the volumetric water content change. Rather, a total change in the volume of soil would be equal to a sum of volume changes of water and air phase.

In addition to stress changes, there are other causes of water content changes that are exclusive to unsaturated soils. As previously explained volumetric water content is related to the matric suction through soil water retention curve (SWRC). Therefore, a change in matric suction produces a direct change in the volumetric water content of the soil (and vice versa). Further, a change in matric suction is analogous to a change in the applied stress, in that it will induce deformations of the soil structure, hence leading to variation in the volume of voids. In turn, this will produce a further change in the volumetric water content of the soil, as already explained.

To account for these differences, a number of additions and adjustments need to be introduced into existing finite element constitutive relationships for saturated soils. The foundations of consolidation theory (coupled hydro-mechanical behaviour) has been laid by (Biot, 1941). By introducing the assumption of incompressible pore fluid, his primary intentions were to derive governing equations for saturated soils. But at the same time, he also allowed water to contain air bubbles, which are essentially compressible (although not explicitly stated in his work), which was contradictory to the first assumption. Thereby, the derived equations are not restricted exclusively to truly saturated conditions, but may be applied for tension-saturated conditions or so-called quasi-saturated states. Other assumptions made during derivation process include: isotropy and linear-elasticity of soil material, infinitesimal ("small") strains and applicability of Darcy's law.

Biot constitutive relationships represent an extension of Hooke's law to multi-phase porous materials. In developing his theory, Biot found it necessary to define three new parameters to describe the soil behaviour in the general case, and in doing so, he actually identified the parameters governing unsaturated soil behaviour. The proposed relationship for the soil structure given in the work of (Biot, 1941) is as follows:

$$\varepsilon_x = \frac{\sigma_x}{E} - \frac{\mu}{E}\left(\sigma_y + \sigma_z\right) + \frac{\sigma}{3H} \qquad \gamma_{xy} = \frac{\tau_{xy}}{G}$$

and similar for ε_y and ε_z, and γ_{yz} and γ_{zx}.

In the given equation, "an additional physical constant" H (as termed by Biot), relates changes in pore water pressure to direct strains in the soil and has similar role as Young's modulus. In contrast, pore water suction has no effect on shear strains, which follows from the fact that shear resistance of fluids is negligible.

In addition, constitutive relation for the water phase is also provided, and takes the following form:

$$\theta = \frac{1}{3H_1}(\sigma_x + \sigma_y + \sigma_z) + \frac{\sigma}{R}$$

It relates the changes in volumetric water content with changes in the applied total stress and pore water pressure. Two additional physical constants H_1 and R are introduced. The "modulus" R links changes in volumetric water content to changes in water stress and therefore is basically directly related to the gradient of the SWRC. The parameter H_1 relates stress to a volumetric water content change.

In his work (Biot, 1941) states that two moduli (physical constants) H an H_1 are equal, under specific hydrostatic (isotropic) stress conditions, and can be defined as single variable H. Based on this assumption, after some rearrangements Biot developed another form of volumetric water content relationship:

$$\theta = \alpha\varepsilon + \frac{\sigma}{Q}$$

Where

$$\alpha = \frac{2(1+\upsilon)}{3(1-2\upsilon)} \cdot \frac{G}{H}$$

$$Q = \frac{1}{R} - \frac{\alpha}{H}$$

with ε being volumetric strain.

Extension of Biot's coupled framework to truly unsaturated soils (both fluid phases are continuous) has been undertaken by (Dakshanamurthy, Fredlund & Rahardjo, 1984; Fredlund & Rahardjo, 1993; Wong, Fredlund & Krahn, 1998). These improvements of Biot's expressions to account for unsaturated stats, are essentially reduced to substitution of water stress, σ, with the matric suction, $(u_a\text{-}u_w)$, and some notation modifications, most notably $3H$ in the denominator of water phase constitutive relationship is redefined as just H.

In the work of (Dakshanamurthy, Fredlund & Rahardjo, 1984) constitutive relation for soil structure (solid phase), in general 3-dimensional 3-phase case is given by the following expression:

$$\varepsilon_x = \frac{(\sigma_x - u_a)}{E} - \frac{\nu}{E}(\sigma_y + \sigma_z - 2u_a) + \left(\frac{u_a - u_w}{H_1}\right)$$

and similar for the y and z axis. Same equation is provided by (Fredlund & Rahardjo, 1993), with an exception of denoting H_1 parameter with H. By comparing with Biot's expression, it can be seen that they are practically the same, but with the inclusion of pore air pressure term (and already explained replacement of $3H$ with H).

After rearranging the equations so that change in stress is expressed in terms of strains, the matrix form of constitutive relations for soil skeleton, takes the following from:

$$\{\Delta\sigma\} = [D]\Delta\varepsilon - [D]\left(\frac{\Delta(u_a - u_w)}{H}\right) + \{\Delta u_a\}$$

Simplification that is commonly made, involves omitting continuity equation of the air phase, independently of the saturation state, by assuming that gas pressure is constant and equal to atmospheric pressure. This means that the air pressure is equal to zero-gauge pressure (atmospheric pressure) and is free to flow through the void space. By introducing:

$$\{m_H\}^T = (1/H\ 1/H\ 1/H\ 0\ 0\ 0)$$

The final form of constitutive equation of the soil structure for unsaturated case is obtained:

$$\{\Delta\sigma\} = [D]\Delta\varepsilon + [D]\{m_H\}(\Delta u_w)$$

Comparison of derived equation with the classical one for the saturated state (Potts & Zdravković, 1999), given below, shows that H modulus could be expressed in terms of linear elastic stiffness parameters, Young's modulus E and Poisson's ration v, as $H = \frac{E}{1-2v}$

$$\{\Delta\sigma\} = [D]\Delta\varepsilon + \{m\}(\Delta u_w)$$

The finite element formulation of the of the ICFEP constitutive relationship for soil structure, for the general case of saturated or unsaturated soils, is provided in the thesis by (Smith, 2003), and has the following form:

$$[K_G]\{\Delta d\}_{nG} + [L_d]\{\Delta p_f\}_{nG} = \{\Delta R_G\}$$

where

$$[L_d] = \sum_{i=1}^{N} \left(\int_{vol} [D]\,\{m_H\}[B]^T [N_p] dVol \right)_i$$

Regarding the water phase relations, the one proposed by (Dakshanamurthy, Fredlund & Rahardjo, 1984) was proved to be in error and is hance incorrect. This was brought about by (Wong, Fredlund & Krahn, 1998), who have shown that the change in the volumetric water content of the soil, θ_w, may be expressed as follows:

$$\theta_w = \beta_\varepsilon + \omega(u_a - u_w)$$

Where:

$$\beta = \frac{E}{H(1-2v)}$$

$$\omega = \left(\frac{1}{R}\right) - \left(\frac{3\beta}{H}\right)$$

with ε being the volumetric strain, H as before, being the elastic modulus of the soil structure with respect to $(u_a\text{-}u_w)$, and R being a modulus relating a change in volumetric water content to change in matric suction $(u_a\text{-}u_w)$. The given expression is derived in accordance with the Biot's work, and resembles the equation given previously.

It is important to note, that in all works except (Fredlund & Rahardjo, 1993) authors implicitly assumed that two moduli H and H_1 remain equal. In the mentioned work, a difference is made between the two, which is essentially accurate from the physical point of view.

$$\frac{dV_w}{V_o} = \frac{3}{E_w} d(\sigma_{mean} - u_a) + \frac{d(u_a - u_w)}{H_w}$$

The two moduli, one governing the effect of matric suction on the direct strains, H, and the other governing the effect of net stress on the volumetric water content, E_w, represent fundamentally

different facets of the soil/water behaviour and there is no justified reason for them to be identical, in particular for truly unsaturated soils containing continuous air.

In his thesis (Smith, 2003), for the purpose of formulating governing finite element consolidation equations for unsaturated soils, author employed the expression for water phase by (Wong, Fredlund & Krahn, 1998), but with the adjustment in the β function to include E_w modulus instead of erroneous one, H. Also, the β symbol was replaced by Ω, since the former one was already reserved in ICFEP (Imperial College Finite Element Program). Therefore, the water phase constitutive equation thus becomes:

$$\theta_w = \Omega\varepsilon + (u_a - u_w)(\frac{1}{R} - \frac{3\Omega}{H})$$

$$\Omega = \frac{E}{E_w}\frac{1}{(1-2v)}$$

ICFEP constitutive relation for the water phase formulated in finite element terms, developed, as previously stated, by (Smith, 2003) for the general case of unsaturated soils is:

$$\Omega[L_G]^T\{\Delta d\}_{nG} - (\beta\Delta t[\Phi_G] + \omega[M_N])\{\Delta p_f\}_{nG} = ([n_G] + \{Q\} + [\Phi_G]\{\Delta p_f\}_{nG})\Delta t$$

where

$$\omega = (\frac{1}{R} - \frac{3\Omega}{H})$$

The two equations, one for the soil structure and the other for the water phase constitute the basis for coupled consolidation analysis. By coupling them, the governing finite element equation for unsaturated soils, as explained and implemented in ICFEP by (Smith, 2003), becomes:

$$\begin{bmatrix} [K_G] & [L_d] \\ \Omega[L_G]^T & -\beta\Delta t[\Phi_G] - \omega[M_N] \end{bmatrix}\begin{Bmatrix} \{\Delta d\}_{nG} \\ \{\Delta p_f\}_{nG} \end{Bmatrix} = \begin{Bmatrix} \{\Delta R_G\} \\ ([n_G] + Q + [\Phi_G]\{p_f\}_{nG})\Delta t \end{Bmatrix}$$

In the unsaturated case, volumetric deformations trigger the flow of both fluid phases, water and air. The Ω parameter in previous equation controls the amount of water that flows in response to a change in the volume of voids. Depending on the state of saturation, quantity of flowing water lies between the total volumetric strain (fully saturated state) and zero (residual saturation state), in which case all of the fluid flow is restricted to air phase. This means that for the saturated state, the Ω should be 1.0, reflecting the equality $\Delta\theta_w = \Delta\varepsilon_{vol}$ is intrinsic to saturated conditions. Assuming Ω = 1.0, also meets the consistency between saturated term ($[L_G]^T\{\Delta d\}_{nG}$ (Potts & Zdravković, 1999)) and unsaturated term ($\Omega[L_G]^T\{\Delta d\}_{nG}$ (Smith, 2003)). Considering that there was a lack of experimental evidence regarding the variation of Ω parameter with degree of saturation, (Smith, 2003) adopted linear distribution, expressed in terms of suction. In his work, he argues that in the case of discontinuous air phase (in the form of occluded bubbles), air bubbles will flow together with water. On the contrary, when the air phase becomes continuous, water flow is becoming rapidly less responsive to compression (volume reduction by loading). This is because the air phase flows much more readily and easily compared to water phase. Once the water phase reaches residual state (becomes discontinuous), no flow occurs afterwards. So, in ICFEP, the value of Ω is varying linearly from 1.0 for saturated conditions (for air-entry value of suction) to 0.0 for some higher value of suction, which is an input parameter, included in the soil-water retention curve (SWRC) models.

It is worth to mention that E_w is not an input parameter, but is instead indirectly accounted for through an alternative parameter Ω. From the equation for Ω, given earlier, it can be concluded that E_w is

progressively increasing as Ω is becoming smaller. When Ω attains zero value, depicting the absence of water flow, E_w has become infinitely large.

3.4 Constitutive Models for Mechanical Unsaturated Soil Behaviour

Two basic groups of unsaturated constitutive models are currently available in ICFEP. The first model that is introduced in the following section is a simple extension of classical elasto-plastic Mohr-Coulomb model. The model introduces only one additional parameter compared to the saturated version and therefore fails at reproducing a number of specific aspects of unsaturated soil behaviour.

The second class of models available in ICFEP are the so-called BBM (Barcelona Basic Model) type models. Numerous modifications and refinements have been introduced into the original framework developed by (Alonso, Gens & Josa, 1990). Despite offering great flexibility in representing various aspects of unsaturated soil behaviour, the 20+ input parameters, which require sophisticated testing equipment, significantly limits their practical application.

3.4.1 Partially Saturated 3D Mohr-Coulomb Model – ICFEP Model 82

This simple unsaturated material model is derived from an existing saturated Mohr-Coulomb type soil model. The model is a part of unsaturated model class that is based on two stress-state variables. The basic data required for the operation of the saturated part of this model are the cohesion *c'*, the angle of shearing resistance *φ'*, and the angle of dilation *v*. The angle of dilation forms part of the flow rule that governs plastic volumetric straining.

The switch between saturated and unsaturated behaviour is achieved through the introduction of suction air-entry value (AEV). In the case pore water pressures are more compressive than the AEV, the model reduces to classical saturated Mohr-Coulomb type model.

On the other hand, if the pore pressures are more tensile than AEV, the model acts as an unsaturated soil model. At that point, ICFEP switches from using effective stresses to operating in net total stresses (which are actually total stresses considering that air pressure is zero) and matric suction, which is consistent with the work of (Fredlund, 1978). The unsaturated part of the model is defined in terms of parameter *H*, which appears in cross-coupling matrix [L_d] (see section 3.3). The soil parameter *H* is a modulus relating the change of volumetric strain in the soil structure to a change in suction (Wong, Fredlund & Krahn, 1998). Within the ICFEP, relatively simple piecewise tri-linear function is adopted for the *H* modulus, as depicted in Figure 3.13.

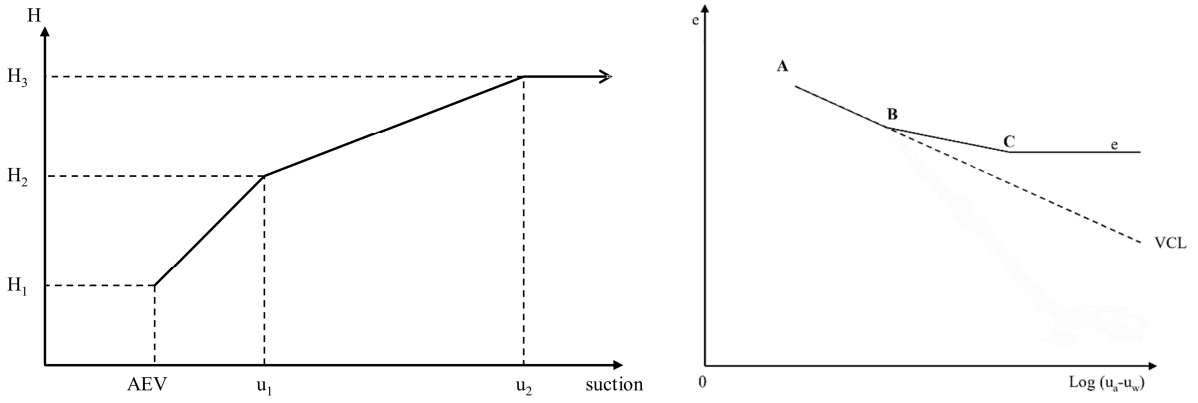

Figure 3.13 Variation of H parameter within ICFEP Model 82 (on the left), Relationship between void ratio and matric suction after (Toll, 1995) (on the right)

The model requires, three values of *H* modulus, each with an accompanying value of suction, to be specified. At suctions beyond the maximum specified, *H* becomes constant, while at suctions with a magnitude less than the AEV, no value for H is given, since in this range, the soil is assumed to behave as saturated soil, as explained earlier.

The piecewise linear increase in *H* parameter approximately reflects the relationship between void ratio and matric suction established by (Toll, 1995) and illustrated in Figure 3.13. Point A in the figure, represents some initial, fully saturated condition. Point B indicates the commencement of desaturation, which is effectively the AEV. Between these two points, the soil is quasi-saturated (actually, tension-saturated), which means that air phase is still discontinuous and not in direct contact with the surrounding air, and behaves effectively as saturated geomaterial. At suctions beyond point B, water and air will both be continuous in the pore space, and in turn soil structure sensitivity to changes in matric suction will gradually decay. This means that the overall change in *e* tends to reduce as matric suction increase. This trend continues until the shrinkage limit corresponding to point C, after which no further change in volume can occur.

The conceptual model presented by (Toll, 1995) provides some theoretical basis for the distribution of H adopted in this simple unsaturated soil model. Additionally, the division in three distinct zones matches with the three different states of saturation inherent to unsaturated soils. Thus, the three values of suction required by the model, AEV, u1 and u2, are readily identified for what they represent, even if assessing a numerical value for them is difficult.

The procedure for obtaining the *H* modulus parameter values from the slope of a void ratio *e* versus matric suction $(u_a - u_w)$ curve is suggested by (Wong, Fredlund & Krahn, 1998). The gradient of this curve is expressed in the following form:

$$\frac{de}{d(u_a - u_w)} = \frac{3}{(1-n)\cdot H}$$

where:
n porosity
e void ratio
u_a - u_w matric suction

Thus, a curve for the *H* modulus can be obtained from a measured void ratio versus matric suction curve. Also, it can be seen from Toll's model and Wong's expression that *H* becomes larger as suction increases, which is as well represented by this simple unsaturated ICFEP model. The use of a constant *H* value beyond the suction value u_2 is not in agreement with the theoretical and experimental evidence, but represents a convenient assumption for dealing with a suction range which is unlikely to be entered for most practical problems.

It should be noted that the effect of matric suction on the increase in shear strength explained by (Fredlund, Morgenstern & Widger, 1978) is not accounted for by the present model. Thus, effectively, this model assumes φ_b (and hence the $(u_a-u_w)\tan\varphi_b$ term in equation (Fredlund, Morgenstern & Widger, 1978)) equals zero in all circumstances.

It must be emphasized that presented model cannot reproduce many of the important aspects of mechanical behaviour of unsaturated soils. Rather, due to its simplicity it was deemed it would allow easier understanding of the impact of soil-vegetation-atmosphere interaction on the hydrological processes taking place within unsaturated infrastructure embankments.

3.4.2 Unsaturated Barcelona Basic Type Model – ICFEP Model 81

Several modifications of the Barcelona Basic Model (BBM) developed by (Alonso, Gens & Josa, 1990) have been implemented into ICFEP numerical code. Most notable are the ones introduced by (Georgiadis, 2003; Georgiadis, Potts & Zdravkovic, 2005; Tsiampousi, Zdravković & Potts, 2013). The BBM covers most important features of unsaturated soil behaviour, including recoverable shrinkage/swelling deformations at low confining stresses, structural collapse at relatively high confining pressure, and expansion of yield surface (increase in preconsolidation pressure) with increase in matric suction. BBM reduces to Modified Cam Clay model when suction falls to zero.

During a course of this research only the Georgiadis version without Hvorslev surface, in the remainder of this section referred as Model 81, has been used. The model is formulated in terms of two stress variables, the equivalent stress σ and the equivalent suction s_{eq}. The concept of two sets of independent stress variables for description of stress state of unsaturated soils was established by (Fredlund & Morgenstern, 1977). Figure 3.14 illustrates the difference in stress state variables for saturated and unsaturated soil mechanics. It shows that when the pore water pressure is negative (tension), the effects of total stress and water stress need to be separated. The stress state variables suggested by the authors are net total stress, $(\sigma - u_a)$ and matric suction, $(u_a - u_w)$, where σ is the total stress, u_a is the pore-air pressure and u_w is the pore-water pressure. In the paper by (Bishop & Blight, 1963), it was demonstrated that the strain response to change in matric suction $(u_a - u_w)$, differs from the respond to change in net normal stress $(\sigma - u_a)$. This confirms the inability of effective stress principle in the formulation of mechanical constitutive behaviour of unsaturated soils.

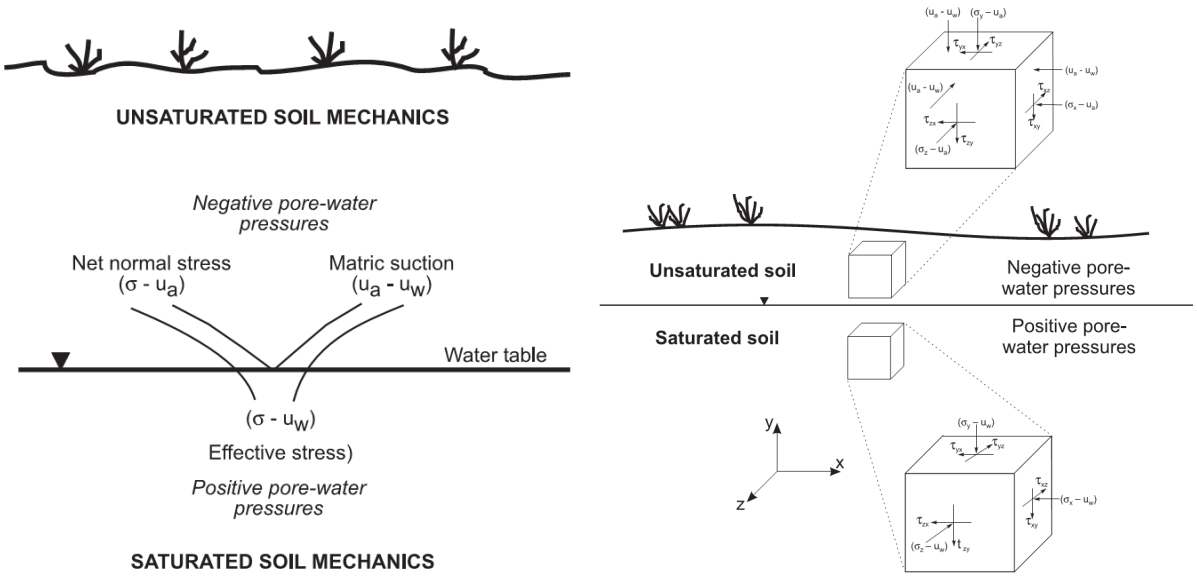

Figure 3.14 Differences in saturated and unsaturated stress state variables, after (Fredlund, 2000)

The two stress variables adopted in ICFEP are, as mentioned in the previous paragraph, the equivalent stress:

$$\sigma = \sigma_{net} + s_{air}$$

and the equivalent suction:

$$s_{eq} = s - s_{air}$$

One of the primary upgrades of Model 81 compared to original BBM, represents the introduction of air-entry value of suction s_{air}, in the definition of stress variables, which allows the transition from saturated to unsaturated behaviour to be shifted from zero suction, to deeper within quasi-saturated zone. This effectively means that for suctions $s < s_{air}$, the effective stress principle with single stress variable still applies. For suction values in excess of air-entry suction value, rapid desaturation takes place, and two independent stress variables introduced previously are required to model partially-saturated soil behaviour.

For the formulation of constitutive models, alternative stress state invariants are commonly employed. In the case of unsaturated soils constitutive models are defined in the 4-dimensional stress space J - p - θ - s_{eq}, where J is deviatoric stress, p is mean equivalent stress, θ is Lode's angle and s_{eq} is equivalent suction.

$$J = \frac{q}{\sqrt{3}}$$

$$p = \frac{(\sigma_x + \sigma_y + \sigma_z)}{3}$$

$$\theta = -\frac{1}{3} \cdot \sin^{-1}\left[\frac{3\sqrt{3}}{2} \cdot \frac{dets}{J^3}\right]$$

$$dets = \begin{bmatrix} \sigma_x - p & \tau_{xy} & \tau_{xz} \\ \tau_{yx} & \sigma_y - p & \tau_{yz} \\ \tau_{zx} & \tau_{zy} & \sigma_z - p \end{bmatrix}$$

For the saturated case, the problem reduces to 3-dimensional stress space J - p' - θ, where p' is mean effective stress.

Yield (YS) and Plastic Potential (PP) Surfaces

The model is based on the concept of loading-collapse (LC) and suction increase (SI) curves (see Figure 3.15), which were originally introduced by (Alonso, Gens & Josa, 1990). In comparison to BBM the elastic region is expanded in the tensile equivalent stress domain (the zone on the left from ordinate), in order to capture the experimentally observed increase of apparent cohesion with suction. In the p - J stress plane the yield and plastic potential functions, F_1 and G_1, are defined by the expression proposed by (Lagioia, Puzrin & Potts, 1996) modified for the unsaturated states.

$$\left.\begin{matrix} F_1 \\ G_1 \end{matrix}\right\} = \frac{p + f(s_{eq})}{p_0 + f(s_{eq})} - \frac{\left(1 + \frac{\eta}{K_2}\right)^{\frac{K_2}{\beta_f}}}{\left(1 + \frac{\eta}{K_1}\right)^{\frac{K_1}{\beta_f}}} = 0$$

Where:

p_0	isotropic yield stress at the current value of equivalent suction
$f(s_{eq})$	measure of the increase in apparent cohesion with suction and controls the expansion of the yield surface into the tensile region
K_1, K_2, β_f	constants
η	generalised normalised stress ratio

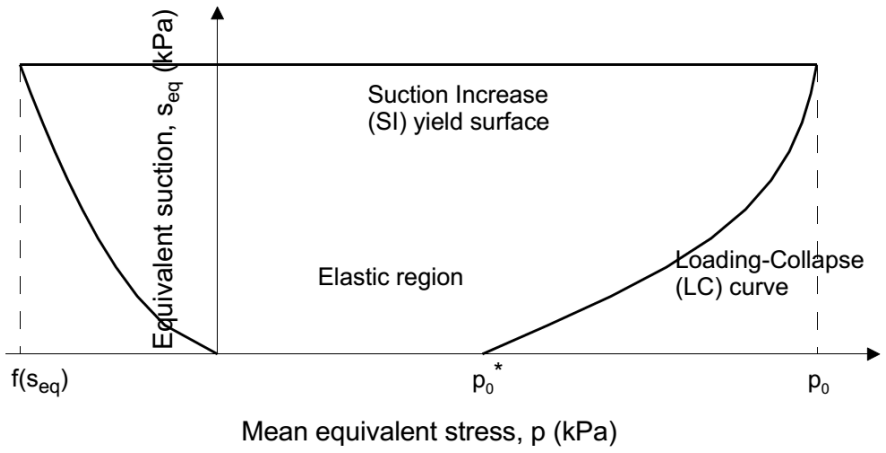

Figure 3.15 Loading-Collapse (LC) and Suction Increase (SI) surfaces, after (Georgiadis, 2003)

The expression proposed by (Lagioia, Puzrin & Potts, 1996) is very flexible, in a sense it can reproduce a wide range of shapes through adjustment of model parameters. This adaptability is schematically illustrated in Figure 3.16, where several well-known yield surfaces have been replicated applying (Lagioia, Puzrin & Potts, 1996) expression. For unsaturated conditions the hardening/softening parameter is the equivalent fully saturated isotropic yield stress p_0^*, corresponding to zero equivalent suction, s_{eq}.

There are to options available within the Model 81 with respect to the type of function which controls the expansion of the yield surface into the tensile stress domain $f(s_{eq})$. The first one relates the $f(s_{eq})$ with equivalent suction, while the second one links it with degree of saturation. The second option better agrees with experimental observations and provides direct coupling between mechanical and hydraulic behaviour of unsaturated soils. The measure of the apparent cohesion is depicted in Figure 3.17 as the intercept on the deviatoric stress axis.

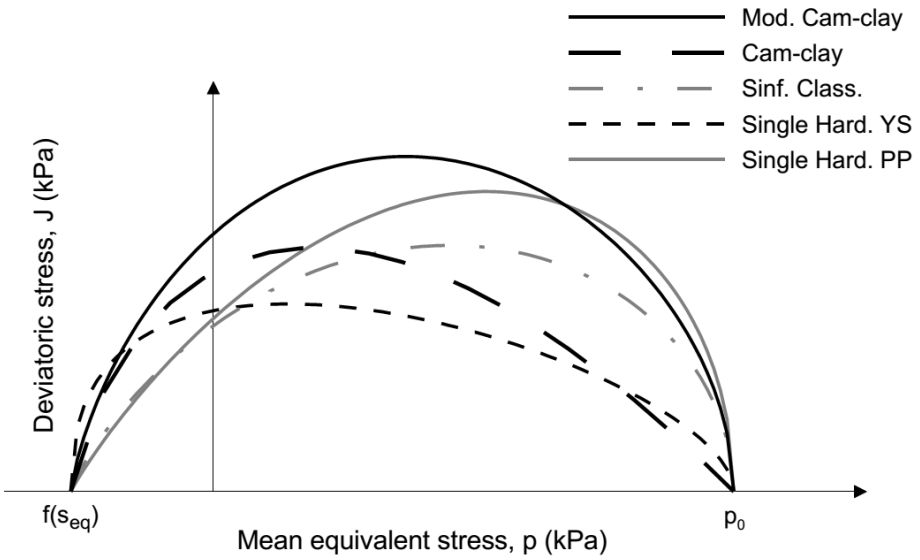

Figure 3.16 Examples of yield (YS) and plastic potential (PP) functions reproduced by the (Lagioia, Puzrin & Potts, 1996) expression

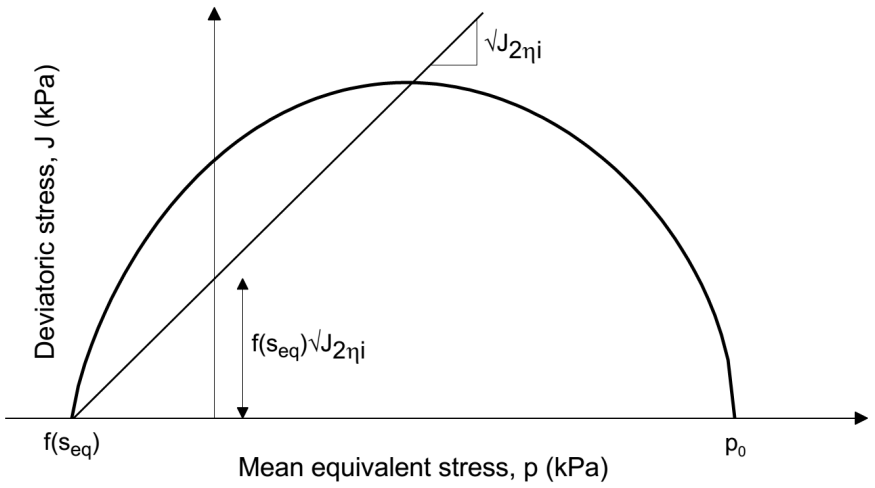

Figure 3.17 Apparent cohesion in the p-J plane after (Georgiadis, 2003)

The suction increase (SI) yield surface present in Model 81, was taken from the work of (Alonso, Gens & Josa, 1990). The hardening/softening parameter linked to this surface is suction value s_0. The expression for suction increase (SI) yield surface (and plastic potential surface, assuming associated flow rule), hereafter termed the secondary yield surface, is as follows:

$$F_2 = G_2 = \frac{s_{eq}}{s_0} - 1 = 0$$

This surface is actually a plane perpendicular to the equivalent suction axis s_{eq} axis, and projects as a straight line in the isotropic stress plane p - s_{eq}, as can be seen in Figure 3.15. Considering that this secondary yield surface is rarely used, significantly high value should be assigned to yield suction s_0, in order to eliminate the effect of this yield surface on the model predictions.

Unsaturated Isotropic Compression Line (ICL) and Yield Stress

Two options are available in ICFEP regarding the shape of the isotropic compression line. Either linear/bi-linear (Model 81) or nonlinear relationship (Model 84) could be employed. In the remainder of this section, only the linear/bi-linear will be discussed.

The linear unsaturated isotropic compression line was initially introduced by (Alonso, Gens & Josa, 1990), and is illustrated in Figure 3.18. As can be seen, for some fixed value of equivalent suction, the unsaturated ICL is constantly diverging from the ICL for fully saturated conditions. Additionally, the rotation of the ICL in the anti-clockwise direction, indicates that the soil is becoming more stiffer with the increase in suction. The equation of unsaturated ICL is given in the following form:

$$v = v_1(s_{eq}) - \lambda(s_{eq}) \cdot \ln p$$

Where, $v_1(s_{eq})$ is the specific volume determined on the current unsaturated ICL for p = 1.0 kPa, $\lambda(s_{eq})$ is the coefficient of soil compressibility at equivalent suction. The coefficient of soil compressibility can be calculated based on the empirical expression proposed originally by (Alonso, Gens & Josa, 1990).

$$\lambda(s_{eq}) = \lambda(0) \cdot [(1 - r)e^{-\beta \cdot s_{eq}} + r]$$

where r and β are model parameters which govern the shape of the loading-collapse (LC) curve.

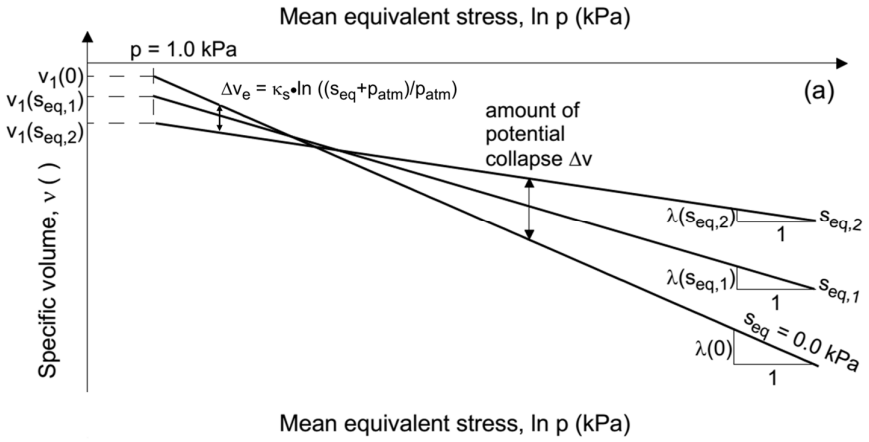

Figure 3.18 Linear unsaturated isotropic compression line (ICL), after (Alonso, Gens & Josa, 1990)

For the linear expression of the unsaturated ICL, (Alonso, Gens & Josa, 1990) has derived the relationship between the hardening/softening parameter p_0^*, mentioned earlier, and the isotropic yield stress p_0 corresponding to the current value of suction, which actually represents the LC curve in the isotropic stress space p - s_{eq}

$$p_0 = p^c \left(\frac{p_0^*}{p^c}\right)^{\frac{\lambda(0)-\kappa}{\lambda(s_{eq})-\kappa}}$$

Where:

p^c	characteristic pressure
$\lambda(0)$	coefficient of soil compressibility for fully saturated conditions
κ	coefficient of compressibility along an elastic path

On the Figure 3.18, the marked distance between ICL corresponding to equivalent suction $s_{eq,2}$, and ICL for saturated conditions ($s_{eq} = 0$), represents the amount of potential collapse induced by wetting (suction decrease). The main shortcoming of the Alonso's linear ICL is that the magnitudes of wetting induced structural collapse (contractive volumetric strains) are overestimated, especially in the region of relatively high confining stresses. To overcome this deficiency, the bi-linear unsaturated ICL was developed for ICFEP by (Georgiadis, 2003). The shape of the bi-linear ICL introduced by (Georgiadis, 2003) is illustrated in Figure 3.19.

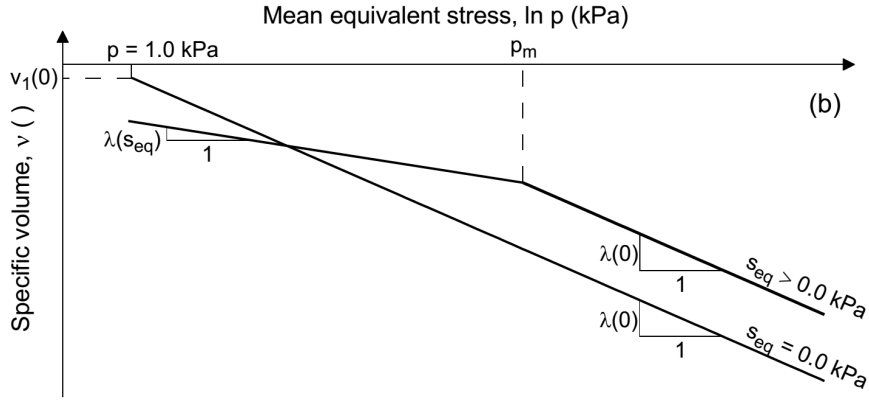

Figure 3.19 Bi-linear unsaturated isotropic compression line (ICL), after (Georgiadis, 2003)

The bi-linear relationship is based on the assumption that the unsaturated and saturated ICLs are collinear for confining stresses in excess of p_m. Therefore, the LC curve for the bi-linear ICL becomes:

$$p_0 = p^c \cdot (\alpha^c)^{\frac{\lambda(0)-\lambda(s_{eq})}{\lambda(s_{eq})-\kappa}}$$

where α^c is a model parameter. For confining stresses lower than p_m the Alonso's expression for LC curve is used. Therefore, for confining stresses beyond p_m the constant amount of collapse is predicted.

For the lower confining stresses (on the left-side of the intersection of the unsaturated and saturated ICL) under the wetting conditions, the model predicts merely elastic swelling.

Suction Induced Wetting/Drying Line (WDL)

Suction induced volumetric strains are expressed in terms of constant elastic and elasto-plastic coefficients of compressibility κ_s and λ_s. The suction induced compression line, also referred as wetting/drying line is depicted in Figure 3.20.

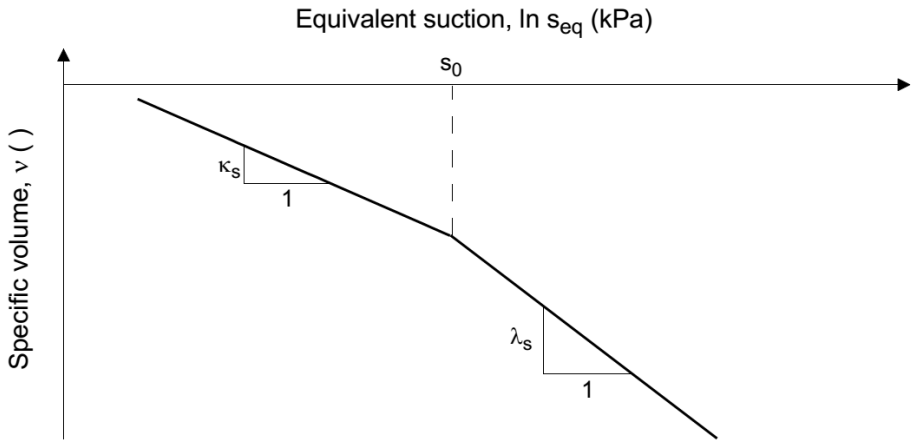

Figure 3.20 Suction induced compression line (wetting/drying line) after (Georgiadis, 2003)

Critical State Line (CSL)

Similar to classical critical state constitutive models, a unique critical state line exists for a fixed value of equivalent suction. The shape of critical state line in $p - J - s_{eq}$ stress space is shown in Figure 3.21. The projections of the critical state line onto the $J - s_{eq}$ and $p - s_{eq}$ planes indicates that the stress coordinates of the critical state point (p_{cs}, J_{cs}) are rising in value with increase of suction.

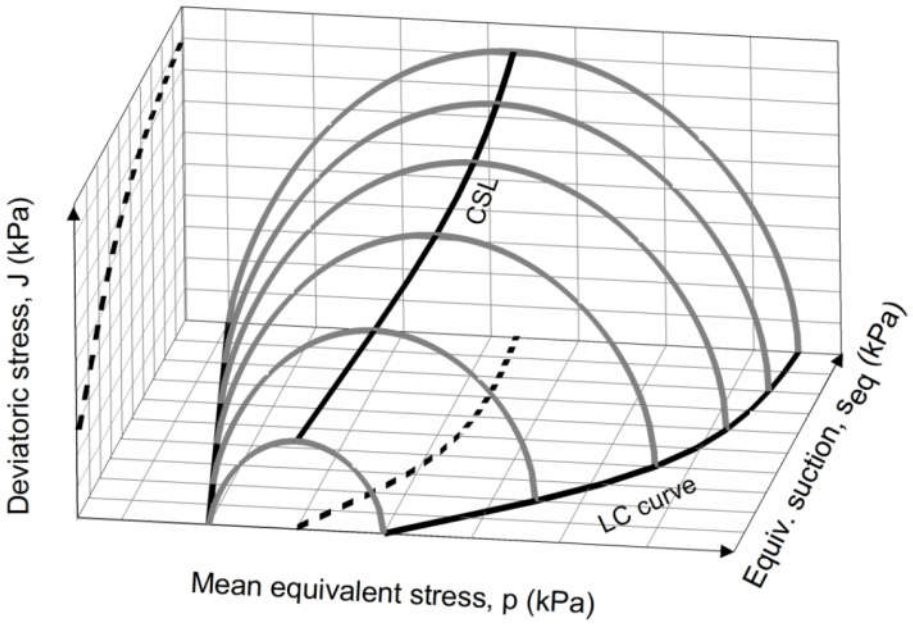

Figure 3.21 Critical state line in $p - J - s_{eq}$ stress space

The critical state line in the $p - J$ stress plane is the same as in the modified Cam Clay model, but with the addition of apparent cohesion term, induced by suction.

$$J = p \cdot \sqrt{J_{2\eta i}} + f(s_{eq}) \cdot \sqrt{J_{2\eta i}}$$

The critical state line in the $v - lnp$ stress-strain space is parallel to the unsaturated ICL, and is given by the following equation

$$v_{cs} = v(p_0) - \kappa \ln \frac{p_{cs}}{p_0}$$

where $v(p_0)$ is the specific volume at the yield stress p_0, corresponding to the current value of equivalent suction, s_{eq} (see Figure 3.22). The $v(p_0)$ is obtained from the the equation of the unsaturated ICL as is illustrated in Figure 3.22.

$$v(p_0) = v_1(s_{eq}) - \lambda(s_{eq}) \ln p_0$$

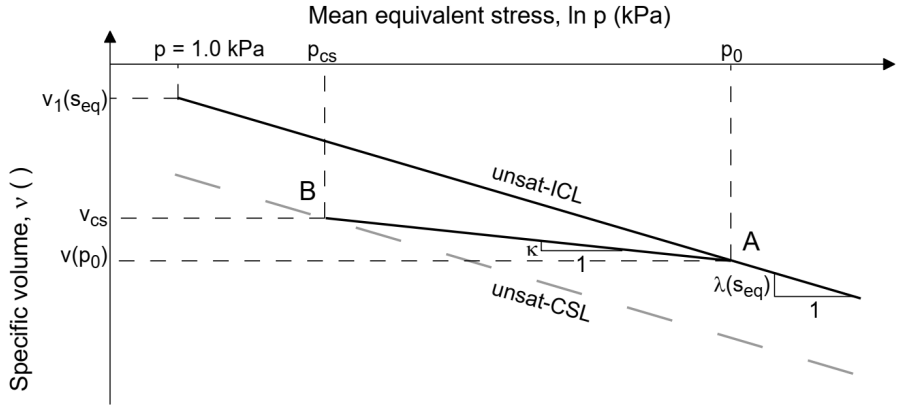

Figure 3.22 Critical state line in the v – lnp stress-strain space

Hardening/Softening Rules

The magnitude of plastic strains generated upon reaching the yield surface are related to the change in the hardening/softening p_0* and s_0, in accordance to the following expressions
For the primary F_1 yield surface:

$$\frac{dp_0^*}{p_0^*} = \frac{\nu}{\lambda(0) - \kappa} d\varepsilon_v^p$$

For the secondary yield surface F_2:

$$\frac{ds_0}{s_0 + p_{atm}} = \frac{\nu}{\lambda_s - \kappa_s} d\varepsilon_v^p$$

The two surfaces are coupled, meaning that the changes (i.e. expansion) in either induces changes of the other one.

The initial value of hardening parameter p_0* is established based on the initial stress state and overconsolidation ratio, *OCR*, which is an input parameter of the model. On the other hand, the initial value of s_0 needs to be directly specified and may be obtained from an unconfined drying test.

Elastic Behaviour

In the elastic region, alterations of either of the two isotropic stress variables induces elastic volumetric strains, which are determined according to the following equations:

$$d\varepsilon_{vs}^e = -\frac{\kappa_s}{\nu \cdot (s_{eq} + p_{atm})} ds_{eq}$$

$$d\varepsilon_{vp}^e = -\frac{\kappa}{\nu \cdot p} dp$$

where all terms on the right-hand side of the equations have already been explained.

Additional parameter required by the model, represents the minimum bulk modulus $K_{min.}$ The parameter is introduced in order to prevent predictions of infinite volumetric deformations when mean equivalent stress, *p,* tends to zero.

The changes in the deviatoric stress are related to incremental deviatoric strains vie shear modulus G, as follows:

$$dE_d^e = \frac{dJ}{G}$$

3.5 Soil Water Retention Curve (SWRC) Model

The basic soil-water retention curve (SWRC) model available in ICFEP is the non-hysteretic, void-ratio independent, non-linear curve shown in Figure 3.23 (Melgarejo, 2004). The model is a form of the (Van Genuchten, 1980) type analytical models and is formulated in terms of degree of saturation, Sr, and matric suction, s, rather than in terms of volumetric water content and suction. The (Melgarejo, 2004) SWRC model is given by the following equation:

$$S_r = \left\{\frac{1}{1 + [\alpha(s - s_{des})]^n}\right\}^m (1 - S_{r,0}) + S_{r,0}$$

where:

s	current value of suction
s_{des}	value of suction at desaturation
$S_{r,0}$	residual degree of saturation
α	fitting parameters controlling the shape of the curve. Note that $\alpha > 0.0$, $n > 0.0$ and $0.0 \leq m \leq 1.0$. The dimension of parameter α is 1/stress (i.e. kPa^{-1}) so that the product $s \cdot \alpha$ is dimensionless

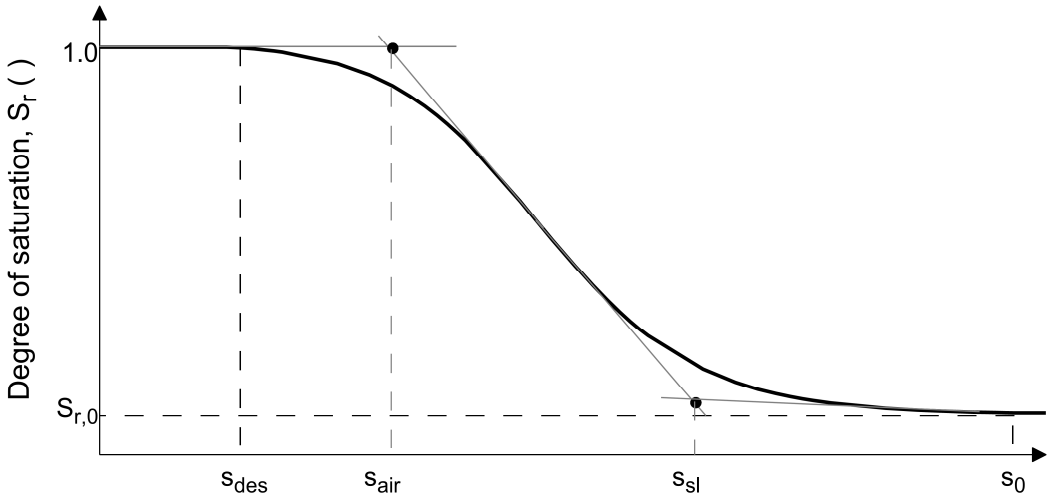

Figure 3.23 Simple non-hysteretic, void-ratio independent, non-linear SWRC implemented in ICFEP by (Melgarejo, 2004)

The slope of the retention curve at the current value of suction, s, is:

$$R = \frac{\partial S_r}{\partial s} = -mn\alpha \cdot (1 - S_{r,0}) \cdot \frac{[\alpha(s - s_{des})]^{n-1}}{[1 + [\alpha(s - s_{des})]^n]^{m+1}}$$

The model is capable to simulate a residual degree of saturation $S_{r,0}$, which is asymptotically reached when the suction tends to infinity, as can be inferred from the mathematical expression of the SWRC. However, as can be seen from the Figure 3.23, the model allows finite value of suction s_0 to be specified, for which the degree of saturation S_r, practically reduces to its residual value. This suction does not represent the suction at shrinkage limit, rather the suction at which the water phase seemingly becomes discontinuous. Theoretically, it is expected that discontinuity of water would occur earlier in desaturation process and that subsequent changes in the degree of saturation and the corresponding suction are restricted to meniscus water at the particle contacts.

The above inconsistency is practically overcome by the introduction of the Ω parameter, which, as explained earlier in this chapter, governs the volume of water that flows in response to a change in the volume of voids and reduces to zero when the water phase becomes discontinuous. The suction at Ω transition, s_Ω, is an input parameter and may well be smaller than s_0. The program, however, checks that $s_\Omega > s_{air}$, s_{air} being the air-entry value of suction, which is an extra model parameter. Furthermore, the value of s_{air} prescribed for the SWRC model needs necessarily to agree with the value input in the elasto-plastic constitutive model adopted.

3.6 Nonlinear Permeability Models

Permeability is the fundamental soil property in the case of pure flow analysis, as well as in fully coupled flow-deformation analysis. Saturated permeability of soil depends on numerous factors, among which void ratio stands out as the most important one. Void ratio is in turn function of mean effective stress level, and therefore nonlinear saturated permeability models are most commonly derived in terms of stress level. Such model exists in ICFEP and is introduced in Chapter 4 of this thesis.

In the case of unsaturated soils, one needs to distinguish between the permeability for water and permeability for air phase. The hydraulic conductivity for water, defines how fast water propagates through the water phase. Considering that in the case of truly unsaturated soils, the cross-sectional area of water is lower compared to saturated case, there is less space for water to flow. Therefore, the permeability of unsaturated soil is lower than for saturated soil, and decreases further as the soil progressively desaturates. The air phase which is also present within the void space, actually blocks the flow of water, in a similar manner the solid particles do. The increase in tortuosity and drag forces additionally hinders the water flow, with the effects becoming more pronounced as the volumetric water content decreases. Therefore, it can be seen that unsaturated soil permeability depends heavily on the degree of saturation, which in turn depends on the soil suction (see SWRC in previous section).

Various permeability models are available in ICFEP numerical code, and some that are thought to be practical for the purposes of the performed analyses are presented in the following sections.

3.6.1 Desaturation Permeability Model

The ICFEP numerical code possess two nonlinear permeability models for simulating the effect of desaturation. The first one is the so-called 'suction switch model', which expresses the hydraulic conductivity in terms of suction. The model acts as classical homogeneous isotropic permeability model as long as pore water pressures are compressive. Once the specified tensile pore water pressure S_1 is reached, the model switches to nonlinear model in which logarithm of permeability varies linearly with suction (see Figure 3.24). As can be seen from given illustration, the permeability decreases from saturated value k_{sat} corresponding to suction S_1 to a limiting value k_{min}, corresponding to suction S_2. At that point permeability again becomes constant regardless of further changes in the suction value. The use of a constant residual permeability is also consistent with the findings of (Fredlund, 1998).

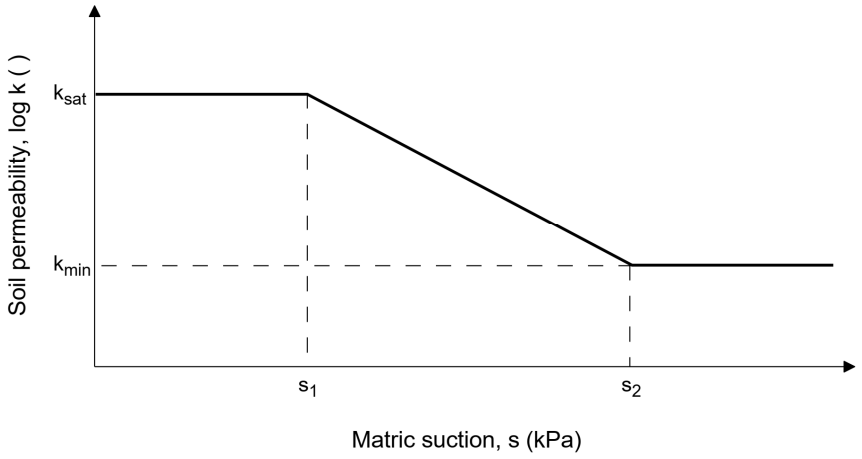

Figure 3.24 ICFEP suction switch permeability model

The magnitude of permeability corresponding to the current suction level, *S,* can be obtained from the following equation:

$$\log k = \log k_{sat} - \frac{s - s_1}{s_2 - s_1} \log(\frac{k_{sat}}{k_{min}})$$

Beside this relatively simple suction dependant unsaturated permeability model, another more advanced model exists in the ICFEP. Instead in terms of suction, the model is expressed as a function of the degree of saturation S_r, and should preferably be employed in combination with the hysteretic retention curve, which is not the scope of the current research.

3.6.2 Desiccation Permeability Model

Clayey soils are generally prone to desiccation cracking as a result of shrinking deformations. During summer dryer months when the outward moisture flux due to evapotranspiration extracts the water from the soil, volumetric contraction induces tensile total stresses, which if exceed soil tensile strength, initiate the opening of cracks and fissures. Such discontinuities affect topsoil shear strength and in particular overall mass permeability, thereby facilitating the infiltration of rainwater. This could potentially rapidly reduce deeper tree-induced suctions and instigate the slope instability.

ICFEP is not capable of explicit modelling of discreet cracks generation. Rather, it can account for variation of soil properties, permeability in specific, in response to cracking. Smeared crack permeability model capable of simulating hydraulic conductivity variations due to cracking is implemented into ICFEP (Nyambayo, 2004). A similar relationship is used as in the case of desaturation model, except that the suction is replaced by tensile total principal stress σ_T.

$$\log k = \log k_{sat} - \frac{\sigma_T - \sigma_{T1}}{\sigma_{T2} - \sigma_{T1}} \log(\frac{k_{max}}{k_{sat}})$$

where σ_T is the current tensile total principal stress and σ_{T1} and σ_{T2} are the tensile stresses illustrated in Figure 3.25. More specifically, σ_{T1} is the tensile stress at which the saturated permeability begins to increase, while σ_{T2} is the limiting value at which maximum permeability is attained.

If both, desiccation and desaturation, permeability models are applied in the same analysis, the code first checks whether the desiccation criterium is satisfied, and only then investigates the occurrence of desaturation. Permeabilities are calculated in accordance with the outcomes of these checks.

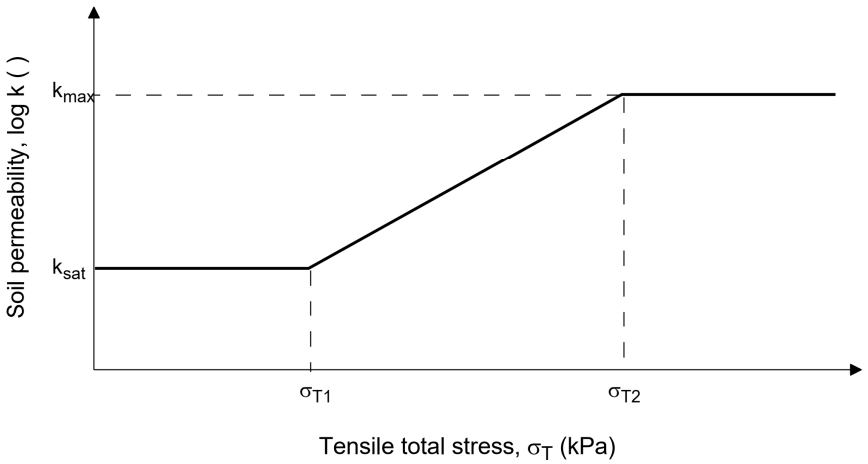

Figure 3.25 ICFEP desiccation permeability model

3.7 Hydraulic Boundary Conditions

Flow and coupled flow-deformation problems require appropriate hydraulic boundary conditions to be specified for all nodes on the outer boundary of the mesh, either in the form of prescribed pore pressure or fluid-moisture flux (Potts & Zdravković, 1999). The default condition in ICFEP is that of a zero nodal flow.

Prescribed values of incremental nodal pore pressure $\{\Delta p_f\}$ affect only the left-hand side of the governing system of equations for coupled problems, both for saturated and unsaturated conditions and are treated in a similar way as prescribed displacements in deformation analysis. Specified nodal flow rates affect the right-hand side vector Q of the governing system of equations and are dealt with in the same fashion as prescribed nodal forces.

Among the numerous hydraulic boundary conditions available in ICFEP, only precipitation and vegetation conditions are explained in detail, bearing in mind that these constitute the essence of the soil-vegetation-atmosphere interaction.

3.7.1 Precipitation Boundary Condition

Simulation of the rainwater infiltration can most easily be achieved by prescribing a classical infiltration boundary condition along the ground surface equal to the rainfall intensity. However, if the rainfall intensity exceeds the permeability of the soil adjacent to the ground surface, unrealistically high compressive pore water pressures would be predicted. In reality, excess rainwater (not penetrating the ground) will either pond or, make for surface run off for sloping ground. It can be seen that the rainfall infiltration depends on various factors, including: the intensity and duration of the rainfall, the geometry of the soil surface and its porosity, and the initial conditions prior to the start of precipitation. Therefore, it is likely that type of the adequate boundary condition will have to change throughout an analysis.

To account for mentioned difficulties a sophisticated dual condition is developed by (Smith, 2003) and implemented in ICFEP, which enables realistic simulation of the inflow part of the water balance. It operates either as an infiltration (specified constant flow) condition, or as a constant prescribed pressure (variable flow) condition, thereby providing automatic and continuous division of the surface reached rainwater into infiltration, run-off and ponding.

The operation of the precipitation boundary condition is schematically illustrated in Figure 3.26 and explained in detail in the following paragraphs. The precipitation boundary condition requires that a flow rate q_n (i.e. the rainfall intensity at the ground surface), along with some maximum threshold value (p_{fb}) of the pore water pressure at the surface boundary, be specified. At the commencement of every increment, pore water pressure at boundary nodes p_f is compared to p_{fb}. In case, it is more tensile than the p_{fb}, an infiltration boundary condition is applied, employing the specified flow rate, q_n. Infiltration is also applied when at the beginning of the increment the flow rate across the boundary exceeds the prescribed value.

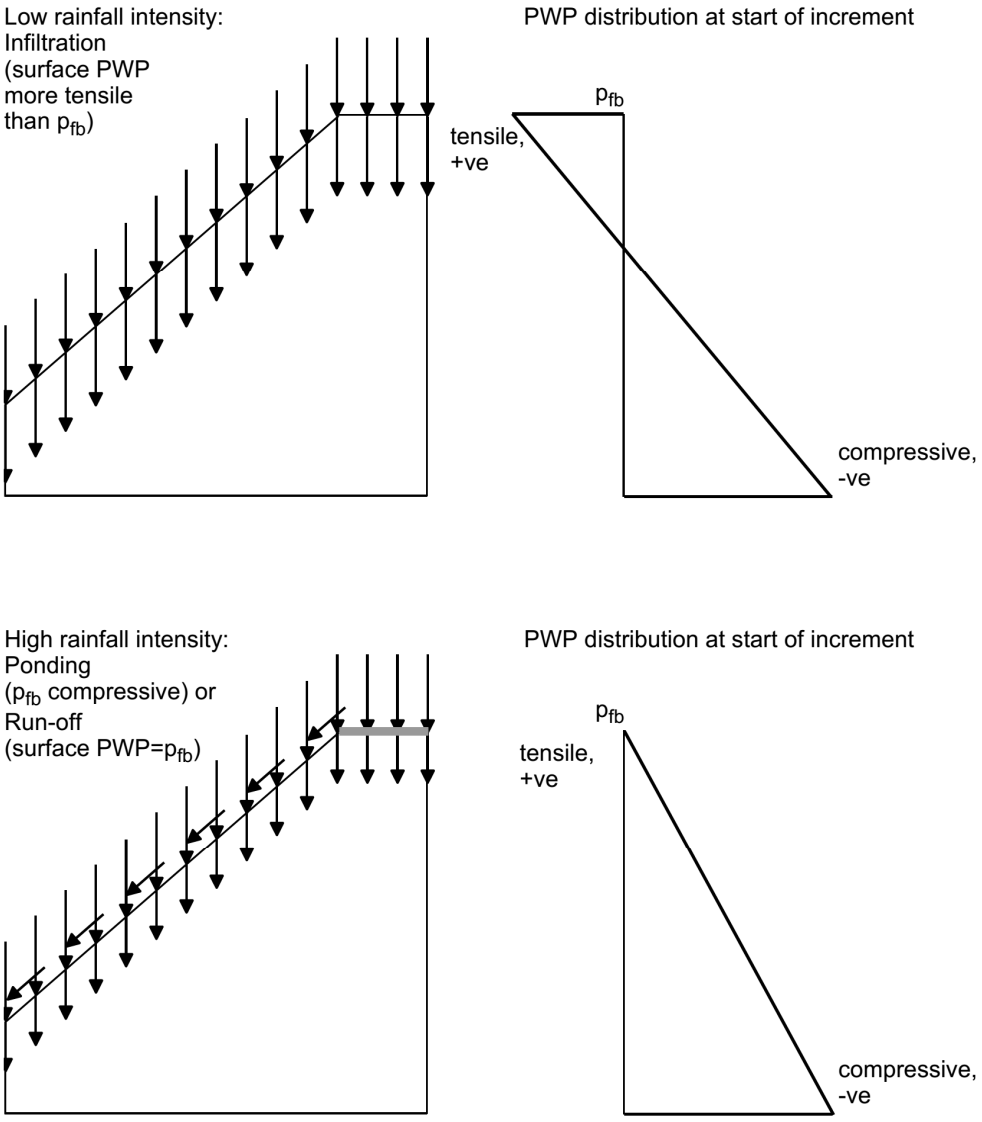

Figure 3.26 Precipitation boundary condition after (Smith, 2003)

Alternatively, if the pore pressure at the beginning of the increment is more compressive than the p_{fb}, then a constant pore water pressure equal to the latter is imposed. In order to maintain the prescribed pore pressure at the boundary, a portion of the specified infiltration is applied, while the rest is considered as run-off and, since the resulting flow occurs outside the finite element mesh, is disregarded.

Typically for sloping ground, the p_{fb} is set to 0.0 kPa, allowing the soil to become fully saturated as a result of intense rainfall, but preventing ponding and generation of compressive pore water at the ground surface. Contrary, compressive pore water pressures should be prescribed for terrain configurations for which accumulation of surface water (ponding) could occur. Finally, tensile values of p_{fb} can be employed to prevent total loss of suction. This is particularly important in situations when vegetation boundary condition is also present at the surface. In that case total loss of suctions would form anaerobic conditions, which in turn would cancel out any future effect that vegetation may have.

The main advantage of the precipitation over the infiltration boundary condition is that ponding and run-off cannot be reproduced with the latter. However, employment of the precipitation boundary condition is not straightforward; depending on the flow rate and on the soil permeability, conditions may change during an increment of the FE analysis, for one or more nodes. In that case a switch of boundary condition is required, which is dealt with by an automatic-incrementation algorithm described in detail in (Smith, Potts & Addenbrooke, 2008). This algorithm automatically divides the current increment into a series of sub-increments when it is required.

3.7.2 Vegetation Boundary Condition

Plants extract water from the ground through the process of transpiration. However, due to distinct seasonal leaf cycles inherent to deciduous trees, transpiration rates vary throughout the calendar year, peaking during the summer and dropping during the winter, modifying the pore pressures within the ground accordingly. In the past, the effect of vegetation on the performance of geotechnical structures was simulated by prescription of seasonal pore pressure profiles, derived to match field observations (Kovacevic, Potts & Vaughan, 2001; Nyambayo, Potts & Addenbrooke, 2004; Russell *et al.*, 2000). These summer and winter pore water pressures profiles were successively applied, in order to mimic the effects of evapotranspiration. Nonetheless, this simplification may lead to unrealistic water flows, which cannot be achieved by vegetation. Besides, hydrological cycle is transient in nature, making the seasonal profiles simplification rather rough. More appropriate approach would be to model the soil–vegetation–atmosphere continuum using rainfall and evapotranspiration as input data, which is achieved through the use of Root water uptake models (RWUMs). Such a procedure allows the pore water pressure profiles to be predicted, rather than prescribed.

A non-linear RWUM has been developed by (Nyambayo & Potts, 2010) and implemented in ICFEP (Imperial College Finite Element Program). The model's main advantage is its flexibility, the fact it does not involve plant-specific parameters and can, therefore, be applied to any vegetation type. The primary input data includes potential evapotranspiration and maximum root depth. The model assumes linear distribution of potential evapotranspiration with depth, from a maximum value corresponding to the ground surface, to zero at depth r_{max}, as illustrated in Figure 3.27. Below the maximum root depth r_{max}, the water uptake is assumed to be zero.

In numerical analysis, root water uptake is taken into account by incorporating sink term into continuity equation of fluid flow (Potts & Zdravković, 1999). The sink term represents the volume of water extracted per unit volume of soil, per unit time, and is calculated based on the potential evapotranspiration rates, which are prescribed incrementally. Potential evapotranspiration rates represent an amount of water that potentially could be extracted from the ground if an unlimited supply of moisture were available. However, under field conditions, the supply of water is commonly limited, which affects the pore pressures and in turn reduces the actual evapotranspiration rates. To obtain the actual evapotranspiration rates, which are a fraction of the potential ones, the relationship introduced by (Feddes, Kowalik & Zaradny, 1978) is employed:

$$S_{acc} = \frac{2 \cdot a \cdot T_p}{r_{max}} \cdot \left(1 - \frac{r}{r_{max}}\right)$$

Where:

S_{acc} is a sink term incorporated in the continuity equation of fluid flow;
T_p is the potential evapotranspiration rate prescribed;
r_{max} is the maximum root depth for which the boundary condition applies (see Figure 3.27);
r refers to the depth below the ground surface (see Figure 3.27) and cannot exceed the value r_{max} (i.e. $0 \leq r \leq r_{max}$);

α is a suction dependent function as shown in (see Figure 3.28). Its value is zero for suction levels lower than S1 (anaerobiosis point) and larger than S4 (wilting point) and equal to 1.0 for suction levels between S2 and S3. It increases linearly between S1 and S2 and decreases linearly from S3 to S4. Suctions S1, S2, S3 and S4 are model parameters, input as evapotranspiration soil properties. As is explained in (Nyambayo & Potts, 2010), the generally accepted magnitudes for S1, S2 and S4 are 0, 5 and 1500 kPa, respectively, while the value of S3 (value at which vegetation begins to become stressed) is tree-species dependent. (Nyambayo & Potts, 2010) have undertaken a parametric study regarding the influence of S3 on overall soil behaviour and showed that the value of S3 within the range common to most vegetation species (50–200 kPa) is likely to have only a small effect on predictions regarding pore pressures and ground movements.

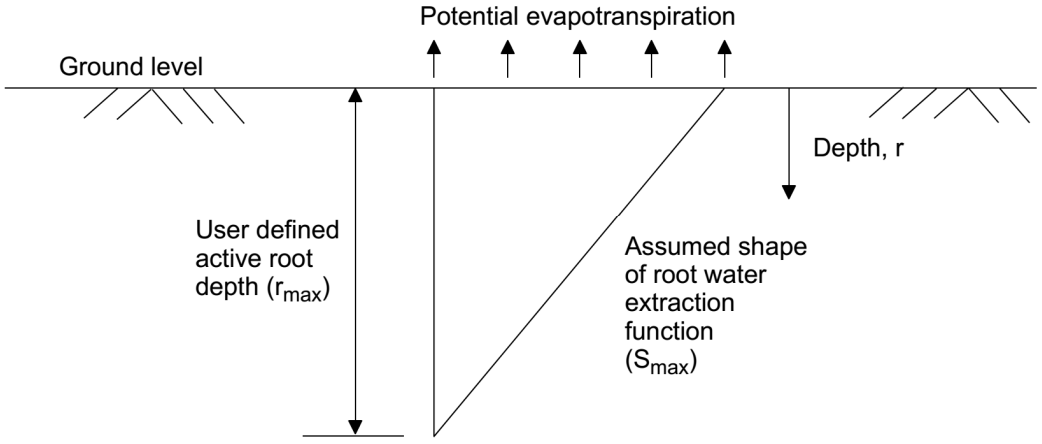

Figure 3.27 Assumed shape of root extraction function in the rooted zone after (Nyambayo & Potts, 2010)

Detailed description of the model implementation, particularly with respect to estimation of equivalent nodal flows and the correction of α coefficient over an increment of the analysis is given in the paper by (Nyambayo & Potts, 2010).

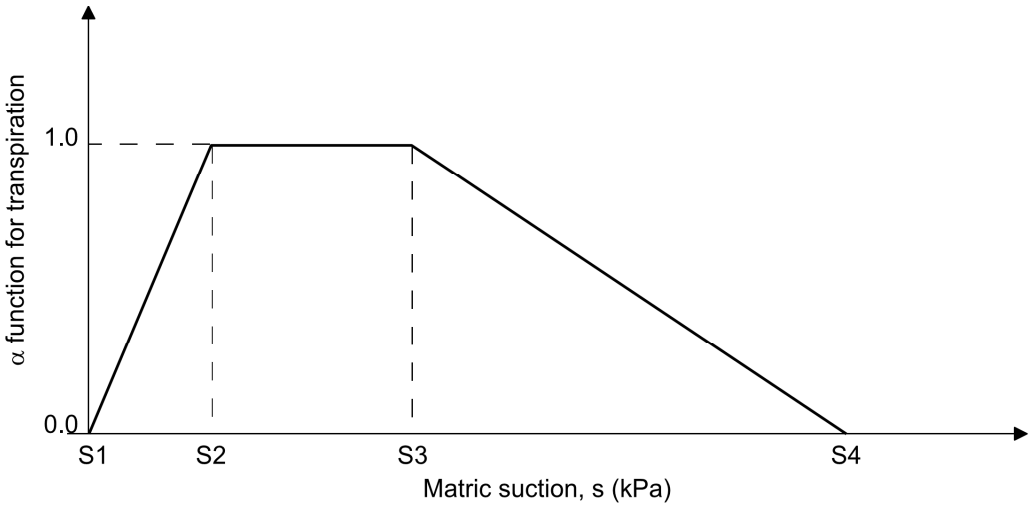

Figure 3.28 Linear variation of α function after (Nyambayo & Potts, 2010)

Chapter 4: Magnolia Road - Case Study

4.1 Introduction

In the first part of this chapter an instrumented embankment suffering from poor ride quality and frequent speed restrictions is presented. The geometrical properties and stratigraphical units that build up the embankment and foundation soil are introduced firstly, followed up by detailed description of utilised instrumentation and monitoring data. The gathered data have been systematically processed and interpreted to establish the patterns of behaviour, as well as to identify the causes of unsatisfactory performance. The case study embankment is of particular importance from the soil-vegetation-atmosphere interaction perspective, as it was monitored both, during the seasonal wetting-drying phase (the period when vegetation was present on the embankment slopes) and following vegetation clearance.

In the second part, a numerical model of the same embankment has been constructed and presented. Extensive explanation regarding the assumptions and calibrations of material parameters, made assumptions relating to general boundary, initial and climatic conditions, and finally framework and course of analysis stages, is provided.

In the final third part of the chapter, the predictions from the two "main" analyses differing primarily in the type of employed constitutive model, have been thoroughly discussed. That section concludes with the comparison of conducted numerical simulations with field measurements summarizing the most important findings.

4.2 Embankment Geometry and Site Characteristics

The instrumented embankment is located on the Shenfield–Southend Victoria railway line near Hawkwell, Essex, UK (OS grid reference TQ856923; Fig. 4.1). The railway line runs north-west to south-east through the site. At this section of the rail track, applied temporary speed restrictions were common in the past and had the highest impact on passenger services. As subsequently explained, the main reason why the speeds have had to be limited, were excessive cyclic shrink-swell movements associated with highly vegetated slopes. Additional expenses, beside losses related to delays, come from frequent maintenance requirements, particularly at the end of summer, when tree water demand is at its peak. Geotechnical Interpretative Report (GIR) and monitoring data were made available by (Arup Geotechnics, 2007) and (Geotechnical Observations, 2013)

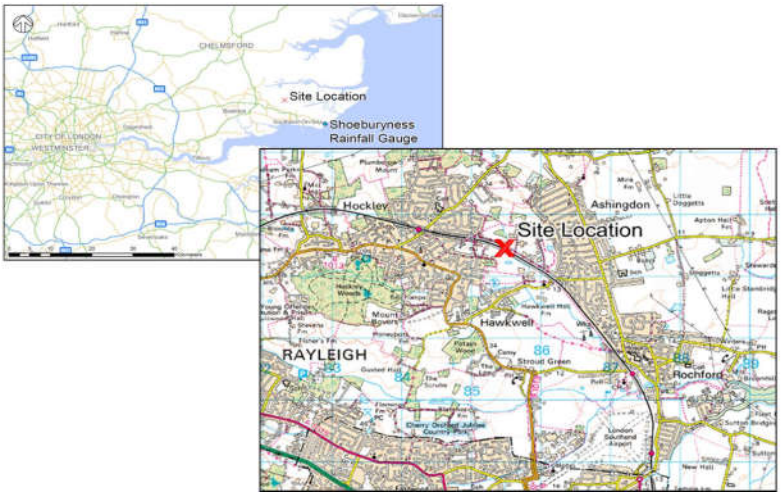

Figure 4.1 Site location after (Ordnance Survey, 2013)

The embankment was constructed around 1887. Along the instrumented section, its height and width are around 5.5 m and 35 m respectively. The slope of the embankment is typically around 20° steepening to around 30° at the shoulder of the embankment, with north side being somewhat steeper compared to the south one. As described earlier, this 'coat-hanger' shape is an indicator that high-water demand trees were present for the prolonged period of time. The embankment consists of intermediate to high plasticity clay fill (indicator of high-volume change potential) of London Clay origin excavated from adjacent areas of cut. As explained earlier, embankments from that era are heterogeneous in nature, containing pockets of coarser granular materials with occasional brick fragments. The underlying stratigraphy consists of high to very high plasticity London Clay Formation of brown-yellowish colour. The embankment is covered with a layer of ash up to 2.3m thick. A layer of ballast approximately 1.3m thick caps the ash. At the start of the monitoring period in March 2006, the embankment was densely vegetated with mature and semi-mature oak (*Quercus robur*) and ash (*Fraxinus excelsior*) trees. According to (NHBC standards, 2007) oak is being classified as high water demand tree, wail ash is more of a moderate type. Beyond the embankment to the north lies predominantly agricultural land with grass vegetation.

In March 2007, the vegetation was removed over the shoulder of the embankment leaving only the vegetation near the toe as indicated in Figures 4.2 and 4.3. Further tree clearance occurred in March 2010, along the full length of the embankment. All of the trees adjacent to the instrumented section were felled, leaving only two semi-mature trees close to the ditch at the toe of the south-facing slope. Between the first and the second tree clearance, small saplings and other scrubby vegetation became re-established on the slopes (Smethurst *et al.*, 2015).

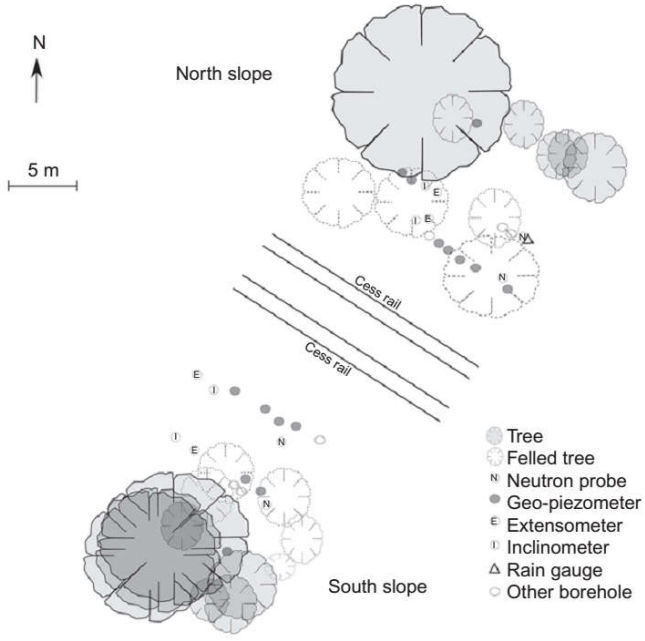

Figure 4.2 Plan view of Hawkwell embankment indicating the extent of first tree removal and location of instrumentation

4.3 Monitoring Data

Monitoring data was available from spring 2006 until March 2011. Most of the data and related interpretations presented in the following sections, correspond to the north section of the embankment, because only that part of the embankment was subsequently used in numerical simulations. Instrumentation was installed predominantly at two sections on each side of the embankment, at the shoulder closer to the crest and at the midslope with some additional piezometers located near the toe of the emabankment (see Fig. 4.2 and 4.3). The instrumentation consisted of:

- Standpipe piezometers installed to a depth of 9 m below the surface at shoulder section of north slope. It is noted by (Arup Geotechnics, 2007) that the standpipe piezometers were not reaching adequate depth to monitor the ground water level. A standpipe piezometer installed on the southern slope of the embankment was somewhat deeper allowing more practical data regarding the water level to be gathered. The standpipe was dry for some of the monitoring period indicating potential fluctuations in level;
- GeO flushable piezometers (by Geotechnical Observations Ltd) at both sections at varying depths within the clay fill and some into the top of the in situ London Clay. In addition to compressive water pressures, the GeO flushable piezometers are capable of measuring suctions (negative pore pressures) up to 100kPa. The geo-piezometer and its installation technique are described by (Ridley *et al.*, 2003).
- Neutron probe access tubes at both previously defined sections for indirect measurements of soil water content. Due to uncertainty of tube-soil contact and employed neutron probe calibration curves, produced water content profiles may potentially be in error.
- Inclinometers measuring lateral displacement perpendicular and parallel to the track. These were installed at both sections to depths between 8 and 10 m below ground level. Inclinometer readings were interpreted assuming the base of the tube to be fixed.
- Extensometers measuring the vertical displacement at both sections to depth around 10 m below the ground surface. Vertical displacements were calculated relative to the deepest magnet, which displacements are assumed to be negligibly small, and therefore it was considerd fixed.
- Datalogged tipping bucket rain gauge installed on the north slope, for the on-site measurements of rainfall.

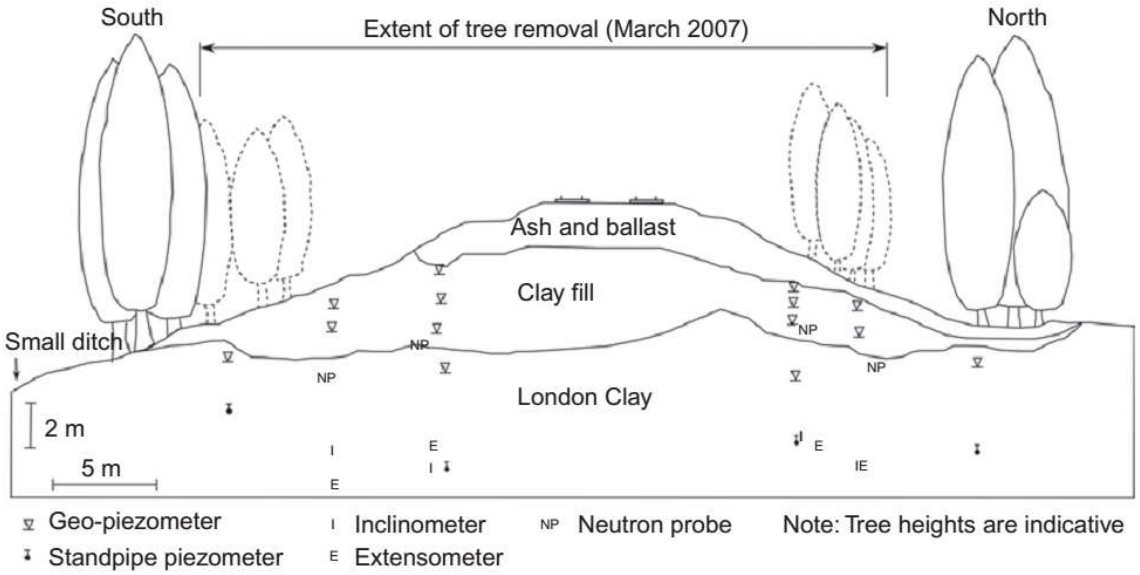

Figure 4.3 Cross-section view of Hawkwell embankment indicating the extent of first tree removal and location of instrumentation

4.3.1 Weather Data

Due to the fact that measured rainfall data was not available for the entire monitoring period (only from April 2006 until February 2009) (Southampton, 2009), for the purposes of completeness and comparison, additional data from the local Met Office weather station at Shoeburyness (see Figure 4.1) located at grid reference TQ96008770, approximately 11.4 km south east from the embankment site, was introduced. Figure 4.4 compares monthly rainfall data measured with the on-site rainfall

gauge, from the local weather station and the long-term average monthly rainfall from 1971 to 2000 from Greenwich, London. Relatively good agreement between the site rainfall data and the Met Office rainfall data ensures reliability in using Met Office rainfall data beyond February 2009.

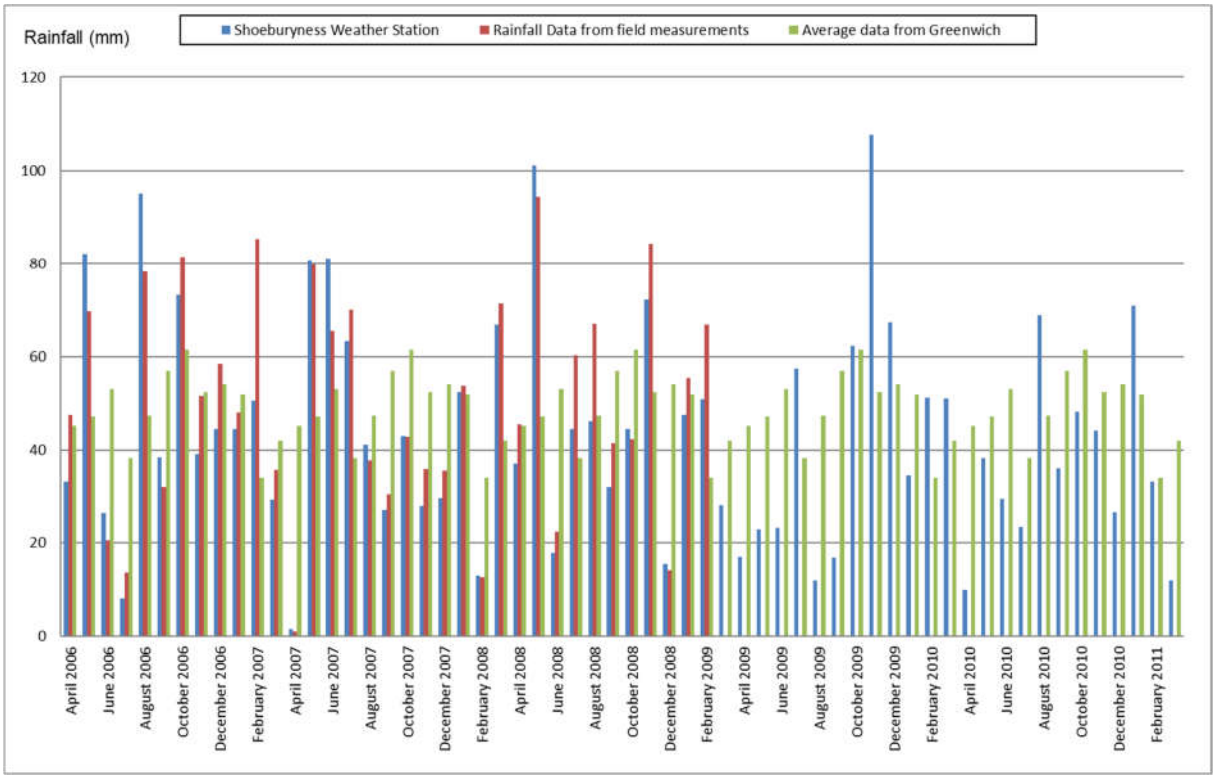

Figure 4.4 Comparison of the monthly rainfall totals measured for the monitoring period

Potential evapotranspiration rates for the Hawkwell embankment were either calculated or taken from literature. The first set of evapotranspiration data was provided by the Met Office for a site near Chattenden in Kent, approximately 25km from the site. The Met Office uses the Meteorological Office Rainfall and Evaporation Calculation System (MORECS) to estimate evapotranspiration rates in the UK for weekly and monthly periods, based on a form of the Penman-Monteith equation (Hough & Jones, 1997). The Met Office regularly publishes the evapotranspiration data for number of different plant species, primarily for agricultural purposes. The data used within this research is for deciduous trees. The same set of data has been previously used by (Nyambayo, Potts & Addenbrooke, 2004; Chalmers, 2013).

The second set of evapotranspiration data was calculated based on the empirical method proposed by (Thornthwaite, 1948), described in detail in Chapter 2. For the evaluation of the monthly mean air temperatures, the monthly minimum and maximum air temperatures between April 2006 and March 2011 for the Shoeburyness weather station were used.

For the third set of data, the FAO Penman-Monteith method was employed. The methodology proposed by the Food and Agriculture Organization (FAO) has been described in Chapter 2. The data required for the calculation of reference evapotranspiration include following: the altitude and latitude of the site location, and the minimum and maximum air temperatures for the time step under consideration. Aforementioned temperature data from the weather station at Shoeburyness were used. The station is located at an altitude z=2m and a latitude of 51.55 in decimal degrees. The value of 0.19, corresponding to a coastal location, was attributed to the adjustment coefficient k_{Ra}, required for the calculation of net solar radiation R_s. Dew point temperature T_{dew} was considered to be equal

to T_{min}. The reference evapotranspiration was calculated, using equations explained in Chapter 2, which account for limited availability of meteorological data.

For the evaluation of crop evapotranspiration ET_c, estimation of the crop coefficient K_c was required. The single crop coefficient approach was selected, considering that the available climatic data were limited and monthly time steps were used. For the deciduous trees, the representative durations of the growth stages, namely the initial, development, mid-season and late season stages are 20, 70, 90 and 30 days respectively (Allen *et al.*, 1998). As the tree vegetation had already been established at the embankment site, the initial phase was neglected and a development stage lasting 90 days (from March to end of May) was assumed. The mid-season stage was assumed to last from June to end of August, whereas the late season stage was assumed to correspond to September. The senescence period, characterized by dropping leaves, was taken to last from October to the end of February. The phases are then repeated annually for the 5-year period under consideration. As there was no information about the type of grass growing on the embankment, the duration of the growth stages recommended for grass pasture were used (Allen *et al.*, 1998). The duration of the development stage was assumed to be 30 days and it was only attributed to March of 2006. The grass is then considered to grow throughout the year for air temperatures above -4ºC.

The crop coefficient values for the deciduous trees were selected based on recommendations for apricots, peaches and stone fruit, using the average values provided for the cases of active and no ground cover (Allen *et al.*, 1998). These were $K_{c,ini}$=0.70, $K_{c,mid}$=1.05 and $K_{c,end}$=0.80. For October, the K_c was assumed to decrease from 0.80 to 0.50, remaining constant until February to correspond to the leaf drop period of the trees. The crop coefficients for turf grass were used to calculate ET_c for grass vegetation. The average values between the recommended for cool and warm season turf grass were used. These are $K_{c,ini}$=0.85, $K_{c,mid}$=0.90 and $K_{c,end}$=0.90 (Allen *et al.*, 1998). In order to account for sparse growth under natural conditions, ground cover fraction ratio of 0.6 was used. The resulting crop coefficients are $K_{c,ini}$=0.65, $K_{c,mid}$=$K_{c,end}$=0.70.

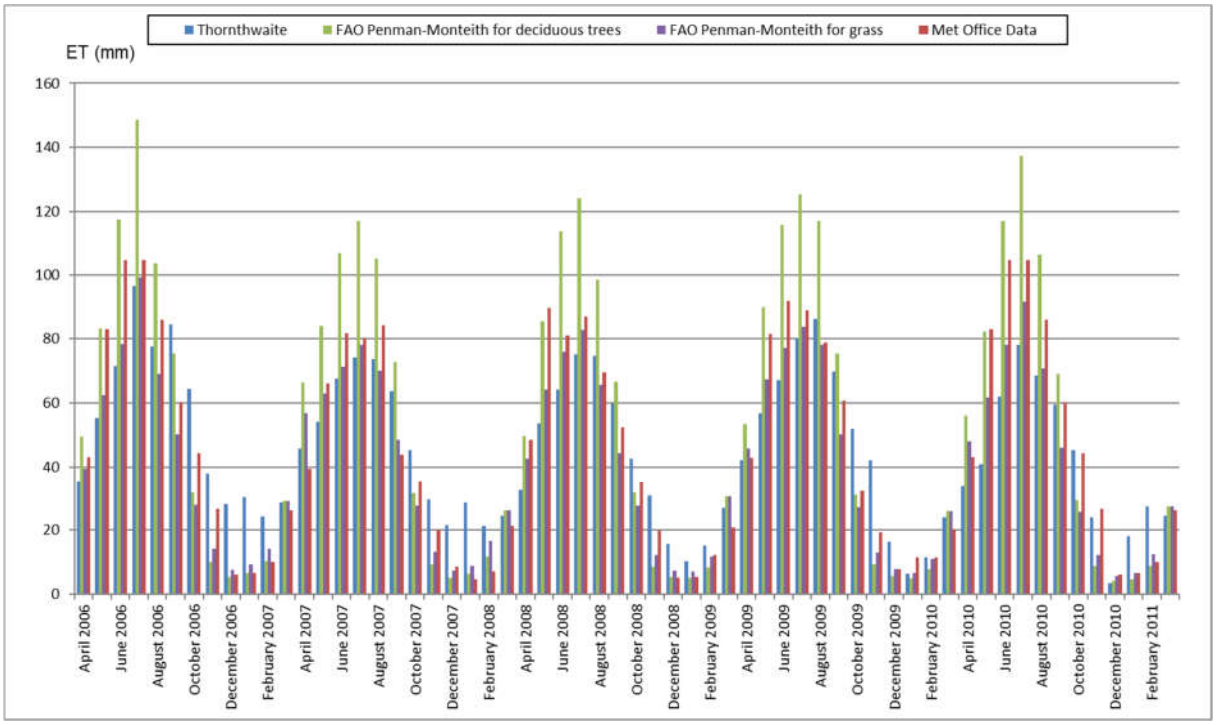

Figure 4.5 Comparison of the monthly evapotranspiration rates for the monitoring period

Comparison of the monthly evapotranspiration rates corresponding to the different calculation methods used, are illustrated in the Figure 4.5. It can be observed that potential evapotranspiration rates for FAO Penman-Monteith method have greatest annual fluctuations, with highest peaks during summer and lowest bottoms throughout the winters. In contrast, yearly changes in potential evapotranspiration obtained on the basis of Thornthwaite's method are less pronounced. Additionally, the FAO Penman-Monteith accumulated annual water outward fluxes significantly exceed those of Thornthwaite and Met Office. The pattern of evapotranspiration is more consistent throughout the years in comparison to the precipitation data.

4.3.2 Displacements

The vertical and horizontal displacements at Section 1 and 2 of the north embankment slope (see Figure 4.6) for the whole monitoring period are shown in Figure 4.7 and 4.8 respectively. All measurement depths shown are from ground level at the top of the installation.

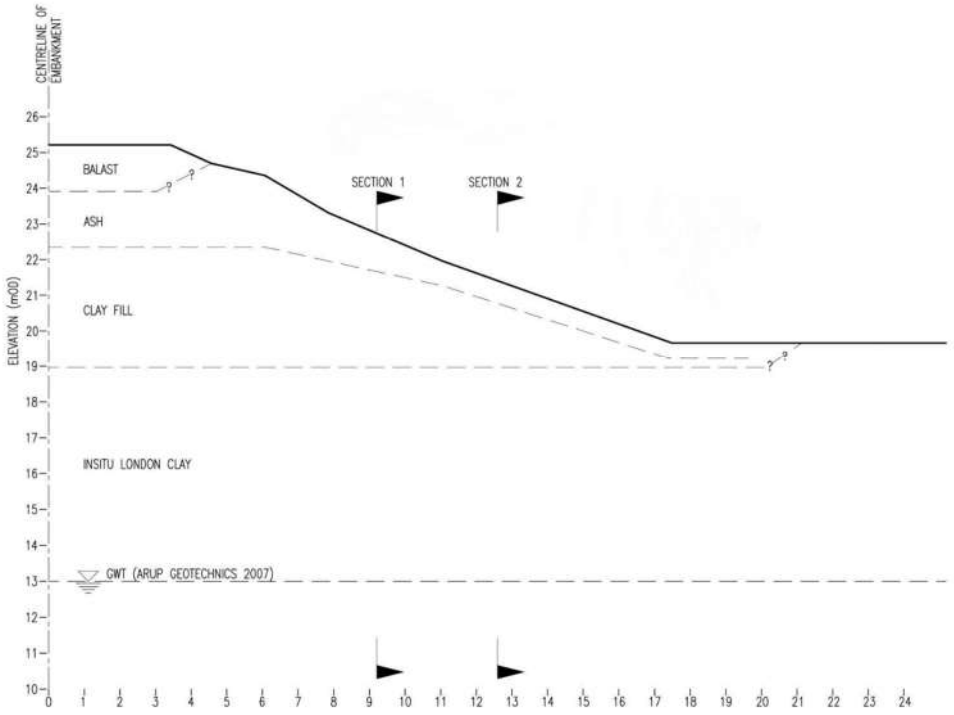

Figure 4.6 Section through north slope of the embankment

Figures 4.7a and 4.8a illustrate the evolution of vertical displacements during the entire monitoring period. During the first summer 2006, when trees were still present on the slopes, downward movements to a depth of around 5 m below the ground surface were observed. The peak of those movements of 40 mm in Section 1 closer to the crest, was reached at the beginning of October. During subsequent autumn and winter, these movements were largely recovered by opposite outward heave. The topmost magnet has returned completely to its original position, while the others have retained some residual settlement, up to 10-15 mm. After vegetation removal in March 2007, heave movements were continuously accumulating through to the end of the monitoring period, reaching at the most 70 mm for Section 1. Rates of heave movements were steadily reducing from June 2008 until March 2011. Some fluctuations in the vertical movements were observed around October 2009 where 20 mm settlement occurred. Correlating this with the rainfall data (Figure 4.4), indicates that observed settlements were triggered by significantly dryer preceding period with rainfall well below average values.

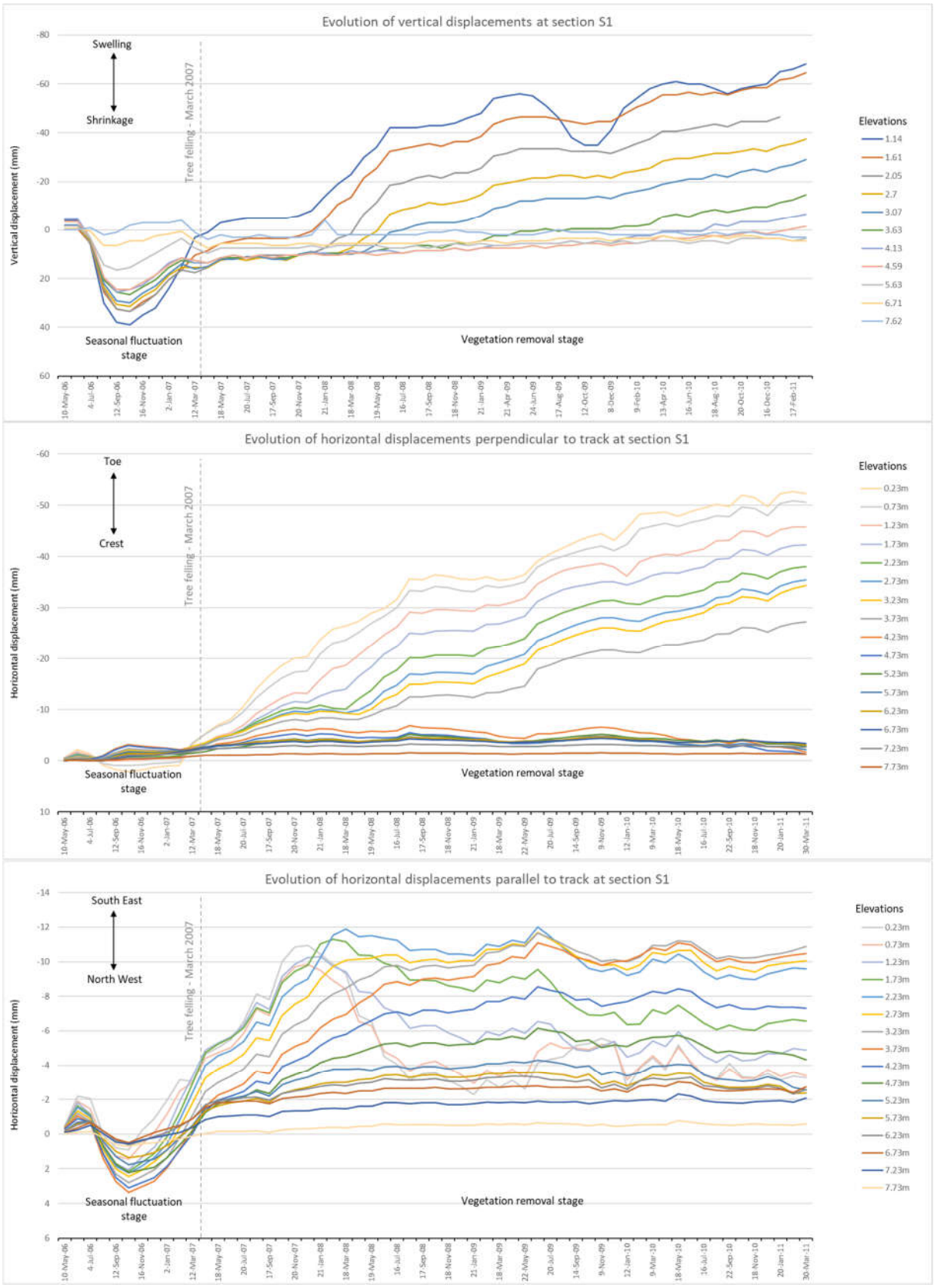

Figure 4.7 Displacements evolution for Section 1 A) vertical B) horizontal perpendicular to track C) horizontal parallel to track

Regarding the Section 2, much smaller swelling movements of the clay fill were recorded. The reason for this could be the fact that this section is closer to embankment toe, beyond which some large trees have remained. The trees are not capable of generating regular seasonal fluctuation at this section, but could possibly mitigate the swelling induced be rainfall infiltration. The magnets 2.5 m below the surface, located within the London Clay foundation exhibit rather peculiar settlements which occur vary rapidly between March and April of each year. The maximum settlement was observed nearing the end of monitoring period, in March 2011, and was around 60 mm. On the other hand, the vertical displacement in the clay fill and ash remains relatively consistent, which indicates that the recording of deeper magnets could be in error.

The vertical displacements for the south section (not illustrated), showed regular seasonal and considerably greater fluctuations, which could be explained by the trees remaining at the toe of the slope and larger evaporation rates for the southerly oriented slope.

The horizontal displacements perpendicular to the railway track at Sections 1 and 2 are shown in Figures 4.7b and 4.8b. Up until the vegetation clearance in March 2007, the magnitudes of horizontal displacements were negligible with no clear trend. Following removal of high-water demand trees there was a steady increase in perpendicular horizontal displacements in outward direction. At the depth corresponding to the clay fill – in situ London clay interface, a discontinuity in perpendicular horizontal displacements was recorded, indicating a possible slip surface. Maximum displacements were observed nearing the end of monitoring period, with magnitudes in excess of 50 mm in direction away from the track.

Figure 4.9 schematically illustrates the evolution of horizontal displacement profiles. As previously stated, the accumulation of relative horizontal displacements within London Clay, close to the interface with embankment clay fill, is progressively increasing from end of summer 2008 (September 2008). This sharp gradient of the horizontal displacement profile indicates that slip surface may be present at this depth.

The displacements parallel to the track are small in comparison to displacements perpendicular to the track (see Fig. 4.7c and 4.8c). The first-year orientation fluctuation and subsequent progression coincide well with the location of the nearest tree.

During the monitoring period, seasonal fluctuation in displacements were shown to be predominantly in the vertical direction. Although, only one full year of monitoring has been conducted prior to vegetation removal, the observed seasonal cyclic shrink/swell movements could clearly be attributed to presence of mature trees on the slopes of the embankment. Additionally, the lack of seasonal cyclic movements following tree felling, supports the aforementioned statement.

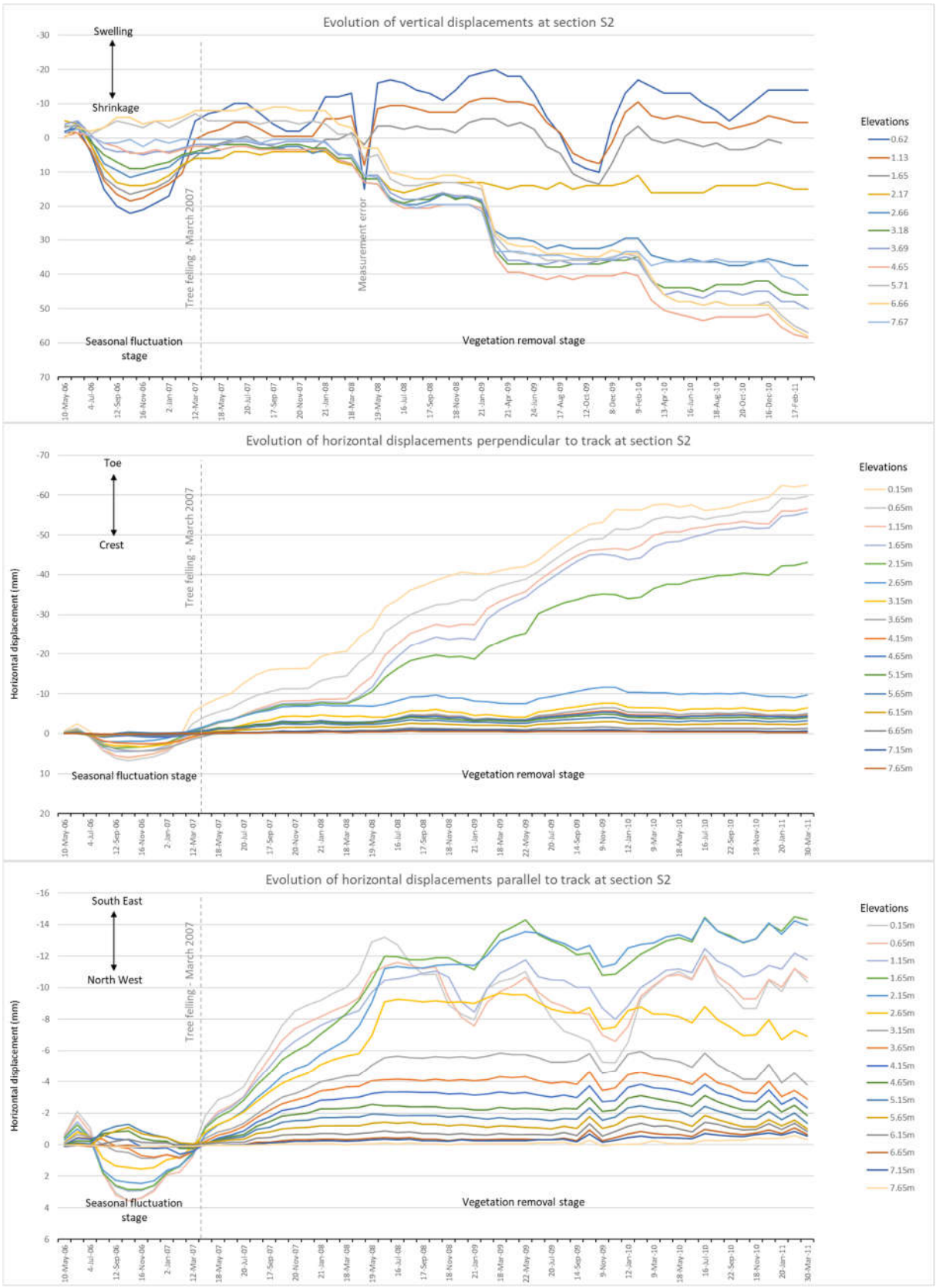

Figure 4.8 Displacements evolution for Section 2 A) vertical B) horizontal perpendicular to track C) horizontal parallel to track

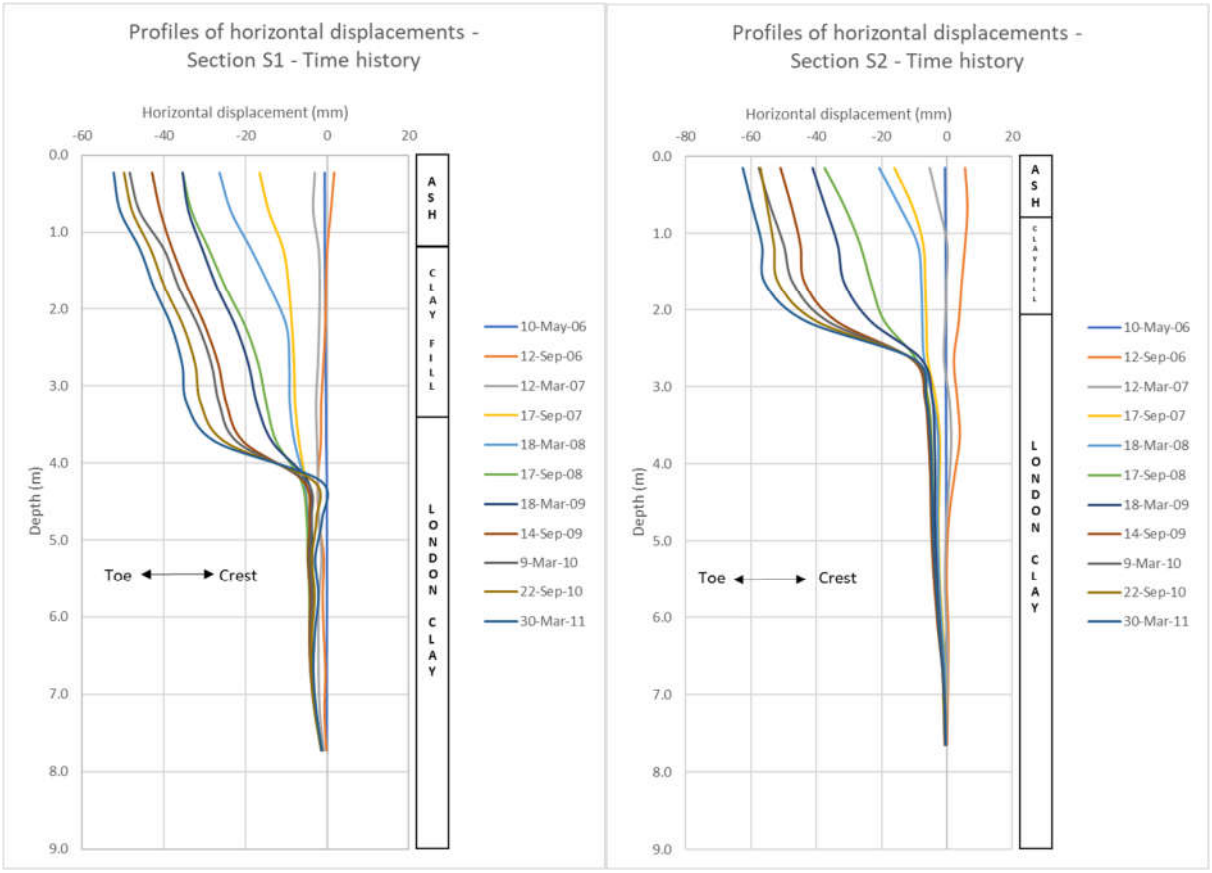

Figure 4.9 Characteristic summer and winter horizontal displacement profiles for the entire monitoring period A) Section, B) Section 2

4.3.3 Pore Water Pressures

The pore water pressure variations within the northern slope were recorded by GeO flushable piezometers (by Geotechnical Observations Ltd). Four of these were installed along Section 1 and two along Section 2. Additionally, one piezometer has been installed at the toe of the embankment and its data has been plotted on the same diagram as data from Section 2. Pore pressure profiles for periods prior and after vegetation removal are depicted in Figures 4.10 and 4.11 respectively.

The graph in Figure 4.10(A) illustrates the pore water pressure variation measured at Section 1 of the embankment slope. Throughout the year, low suctions, up to 20 kPa, were recorded at the ash/clay fill interface. Considerably greater suctions were measured in clay fill and London clay foundation soil materials, ranging from 50 to 95 kPa. The observed difference in measured suctions in ash and clay materials is in agreement with theirs's grain size distributions and retention behaviour. This issue will be discussed later in more detail. The recorded maximum seasonal fluctuation was approximately 35 kPa between 2.5 and 3.5 m depth within the clay fill. The highest suctions were measured in June and the lowest in February/March. In Figure 4.10(B), readings from the piezometers installed in Section 2 are presented. The pore water pressure variation recorded within the clay fill for Section 2 is similar to that of Section 1, with the exception of the measurements corresponding to March. Readings at the lowest elevation on the Section 2 graph, correspond to the piezometer installed near the toe of the embankment. One possible explanation for inconsistently low suction values at this elevation, could be the occurrence of sandy interlayer, as evidenced by the results of CPT test performed from the crest of the embankment (Smethurst *et al.*, 2015).

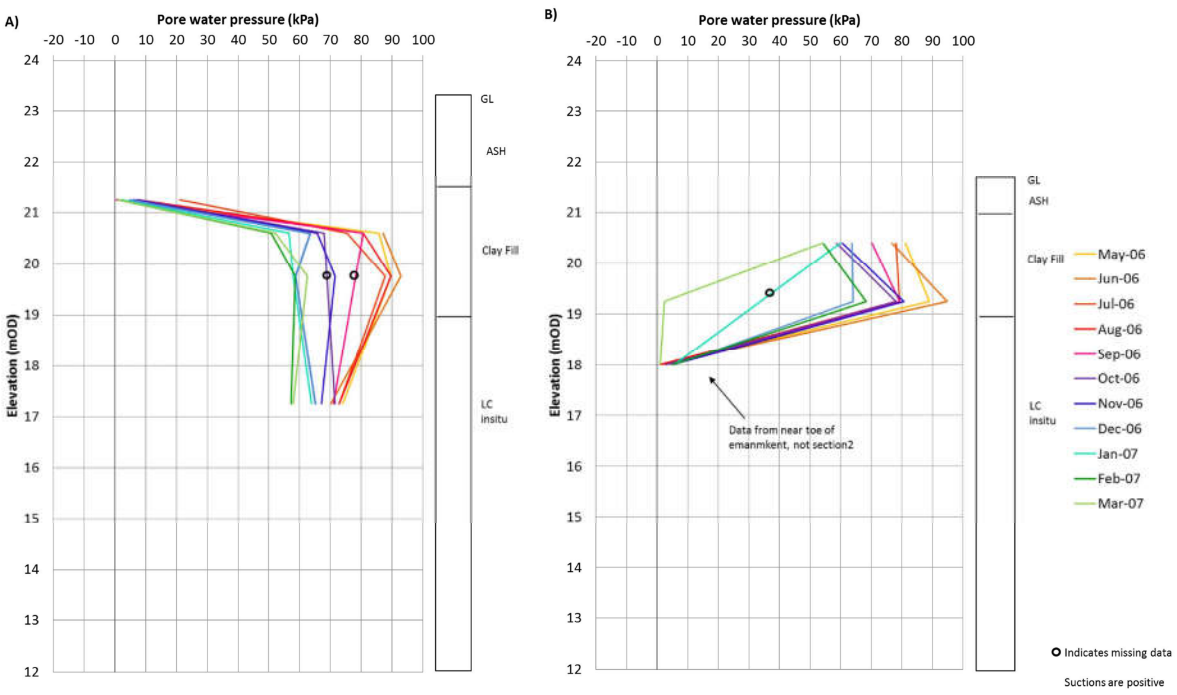

Figure 4.10 Monthly pore water pressure profiles prior to vegetation removal – A) Section 1, B) Section 2 (Chalmers, 2013)

The graphs in Figure 4.11 illustrate the pore water pressure profiles after vegetation removal until the end of monitoring in March 2011. The end of the winter and summer seasons are represented by measurements corresponding to September and March respectively. The profiles obtained for Section1 (Figure 4.11A) show that during the first summer following vegetation removal (2007), despite significantly wetter period with rainfall well above long-term average, suctions were still maintained deeper within the clay fill. This is mainly because wetting front has not reached the depths of 2.8 m and 3.7 m where the piezometers have been installed (see Fig 4.3). In the following years, starting from the winter of 2007/2008, suctions decreased rapidly within the clay fill. Suctions of around 30 kPa recorded in March 2008, closer to the surface (at depth 2.8 m), are probably generated by combination of drier than average winter and higher surface evaporation. Deeper, at the depth of 3.7 m, suctions were already lost, and could not have been recovered by evaporation, whose influence is restricted to the shallow surface zone. From the 2009, compressive pore water pressures between 5 kPa and 10 kPa were measured within the clay fill, at the end of each and every winter season. At the end of summer seasons very small suctions up to 5 kPa were measured in the clay fill. Following vegetation removal and until winter of 2010/2011, suctions were still logged within the London Clay foundation, varying between 35 kPa and 55 kPa and decreasing approximately by 5 kPa each year (readings for the March 2010 are in error (Smethurst *et al.*, 2015)). Piezometric readings of 0 kPa were recorded at the top of the clay fill over the whole monitoring period and were unaffected by vegetation removal. The pore water pressures measured at Section 2 (Figure 4.11B) after vegetation removal were 0 kPa at the clay fill surface. The measurements obtained from the piezometer near the toe of the embankment at 18mOD varied between 5 kPa and -10kPa.

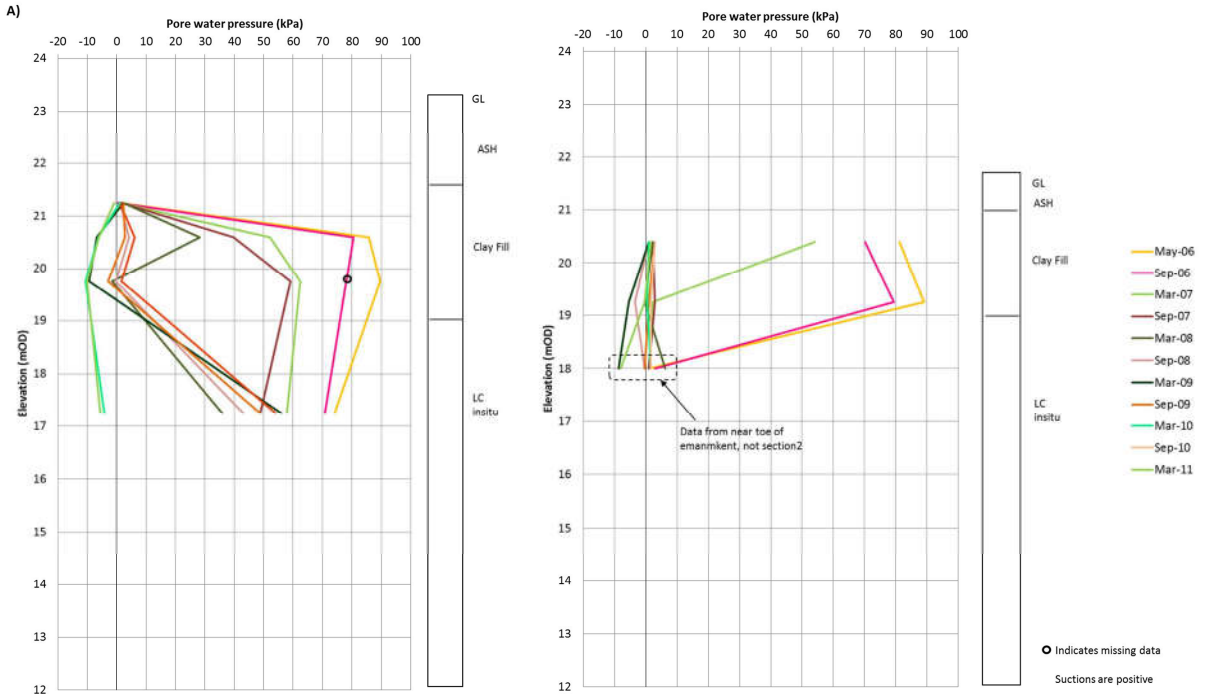

Figure 4.11 Winter and summer season pore water pressure profiles after vegetation removal – Section 1 (A), Section 2 (B) (Chalmers, 2013)

Prior to vegetation removal tensile pore water pressures (suctions) have been constantly recorded over the entire embankment and within the surficial part of in-situ London clay. There was a clear pattern in seasonal hydraulic behaviour, with the highest fluctuations occurring in the clay fill, around 3 m below the surface. Following tree felling, relatively rapid saturation of the clay fill took place, the pwp fluctuation magnitude reduced significantly and was shifted towards zero water stress and closer to the surface. The newly established pore pressure regime is consistent with the "grass" area pore pressure variations as observed by (Scott, Loveridge & O'Brien, 2007). Further progression of the wetting front down the in-situ London clay was distinctly slower, which is consistent with its lower hydraulic conductivity. Particularly, suctions deeper in the foundation soil (piezometer at 5.8 m at Section 1) were maintained for almost four years after tree removal.

Tree clearance at Hawkwell altered seasonal patterns of soil wetting and drying, causing a general increase in soil water content and pore water pressures (more compressive) within the embankment (Smethurst *et al.*, 2015). For the purpose of better understanding of hydrological processes in context of subsequent numerical simulations, the volumetric water content profiles (θ = volume water/total volume) for the Section 1 of the north slope for the first year following tree felling, from (Smethurst *et al.*, 2015), are represented in Figure 4.12.

Sequence of monthly profiles, demonstrates the saturation process of clay fill, induced by rainfall infiltration exceeding evapotranspiration rate. Progression of wetting front (depicted by inclined coloured lines) predicted by neutron probe readings is not as sharp as would be expected in reality, mainly because neutron probe measures the average water content within a sphere of soil of radius ~140 mm.

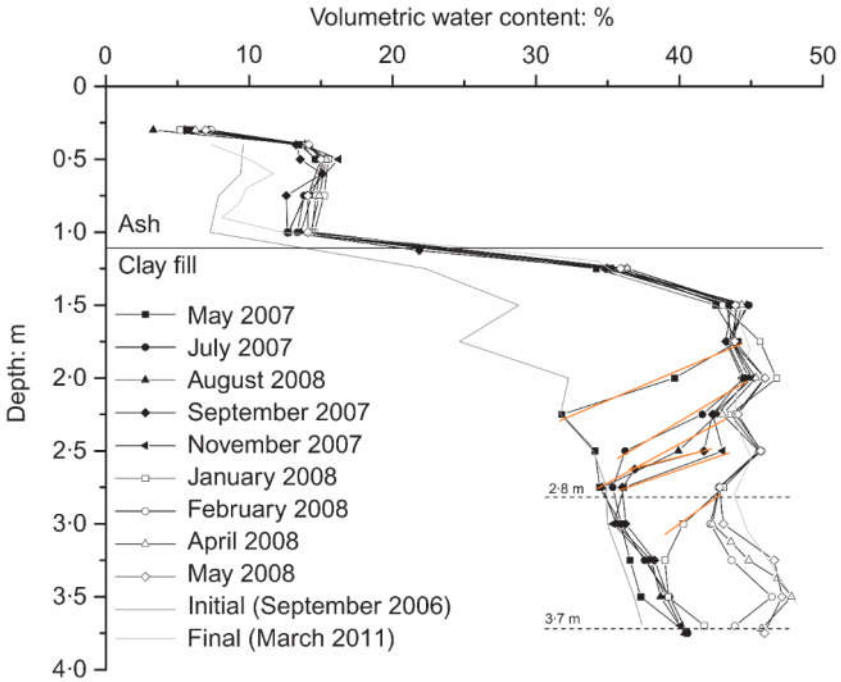

Figure 4.12 North crest volumetric water content variation from May 2007 to May 2008, with initial and final measurements shown for comparison after (Smethurst et al., 2015)

Comparison of the piezometer and neutron probe measurements for the north crest (Section 1) show that the abrupt shifts in pore pressure profiles coincide with the rapid wetting (soil water content reaching saturation state) of the clay fill. The soil profile from 2.8 m to 3.7 m depth reaches saturation ($\theta \approx 45\%$) between November 2007 and April 2008, coinciding with the period in which the pore water pressures also increase significantly. The water content profiles measured after May 2008 show that the soil then remained saturated at 2.8 m and 3.7 m depth, consistent with the continuous measurement of pore water pressures close to 0 kPa over the same period (Smethurst *et al.*, 2015).

The standpipe piezometers within the Hawkwell embankment were not installed to sufficient depth to measure the ground water level, as was demonstrated in (Arup Geotechnics, 2007). Only at one piezometer the ground water table was temporarily observed (at around 7 meters beneath the toe of the embankment), which indicates that there is a fluctuation in the ground water level at the site. However, it was not possible to establish more about fluctuation magnitude.

4.4 Numerical Modelling

The Hawkwell embankment described in detail in previous sections was analysed using Imperial College Finite Element Program (ICFEP) (Potts & Zdravković, 1999). In recent years other researchers have used this embankment and its monitoring data as a benchmark to validate theirs's numerical models. Different approaches have been applied, from simple one dimensional saturated analysis (Papastathis, 2014; Briggs, Smethurst & Powrie, 2014) to more complex 2-dimensional fully coupled saturated (Chalmers, 2013) and 2-dimensional pure hydraulic unsaturated analysis (Briggs *et al.*, 2016). Common for all studies is that advanced hydraulic boundary conditions, which allow for vegetation and infiltration effects to be modelled, have been employed. The main objective of the studies performed by (Papastathis, 2014; Briggs *et al.*, 2016) have been to investigate the influence of mature tree cover and tree removal on embankment hydrology, in particular on pore pressure variations. On the other hand (Chalmers, 2013) fully coupled hydro-mechanical analyses, also provided the insight into the mechanical component of the behaviour (evolution of displacements). All mentioned models were able to simulate overall patterns of hydrological behaviour consistently

with available monitoring data. Main and common limitation was the inability of the models to provide quantitative predictions of the pore water pressures variations. Obtained pwp fluctuations were excessively overpredicted, compared to recorded ones (see Chapter 2).

Therefore, predicting soil-atmosphere interaction is not straightforward, due to the complexity of both the boundary conditions involved and the hydro-mechanical behaviour of soils, which is coupled, highly nonlinear and inherently unsaturated in case of embankments. In order to obtain more "predictive" outputs a different, more advanced approach was followed herein: fully coupled unsaturated flow-deformation finite element analyses have been employed. Such an approach offers considerable advantages in reproducing reality, improving reliability, reducing cost and improving monitoring. Unsaturated hydro-mechanical soil behaviour was represented by appropriate water retention curve, hydraulic conductivity function and partially saturated constitutive model, introduced previously in Chapter 3. Two types of unsaturated constitutive models were applied, specifically simple classic elasto-plastic Mohr-Coulomb type unsaturated model and advanced Barcelona Basic type model. The behaviour of the embankment was investigated in terms of displacements, pore water pressures and water content profiles.

The main objective of this research phase was, to evaluate the ability of this numerical modelling approach to quantitatively reproduce the observed behaviour of the Hawkwell embankment, both prior and after vegetation removal. Particular emphasis was placed on the assessment of the prediction capability of the simple unsaturated model, owing to its more effective practical applicability. In the subsequent Chapter 5, comprehensive parametric analysis was conducted in order to assess the influence of various components of the soil-vegetation-atmosphere system interaction on the performance of this embankment.

4.5 Mesh

The finite element mesh used for the analysis of the Hawkwell embankment is shown in Figures 4.13 and 4.14. Although, some horizontal displacements parallel to the track were observed (probably due to uneven spatial distribution of large trees along the embankment), their magnitude was negligible compared to in-plane displacements. Therefore a 2-dimensional plane strain analysis of the northern half of the embankment was carried out with a line of symmetry assumed through the centre of the embankment. To minimize boundary effects on the area of interest, relatively large (but consistent with general recommendations and the type of analysis) portion of foundation soil was included in the model. The side and base boundaries of the finite element model were located far enough so as not to influence deformations and in particular flow within the embankment slope. As can be seen on Figure 4.14, the mesh was refined closer to the ground surface, in the zones were more highly variable pore water pressures gradients were expected. Remote from the area of interest and where stresses and strains are more uniform, progressively larger elements were adopted. The near surface element sizes were also adjusted in accordance with prescribed maximum root depts, r_{max}. It was demonstrated by (Nyambayo & Potts, 2010), that an element thickness to r_{max} ratio less than 1.0 should not compromise the accuracy of predictions. Vertical far boundary was placed around 100 m away from the toe of the embankment, while bottom boundary extended 120 m below the base of the embankment. The finite element analyses were conducted using isoparametric quadrilateral eight-noded solid elements, with two displacement degrees of freedom at each node, and only one pwp degree of freedom at the corner nodes. By assigning pwp's only at the four corner nodes, same order of variation (linear) between the effective stresses and pore water pressures across the element is achieved.

The upper 3 meters of the foundation soil just below the embankment were treated as unsaturated London Clay but with properties more similar to clay fill material, which is in accordance with the borehole loggings and the fact that the north side toe elevation is well above the south toe part.

For the solution of nonlinear governing equations ICFEP numerical code employs accelerated modified Newton–Raphson solution technique with an error controlled sub-stepping stress-point algorithm.

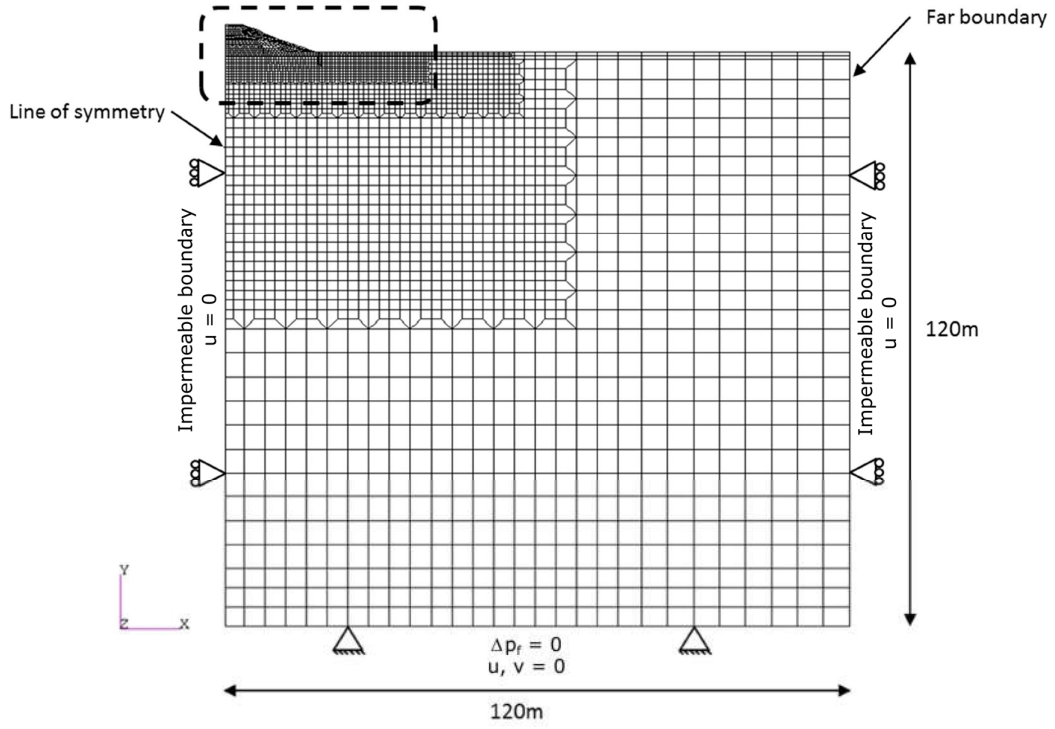

Figure 4.13 Finite element mesh and displacement and hydraulic boundary conditions

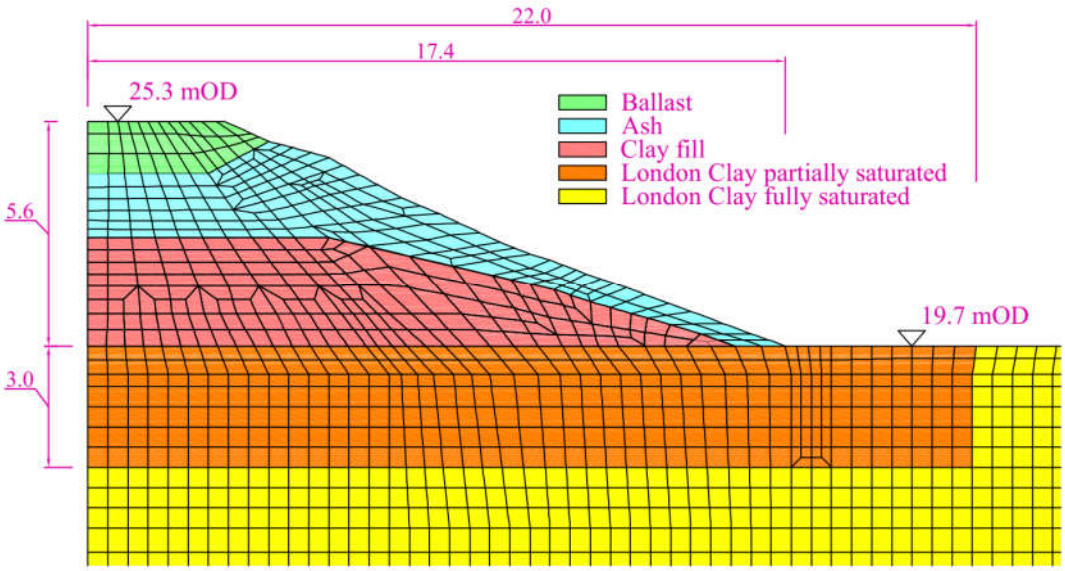

Figure 4.14 Zoomed in view of finite element mesh

4.6 Material Properties

4.6.1 Hydraulic Behaviour

The hydrological soil properties used in the performed analysis are shown in Table 4.1. The ballast at the top of the embankment was treated as drained due to its high permeability. All other stratigraphical units were deemed to be consolidating, and it was therefore necessary to specify appropriate permeabilities *k*. The ash is a granular material with relatively large particles, which grain size distribution resembles closely the one of sandy gravel. Considering that for the ash site specific permeability measurements were not available, the ash was assigned a permeability consistent with a coarse-grained material.

The saturated permeability of the clay fill was adopted from the permeability testing data presented in the work of (O'Brien, Ellis & Russell, 2004). The in situ and laboratory testing results have indicated that dumped clay fill (derived from London Clay) have more than one order of magnitude greater permeability compared to natural London Clay. This difference was attributed to specific internal structure of the dumped clay fill, which is characterized by relatively high permeability matrix that acts as preferred flow path. Due to the fact that dumped clay fills are also inherently heterogenous the variability of material properties is likely to be very high. The Figure 4.15 (left side) from (O'Brien, 2013), reveals the wide range of laboratory and in-situ measured permeabilities of dumped clay fill. Throughout this study, the same saturated permeability for clay fill was adopted, equal to median value based on a total of 58 laboratory and in-situ tests from samples deeper within embankment, presented in the paper (O'Brien, Ellis & Russell, 2004). In paper by (O'Brien, 2013) it was reported that Guelph permeameter tests were carried out at many sites along the UK railway network. The Guelph test results are representative of near surface permeability, and the obtained ones indicate significantly greater permeabilities compared to permeabilities measured at depth within the embankment (two to three orders of magnitude difference). The effect of this higher surface permeability on the overall hydraulic behaviour was investigated, particularly in the vegetation removal stage, as explained later.

Table 4.1 Summary of hydraulic properties used in the main finite element analysis

	Clay fill	**London Clay**	**Ash**	**Balast**
Isotropic/Anisotropic	Isotropic	Isotropic	Isotropic	Free draining
Saturated coefficient of permeability K_0 [m/s]	$2x10^{-9}$	$5x10^{-10}$	$4x10^{-5}$	
Nonlinear permeability model	none	logarithmic	none	
a	/	0.007	/	
Unsaturated hydraulic constitutive model	Van Genuchten type	none	none	
s_{air} *(kPa)*	20	/	/	
a	0.0125			
n	1.5			
m	0.33			

Non-linear isotropic permeability model proposed by (Vaughan, 1994), was assumed for the characterization of hydraulic conductivity of the natural London Clay. High quality permeability

database was assembled over the course of half a century of permeability testing and is illustrated here (Figure 4.15 right side) together with the adopted initial permeability distribution with depth. Non-linear permeability model by (Vaughan, 1994) relates permeability to mean effective stress in a following manner:

$$k = k_0 \times e^{-ap'}$$

where, k_0 is the permeability at zero mean effective stress (m/s), and a is a fitting parameter that has dimensions m^2/kN. It is well known that permeability is actually dependent on void ratio, which is in turn controlled by effective stress. Therefore, the initial void ratio is incorporated into parameter a.

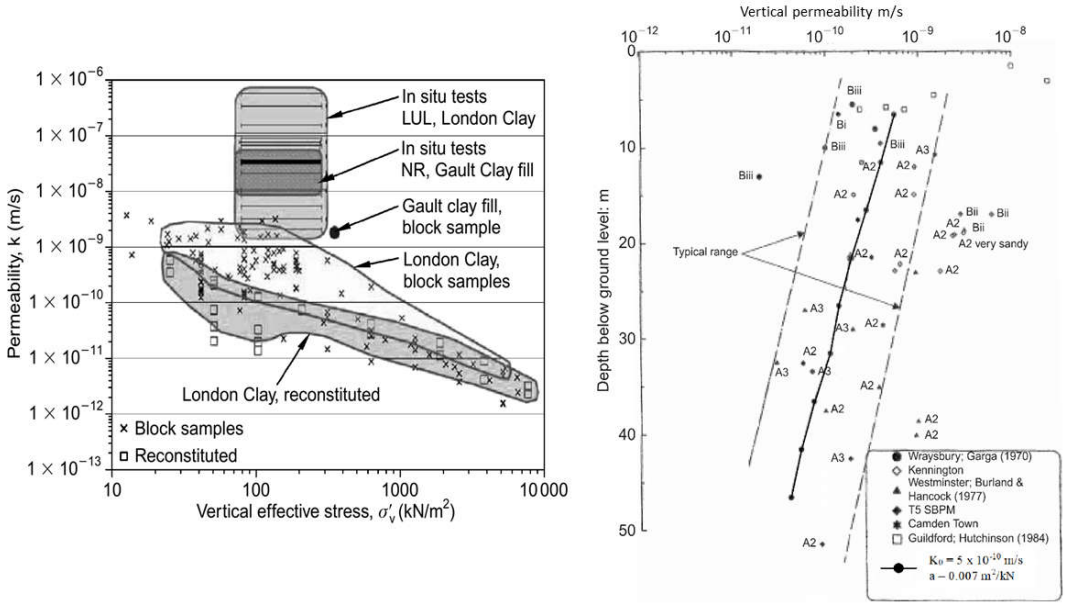

Figure 4.15 Permeability data for A) dumped clay fill (O'Brien, 2013) and B) London Clay from in situ tests (Hight et al., 2003)

Considering that soil is treated as unsaturated, additional constitutive relationships and parameters need to specified, to effectively capture the reduction of water content, degree of saturation and flow rates, resulting from desaturation process. For that purpose, in the current analysis non-hysteretic soil water retention curve (SWRC) available in ICFEP and described in detail in previous chapter was utilised. Beside this rather simplified representation of retention behaviour, numerical code ICFEP possesses more sophisticated SWRC models. These account for the effects of void ratio on the position of the retention curve, as well as the hysteretic behaviour inherent to cyclic suction changes. Although it is generally suggested that advanced unsaturated constitutive models should be combined with advanced formulations of SWRC (Elia *et al.*, 2017), that was not possible within the present analysis. The lack of reliable data required for calibration of additional parameters, prevented the use of such complex retention models.

The shape of the SWRC was deemed as one of the most important factors controlling the key outputs of the soil-vegetation-atmosphere interaction, particularly pore suction distributions. The gradient of the SWRC is crucial in a coupled analysis, because it affects the flow of water generated by the changes in water content. Therefore, the influence of various parameters defining the shape of SWRC is examined within parametric analyses presented in the next chapter.

Considering that laboratory measurements of clay fill SWRC for the Hawkwell embankment were not available, the retention curve for current main analysis was calibrated against in situ

measurements of volumetric water content and corresponding pore water suctions (see Figure 4.16, Run_IR). Compared to primary drying and wetting SWR curves corresponding to reconstituted London Clay established by (Melgarejo, 2004; Croney, 1977) and depicted in Fig 4.16, the adopted clay fill SWRC is characterized by somewhat steeper slope and significantly lower air entry suction value (s_{air}= 20 kPa). This should reflect the specific structure of dumped clay fill, rendered by higher specific volume and much broader pore size distribution curve.

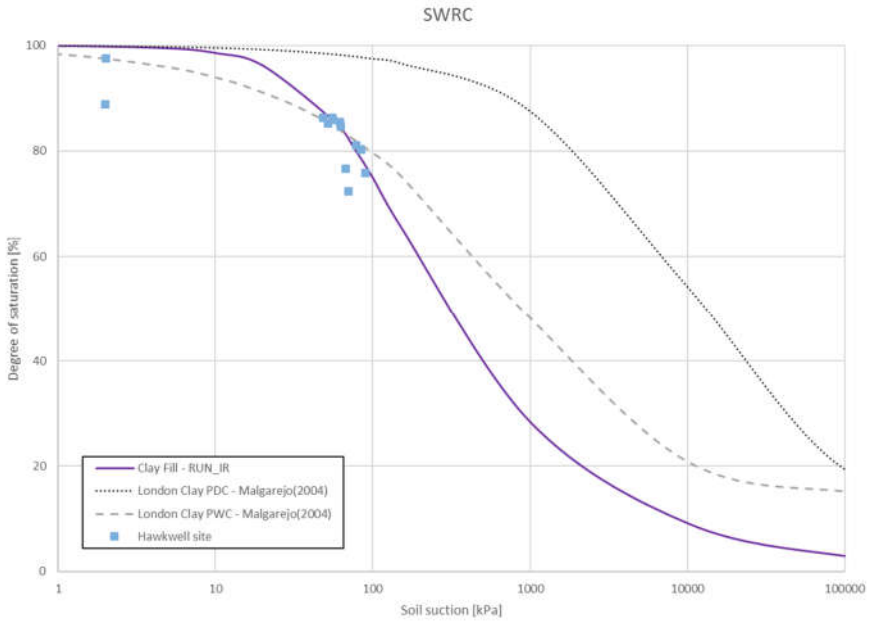

Figure 4.16 Comparison of the adopted and measured drying/wetting SWRC for reconstituted London Clay after (Melgarejo, 2004), together with volumetric water content and suction measurements from Hawkwell embankment

Although it is well documented (Fredlund, 2000), that in the case of unsaturated flow permeability depends on the suction level (or degree of saturation), in the present analysis hydraulic conductivity function was assumed to be constant. Considering that the observed pore water suction magnitudes were relatively low, it was deemed that the reduction of coefficient of permeability due to desaturation would be insignificant. This assumption was further investigated within parametric study, employing two unsaturated permeability models available in ICFEP.

Desiccation cracking represents another important phenomenon which could potentially alter the overall permeability patterns of the embankment slopes. During summer months, when the evapotranspiration rate greatly exceeds rainfall infiltration, shrinking of high plasticity clays takes place. This volumetric contraction generates tensile total stresses, which if exceed soil tensile strength, initiate the opening of cracks and fissures. Cracks formed at the ground surface allow for more rapid infiltration of rainwater during the subsequent winter months, which could generate compressive pore water pressures and compromise the slope stability. Smeared crack model capable of simulating hydraulic conductivity variation due to cracking is implemented into ICFEP. The effects of increased permeability resulting from desiccation cracking on seepage response of Hawkwell embankment are investigated in the next chapter as part of the parametric study.

4.6.2 Mechanical Behaviour

The majority of used stiffness and strength input parameters, of existing stratigraphical units, are not site specific. Rather, they are representatives of similar (in most cases identical) materials sampled

across the railway network and tested extensively in the past. The ash and ballast were assumed to behave as saturated materials and were therefore modelled with a linear elasto-plastic Mohr-Coulomb constitutive model. Stiffness and strength parameters are provided in Table 4.2.

The in-situ London Clay foundation soil was also treated as saturated, except the shallow part just beneath the embankment, as explained earlier when the mesh features were discussed. Considering that the emphasis is placed on slope's serviceability, particularly during the pre-vegetation removal stage of the analysis, simple Mohr-Coulomb elastic-perfectly plastic model is coupled with nonlinear elastic small strain stiffness model. The details of adopted stiffness degradation model are provided in next section. The plastic part of the model was defined by non-associated Mohr–Coulomb yield and plastic potential functions with parameters as given in Table 4.2.

Table 4.2 Basic material properties used in the analysis

Parameter	**Balast**	**Ash**(1)	**Clay fill**(2)	**London Clay**(3)
Model	Mohr-Coulomb	Mohr-Coulomb	Unsaturated Mohr-Coulomb	Mohr-Coulomb
Bulk unit weight γ [kN/m³]	18.0	11.0	18.1	18.8
Shear strength parameters φ [°], c [kPa]	φ' = 40°, c' = 0 kPa	φ' = 35°, c' = 2 kPa	φ' = 22.9°, c' = 5 kPa	φ' = 20.0°, c' = 2 kPa
Angle of dilation ψ [°]	0	0	0	0
Elastic stiffness parameters (E,ν) or (K,G)	E = 30000kPa ν = 0.2	E = 30000kPa ν = 0.3	K = 2000 kPa G = 923 kPa *	**
H modulus [kPa]	-	-	6000***	-

(1)Ash properties from (Arup Geotechnics, 2007)

(2)Clay fill properties from (Arup Geotechnics, 2007; O'Brien, Ellis & Russell, 2004)

(3)London Clay properties from (O'Brien, Ellis & Russell, 2004)

*The parameters values adjusted according to expected strain levels based on (Nyambayo, Potts & Addenbrooke, 2004; O'Brien, Ellis & Russell, 2004).

**Small-strain stiffness parameters used; see next section

***Constant throughout entire suction range

The plastic potential function is defined by the angle of dilation ψ. For all materials the dilation angle was assumed to be zero, because in previous studies on this subject this value was approved to be appropriate. However, care must be exercised with the selection dilation angle values in excess of 0. In a book by (Potts & Zdravković, 2001) it was stated that dilation upon yielding may generate excessively high mean effective stresses, which in turn can drastically lower the permeability value (as demonstrated in previous section). The issue with Mohr-Coulomb plastic potential function originates form the fact that in cases $\psi \neq 0$, once the yield surface is attained the soil will dilate indefinitely, which is in contrast to the real soil behaviour. On the contrary, if no yielding occurs and only the elastic part of the model is active, the adopted value of dilation angle is essentially insignificant.

The clay fill within the embankment was simulated as partially saturated. Although, the embankments are most commonly unsaturated during the construction stage due to the fact that compacted fill materials are intrinsically unsaturated, in later stages during their service life the saturation conditions may change. In the case of Hawkwell embankment, several factors contribute to permanent truly unsaturated conditions. These include relatively deep elevation of ground water table and in particular the fabric (internal structure) of the dumped clay fills. They are characterized by very wide range of

pore sizes. The existence of relatively large void spaces due to the presence of silt and sand fractions and distinct structure, significantly reduces the air entry value of suction, facilitating the desaturation process. An opposite is true for in-situ London clay, which can resist very high suctions (up to 1 Mpa)(Croney & Coleman, 1954), before receding of water menisci into the soil and entering of air commences. Hence, it was justified to model the foundation London Clay as saturated material, despite relatively deep ground water table (after Initialisation stage, see section 4.7). Es explained earlier in section 4.5, the part of the London Clay foundation soil, underneath the embankment, was assumed to be partially saturated. The reason for such decision lies in the fact that, mature deciduous trees were present in a narrow zone beyond the toe of the embankment. These high water demand trees may generate very high suction values within fully saturated coupled analysis as was demonstrated by (Chalmers, 2013). These could trigger instabilities arising from high pore suction gradients between foundation soil beyond the toe and clay fill material within embankment. Considering probable that a wider zone of the foundation soil around embankment has remnants of clay fill and pockets of granular materials, it was deemed reasonable to assume that the mentioned zone would more easily desaturate and behave analogously to clay fill inside embankment. To test this hypothesis, analysis in which the entire foundation soil was treated as fully saturated London clay was performed as a part of a parametric study, presented in Chapter 5. All parameters values for this zone are equal to those specified for clay fill, except stiffness parameters (*K, G, H*) which are ~50% higher.

Two different unsaturated constitutive models available in the ICFEP are applied in two separate analysis. The main goal was to evaluate relatively simple partially saturated model of the Mohr-Coulomb type against more comprehensive one which practical application is limited by a large set of input parameters. Considering that majority of the observed movements are occurring within clay fill embankments and that the measured magnitudes are relatively large (reflecting higher strains), it was deemed inessential to include the small strain stiffness model into elastic part. This would just unnecessarily impede the already excessively non-linear and cumbersome model, prolonging computational time and strongly affecting computer resources. Instead, isotropic linear elastic soil model, specified in terms of bulk modulus *K* and shear modulus *G*, was employed. The prescribed values for two moduli (*K,G*) were derived based on recommendations given in papers by (Nyambayo, Potts & Addenbrooke, 2004; O'Brien, Ellis & Russell, 2004), accounting for expected strain range and average mean effective stress within the embankment.

In the following sections, details of employed mechanical constitutive models are discussed.

Small Strain Stiffness model

In various types of interaction problems when serviceability is of concern, it is of great importance to account for small-strain stiffness nonlinearity. Keeping in mind that Hawkwell embankment is suffering from serviceability issues, related to slope-vegetation interaction, it was judged necessary to incorporate the effects of stiffness degradation into numerical model. Therefore, the pre-peak behaviour of in-situ London Clay was formulated in terms of small strain stiffness model developed by (Jardine *et al.*, 1986) and implemented into ICFEP. It is a nonlinear elastic model in which tangent shear G_{tan} and bulk K_{tan} moduli are dependent on both, current stress and strain levels. The expressions for the two moduli are given in the following form:

$$\frac{G_{tan}}{p'} = \frac{A}{3} + \frac{B}{3}\cos(\alpha X^{\gamma}) - \frac{B\alpha\gamma X^{(\gamma-1)}\sin(\alpha X^{\gamma})}{6.909}$$

$$\frac{K_{tan}}{p'} = R + S\cos(\delta Y^{\mu}) - \frac{S\delta\mu Y^{(\mu-1)}\sin(\delta Y^{\mu})}{2.303}$$

Where:

$X = \log_{10}(\frac{E_d}{C\sqrt{3}})$ $\quad$ $Y = \log_{10}(\frac{\varepsilon_{vol}}{T})$

In the previous equations, $p' = (\sigma_1' + \sigma_2' + \sigma_3')/3$ represents the mean effective stress, E_d is the deviatoric strain invariant $Ed = \frac{2}{\sqrt{6}}\sqrt{(\varepsilon_1 - \varepsilon_2)^2 + (\varepsilon_2 - \varepsilon_3)^2 + (\varepsilon_3 - \varepsilon_1)^2}$, $\varepsilon_{vol} = \varepsilon_1 + \varepsilon_2 + \varepsilon_3$ is volumetric strain, and A,B,C,R,S,T,α,γ,δ,μ are all model parameters, provided in Table 4.3. In addition, model requires the strain limits, as well as minimum stiffness values to be specified. Beyond the strain limit, moduli are dependent solely on the mean effective stress level.

The model parameters are calibrated to match shear stiffness curve measured for the London clay at Terminal 5, Heathrow Airport (Hight *et al.*, 2003). The parameters of the bulk stiffness curve are the same as the ones used by (Kovacevic, Hight & Potts, 2004). The modelled and measured shear moduli together with modelled bulk stiffness curve are illustrated in Figure 4.17.

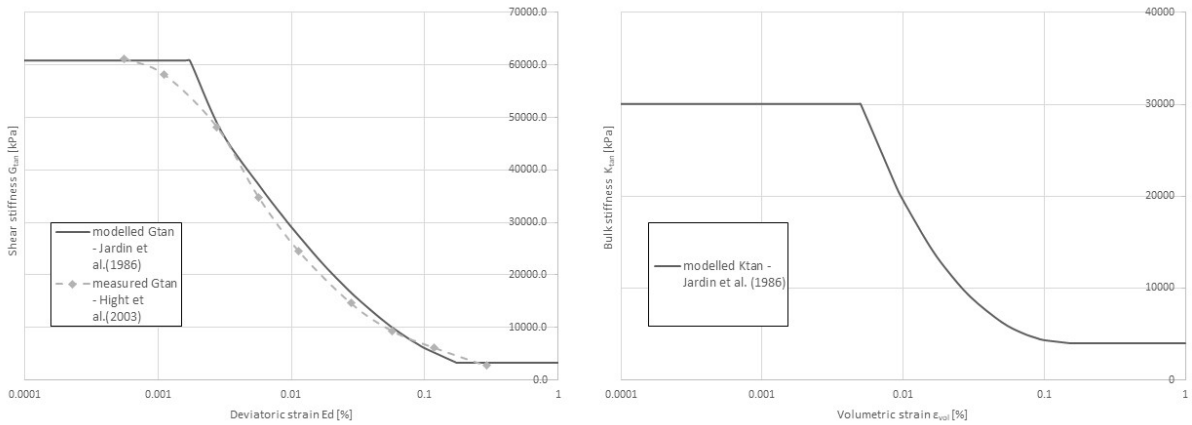

Figure 4.17 Small strain stiffness curves employed for elastic behaviour domain of London Clay foundation soil

Table 4.3 Parameters values of the small strain stiffness model by (Jardine et al.*, 1986)*

Shear	**A**	**B**	**C [%]**	**α**	**γ**	**$E_{d,min}$**	**$E_{d,max}$**	**G_{min}**
	970	890	0.001	1.47	0.7	0.00173	0.173	3333.3
Bulk	**R**	**S**	**T**	**δ**	**μ**	**$\varepsilon_{v,min}$**	**$\varepsilon_{v,max}$**	**K_{min}**
	772.5	712.5	0.001	2.069	0.42	0.005	0.15	4000

As a part of this research the same nonlinear elastic model with another set of parameters fitted to reproduce the stiffness degradation curves provided by (O'Brien, Ellis & Russell, 2004) was investigated. The results were insensitive, therefore not reported later in the discussion. The goal was to evaluate the impact of nonlinear elastic stiffness on the seasonal deformation behaviour of embankment.

Besides, the employed model (Model 2), ICFEP within its database possesses other small-strain stiffness models. In the study by (Chalmers, 2013), it was shown that the effect of the selected small-strain stiffness model has little to no effect on the predicted pore water suctions. The effect on the computed displacements was somewhat more pronounced, whereby "Model 2" has most realistically reproduced observed displacement patterns.

Partially Saturated Mohr-Coulomb Model – ICFEP Model 82

In recent times, constitutive modelling of partially saturated soils is getting ever increasing attention from numerical geotechnical research groups. Some of the most common applications include analysis of rainfall triggered landslides and geological disposal of nuclear waste (in particular thermo-hydro-mechanical (THM) behaviour of compacted bentonite buffers). More sophisticated partially saturated soil models usually require increasingly more parameters to be defined. These parameters are sometimes functions of matric suction, water content or degree of saturation but are sometimes empirical and do not have direct physical meaning. Another drawback in their application represents the fact that experimental measurements are often very time consuming and require very complex unconventional testing equipment. Therefore, the higher order unsaturated model parameters are difficult and costly to obtain. For that reason, there must be a compromise between accuracy and practicality. When considering infrastructure slopes, where there may be so many inherent variables within the material of the slope, there is no practical advantage in using more complex constitutive models. Therefore, it is clear that at some point increased accuracy offered by additional complexity of the constitutive model will be outweighed by the practicality in obtaining the specific data. This will then lead to uncertainty in the material parameters.

One of the primary goals of the current research is the assessment of the capability of quantitative predictions of hydrological aspects of embankment behaviour (especially pore suction values), which has proven to be a common limitation of all previous studies on this topic (Chalmers, 2013; Papastathis, 2014; Briggs *et al.*, 2016). As it is expected that embankment hydrology is dominantly governed by hydraulic soil properties, it is deemed that advanced mechanical constitutive models would provide a limited increase in accuracy but with the added complexity of defining significantly more parameters for which data are scarce. Therefore, simple partially saturated Mohr-Coulomb model, with only one additional parameter *H*, governing deformations due to changes in matric suction, was assumed to be satisfactory for the established goal. Additionally, since the base model is relatively simple, it was anticipated that this would make it easier to understand the influence of the unsaturated aspects of behaviour and identify key parameters governing the embankment hydrology patterns.

As was explained earlier in Chapter 3, partially saturated Mohr-Coulomb model, beside standard parameters, requires the specification of variation of *H* modulus with suction. Since there was no reliable data on the value or variation of the *H* parameter, a constant value was set, regardless of suction level. The assigned value was calculated on the basis of elastic stiffness parameters (Young's modulus and Poisson's ratio) from the following relationship, derived from consistency requirement between saturated and unsaturated elastic constitutive relation of the soil structure:

$$H = \frac{E}{(1 - 2\nu)}$$

The expression is valid for the range of suction values from zero to air entry value, for which soil is basically saturated in spite of water stress being inherently tensile. The established H value is essentially correct for the air entry value of suction, and therefore this value is taken to apply for the entire pore suction domain.

Modified Barcelona Basic Type Model – ICFEP Model 81

The Barcelona Basic type model, modified by (Georgiadis, 2003) was used as part of this study to simulate the mechanical behaviour of clay fill. The original BBM was developed by (Alonso, Gens & Josa, 1990) and represents the elasto-plastic constitutive model for unsaturated soils that has been most commonly used to date. However, its application is generally restricted only to geotechnical research community. The possible contributory factors include the uncertainty in selection of BBM

model parameters based on laboratory testing results and questionable robustness of parameter value selection procedures (D'Onza *et al.*, 2015).

The Model 81 implemented into finite element code ICFEP requires a minimum of 23 parameters to defined in the pre-processing stage. The significantly greater number of model parameters compared to original BBM is primarily linked to the extended (Lagioia, Puzrin & Potts, 1996) expression, which allows reproduction of wide range of yield and plastic potential surfaces. For the purposes of the calibration of model parameters an adequate testing programme is needed, and should include in minimum the following laboratory tests:

- one fully saturated undrained triaxial compression test from which parameters M_g, M_f and G could be derived. If the shapes of yield and plastic potential surfaces are also required, additional triaxial compression tests, both on the wet and on the dry side of the critical state, should be undertaken, in order to calibrate the α_i and μ_i;
- one fully saturated isotropic or K_0 loading and unloading test to establish the parameters $\lambda(0)$, κ, v_1 and p_0*;
- two isotropic or K_0 compression tests at different suction levels to obtain the parameters r, β and α_c;
- one drying/wetting cycle at constant mean net stress to determine the SWRC and the parameters s_{air}, s_0, κ_s and λ_s;
- one unsaturated drained triaxial compression test. This test is optional and is not required if the increase in apparent cohesion is assumed to vary with the degree of saturation S_r.

In this thesis the calibration exercise of Model 81 was based on the data published in the work of (Monroy, 2005). In his thesis the author performed a number of conventional and osmotic oedometer tests on reconstituted and compacted London Clay. The osmotic oedometer tests allow water stress (suction) to be controlled, and thereby different combinations of stress paths and strain states were simulated. These include loading/unloading cycles at constant suction, wetting/drying cycles under constant confining (vertical) stress and wetting paths under no volume change.

The Model 81 parameter values adopted throughout this study are given in Table 4.4.

Table 4.4 Model 81 parameters values

Model 81 parameter	Value	Description	Model 81 parameter	Value	Description
α_g	0.4	Plastic Potential function parameters	κ_s	0.07	Elastic coefficient of compressibility for suction changes
μ_g	0.9		λ_s	0.3	Coefficient of compressibility for suction changes
M_g	0.89	Slope of the critical state line in the q–p space for triaxial compression	ν_1	2.75	Specific volume at unit pressure for fully saturated conditions
α_f	0.4		χ	1	Factors the coefficient κ_s
μ_f	0.9	Yield surface parameters	ω	0	Controls the effect of S_r on the coefficient $\kappa_s^*=(\kappa_s)^{\chi}\cdot(S_r)^{\omega}$
M_f	0.89		s_{air} (kPa)	20	Air-entry suction value
α_c	1.98	Characteristic stress ratio	s_0 (kPa)	1.0E+6	Yield suction
$\lambda(0)$	0.152	Coefficient of compressibility for fully saturated conditions	p_{atm} (kPa)	100	Atmospheric pressure
κ	0.02	Elastic Coefficient of compressibility (along elastic paths)	OCR	10	Overconsolidation ratio
r	0.45	Maximum soil stiffness parameter	K_{min} (kPa)	2000	Minimum bulk modulus
β	0.011	Soil stiffness increase parameter	μ	0.35	Poisson's ratio
k	SWRC	Cohesion increase parameter r			

The model features and meaning of individual parameters are explained in detail in Chapter 3.

The associated plasticity was assumed, and therefore same set of values was assigned to both yield and plastic potential parameters α_i, μ_i and M_i. Adopted values of α_i, μ_i parameters produce the shape of the yield curve that very closely resembles an ellipse of the MCC (Modified Cam Clay) model. The inclination of the critical state line, M_g, was derived from the critical state angle of shearing resistance of the clay fill.

Adopting the α_c instead of p_c means that the bi-linear isotropic compression line (ICL) is employed, rather than linear, which more realistically captures the amount of potential collapse upon wetting. The fully saturated coefficients of compressibility are calculated from compressibility and swelling indices obtained by (Monroy, 2005) based on data from classical oedometers tests, $\lambda(0) = {}^{C_c}/_{2.303}$ and $\kappa \cong {}^{C_s}/_{2.303}$.

The parameters defining the shape of the loading collapse (LC) curve, r and β, are derived based on the geometry of the LC line established by (Monroy, 2005), based on the shape of the isotropic compression and swelling lines at different values of suctions. The three LC curves with same r and β values but different initial hardening parameter p_0*, fitted to match the data from (Monroy, 2005), are depicted in Figure 4.18. Generally, the anchoring position of the LC curve, p_0*, depends on the choice of the OCR value, and current isotropic yield stress p_0, which in turn is a function of current suction level. It is well known that the surficial layers of London Clay, from which the fill material was sourced, are highly overconsolidated due to unloading caused by massive erosion (Grammatikopoulou, Zdravkovic & Potts, 2008). Therefore, an OCR value of 10 was adopted in the present study.

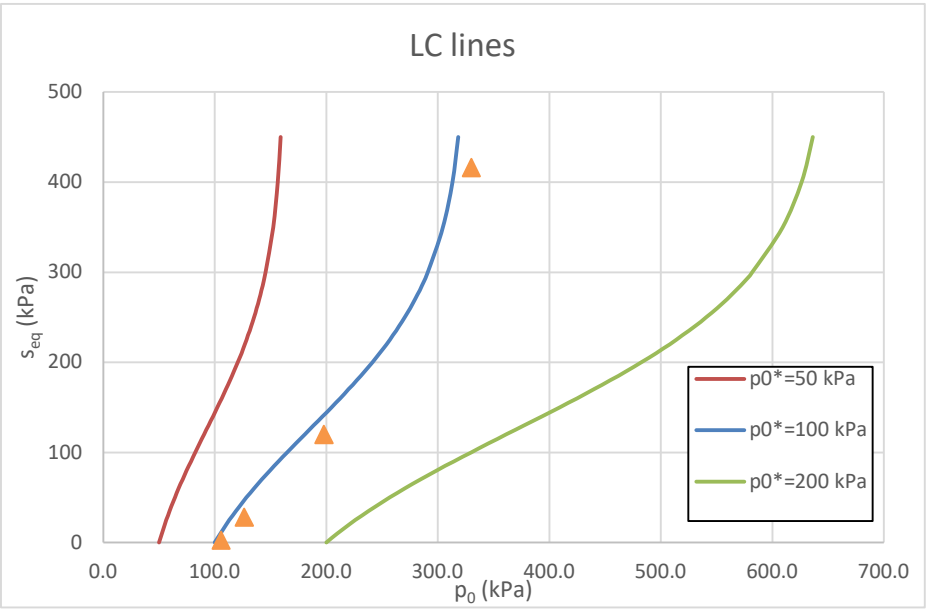

Figure 4.18 Family of loading collapse (LC) yield curves based on r and β values used in the performed analyses

The evolution of slope of isotropic compression line (ICL) with suction is schematically illustrated in Figure 4.19. It can be seen how the stiffness progressively increases with suction. The rate of increase is controlled by parameter β.

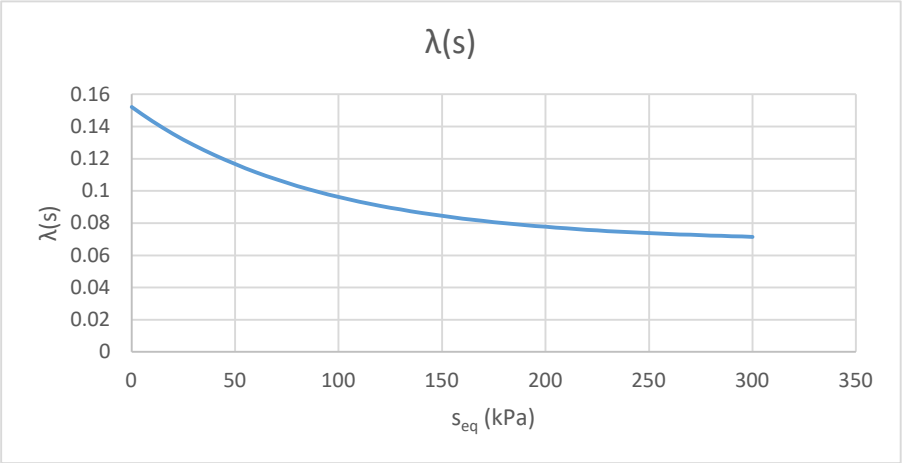

Figure 4.19 Coefficient of compressibility vs suction relationship

It should be noted that very high value was assumed for secondary hardening parameter s_0, which translates to the fact that the adopted value of plastic coefficient of compressibility related to suction changes λ_s is practically irrelevant. Considering that the suction range expected in the analyses is well below the prescribed s_0, the secondary yield surface will not be violated, and therefore the assigned λ_s will not be used by the code. This observation is illustrated in Figure 4.20.

The elastic coefficient of compressibility related to suction changes κ_s, was deemed to be the parameter of utmost importance for the present analysis. This is particularly true for seasonal fluctuation stage prior to vegetation removal, which is characterized by successive cycles of wetting and drying. Considering that external loading is essentially constant throughout the analysis, cyclic variations of suction represent primary stress paths associated with the soil-vegetation-atmosphere system interaction. Therefore, special attention was given to calibration and interpretation of κ_s parameter. The value adopted is based on tests of consecutive wetting and drying tests under constant vertical stress, conducted by (Monroy, 2005), the results of which are presented in the Figure 4.21. As can be seen, the mean value of the slopes of two suction induced compression lines 0.07, was adopted for the main analysis. The effect of this parameter is further investigated as part of the parametric study presented in Chapter 5.

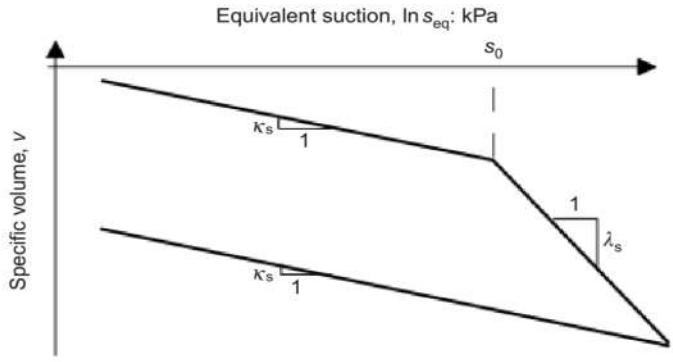

Figure 4.20 Elastic and plastic compressibility coefficients κ_s and λs (Georgiadis, Potts & Zdravkovic, 2005)

The air entry value of suction was assumed to be 20 kPa, in order to be in compliance with the previously defined SWRC. Under unsaturated conditions, apparent cohesion was assumed to be a function of degree of saturation. This option more realistically simulates the rapid increase in apparent

cohesion in quasi-saturated region and later stabilisation and asymptotical approach towards some limiting value as desaturation progresses.

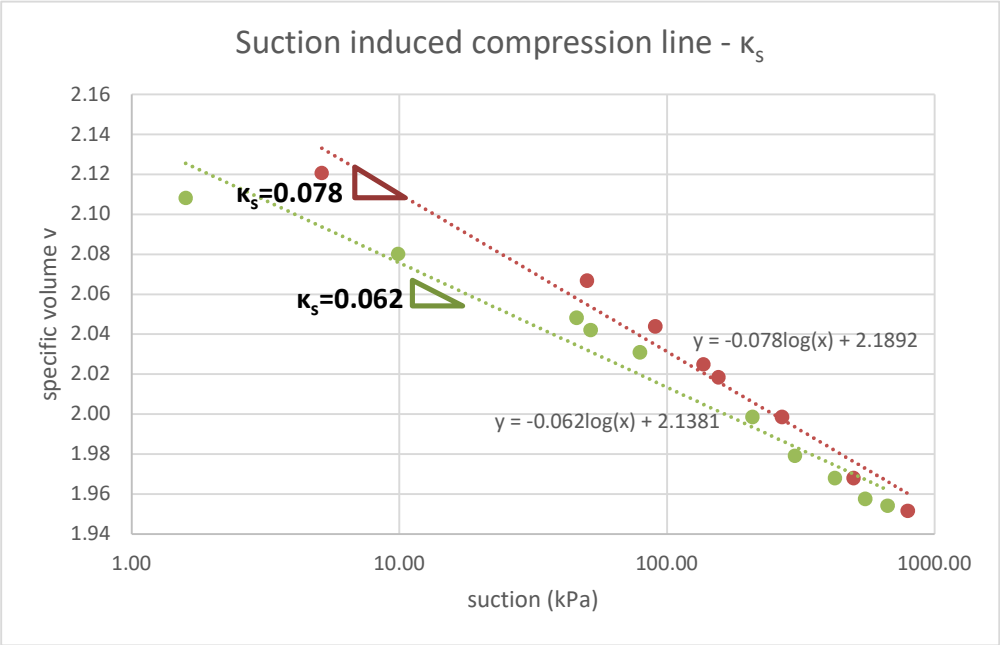

Figure 4.21 Suction induced compression lines, after (Monroy, 2005)

4.7 Sequence of Analysis

The sequence of finite element analyses is illustrated in Table 4.5. All phases/conditions of the embankment's working life that were considered relevant, are included into the analysis. The analysis stages were systematically assembled in order to replicate as closely as possible previous stress and strain history of Hawkwell embankment.

Table 4.5 Sequence of analyses

Increment number	Description of analysis stage	Duration
0	Setting of the initial conditions	-
0	Deactivation of the elements representing the embankment	-
1-17	Construction of the embankment	6 months
18-29	Increments not used – reserved for some trial analysis steps	-
30-605	Initialisation	4 years
606-749	Seasonal flustuation stage – first year of monitoring period	1 year
750-1325	Vegetation clearance	4 years

4.7.1 Initial Conditions

Definition of initial soil state is of great importance, especially when advanced elasto-plastic constitutive models are employed. Therefore, all geo-hydro-mechanical process, that were thought to be relevant, were appropriately taken into account.

In the initial conditions, at increment 0, only the London Clay foundation layer was activated. The stress state was initialised employing a unit weight of 18.8 kN/m^3 above and below the ground water table (GWT) and appropriate K_0 profile. The coefficient of earth pressure at rest K_0 was assumed to vary linearly from the ground surface to a depth of 15 m, below which it was assumed to be constant. The K_0 value at the ground level was 2.1, reducing to 1.0 at 15 m depth. The excessive K_0 values indicate highly overconsolidated strata, typical to London Clay basin. The overconsolidation is a consequence of unloading triggered by the massive erosion that occurred in the late Tertiary and Pleistocene times. As reported by (Chandler, 2000) the estimated amount of eroded overburden was in the range of 200 m. The assigned K_0 profile has been proven by both experimental testing (Hight *et al.*, 2007) and numerical simulations (Tsiampousi *et al.*, 2014). In her paper (Tsiampousi *et al.*, 2014), studied the effect of previous stress history on K_0, investigating various unloading/reloading scenarios. Additionally, the seasonal effects of wetting and drying, caused by combined influence of rainfall infiltration and vegetation, on the K_0 evolution were also examined. The results demonstrate that the effects could be significant, particularly in surficial shallow zone, where during dry seasons outward transpiration fluxes generate high suctions which in turn act as reloading event, thereby inducing an overall decrease in K_0 value. However, it was also demonstrated that the effect of vegetation is likely to be erased by subsequent deposition and concurrent rise of the ground water table.

The pore water pressure profile before the embankment construction was assumed to be hydrostatic, with the groundwater table located at 1m depth, resulting in a suction of 9.81 kPa at the surface. The assigned value of suction matches the average value measured in-situ across the UK (Vaughan, 1994). The adopted position of the initial phreatic surface was found to have no effects on the pore water pressures at the beginning of the monitoring period. As explained later, initialisation stage compensates for differences in assigned initial water levels, and allows pore water pressure regime consistent with long-term environmental effects to be established.

4.7.2 General Boundary Conditions

The prescribed displacement and general hydraulic boundary conditions, excluding vegetation and precipitation, used throughout all analysis stages are illustrated in Figure 4.13. The bottom boundary of the mesh was assumed to be rigid with prescribed zero displacements in the vertical and horizontal directions. For the line of symmetry and the far boundary, the displacements were fixed at zero in the horizontal direction and free in the vertical direction.

The vertical boundaries of the mesh were assumed to be impermeable (no flow boundaries). For the bottom boundary of the FE mesh it was assumed that pore water pressures remain unchanged from the initial state. Therefore, zero incremental pore water pressure Δp_f=0 was specified along the base of the model. The impermeable lateral boundaries allow water table to fluctuate vertically, while the constant water pressure at the base allows groundwater recharge according to regional hydrogeological conditions.

4.7.3 Construction of the Embankment

Prior to the construction, elements of the mesh representing the embankment need to be deactivated. This is done through fictitious excavation, which excludes the prescribed finite elements but without applying equivalent forces at the interface between excavated and unexcavated materials.

The simulation of embankment construction is performed over 17 increments, with a total duration of 6 months. Firstly, clay fil was constructed in 8 layers (increments 1-8), then ash in 6 layers (increments 9-14) and finally construction of ballast was performed in 3 layers (increments 15-17). The assumed construction duration is not entirely representative of end-tipping technique, characterized by very rapid erection and thereby negligible consolidation of foundation soil at the end of construction. However, considering that aim of the initialisation stage, explained in detail later, was to approximately capture 120 years following construction of the embankment until the start of monitoring, it was deemed that the prescribed construction time was generally insignificant.

Over the increments in which the elements are constructed, the numerical code ICFEP by default assumes linear elastic material behaviour, with a Poisson's ratio υ=0.45 and a Young's modulus $E = 0.0001 \times E_{min}$. Modulus E_{min} is the minimum prescribed value of E for all materials present in the analysis. Immediately after construction, displacements, strains and void ratios within the constructed elements are reset to zero, and also valid material properties are assigned. During construction, the surface boundary was modelled as a no flow boundary.

The ash and the clay fill were constructed with an initial suction of 50 kPa. The assumed magnitude of suction represents an average value for fill material excavated from a nearby cutting of typical depth of 5m. In his thesis (Nyambayo, 2004), argues that for materials sourced from deeper elevations, like in case of tunnel excavations, the suctions generated due to stress relief would have been higher. However, frequent precipitation, common to the UK, during transport and handling phases would definitely reduce suctions to some extent. Therefore, a value of 50 kPa was considered sensible.

Due to the construction methods introduced in the Chapter 2, the clay fill initially (upon construction) probably had low lateral earth pressures and a high void ratio. Therefore, clay fill and ash were assigned the initial void ratio of 1.0 and the initial coefficient of earth pressure at rest K_o equal to 0.5.

4.7.4 Initialisation

The purpose of the initialisation stage was to cover as realistically as possible 120 years of embankment existence prior to the start of monitoring, but at the same time without overly compromising the analysis duration.

It is well documented (Smethurst *et al.*, 2015), that until 1960s, the embankment slopes were regularly maintained. The primary task included vegetation maintenance (clearance and felling operations), in order to reduce the risk of fire, given that steam locomotives were the predominant type of railway transport vehicles. In 1968, the electrification of British railway was completed, which resulted in the end of vegetation management. This allowed large mature trees to establish themselves on the slopes of the embankments. In preliminary-trial analyses the establishment of vegetation was simulated by allowing the embankment to consolidate/swell for 5 years under suction of 10 kPa acting along the embankment slope and top of the foundation soil. Swelling was simulated in finite element analysis by applying increments of time Δt, without changes to other boundary conditions. However, inclusion of this transitional phase had no real impact on the later analysis stages, and was therefore omitted from further simulations.

In order to achieve the initial conditions that were present on site at the start of monitoring, 5 years of combined effect of rainfall and vegetation was applied to simulate the environmental effects. It has been proven (additional trial analysis lasting 10 years was also conducted, but not reported) that five years is enough to establish a stable pore water pressure and stress regime that reflects the effect of precursory precipitation and evapotranspiration. A similar conclusion has been drawn by (Tsiampousi, Zdravkovic & Potts, 2017), who in their study simulated climate/vegetation effects for a period of 9 years, to establish initial conditions prior to excavation of a generic cutting. The last

fifth year of the initialisation stage, was treated as the pre-vegetation removal phase of the conducted embankment monitoring (referred to later as seasonal fluctuation stage), for the purpose of results discussion.

The hydraulic vegetation and precipitation boundary conditions, explained in Chapter 3, were utilised for this purpose. Monthly climatic data (rainfall and evapotranspiration) were used, with each month simulated using 12 increments, as suggested by (Nyambayo, 2004) for computational stability reasons. The use of monthly precipitation and evapotranspiration data was considered adequate, especially since the main goal was to assess the long-term embankment performance in response to recurrent cycles of wetting and drying. However, the adopted approach is ineffective in the case when embankment response to short-term extreme rainfall events is pursued, which was not the scope of this research.

The precipitation boundary condition (BC) simulating inflow of water due to rainfall was applied over the top surface of the ash, clay fill and London Clay foundation. The ballast material was considered drained throughout the analysis and so precipitation BC was applied along the internal interface between the ash and the ballast. The position of precipitation BCs is schematically illustrated in Figure 4.22. From the Figure it can be seen that the precipitation flow rate assigned at the ballast-ash interface was taken as 50% of the rainfall applied at the slope surface. It was assumed that some of the infiltrated water would be intercepted within the ballast, and that only half of the total precipitation would reach the ash layer. Interception by the vegetation canopy was not included in the analysis. The onsite measurements of the amount of water intercepted by plant leaves were not available. Based on the assumption of complete rainfall interception and a daily canopy storage capacity of 1 mm for an Oak tree for full leaf coverage (Rutter & Morton, 1977), approximate interception loss measures around 10-15% of the total annual rainfall. This means that the prescribed precipitation rates are greater than the amount of rainwater actually reaching the ground surface, especially during late spring and summer months when leaf area index is high.

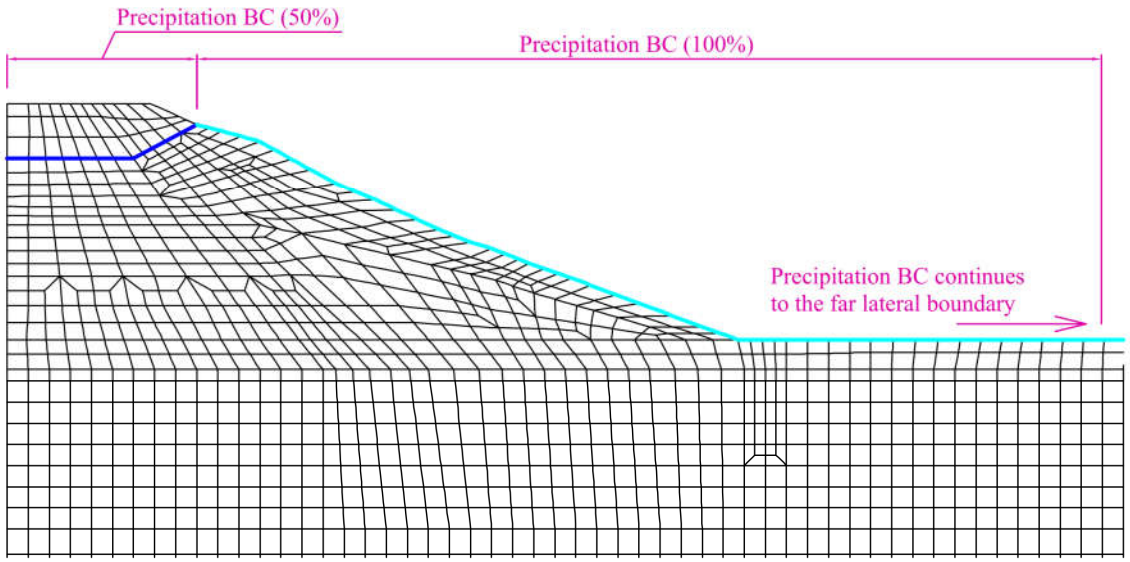

Figure 4.22 Contours of precipitation boundary condition for Initialisation stage

The rainfall data used in the current analysis corresponds to the Shoeburyness weather station rainfall measurements for a period 2006-2011, introduced in section 4.3.1 of this chapter. It should be noted that the rainfall data for the last fifth year of initialisation phase, correspond to year 2006 instead of 2011. The reason for such a change is that the last year of initialisation phase is, as explained previously, also the first and only year of seasonal fluctuation stage (the first year of monitoring). So,

this adjustment was essentially made, to allow predicted results to be comparable with the monitoring data. The pore pressure threshold value (see Chapter 3, Precipitation BC) was input as 0 kPa, implying that no ponding of water was allowed to develop on both the embankment slope and the ground surface beyond the toe.

The extent over which vegetation was applied is shown in the Figure 4.23. The mature deciduous trees over the embankment were modelled with maximum root depths of 2m. Beyond the embankment the root depth was reduced to 0.3m to simulate grass vegetation that can be seen in aerial photographs of the site. The assumed root depth does not represent actual root biomass (Leung, Garg & Ng, 2015), or average root length observed at the site (Garg, Leung & Ng, 2015), but it is a measure of vegetation drying zone, identified through previous water content and pore pressure recordings.

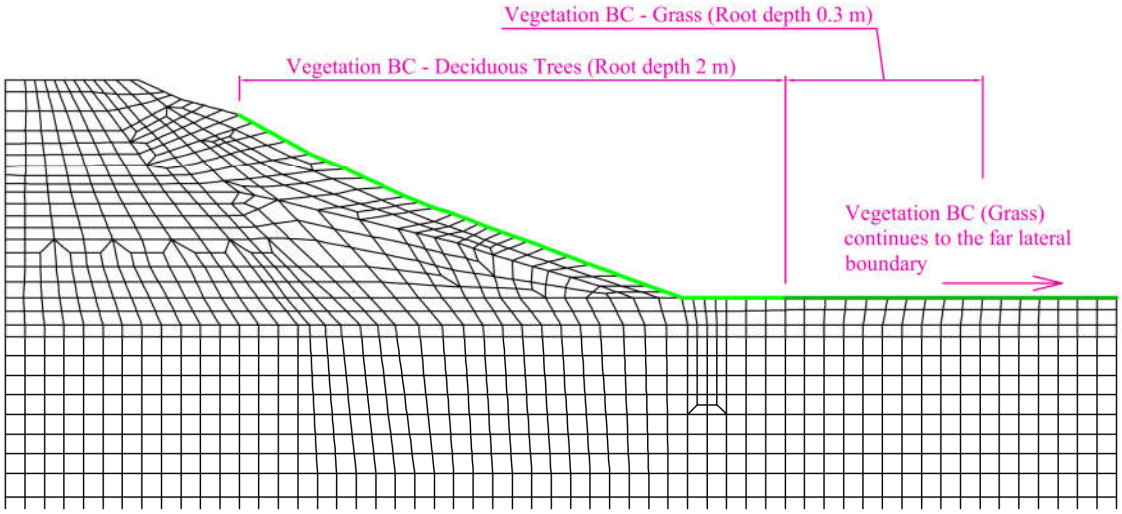

Figure 4.23 Contours of vegetation boundary condition for Initialisation stage

The root water uptake model implemented into ICFEP and described in Chapter 3, beside root depths, requires potential transpiration rates and suction-dependent reduction function to be specified. The potential evapotranspiration data for deciduous trees employed in current analysis correspond to ones calculated using the FAO Penman-Monteith method, as explained in detail in section 4.3.1. For the grass, a somewhat lower potential transpiration rate, estimated again based on the same method, was adopted. Again, same adjustment of the data for the last year, as in the case of precipitation, was made. However, in this case data modification was not necessary, given the fact that evapotranspiration rates are generally very unform from year to year. The specific pore suction values relevant to characterization of reduction function α, are provided in Table 4.6. As explained in Chapter 3, S3 value is species dependant and therefore generally recommended values for Oak tree and grass were adopted respectively. In a paper by (Nyambayo & Potts, 2010), it was demonstrated that the effect of S3 suction value on the pore water pressure and deformation predictions was small. The assumed values of S1, S2 and S4 are generally recommended for the conditions in the UK (Feddes, Kowalik & Zaradny, 1978).

Table 4.6 Reduction function α(S) properties

Vegetation type	**S1** Anaerobiosis point (kPa)	**S2** (kPa)	**S3** (kPa)	**S4** Wilting point (kPa)
Deciduous trees	0	5	200	1500
Grass	0	5	50	1500

4.7.5 Vegetation Clearance

The initialisation stage lasted for 5 years, with the last one being treated as the first year of monitoring period (between March 2006 and March 2007), the so-called seasonal fluctuation stage. In the April 2007 the vegetation was cleared from upper part of the embankment slope, which represented the start of the vegetation clearance phase. In the present analysis the felling of large deciduous trees was modelled by reducing the root depth and potential evapotranspiration rates to match the root system characteristics of the small and sparse vegetation. The root depth was decreased to 0.3 m, the same value as previously assigned to grass vegetation. Potential evapotranspiration was reduced to 10% of rates employed when mature trees were present on the slope. Although the assigned rates seem very low even for the grass vegetation, they are justified by the fact that the north-facing slope is investigated, which gets drastically less solar radiation which directly affects evaporation rates. If the entire embankment had been modelled, it would be sensible to specify higher evapotranspiration rates for the south slope, to reflect higher evaporations inherent to southerly oriented slopes. The explained differences together with some variations in geometry and vegetation cover, essentially means that the problem is non-symmetrical. However, in order to reduce the size of the numerical model only the northern slope was simulated, which is generally the more critical one in terms of stability. The evaluation of stability is one the important goals, particularly for the vegetation clearance phase.

The extent of the vegetation removal zone is illustrated in the Figure 4.24. As can be seen, deciduous trees were removed from the entire embankment slope. Some mature trees were left along a narrow zone just beyond the toe of the embankment. The precipitation boundary conditions remained unchanged compared to previous analysis stage (the same as in Figure 4.22). The used evapotranspiration (FAO Penman-Monteith) and precipitation (data is given in section 4.3.1 and correspond to period between 2007-2011.

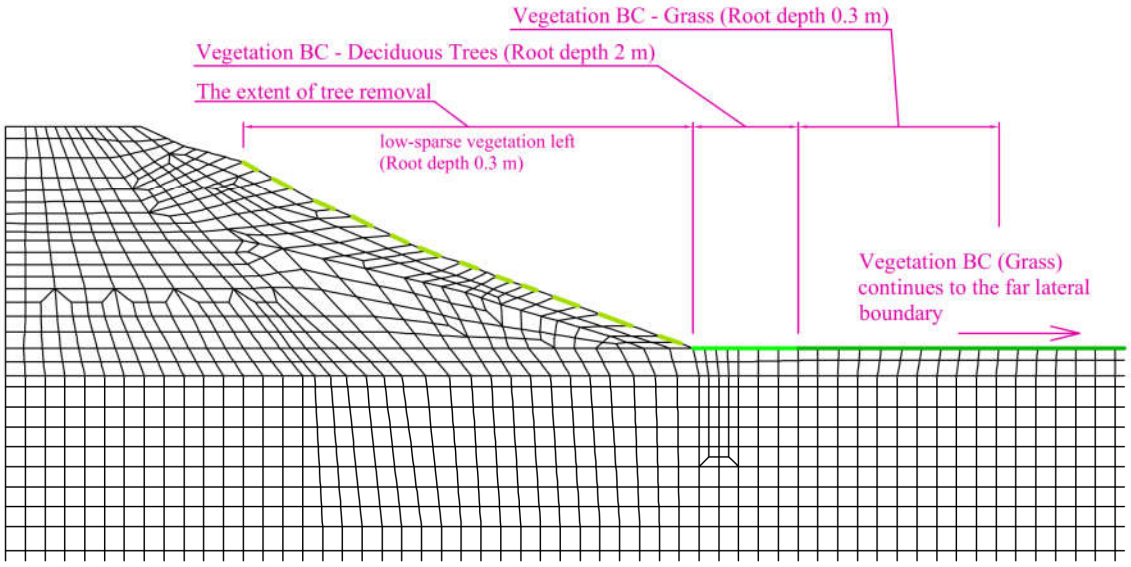

Figure 4.24 The extent of vegetation clearance

4.8 Discussion of Results

The discussion and interpretation of results is structured to follow the sequence of analysis. First the results of construction phase will be briefly presented. Afterwards, the initialisation stage will be discussed, with emphasis on the evolution of embankment and foundation soil hydraulic regime, as respond to environmental effects. The final year of the initialisation stage – seasonal fluctuation

phase, is extracted from the rest of the results and more thoroughly investigated. Finally, the vegetation clearance stage is elaborated.

Considering that, two distinctly different mechanical constitutive models have been employed in this main analysis, the presentation of numerical results is further divided into two branches. For completeness of the evaluation and in order to gain deeper insight into the complex nature of coupled unsaturated flow-deformation analyses, the comparison between analysis outputs of two models and also field measurements, is provided at the end.

4.8.1 Construction Stage

The contours of pore water pressure and degree of saturation for three increments of the construction stage are shown in Figure 4.26. The increment no. 17 corresponds to the end of construction. During construction, the clay fill and ash were assumed to have a suction of 50 kPa upon placement. It can be seen that at the end of construction the pore water stress field has not reached equilibrium conditions, but that some redistribution has occurred in particular within more permeable ash and clay fill layers. In contrast, lower permeability London Clay has allowed excess pore water pressures to be generated. The same conclusion can be drawn from the pore pressure profiles for two sections (one in the line of symmetry and other corresponding to S2) illustrated in Figure 4.25. The degree of pore water pressure dissipation at the end of construction is in excess of 50%, indicating that conditions are rather undrained. The end tipping technique used back in the 19th century was considerably quicker than the simulated construction time, suggesting that the truly undrained conditions have prevailed during the time of construction.

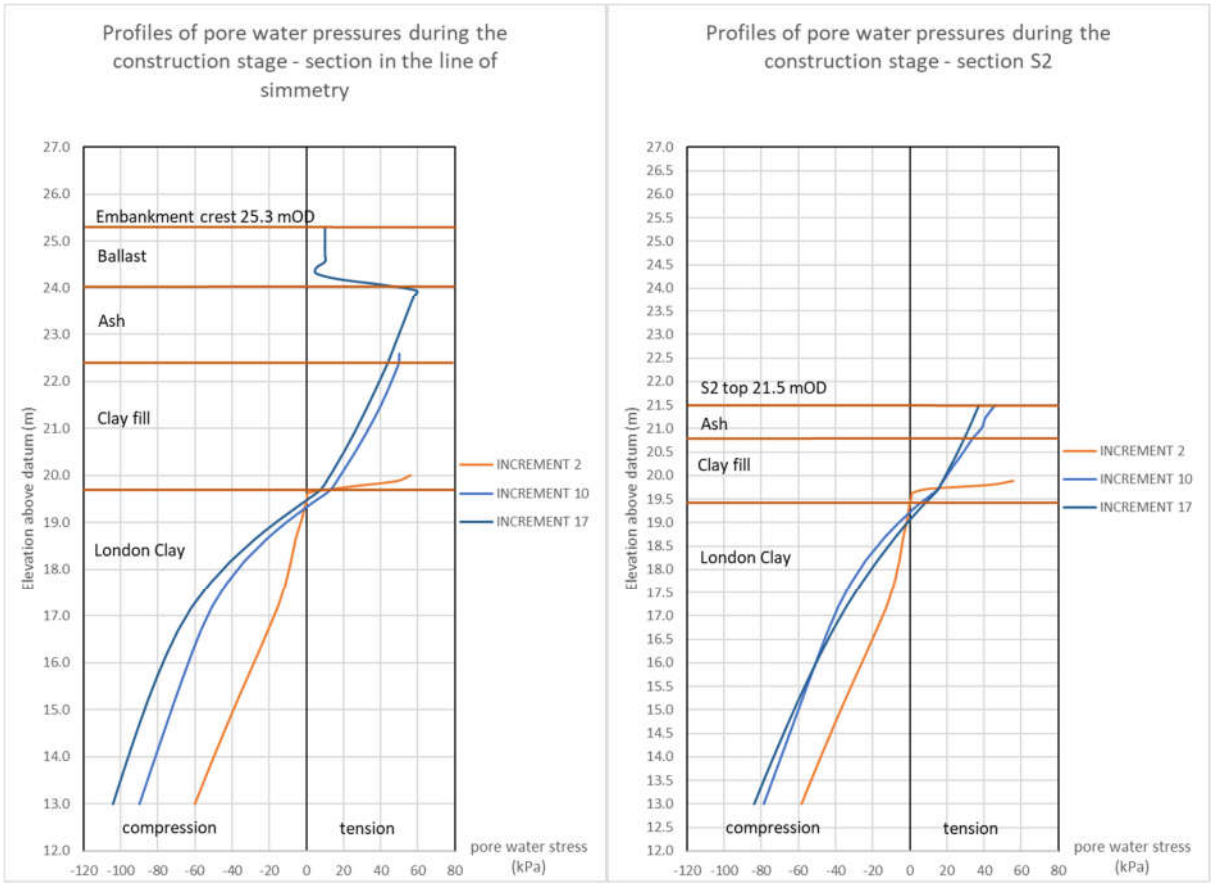

Figure 4.25 Pore water pressure profiles during the course of embankment construction

The Figure 4.27 shows the contours of accumulated deviatoric plastic strains at the end of the construction stage. It can be seen that relatively rapid construction has induced some plastic shear deformations in the London Clay below the toe of the embankment of the order of 1.5% and some very small plastic shear strains at the toe surface. This observation combined with the previously established finding of undrained behaviour could explain the fact that failures and instabilities were common during the construction of the British railway infrastructure earthworks.

The calculated vertical displacements at the crest of the embankment corresponding to the end of construction were around 0.1 m. The embankment was stable at the end of construction.

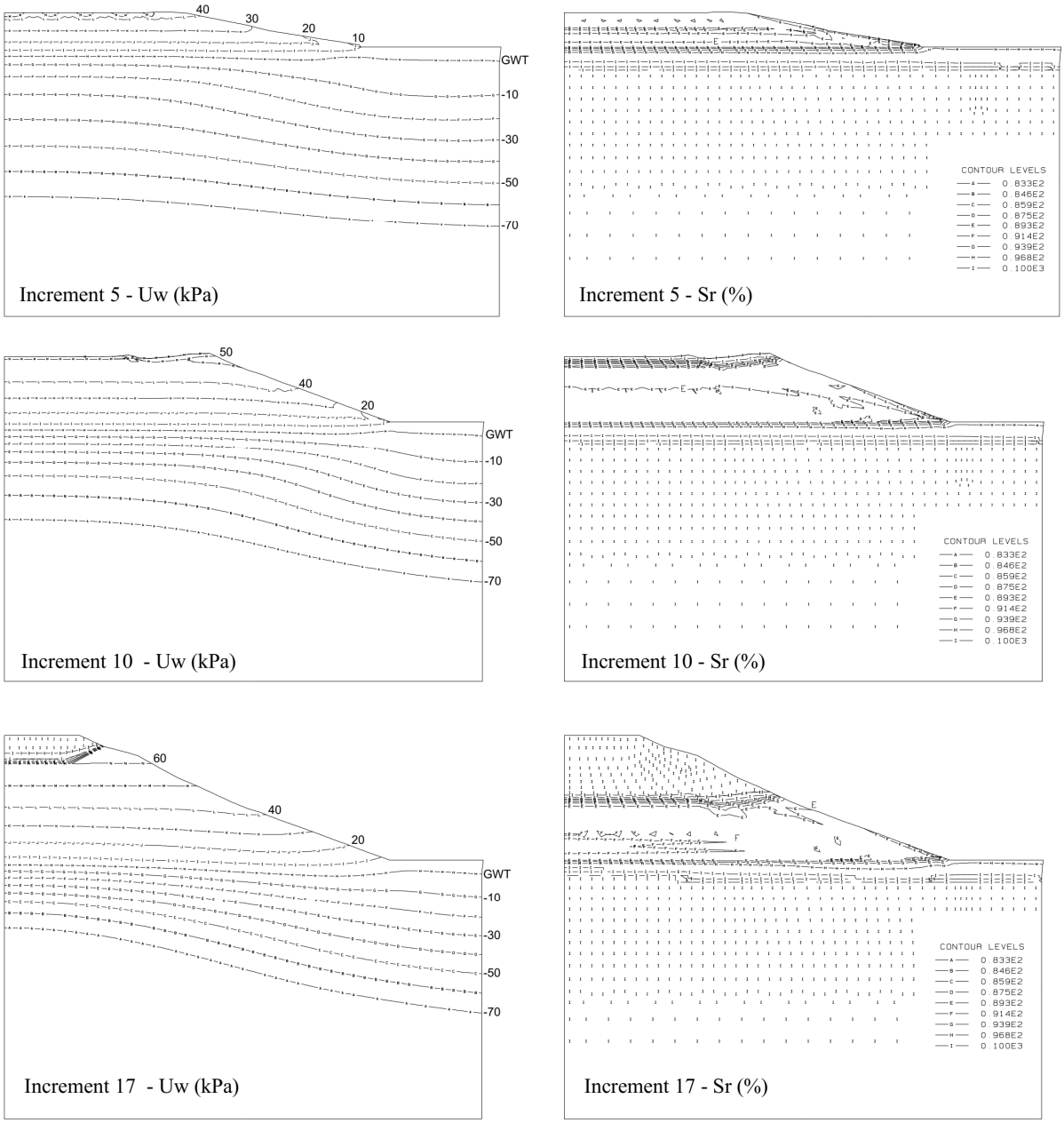

Figure 4.26 Contours of pore water pressures and degree of saturations during the embankment construction

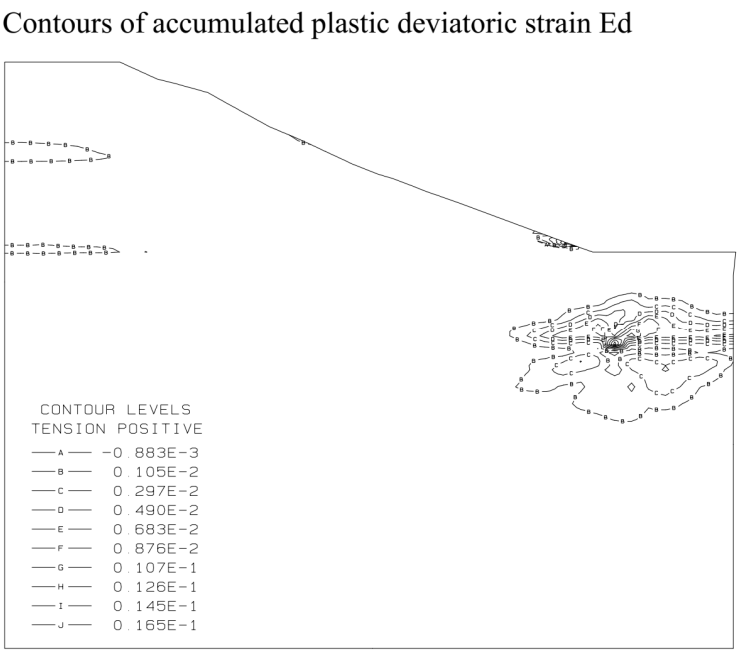

Figure 4.27 Contours of accumulated plastic shear strains at the end of construction stage

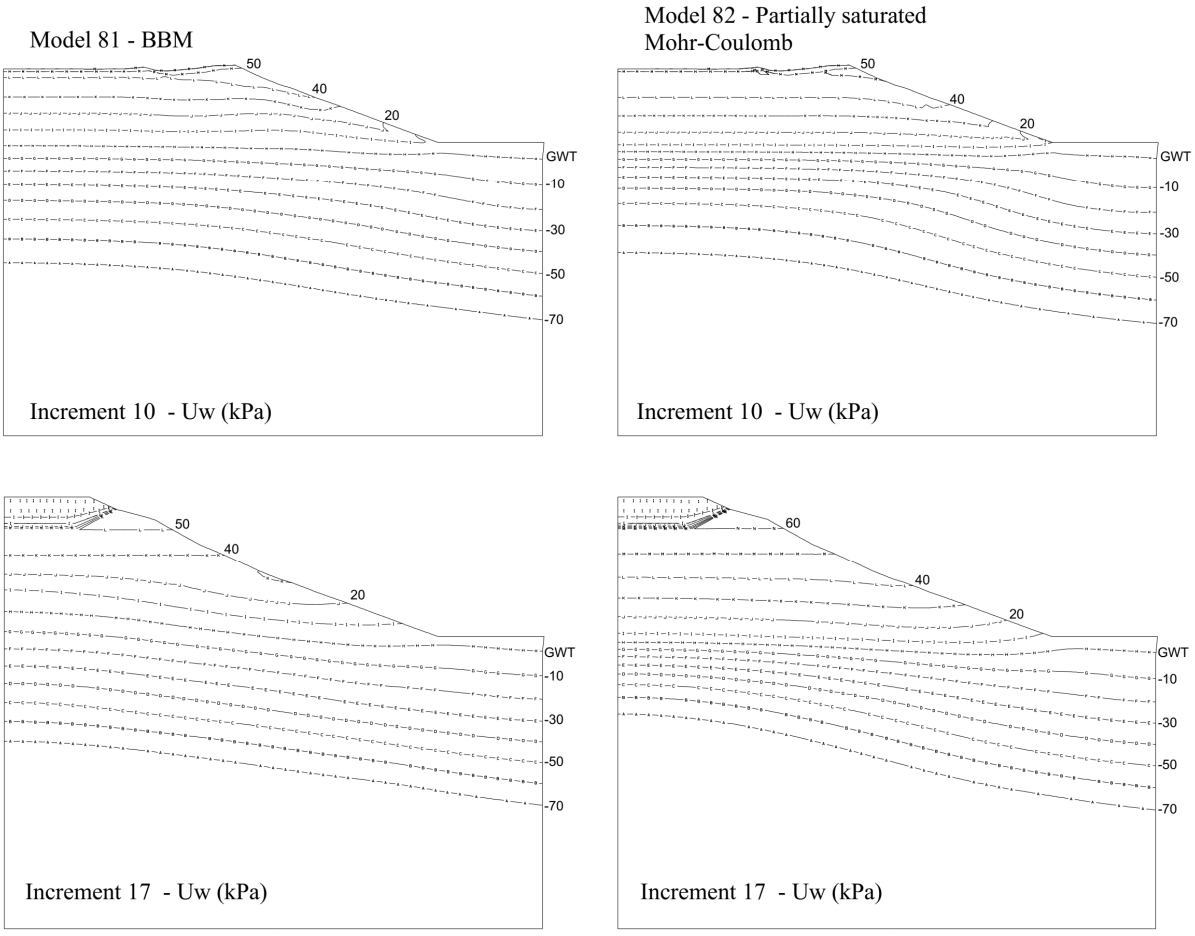

Figure 4.28 Comparison of contours of pore water pressures for unsaturated constitutive Models 81 and 82

In the case of Model 81 (modified BBM) a separate analysis of construction stage was conducted. It is generally accepted that when elastoplastic constitutive models are employed in combination with complex stress histories, it is important to use the same constitutive model throughout all analysis stages (Alonso & Pinyol, 2016). This is particularly true for the construction stage because loading generated due to the placement and compaction of fill material explicitly determines the size of the primary yield surface. Compared to analysis performed with Model 82 (partially saturated Mohr-Coulomb), the permeability of unsaturated section of London Clay was increased from $5 \cdot 10^{-10}$ to $1.25 \cdot 10^{-9}$. The contours of pore water suctions for two increments, no. 10 and 17 (last one), are presented in Figure 4.28. It can be seen that amount of pore water pressure dissipation at the end of construction is significantly higher compared to first analysis. The obvious reason for almost complete loss of excess pore water pressures and establishment of near hydrostatic conditions is, as mentioned earlier, slightly higher permeability of top zone of the London Clay.

4.8.2 Initialisation Stage

Partially saturated Mohr-Coulomb model – ICFEP Model 82

The initialisation stage, as previously discussed, lasted for 5 years, with the last 5th year being nominated as fluctuation stage. Figure 4.29 illustrates the variations of pore water pressures for several elevations along the sections S1 and S2. To allow comparison with field measurements, the same sections were used as those where the instrumentation was installed. It should be noted, prior to presentation and interpretation of results, that the thickness of the ash layer, overlying the clay fill, in sections S1 and S2 equals around 1.2 m and 0.7 m respectively. Successive cycles of wetting and drying, governed by climatic (vegetation) boundary conditions, induce seasonal cyclic variations of pore water stresses. Positive values mark tensile water stress, termed previously as matric suction (in the remainder of the discussion, they will be referred to only as suction).

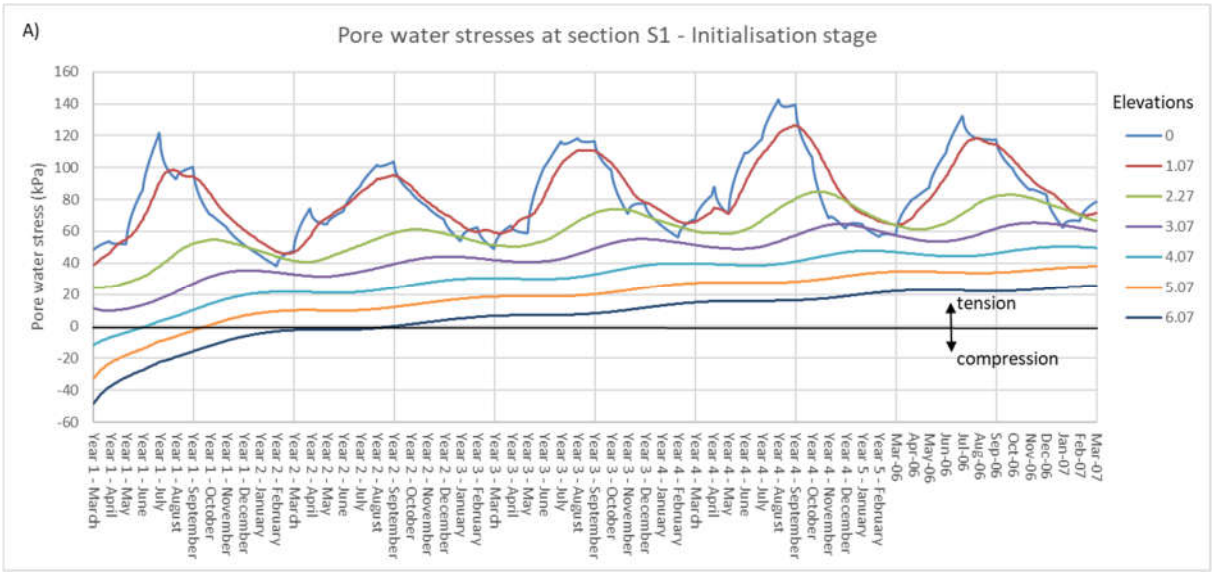

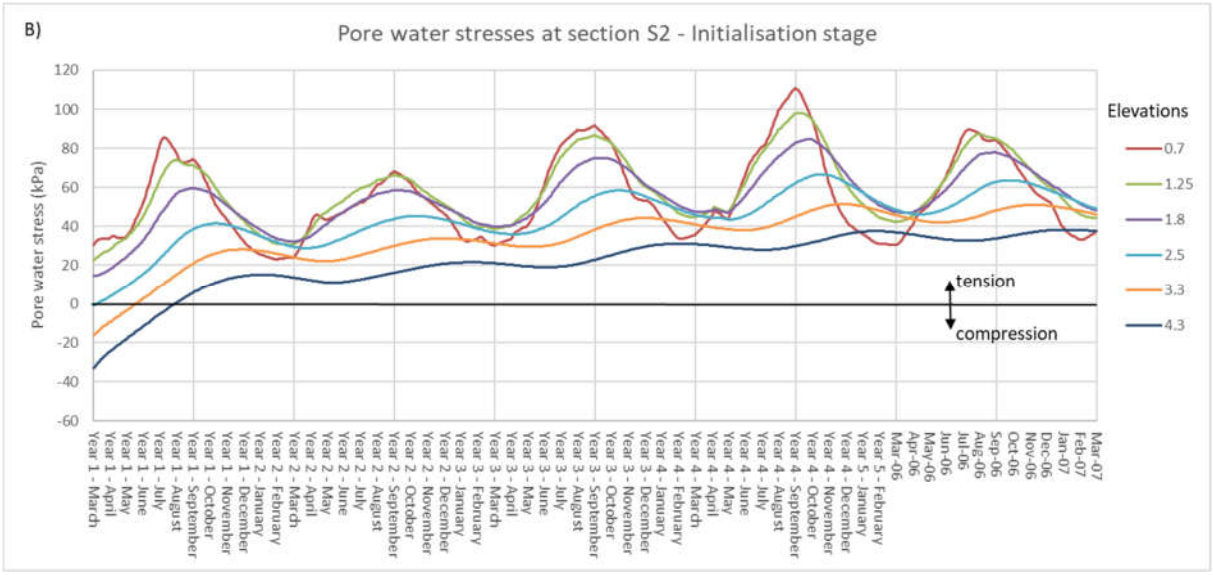

Figure 4.29 Pore water pressure variation at sections S1 and S2 of the north-facing embankment slope

The pore water pressure variations are most pronounced at top 2 meters of the embankment slope. As can be seen, at depths very close to the soil surface (in the ash layer), the predicted suctions are mostly reversible. In contrast, at deeper levels within clay fill and London Clay foundation, a gradual increase in suction is observed. The suction increase is accompanied by the steady lowering of ground water table, which is illustrated in Figure 4.30. The Figure depicts the contours of pore water pressures, which indicates that during first 18 months the ground water table has been lowered from around 1.0 m depth to about 4.0 m. In the next two years the combined influence of evapotranspiration and precipitation has lowered ground water table for additional 1.0 m, reaching approximately an average depth of 5.0 m below the ground surface. The continuous drying of the hydrological domain, caused by high water demand trees, established along and beyond the embankment slope, is consistent with the evapotranspiration and rainfall rates calculated for period 2006-2011 (see section 4.7.4). For illustration purposes the potential evapotranspiration, precipitation and net rates for the period April 2006 – March 2007 are shown in Figure 4.31. The figure shows that the net total moisture flux is negative, indicating that the water is being extracted from the soil. For all five years outward (negative) net total water flux has been calculated based on the available climatic data and methods described in Chapter 2. However, it should be noted, that the actual evapotranspiration rates depend on the soil water supply and are lower compared to potential ones, which means that long-term input and output rates are essentially balanced. As for the duration of the initialization phase, this means that further cycles would have decreasingly less impact, and that a deeper hydraulic regime would reach steady-state conditions.

The Figure 4.29 shows that relatively high pore water suctions, particularly for the winter months, have been predicted in the ash layer throughout the entire initialisation stage. In reality, it is expected that during winter months, when precipitation rates significantly exceed evapotranspiration, water suctions are completely lost within the highly permeable ash stratum. The possible reasons for discrepancy with field observations, could be the fact that the ash is modelled as a fully saturated material, and that its hydraulic response is mainly controlled by the behaviour of underlying lower permeability clay fill. This issue would be further discussed later in the fluctuation stage. On the other hand, progressive increase of pore suctions within clay fill and underlying London Clay, with less responsive seasonal behaviour, are clear indications of the development of persistent suctions (Loveridge *et al.*, 2010). Although the extreme wet scenarios have not been examined, it is likely that

as long as the high-water demand trees are present on the embankment slopes, these deep persistent suctions will be maintained and would prevent any type of deep-seated instability.

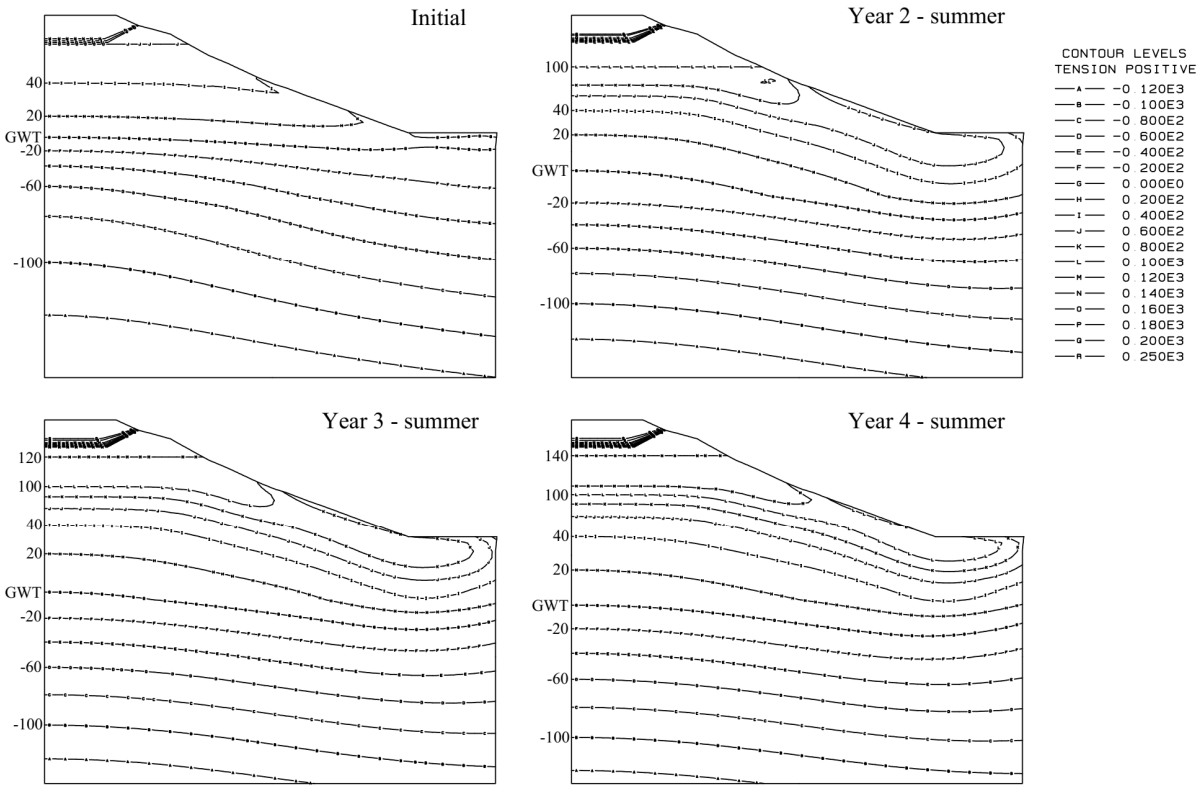

Figure 4.30 Contours of pore water pressures corresponding to the start and three subsequent years of the initialisation stage

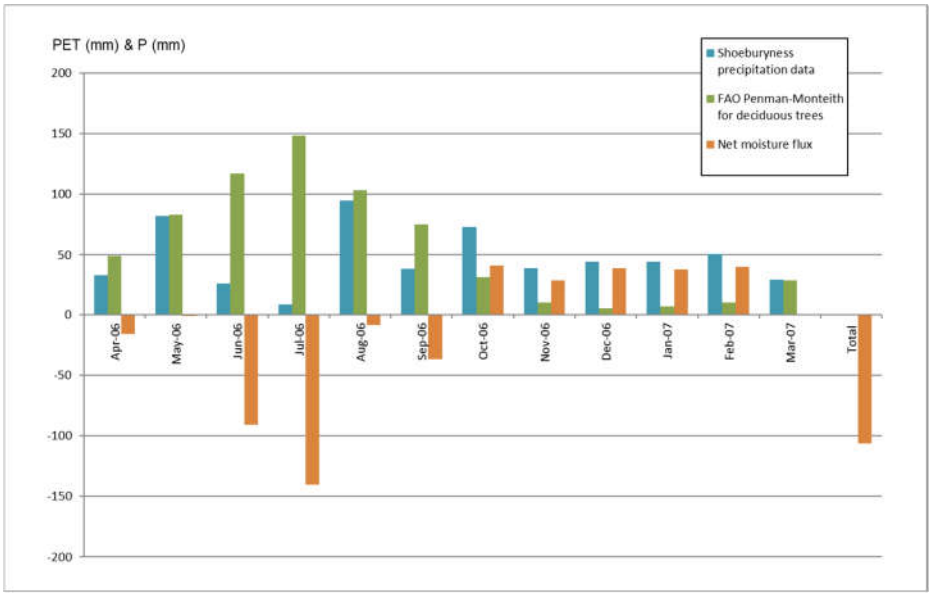

Figure 4.31 Potential evapotranspiration, precipitation and net rates for first year of monitoring period

The calculated vertical and horizontal displacements have been depicted in Figures 4.32 and 4.33 respectively. The predicted seasonal deformational behaviour is less responsive to combined effects of vegetation and precipitation. The seasonal displacement fluctuations are restricted mainly to surficial slope zone. There is a clear trend of overall embankment shrinkage deformation. Both vertical and horizontal displacement patterns confirm that tree-induced desaturation is governing mechanism for the investigated period. The deformation behaviour (shrinkage) is consistent with calculated negative net moisture fluxes.

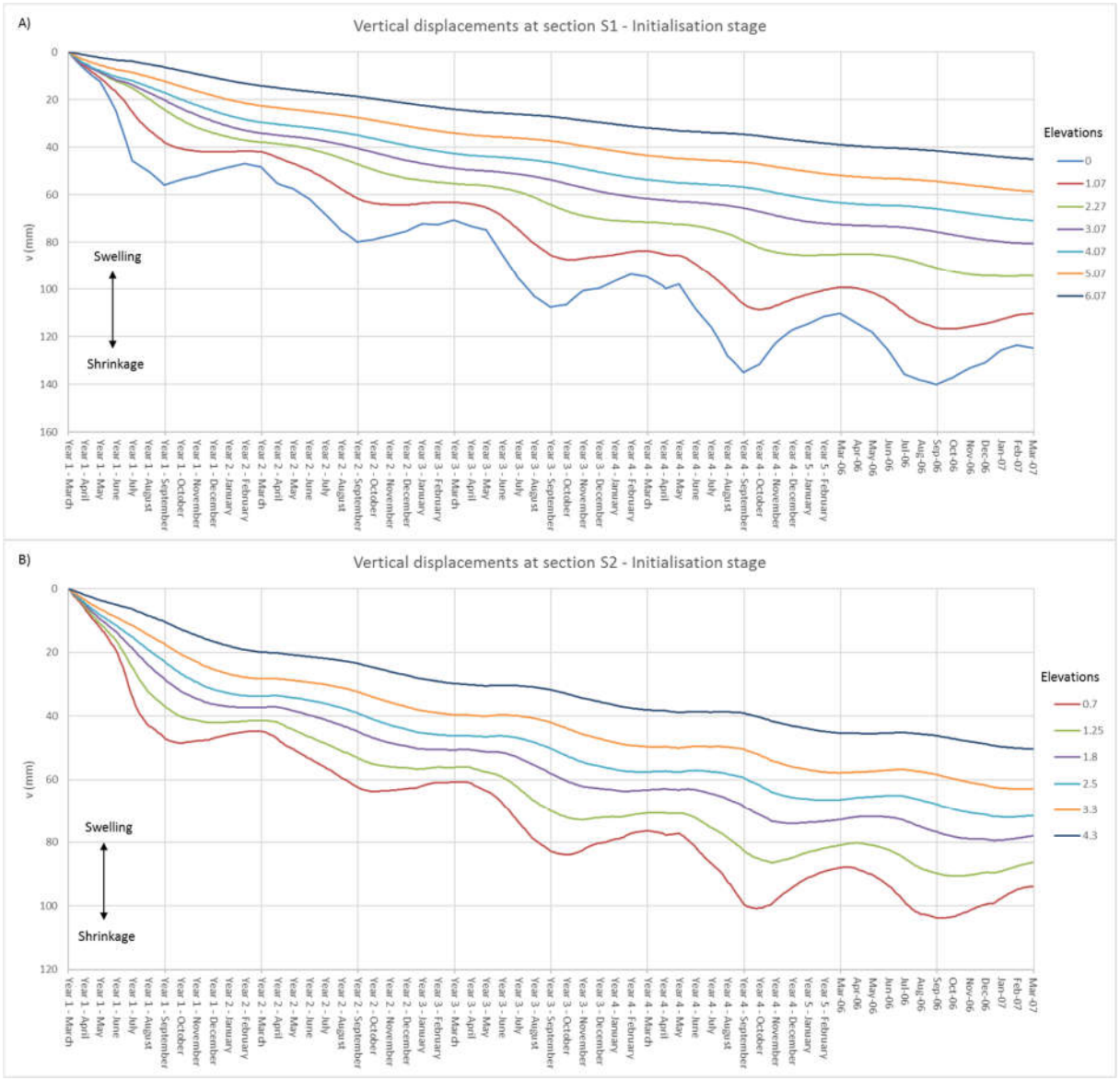

Figure 4.32 Predicted vertical displacements at sections S1 and S2 of the north-facing embankment slope

The horizontal displacements shown in Figure 4.33 demonstrate that the movements induced by climatic boundary conditions are oriented towards the embankment crest. The ratio of vertical and horizontal displacement magnitudes at two sections, indicate that in section S1 (located at the upper half of the embankment slope) movements are dominantly vertical. In section S2, portion of horizontal component is moderately higher, suggesting that the direction of movements is more perpendicular to the slope rather than vertical. The vectors of sub accumulated displacements shown in Figure 4.34, support previous findings. Sub accumulated means that presented vectors correspond

to the sum of incremental displacements for two distinct seasons. In particular, the summer season represents the time span from end of winter (March) to the end of summer (August), whereas winter season comprises the period from August to March.

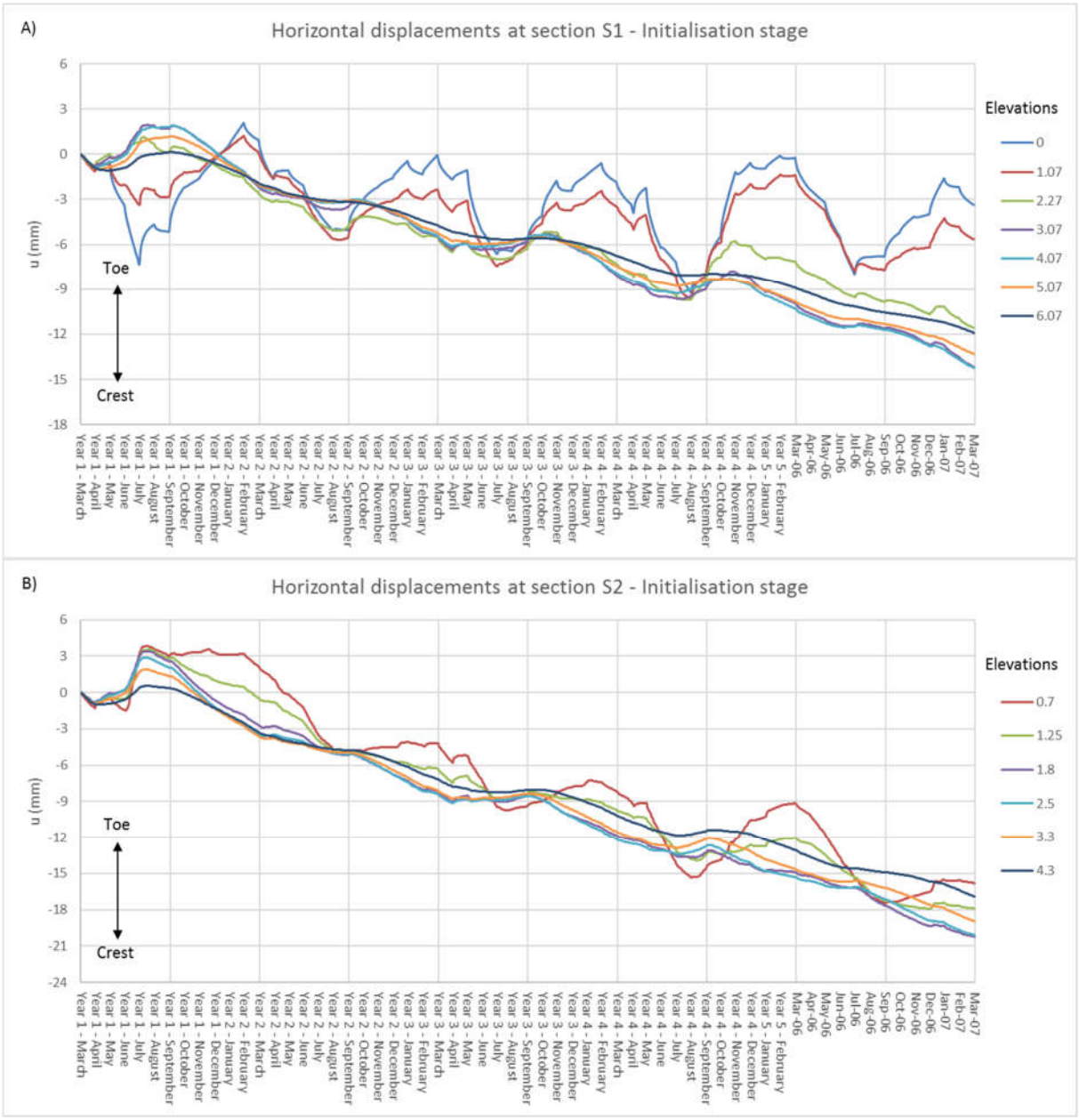

Figure 4.33 Predicted horizontal displacements at sections S1 and S2 of the north-facing embankment slope

The process of desaturation is further investigated through volumetric water content θ_w and degree of saturation S_r profiles, presented in Figures 4.35 and 4.36. In Figure 4.35 the θ_w and S_r profiles for successive winters (March) is shown. It can be seen that the vegetation via the process of evapotranspiration progressively dries the embankment and underlying foundation soil. The abrupt cut-off at a level of around 17 mOD, present on both sets of curves θ_w and S_r, coincides with the change of material model. Below 17 mOD the London Clay foundation soil was modelled as fully saturated without SWRC, and therefore ICFEP cannot compute true degrees of saturation, but automatically gives S_r equal to 100%.

Figure 4.36 illustrates the differences between summer and winter θ_w and S_r profiles, for an arbitrarily selected year. As can be seen, the zone of seasonal wetting and drying propagates to a depth of around 2.0 m. Below that level there are practically no seasonal changes of volumetric water content, and the persistently dry soil zone has been developed. The hatched zone between initial and "long-term" volumetric water content profiles, represents the continuously dry region, referred as zone of persistent soil moisture deficit (SMD) (Hough & Jones, 1997). The SMD is defined as the amount of water a soil needs to reach field capacity, the maximum amount of water a free draining soil can hold under gravitational forces (Rushton, 2003). At field capacity the SMD equals zero.

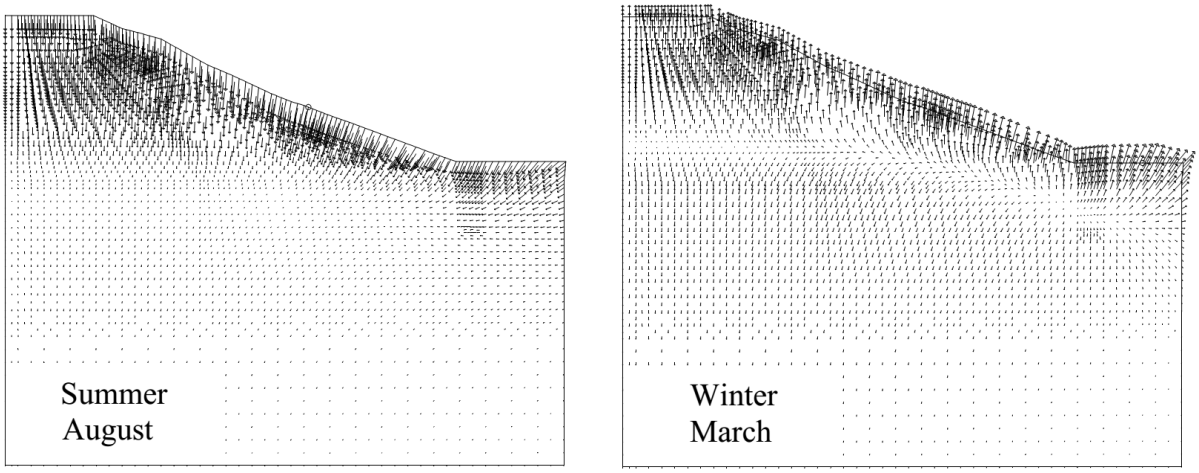

Figure 4.34 Vectors of sub accumulated displacements for periods spring/summer and autumn/winter

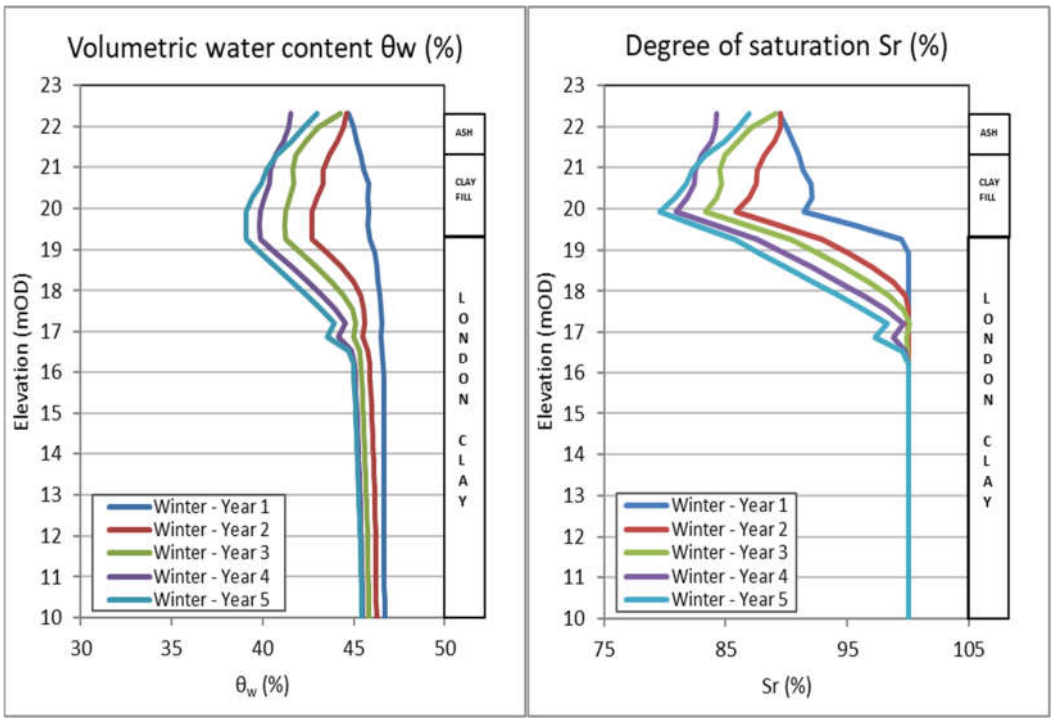

Figure 4.35 Predicted volumetric water content θ_w and degree of saturation S_r profiles at the end of winter season (March) at section S1

The obtained results demonstrate that the effects of tree roots spread significantly deeper compared to the maximum root depth. In current analysis maximum specified root depth was 3.0 m, while the water abstraction generated by roots propagated to 6.0 m. Considering that below 6.0 m the London Clay, as previously explained, was simulated as fully saturated material, the vegetation depth of influence is likely even greater. The position of ground water table at the end of initialisation stage corroborates this hypothesis.

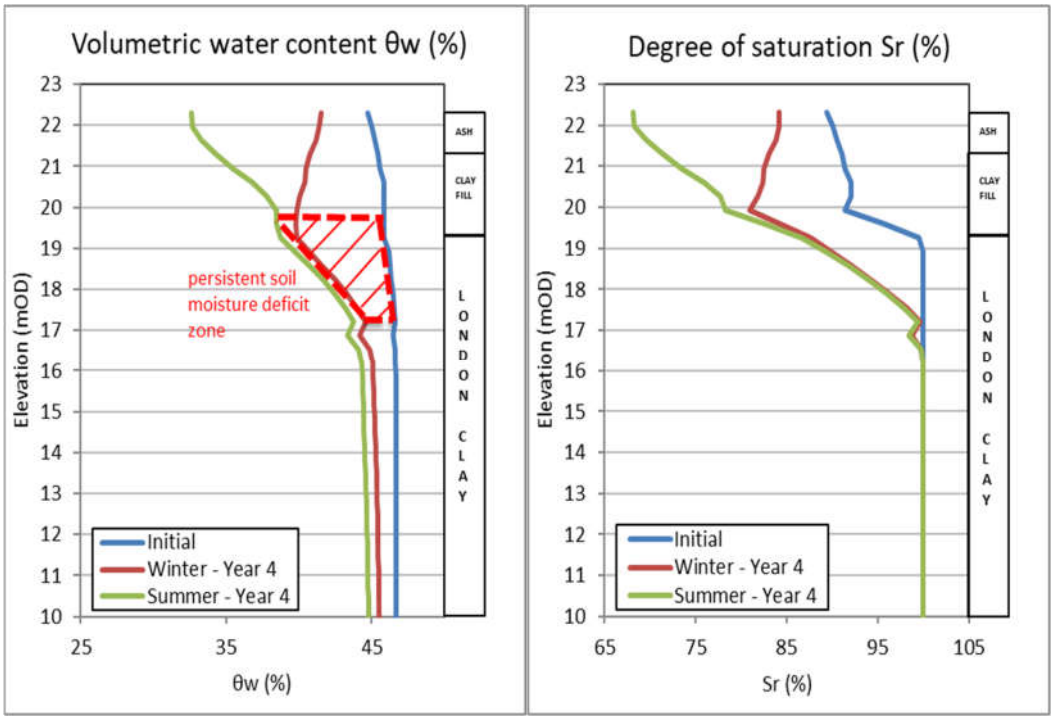

Figure 4.36 Volumetric water content θ_w and degree of saturation S_r profiles for the summer (August) and winter (March) seasons of year 4 at section S1

Modified Barcelona Basic Type Model – ICFEP Model 81

It has been seen in first analysis (with Model 82) that variation of key outputs was restricted to a shallow surface zone (predominantly the ash layer), most likely due to low permeability assigned to the clay fill. The in-situ permeability tests undertaken by (O'Brien, Ellis & Russell, 2004), suggest that the hydraulic conductivity of the clay fill (of London Clay origin) varies in a wide range from $6 \cdot 10^{-7}$ to $2 \cdot 10^{-9}$ m/s. Therefore, instead of prescribing higher constant permeability, a nonlinear permeability model was applied. The desaturation model with permeability varying with suction have been adopted (Figure 4.37). It is well known that the permeability of the unsaturated soils decreases as the water content reduces, as a result of tapering of the water corridors within void spaces, through which seepage takes place. As can be seen from given plot (Fig 4.37), the permeability decreases from saturated value $k_{sat}=2 \cdot 10^{-7}$ m/s corresponding to zero suction to a limiting lowest value $k_{min}=2 \cdot 10^{-9}$ m/s, corresponding to suction of 100kPa.

The evolution of pore water pressures for five years of the initialisation stage is presented in Figure 4.38. It is clear that somewhat higher permeabilities, especially during winter season when corresponding suction magnitudes are lower, generate more uniform seasonal variations over the whole depth of the clay fill layer. This pattern of behaviour is more consistent with field observations at the Hawkwell embankment.

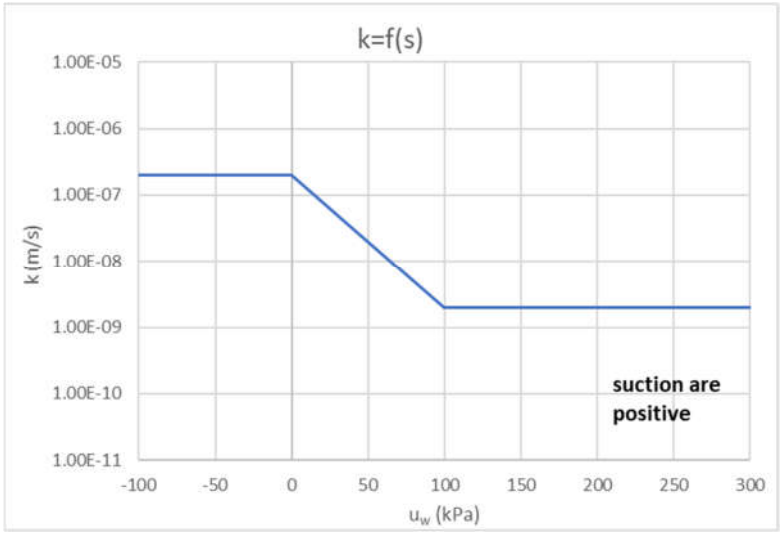

Figure 4.37 Unsaturated permeability model adopted for the clay fill layer

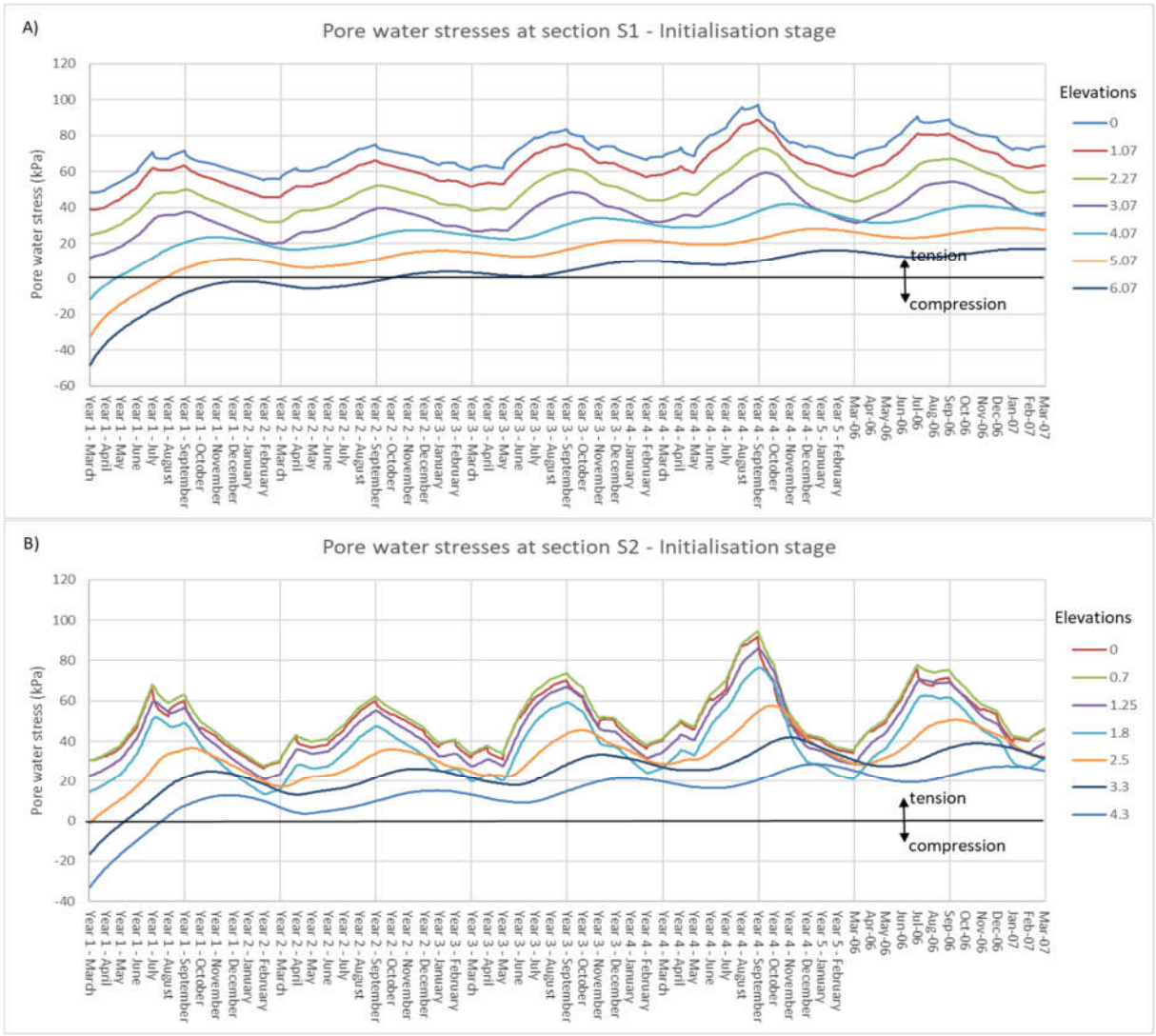

Figure 4.38 Pore water pressure variations at sections S1 and S2 for the analysis employing modified BBM

The Figure 4.39 shows the evolution of vertical movements over the initialisation stage. The same trend of accumulating shrinkage deformations, as in the case of Model 82, is predicted. Despite similar magnitude of seasonal suction variations for the top 3.0 m and 2.0 m at sections S1 and S2 respectively (Fig 4.38), the deformational seasonal fluctuations do not follow the same shape. The points (nodes) within the ash layer exhibit larger annual changes compared with the points located in the clay fill. The probable reason for this is that deformational behaviour of the ash material is governed by effective stress stiffness parameters, whereas in the case of clay fill, modelled as unsaturated modified BBM, the deformation response is mainly controlled by the elastic compressibility coefficient related to suction changes κ_s. Recalling that the initial yield suction, defining the position of secondary yield surface, was assigned extremely high value, the elastoplastic coefficient of compressibility associated to suction changes λ_s, has essentially no effect.

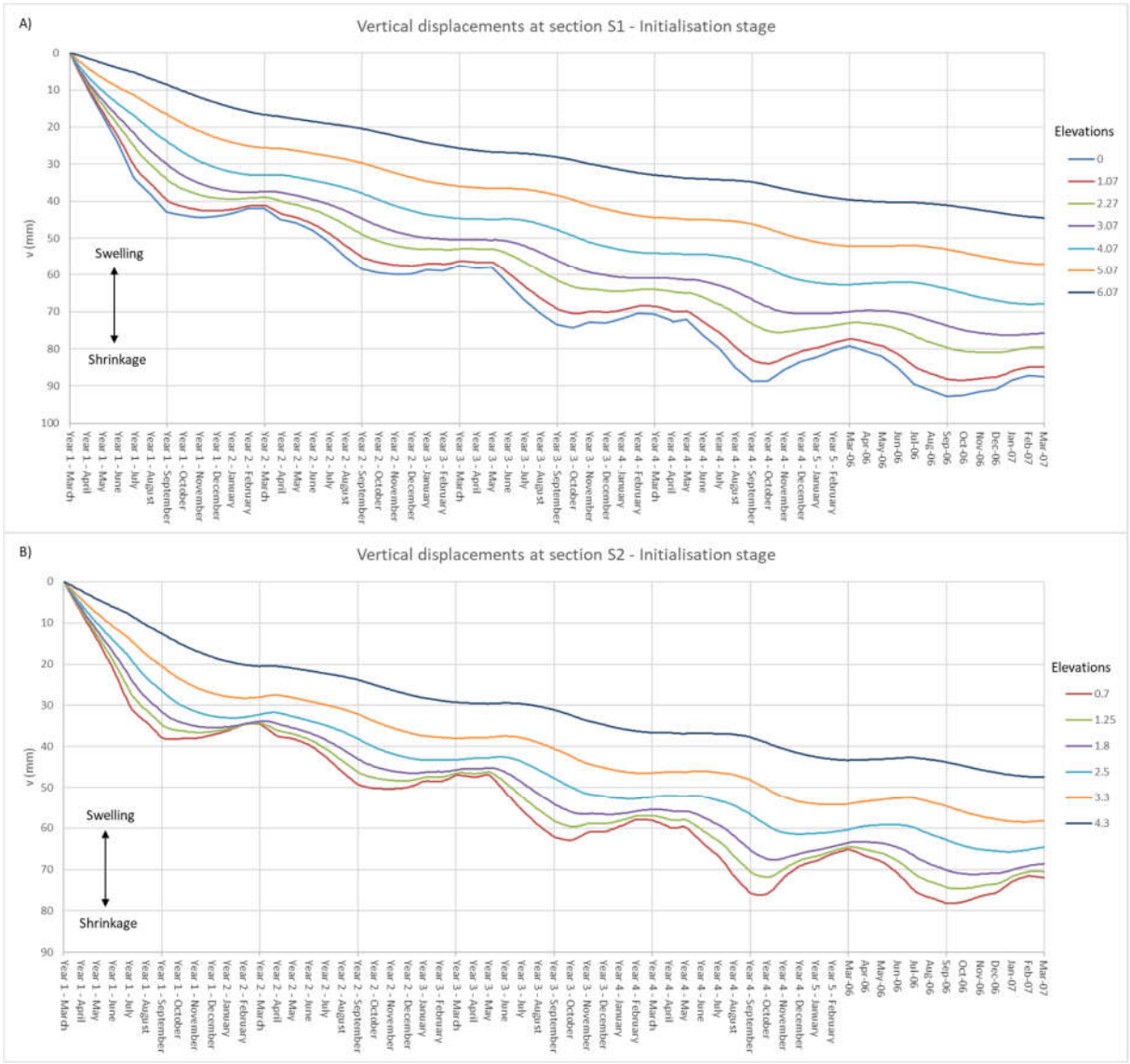

Figure 4.39 Evolution of vertical movements at sections S1 and S2 for the analysis employing modified BBM

The total cumulative settlement in this analysis is lower compared to the first one (using constitutive Model 82 and constant permeability for the clay fill). This could be explained by slower desaturation of the analysed domain, which in turn is a consequence of somewhat deeper zone of seasonal wetting

and drying, directly related to higher permeability of the clay fill. These points are schematically illustrated in Figures 4.40 and 4.41 which depicts the long-term development, as well as seasonal variation of volumetric water content and degree of saturation profiles. It can be seen that higher permeability of clay fill during winter season allows more water to be infiltrated deeper into the clay fill, thereby limiting the drying of the clay fill and underlying London Clay.

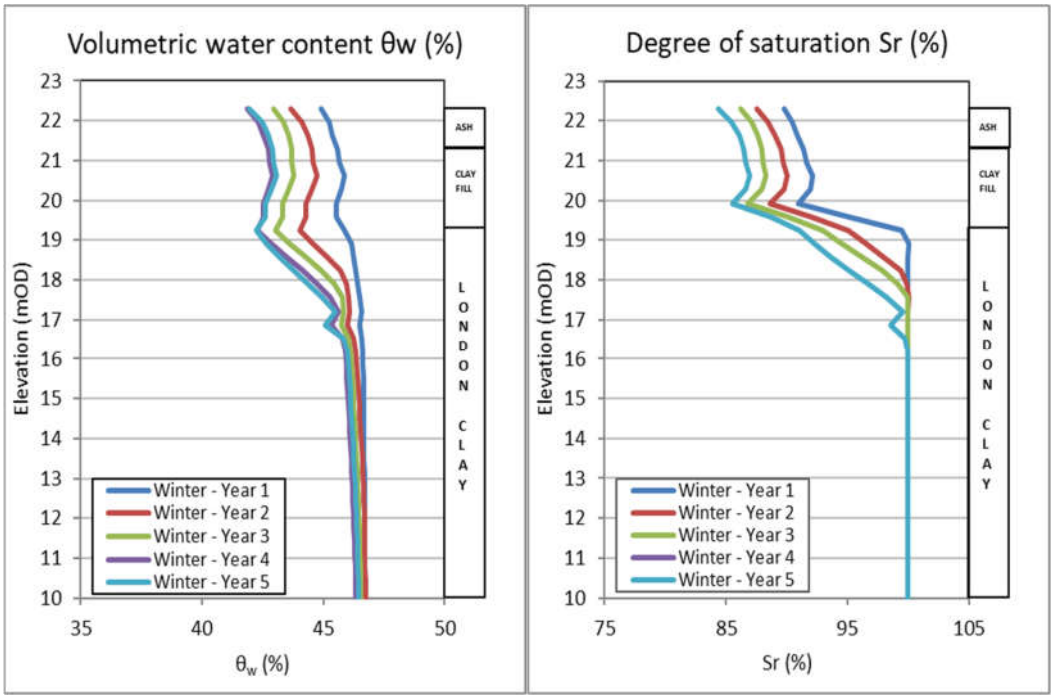

Figure 4.40 Predicted volumetric water content θ_w and degree of saturation S_r profiles at the end of winter seasons (March) at section S1 for the analysis with modified BBM

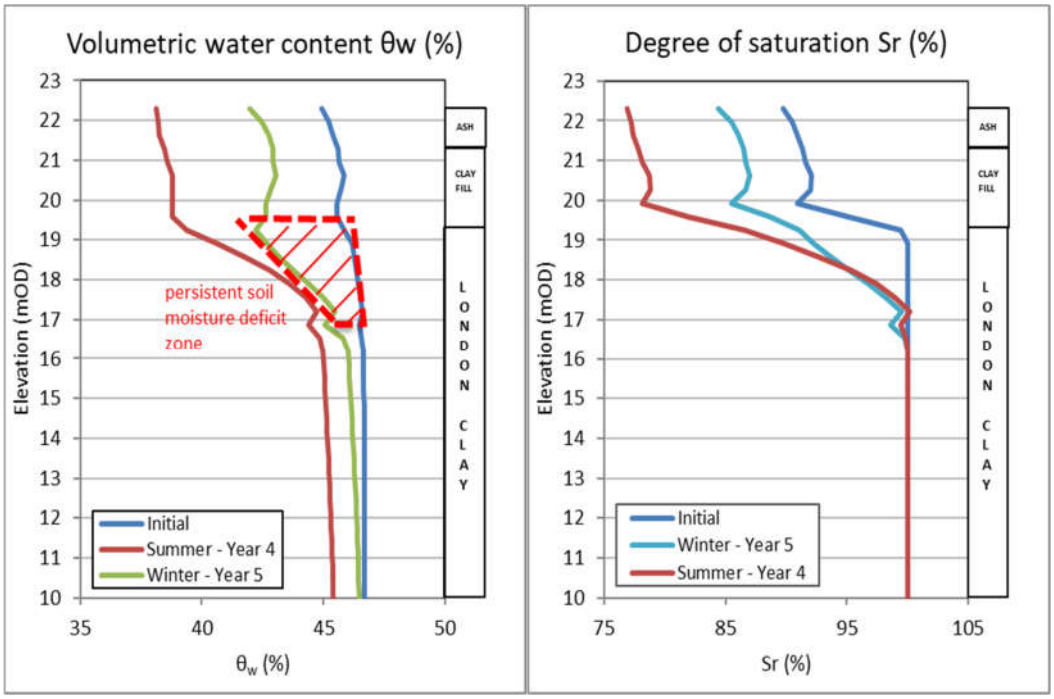

Figure 4.41 Volumetric water content θ_w and degree of saturation S_r profiles for typical summer (August) and winter (March) seasons at section S1 for the analysis with modified BBM

The predicted evolution of horizontal movements for points along the depth of sections S1 and S2 is shown in Figure 4.42. In a similar fashion to first analysis (based on constitutive Model 82 and constant permeability assigned to the clay fill), the overall trend of horizontal displacements directed towards the embankment crest, is obtained. This is consistent with the abstraction of water, governed by the prevailing evapotranspiration component of the hydrological cycle. The ratio of vertical and horizontal componential displacements confirms that shrinkage/swelling mechanism is predominantly vertically oriented.

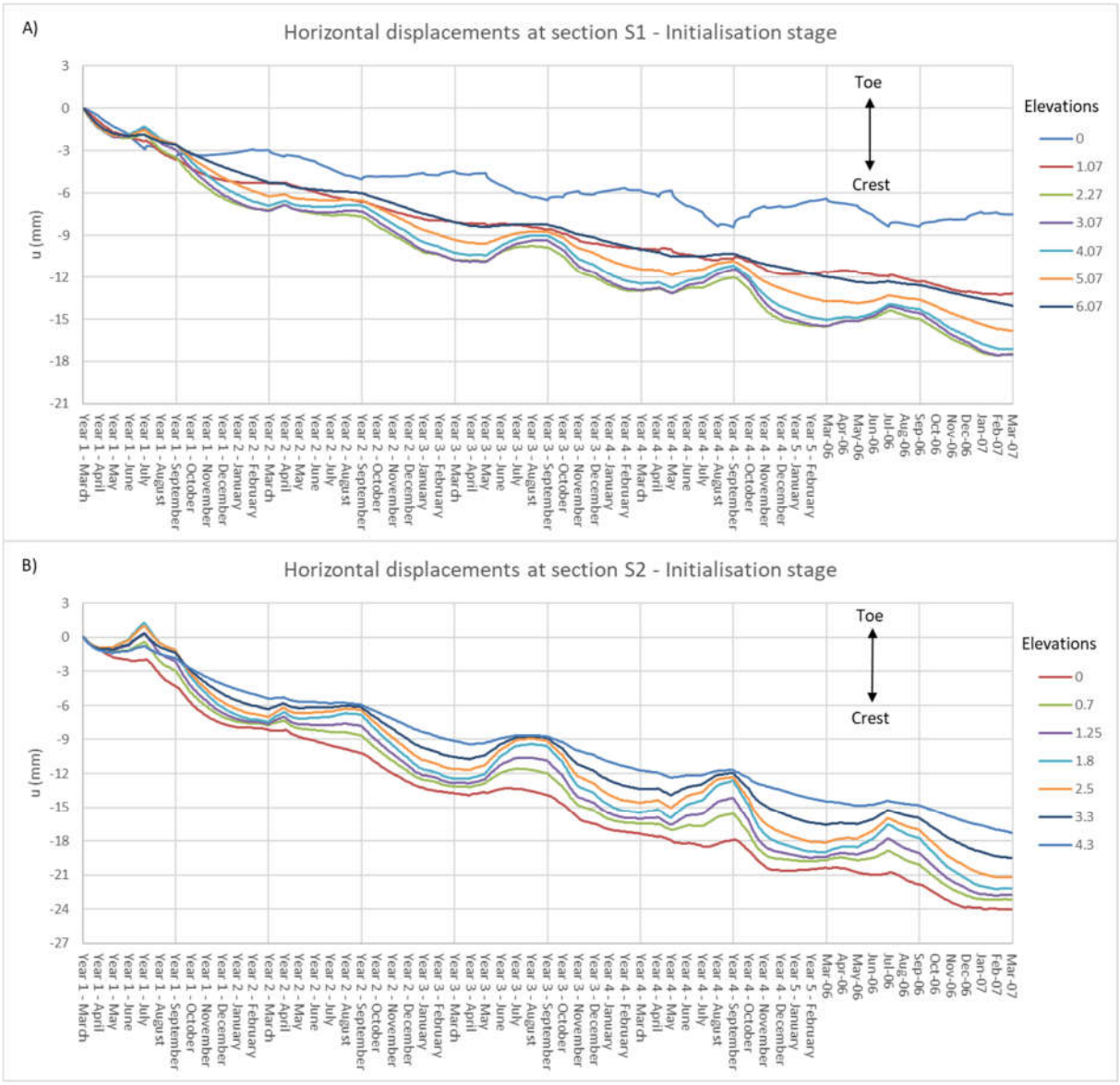

Figure 4.42 Evolution of horizontal movements at sections S1 and S2 for the analysis employing modified BBM

Seasonal variations of horizontal displacements are of the order of few millimetres. On the site, their directions were correlated well with the position of the nearest tree. Considering that utilised vegetation boundary condition is one-dimensional, and therefore unable to model individual tree effects, the seasonal direction patterns are governed by the hydraulic response of wider area. In particular, the zone of foundation soil beyond embankment toe, were large trees are also present, controls the direction of horizontal movements within the clay fill. This is illustrated in Figure 4.43,

which shows the vectors of accumulated summer and winter displacements. Larger seasonal pore water suction variations caused by lower permeability of this material, makes this zone behave numerically likewise the effect individual tree would have in the field. It can be seen that in the lower half of the slope during summer season vectors are oriented towards embankment toe, whereas during winter wetter months the swelling of the highlighted zone pushes the surrounding soil away, driving the clay fill towards the crest. Once again it should be emphasized that the corresponding annual horizontal movements are relatively small and do not compromise the serviceability of infrastructure, but could potentially have detrimental implications for stability. This is particularly true for overconsolidated high plasticity clays prone to progressive failure type mechanism.

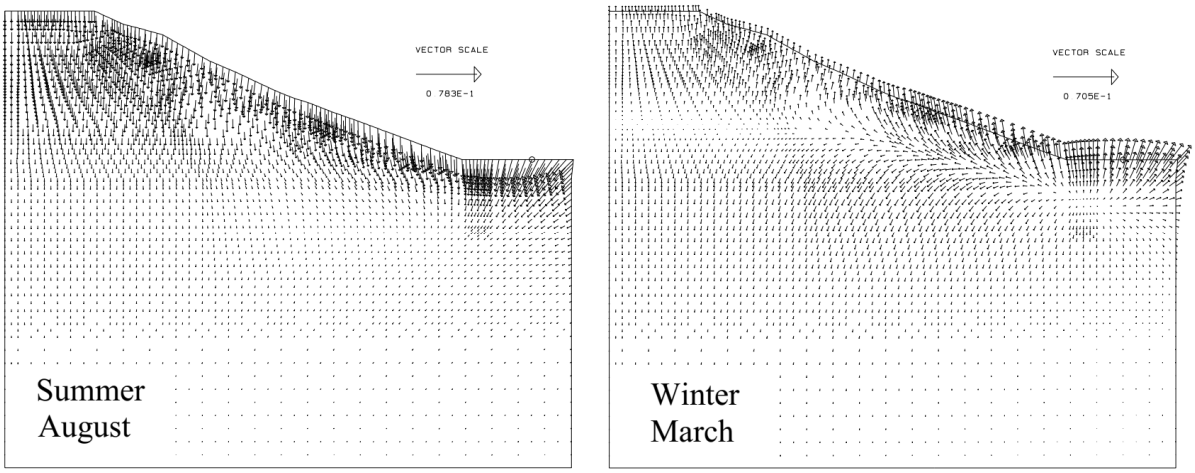

Figure 4.43 Vectors of sub accumulated displacements for periods spring/summer and autumn/winter for the analysis employing modified BBM

4.8.3 Fluctuation Stage

Partially saturated Mohr-Coulomb model – ICFEP Model 82

As already explained, the last year of the initialisation stage was chosen to symbolise the first year of monitoring period, and was referred to as the fluctuation stage. Therefore, the results of performed numerical analyses would be discussed in connection to processed field measurements.

Figure 4.44 illustrates the predicted monthly pore water pressure profiles for the first year of monitoring period. It can be seen that the highest suctions predicted in clay fill stratum are of the order of 120 kPa and 90 kPa for sections S1and S2 respectively, and correspond to the August 2006. (end of summer). On the other hand, lowest suctions in clay fill are predicted in March 2006 and March 2007 (end of winter), with magnitudes of about 60 kPa and 45 kPa. The maximum predicted seasonal variations are in the range 40 to 60 kPa, depending on the section and elevation. All stated values, except the maximum suction value in section S1, are essentially identical to the measured ones. It should be noted, that GEO flushable piezometers have a measuring range of negative pore water pressures up to 100 kPa tensile water stress. Therefore, it could be argued that the slight overestimate is not erroneous, but its accuracy could not be adequately assessed. Further distribution deeper into the London clay, both over space and time, is also in good agreement with the measurement data.

The point where numerical model fails to reproduce the observed behaviour are suction values induced within the ash layer. The predicted results significantly overestimate the recorded values.

The reason for such discrepancy could lie in the fact that ash, as opposed to clay fill, is modelled as fully saturated material. Without SWRC to control the desaturation process, the hydraulic response of the ash is mainly governed by the hydraulic behaviour of considerably less permeable underlying clay fill layer. This finding is demonstrated in particular in section S1, where relatively high suctions have been predicted for wetter winter months. In reality, due to its high permeability ash respond is more sensitive to changes in climatic/vegetation moisture fluxes. The absence of sharp change in pore water pressure gradients between ash and clay fill layers, indicates that the pore water pressure distribution over the depth of ash layer is controlled and in equilibrium with clay fill suction field.

If appropriate SWR curve has been assigned to ash layer, the predicted pore water suctions would have been significantly lower. To demonstrate this point, SWR curves for the clay fill and the ash (Duong *et al.*, 2013) are illustrated and compared in Figure 4.45. It can be seen that for the same degree of saturation, corresponding suction for the ash material is notably lower compared to the clay fill suction.

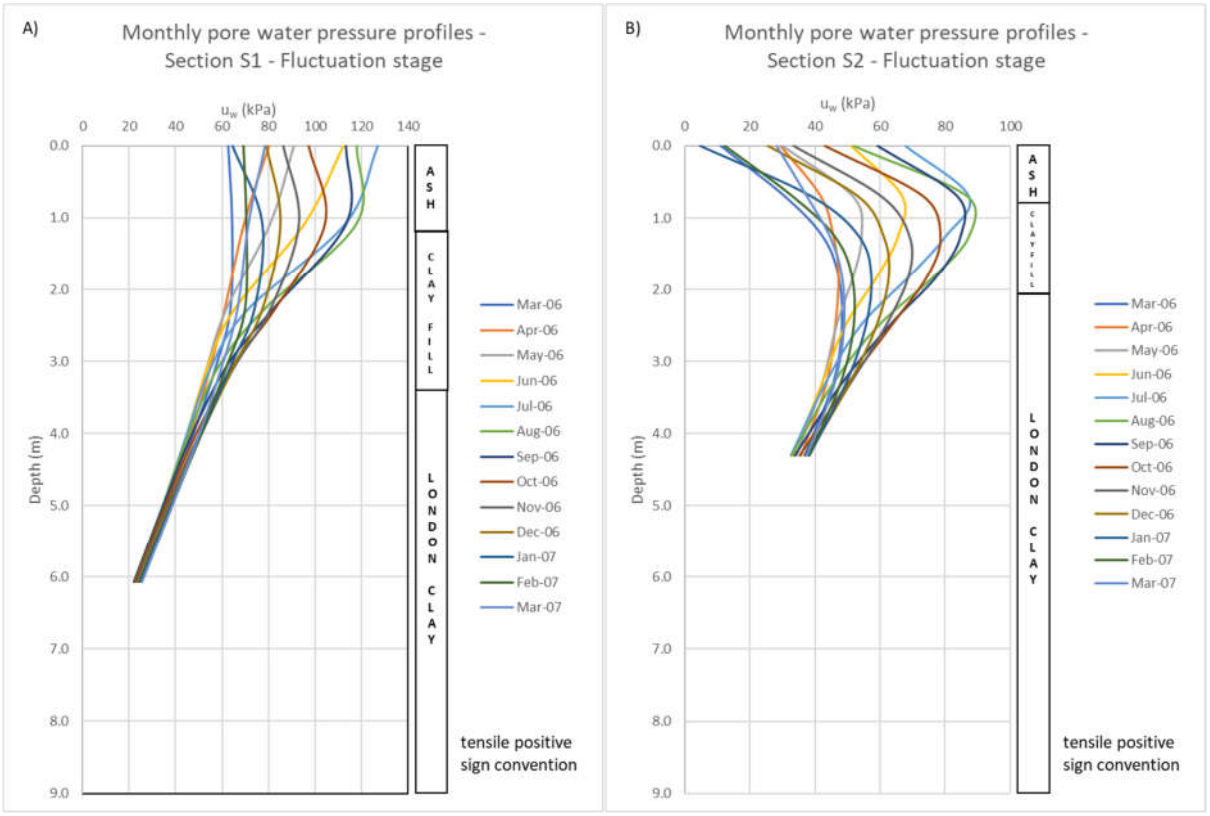

Figure 4.44 Predicted monthly pore water pressure profiles for sections S1 and S2

In contrast, at the surface of section S2, suctions are almost entirely lost at the end of winter. The fact that the suctions are generally lower in this section, especially in ash layer, could be explained by the lateral water inflow from the upper parts of the slope. Once the infiltrated water reaches the ash-clay fill interface, due to the large difference in permeability, further water flow is directed towards the embankment toe, driven by gravitational forces. Section S2 is located in the lower part closer to the toe, and is therefore recharged by lateral seepage.

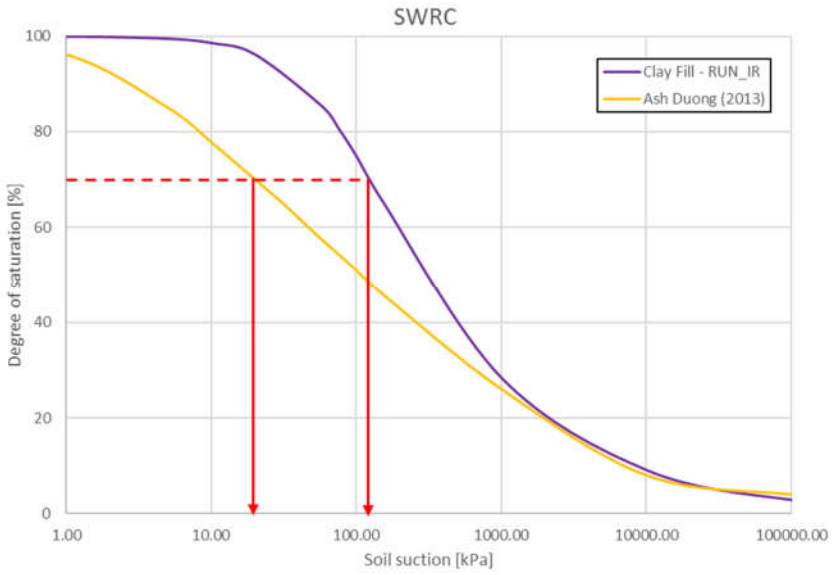

Figure 4.45 SWR curves for the clay fill and the ash (not used in the present study)

The annual distribution of vertical displacements at several points along the depth of sections S1 and S2 is illustrated in Figure 4.46. The obtained results show that maximum vertical displacements are somewhat lower compared to field measurements. Specifically, in section S1 the numerical model significantly underestimates vertical displacements at levels corresponding to clay fill and London clay. Additionally, the model is incapable of capturing seasonal variations at depths greater than 2.0 m, which were observed at the site. However, the top soil displacements, relevant to the assessment of serviceability, are generally in accordance with the field measurements. The profound difference in displacement magnitudes of nodes close to the surface and at depths greater than 2.0 m, indicates that strains are essentially localised within the ash and top zone of the clay fill. Although inconsistent with recorded data, these results correlate well with pore suction profiles, in particular with magnitudes of seasonal fluctuations. As can be seen from Figure 4.44 the differences between summer and winter limiting suctions decrease rapidly below a depth of 2.0 m. It should be emphasized that deformations are induced only by suction changes, as no force boundary conditions are applied.

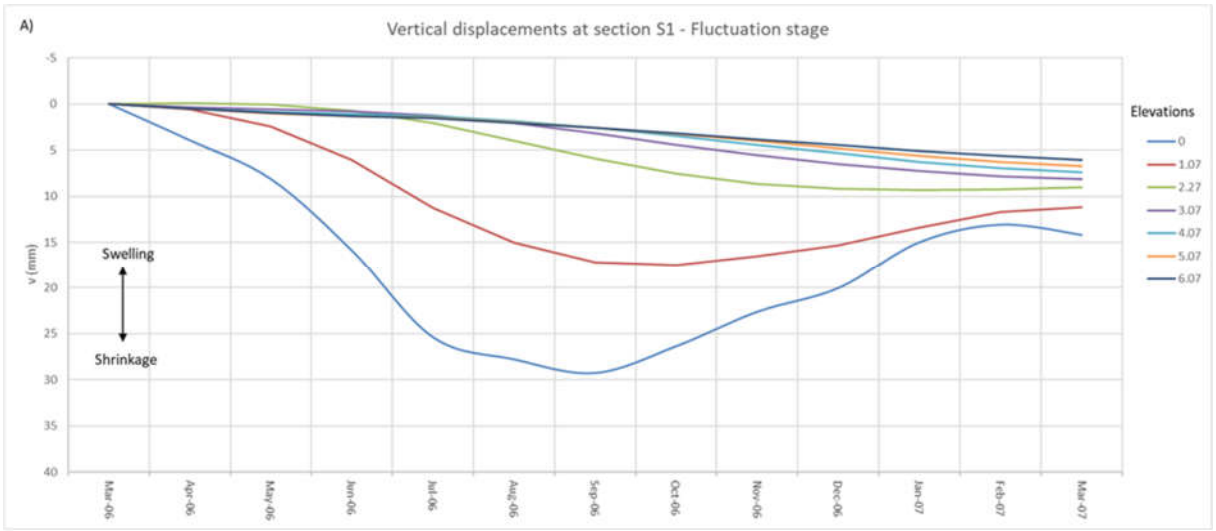

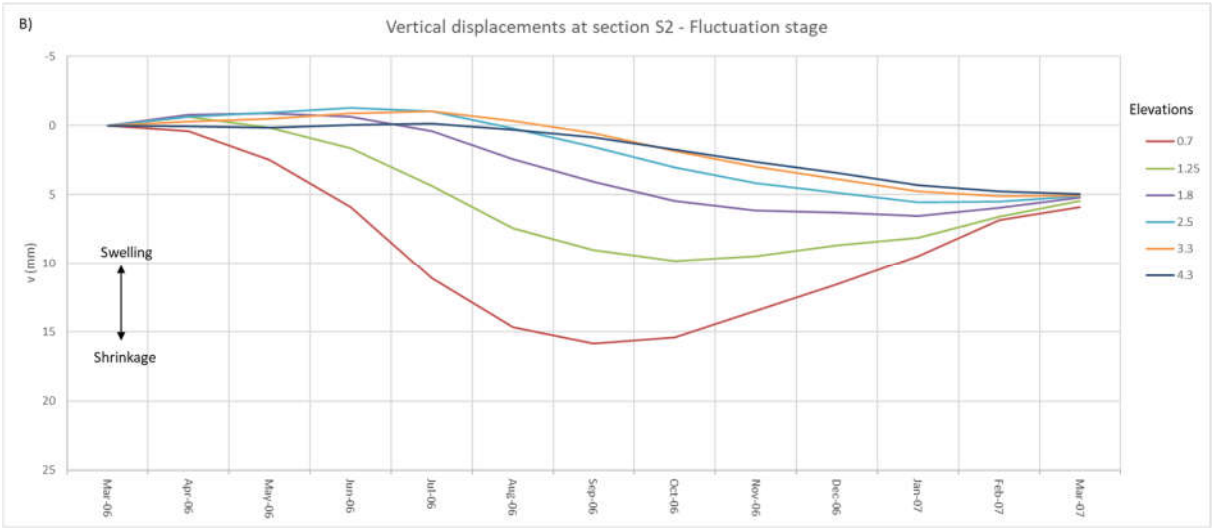

Figure 4.46 Predicted vertical displacements along the depth of sections S1 and S2 for the first year of monitoring period – fluctuation stage

The vertical displacement peak corresponds to the September-October 2006, depending on the depth, which agrees with monitoring data. The delay that exists between the deformational and hydraulic response (maximum pore suctions are predicted in August, whereas maximal vertical displacements are obtained in September-October) is a consequence of soil permeability. Also, similarly to field observations the model predicts that vertical displacements at depths greater than 1.5 m are irreversible. This reflects the fact that the total annual evapotranspiration for first monitoring year is greater than precipitation, which was depicted in Figure 4.30.

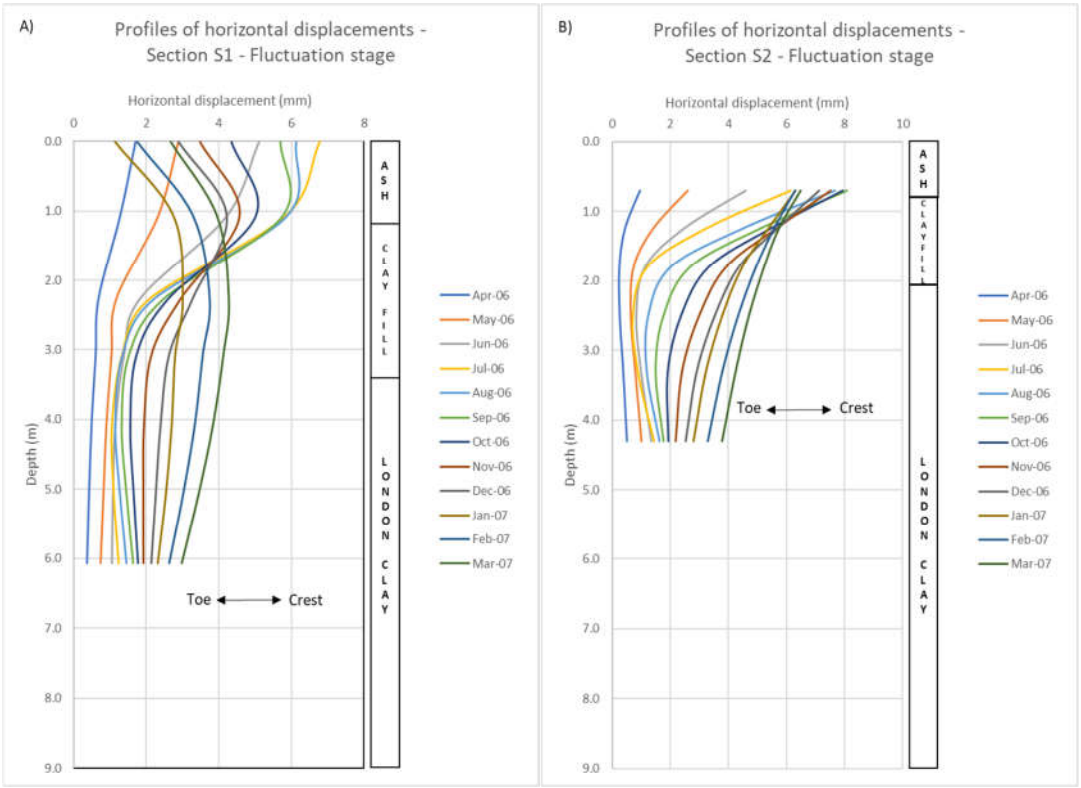

Figure 4.47 Predicted horizontal displacement profiles at sections S1 and S2 for the first year of monitoring period – fluctuation stage

The monthly profiles of horizontal displacements for two sections are shown in Figure 4.47. The whole section S1 is moving towards the crest which is in accordance with the overall shrinkage deformational mechanism governed by negative net moisture fluxes. The surficial 2.0 m at section S1 are more sensitive to alterations in climatic boundary conditions, and by comparison with Figure 4.30 it can be seen that horizontal displacement direction changes perfectly match the monthly net moisture flux rate pattern. In section S2 the entire profile is oriented towards the embankment crest with maximal displacement value of about 8 mm, which complies with inclinometer data.

Modified Barcelona Basic Type Model – ICFEP Model 81

The predicted pore water pressure profiles for the last year of initialisation phase are presented in Figure 4.48. In comparison to the first analysis, more uniform seasonal fluctuation over the entire depth of the clay fill is predicted, which better agrees with piezometer recordings. As explained earlier, this results from the nonlinear desaturation permeability model adopted for clay fill, which taking into account the magnitudes of suctions, obviously gives higher permeabilities. However, the shapes of the profiles are not as would be expected in the field. The predicted monthly profiles are shifting, in top 2 to 3 m, instead of rotating and bending. This is due to nonuniform distribution of permeability across the clay fill depth. Higher permeability in deeper part of the clay fill relative to upper zone, resulting from lower suctions (see Fig. 4.37), eases the propagation of infiltrated water, thereby reducing suctions further. Consequently, the shifting of the profile is produced.

The magnitudes of estimated seasonal variations are in accordance with field measurements, whereas the absolute values are lower.

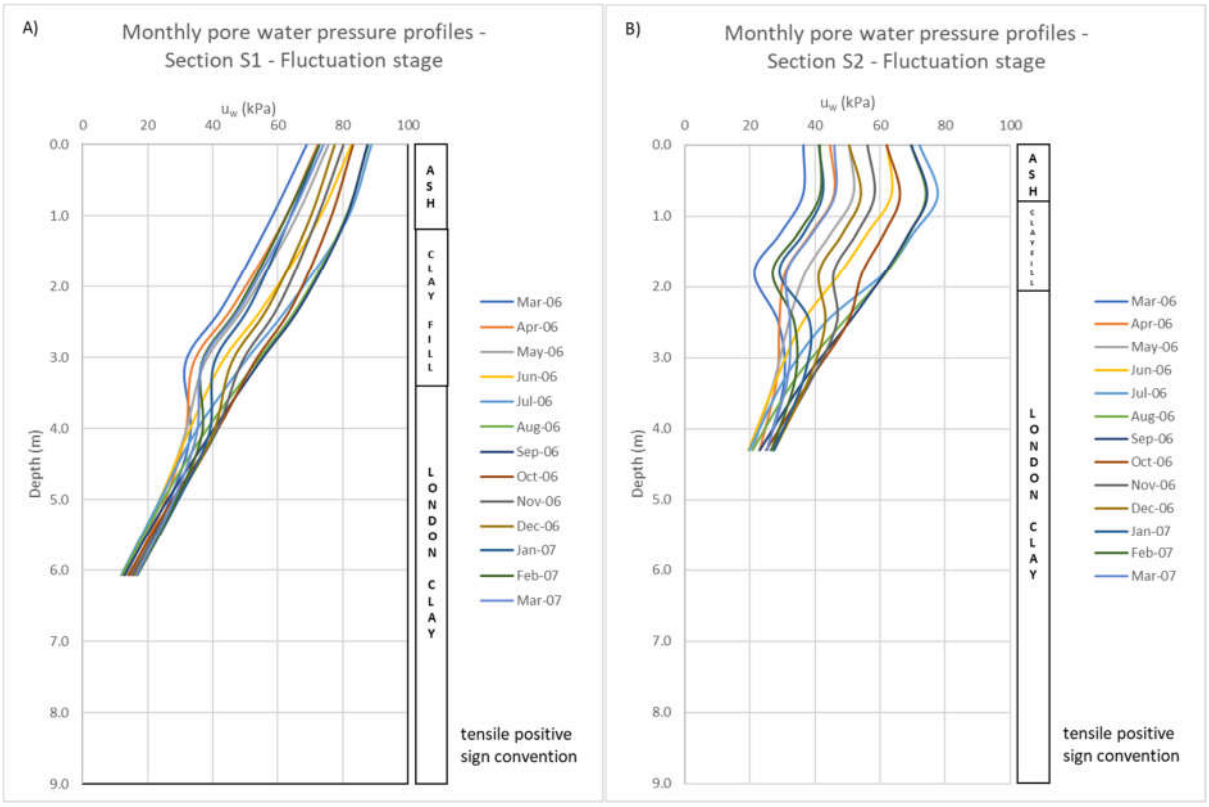

Figure 4.48 Predicted monthly pore water pressure profiles for sections S1 and S2 for the analysis employing modified BBM

The Figure 4.49 shows the evolution of vertical movements for the fluctuation stage. Once again, the higher permeability of the clay fill, allowed the deeper zones of the embankment to be affected by

the process of water exchange with the atmosphere, resulting in more pronounced seasonal variations of deformations compared to the first analysis. The magnitudes of movements are generally lower compared to results of the first analysis and extensometer data, especially in section S1. The reason is that the compressibility of the clay fill in this analysis is mainly governed by elastic compressibility coefficient related to suction changes κ_s, whereas in the case of partially saturated Mohr-Coulomb is essentially controlled by H modulus. Additionally, while the H modulus was assumed to be constant for the entire suction range, that is not the case with modified BBM (Model 81). The constant κ_s value, is equivalent to continuously increasing modulus of deformation relating volumetric strains to suction changes.

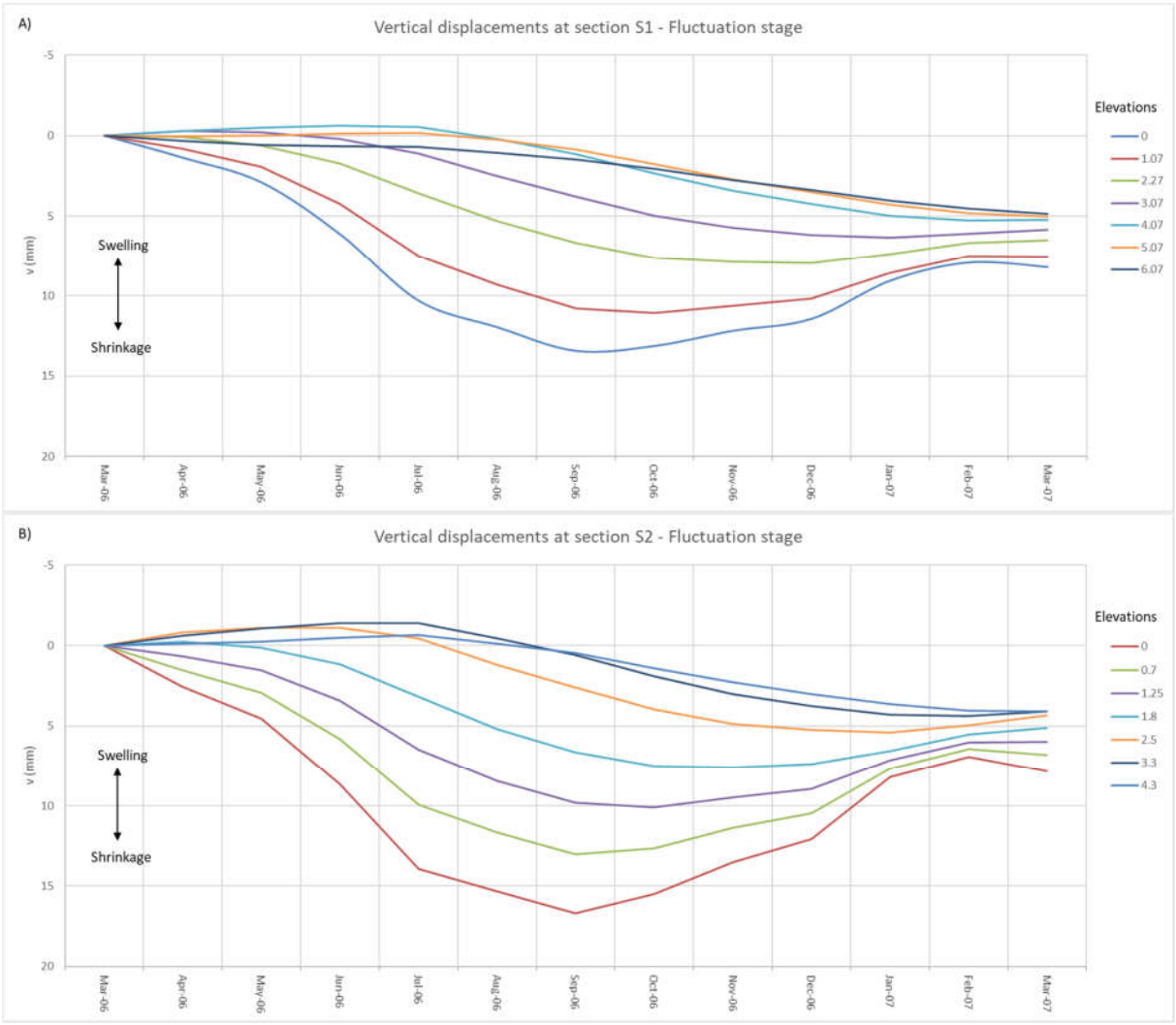

Figure 4.49 Predicted vertical displacements along the depth of sections S1 and S2 for the first year of monitoring period, for the analysis employing modified BBM

4.8.4 Vegetation Clearance Stage

Partially saturated Mohr-Coulomb model – ICFEP Model 82

In March 2007, vegetation has been removed from most part of the slope, leaving only several mature oak trees very close the embankment toe. In main analysis, as was explained in section 4.7.5, the tree clearance was simulated through reduction of maximum root depth from 2.0 to 0.3 m and lowering of potential evapotranspiration rates. In numerical model, the high-water demand trees were left only in a confined zone beyond the embankment toe. The pore water pressure profiles corresponding to

ends of winter and summer seasons (March and September) for the full monitoring period have been presented in Figure 4.50. It can be seen that previously accumulated pore suctions are relatively rapidly decreased, as a result of tree felling. The water extraction rate of grass cover, that has replaced the mature trees along the slope, is insufficient to dry the soil. It is inherent to the UK that precipitation is fairly uniform throughout the year, and that is the main reason why, even during the summer drier months, the evapotranspiration rates of small bushy vegetation are inferior to rainfall.

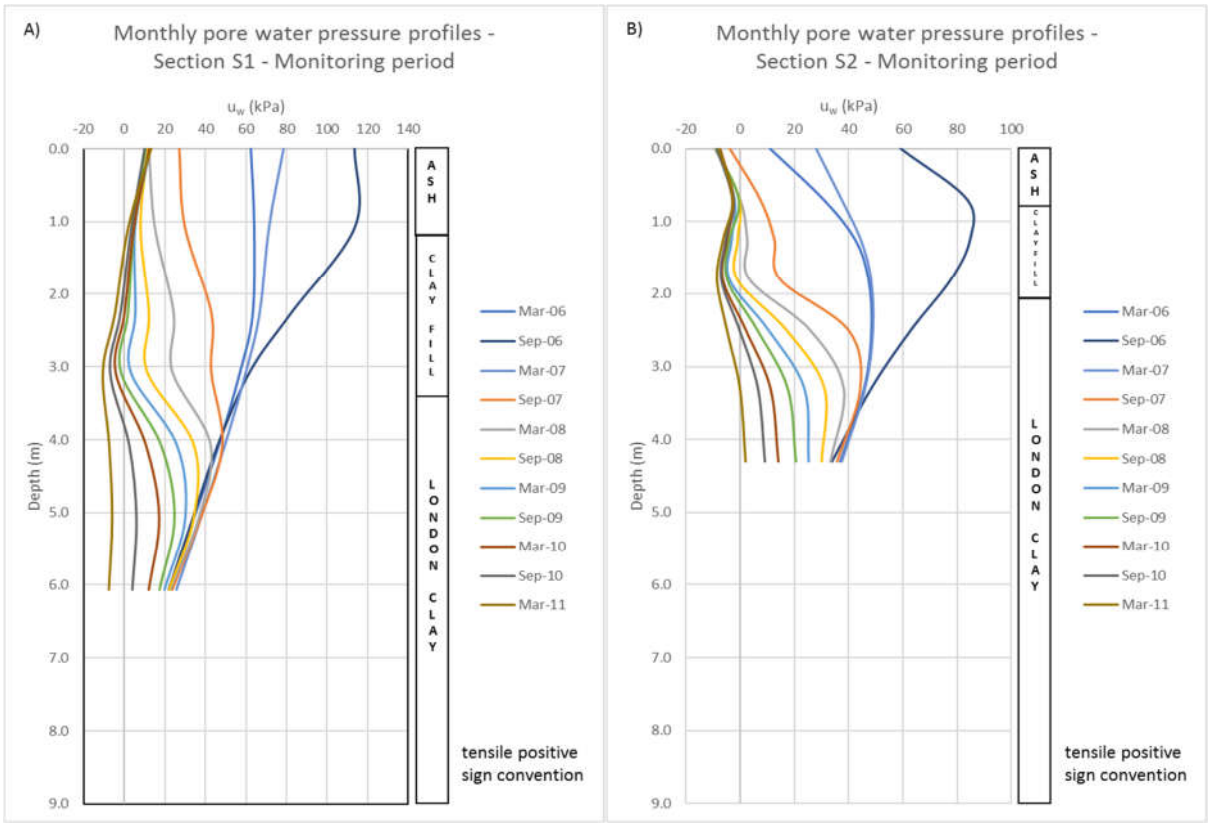

Figure 4.50 Predicted winter and summer pore water pressure profiles at sections S1 and S2

The predicted profiles suggest that suctions within clay fill are essentially completely lost during the second year following vegetation clearance, which agrees reasonably well with field measurements. On the other hand, markedly slower reduction of pore suctions in London Clay stratum is obtained. The steadier "dissipation" of persistent London Clay suctions over several years closely resembles the site observations. The GEO flushable piezometers installed within London Clay have shown that it took almost 4 years for suctions to be completely lost, exactly the same time span as predicted by the numerical model.

The distribution of pore water pressures for several characteristic points (nodes) down the two sections is illustrated in Figure 4.51. Unlike true sharp drop in suctions produced by propagation of the wetting front, the model predicts more gradual decrease, especially in less permeable layers. The top two points, located in the ash, seemingly achieve to reasonable replicate the water front infiltrating from the soil surface. This does not mean that the present numerical model is capable of capturing this complex phenomenon, rather several order of magnitude higher permeability of ash compared to underlying strata produce false impression of sharp reduction on coarse time scale axis.

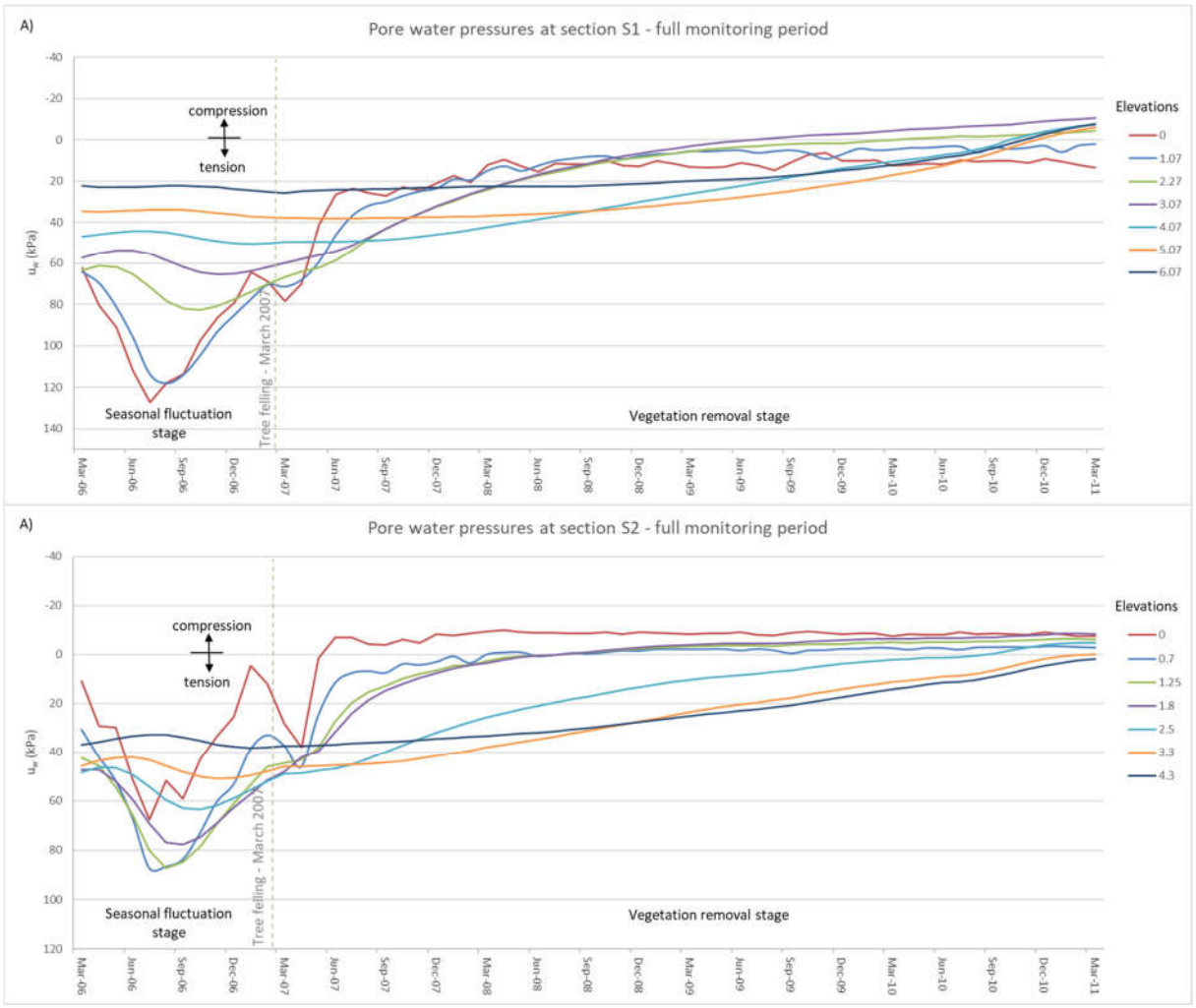

Figure 4.51 Predicted pore water pressure distribution for several levels along the depth of sections S1 and S2

The former discussion regarding the inability of the model to simulate realistically propagation of distinctive wetted zone is schematically illustrated through volumetric water content and degree of saturation profiles, presented in Figure 4.52. As can be seen, the transition from fully to partially saturated zone is not quite sharp as was measured on the site. However, it should be noted that for fine-grained soils, wetting front becomes diffusive and water content and pressure changes occur more uniformly along the depth. Clear wetting front observed on the site, most likely results from specific structure of the dumped clay fill, characterized by more permeable matrix, and preferential seepage path created by decayed tree roots. In addition, it can be seen that deep residual suctions (persistent soil moisture deficit) induced by mature trees and preserved even during the wetter winter months before vegetation has been removed, upon tree felling are rapidly lost in less than two years.

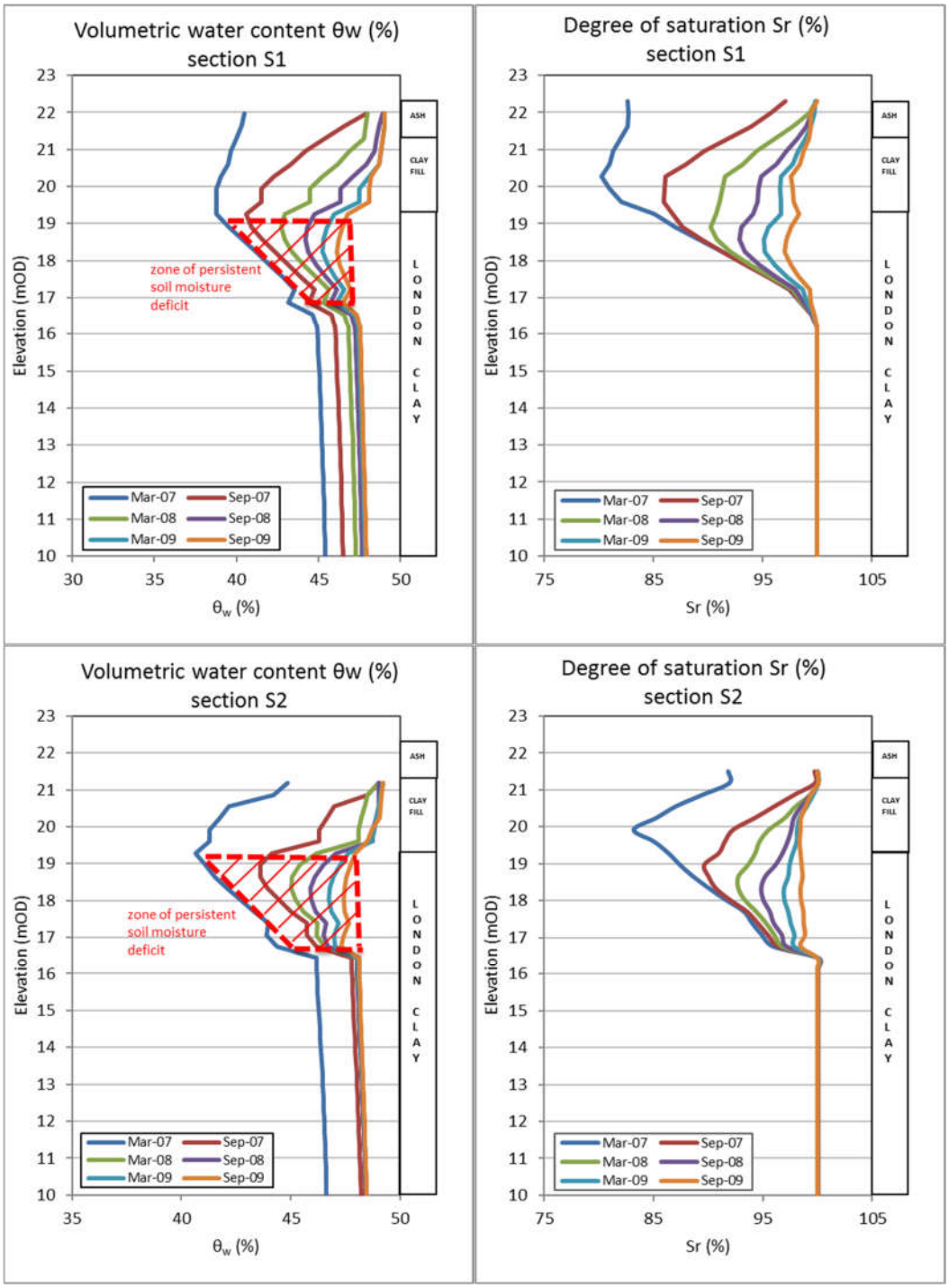

Figure 4.52 Predicted volumetric water content θ_w and degree of saturation S_r profiles for the first two years following vegetation clearance

Figure 4.53 shows contours of winter pore water pressures for the period following vegetation removal. The remaining high-water demand trees at narrow zone beyond the embankment toe are capable, in spite of lateral water inflow from the embankment slope, to maintain persistent soil suctions, which act preventively against formation of deep-seated instabilities.

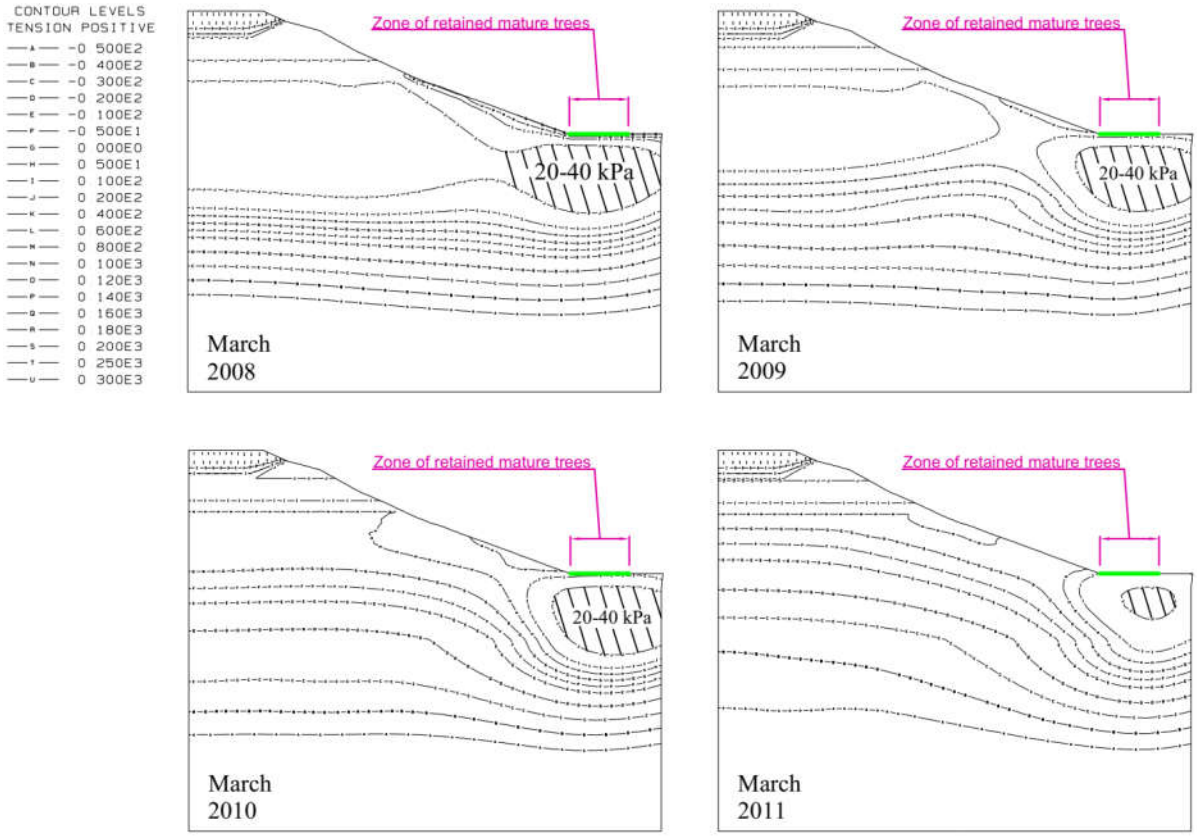

Figure 4.53 Contours of winter pore water pressures following vegetation removal

In a period between March 2008 and September 2008 (increments 894-966), more than one year after the trees were removed from the embankment slope, the failure mechanism was formed in the upper part of the slope. As can be seen from Figure 4.54, the sliding soil mass is located entirely in ash layer. Both, the relative ratio of displacement vectors magnitudes and distribution of plastic deviatoric strains clearly indicate that failure has developed. However, despite the large displacements have been predicted in part of the finite element mesh, the convergence of the solution was not compromised, and the execution of program routine has not terminated. It should be noted that sliding block has encompassed small upper part of the section S1, and those results are therefore excluded from the following discussion.

The failure is relatively shallow, around 1.2 m deep, and has cylindrical shape. The inclination of the failure surface, as expected, is equal to the angle of shearing resistance of the ash layer (see Fig. 4.54). It can be argued that several factors have contributed to the initialisation of the failure. Firstly, the ash-clay fill permeability ratio is very adverse in a sense that lower permeability clay fill will prevent drainage of infiltrated water, which would eventually lead to generation of compressive pore water pressures and establishment of hydrostatic conditions above top clay fill boundary. The clay fill layer in this case acts as an impermeable boundary with respect to ash and allows the formation of so-called perched water conditions. Additionally, the geometry of the upper part of the slope further exacerbates the stability conditions, in that it is somewhat steeper compared to lower part. The rapid infiltration of surface water induced by removal of mature trees, combined with listed factors, triggers the local failure at the embankment crest.

The predicted local failure, and the possible reasons why it has not been observed on the site, is further investigated in next chapter, as part of the parametric study.

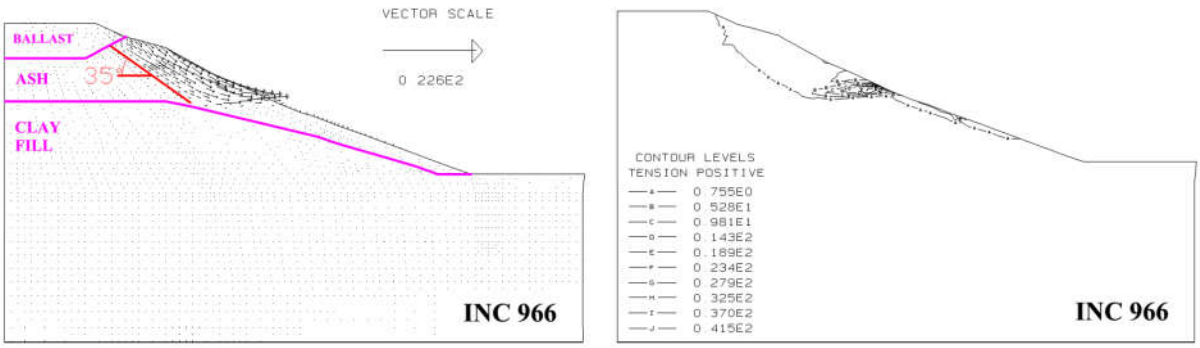

Figure 4.54 Predicted vectors of accumulated displacements and contours of accumulated plastic deviatoric strain

The vertical movements at two sections of north-facing slope are presented in Figure 4.55. As stated earlier, the predictions for the point (node) closest to the surface at section S1 are omitted from displacement plots due to excessively high values related to the local failure. Following tree removal, the continuous swelling, initially rapid and afterwards more gradual, is predicted. Similarly to field measurements the top 3.0 m exhibit heave deformation, whereas deeper strata either return to initial position or retain some permanent settlement. The magnitude of heave movement at section S1, at the end of monitoring period, is lower compared to measured ones (maximum predicted 40 mm vs measured 60 mm).

On the other hand, the magnitude of surficial vertical movements at section S2 is distinctively lower (about 15-20 mm), and shows good agreement with extensometer data. The results from current numerical model support the earlier judgment, that remaining trees at the embankment toe minimise the swelling movements at section S2. However, model fails to provide any answers about peculiar settlements that have been observed at section S2 below 2.0 m depth.

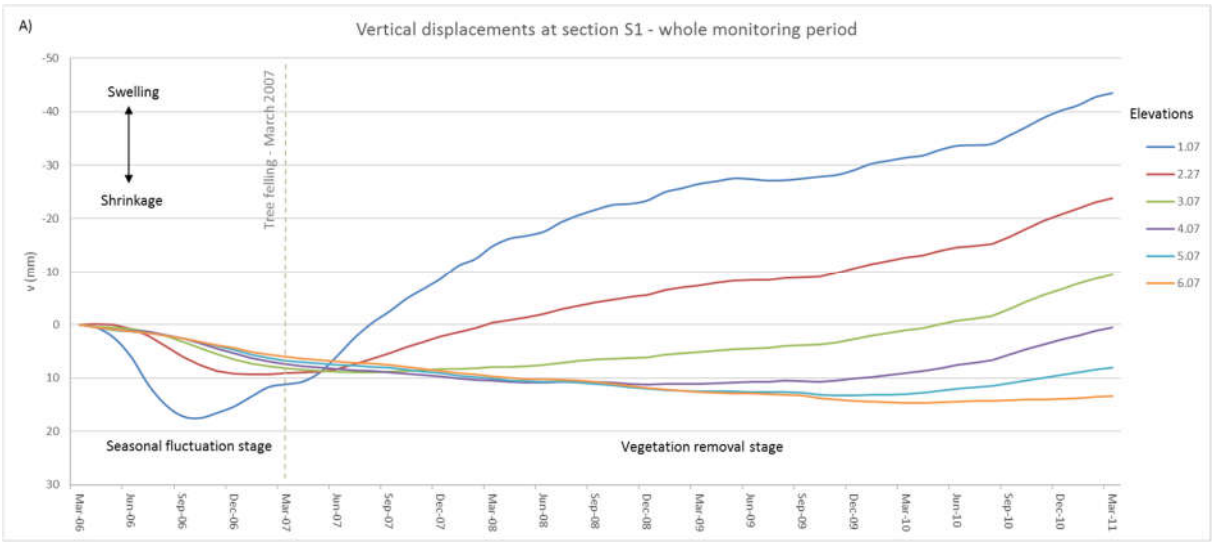

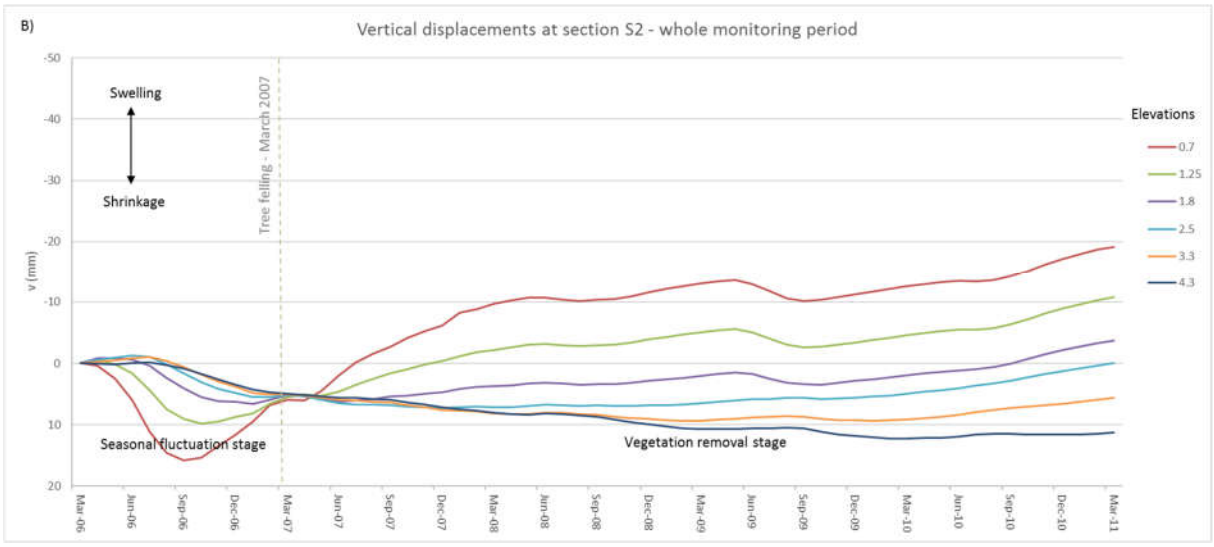

Figure 4.55 Predicted vertical displacements at sections S1 and S2 following vegetation removal

It can also be noticed from Figure 4.55 that during the last winter the rate of the heave deformation is accelerating. This abrupt change in swelling rate, nearing the end of monitoring period, matches with the field loggings.

The evolution of horizontal movements is shown in Figure 4.56. It is clear that the movements are oriented towards the embankment toe, which is consistent with swelling mechanism taking place after the felling of large trees. The maximum horizontal displacements at the highest presented elevations (not affected by upper slope collapse) at sections S1 and S2 are of the order of 45 mm and 65 mm respectively, whereas the corresponding recorded ones are 45-50 mm and 55-60 mm. Additionally, the general trend of progression of horizontal displacements, in particular the acceleration of movement rates during every spring (starting from March) is very accurately reproduced.

It should be recalled that inclinometer measurements suggest that a form of a slip surface is present within the London Clay foundation soil in close proximity to the clay fill boundary. However, the model results do not indicate any slippage or accumulation of plastic deviatoric strains within London Clay layer. This is also illustrated in Figure 4.57, which plots profiles of horizontal movements at sections S1 and S2 of the north embankment slope. It can be seen that the profile gradients are fairly uniform along the depth, especially in section S1.

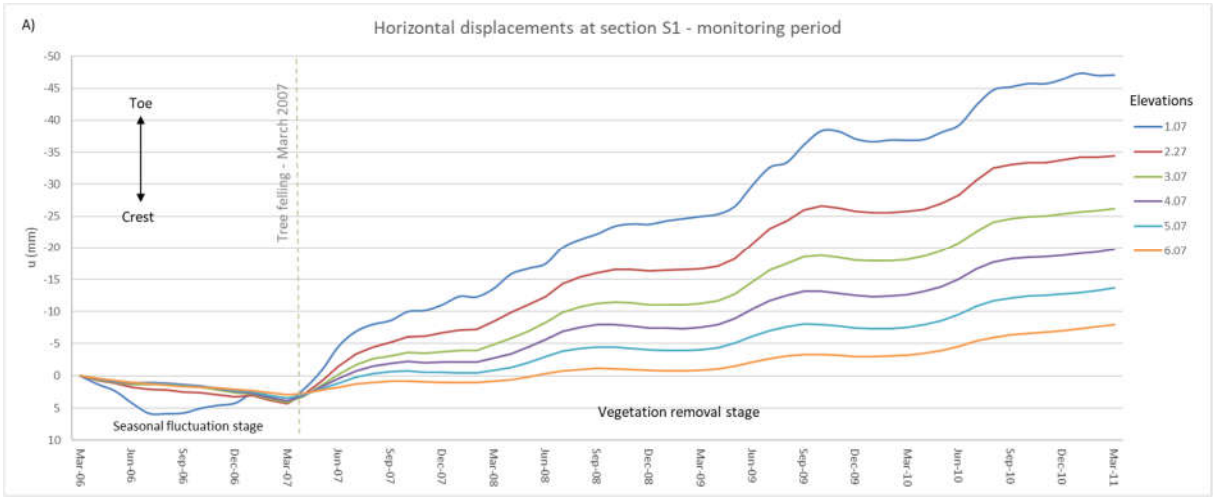

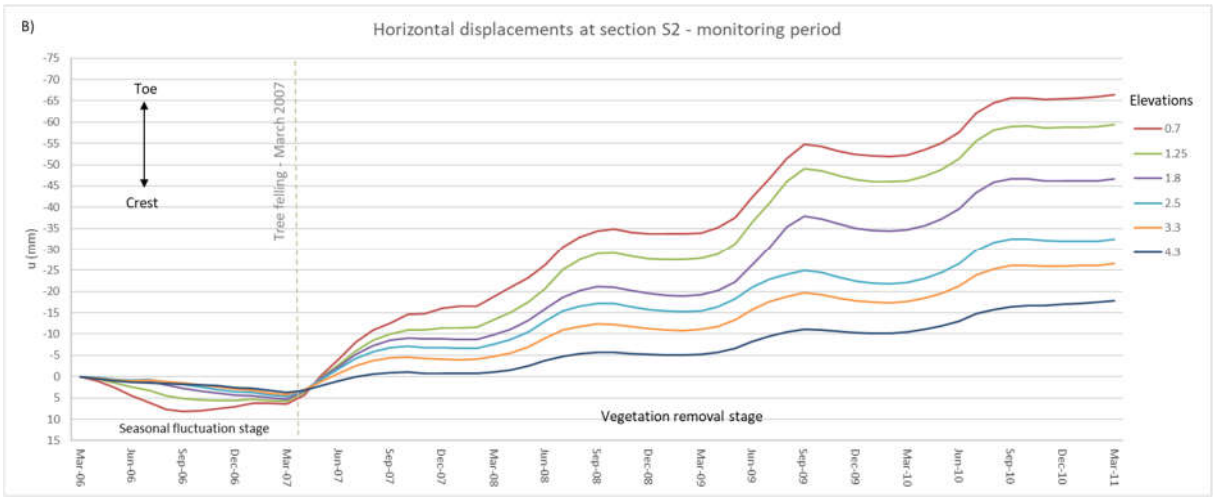

Figure 4.56 Predicted horizontal displacements at sections S1 and S2 following vegetation removal

The reason for observed sliding is possible presence of relic (tectonic) shear surfaces with strengths close to residual (Kovacevic, Hight & Potts, 2007). Within parametric study, presented in Chapter 5, the allowance for potential existence of low-strength shear zone was made, in order to investigate its effect on the overall deformational and stability behaviour.

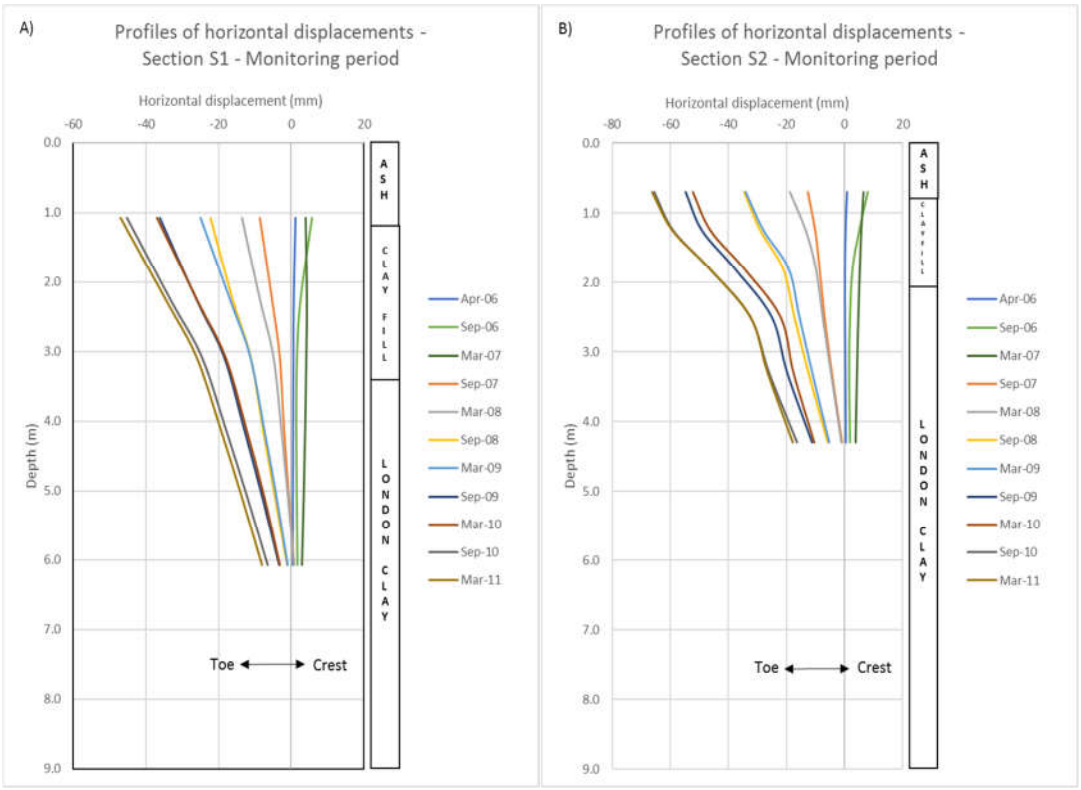

Figure 4.57 Predicted profiles of horizontal displacements following vegetation removal

The winter and summer (March/September) pore water pressure profiles for the entire monitoring period are shown in Figure 4.58. As a result of higher permeability, which even increases as suctions are lost due to prevailing infiltration, soil domain is being rapidly saturated. The pore suctions within the clay fill layer, persistently maintained prior to tree cutting, are completely lost in under 18 months after vegetation clearance (around the autumn of 2008). In addition, even compressive pore water pressures, up to -10 kPa, are generated at the surface of section S2. The transition to compressive pore pressures in root zone, essentially means that vegetation boundary condition is no longer active, as the reduction function $\alpha(s)$ falls to zero. To prevent this from happening threshold pore water pressure p_{fb} should be assigned small tensile (pore suction) value, consistent with the potential evapotranspiration function α. However, it should be emphasized that the prescribed zero threshold pore water pressure value is physically realistic, especially for sloping ground. In that case the excess water, that has not penetrated the ground, would turn into run-off, rather than being ponded on the surface. Additionally, the calculation of negative pore water pressures at the surface is likely related to inadequate set up of automatic incrementation scheme linked specifically to vegetation boundary condition.

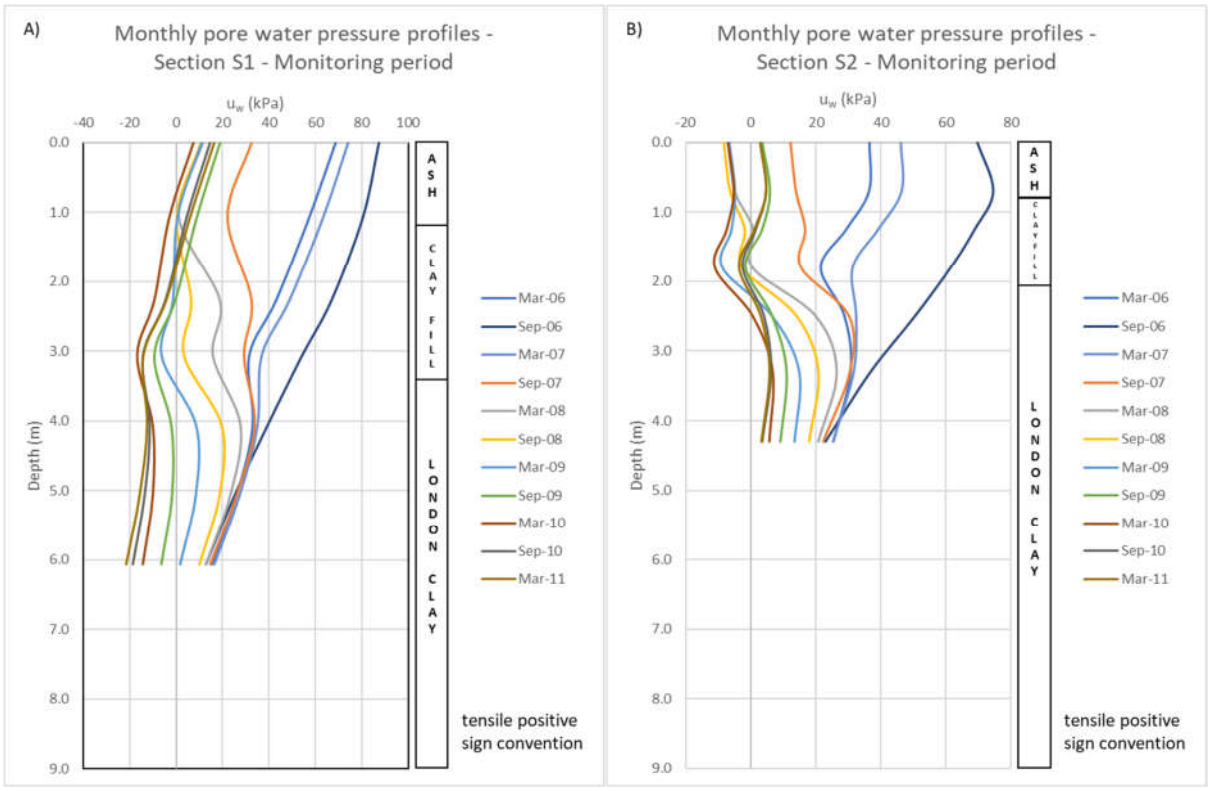

Figure 4.58 Predicted winter and summer pore water pressure profiles at sections S1 and S2 for the entire monitoring period

The distribution of pore water pressures for several characteristic points (nodes) down the two sections, S1 and S2, is illustrated in Figure 4.59. The same type of response with respect to the rate of reduction of pore suctions induced by water infiltration from the soil surface is predicted. It is evident that the more sophisticated mechanical model has no advantage over simpler one with respect to modelling water front propagation. For improved prediction, which would account for propagation of wetted zone, fundamentally different SWR curves should be employed.

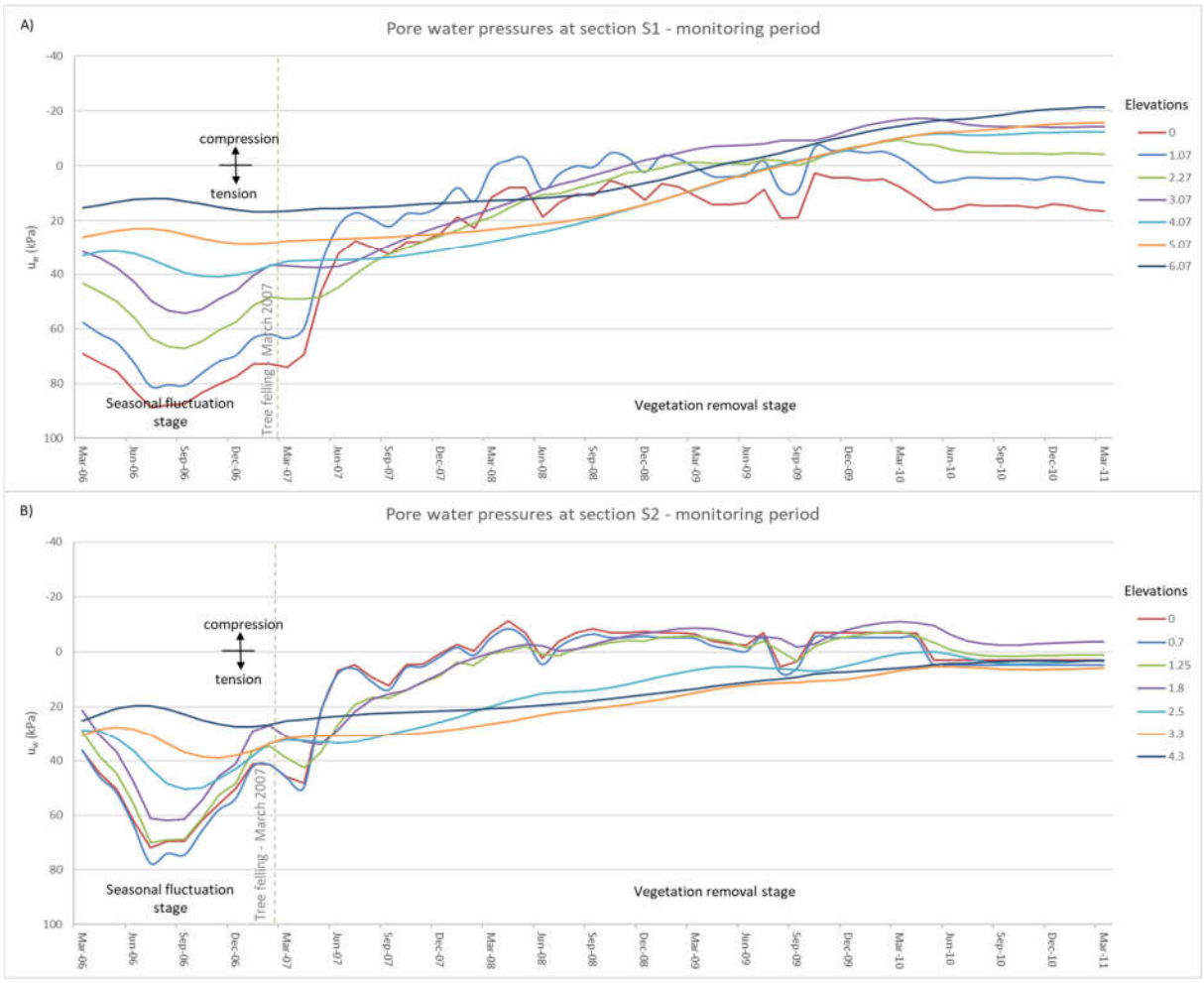

Figure 4.59 Predicted pore water pressure distribution for several levels along the depth of sections S1 and S2 for the analysis with Model 81

Unlike the first analysis with partially saturated Mohr-Coulomb model, the shallow failure of the upper slope has not occurred in this one. The primary reason stems from the fact that effective stress cohesion of the ash material was raised from 2 kPa to 30 kPa. The detailed explanation for this correction is provided within parametric analysis of Chapter 5.

The evolution of vertical displacements for seven nodes along the sections S1 and S2 is illustrated in Figure 4.60. Considering that the failure has been prevented, the prediction for the top most node in section S1 is also included. Compared to first analysis slightly lower maximum heave movements are predicted. Also, more uniform rate of vertical movements is predicted for the first three years following vegetation removal, after which the swelling deformation is gradually stabilising.

In section S2, the current analysis is able to capture some fluctuations observed in the measured heave. Recall that vegetation boundary condition along the slope representing grass cover, that has left upon cutting of the trees, is essentially inactive due to the complete loss of the pore suctions. This means that the estimated variations for the end of summer 2009 and 2010, which correlate well with the climatic data for the same period, were induced by large trees kept beyond the embankment toe.

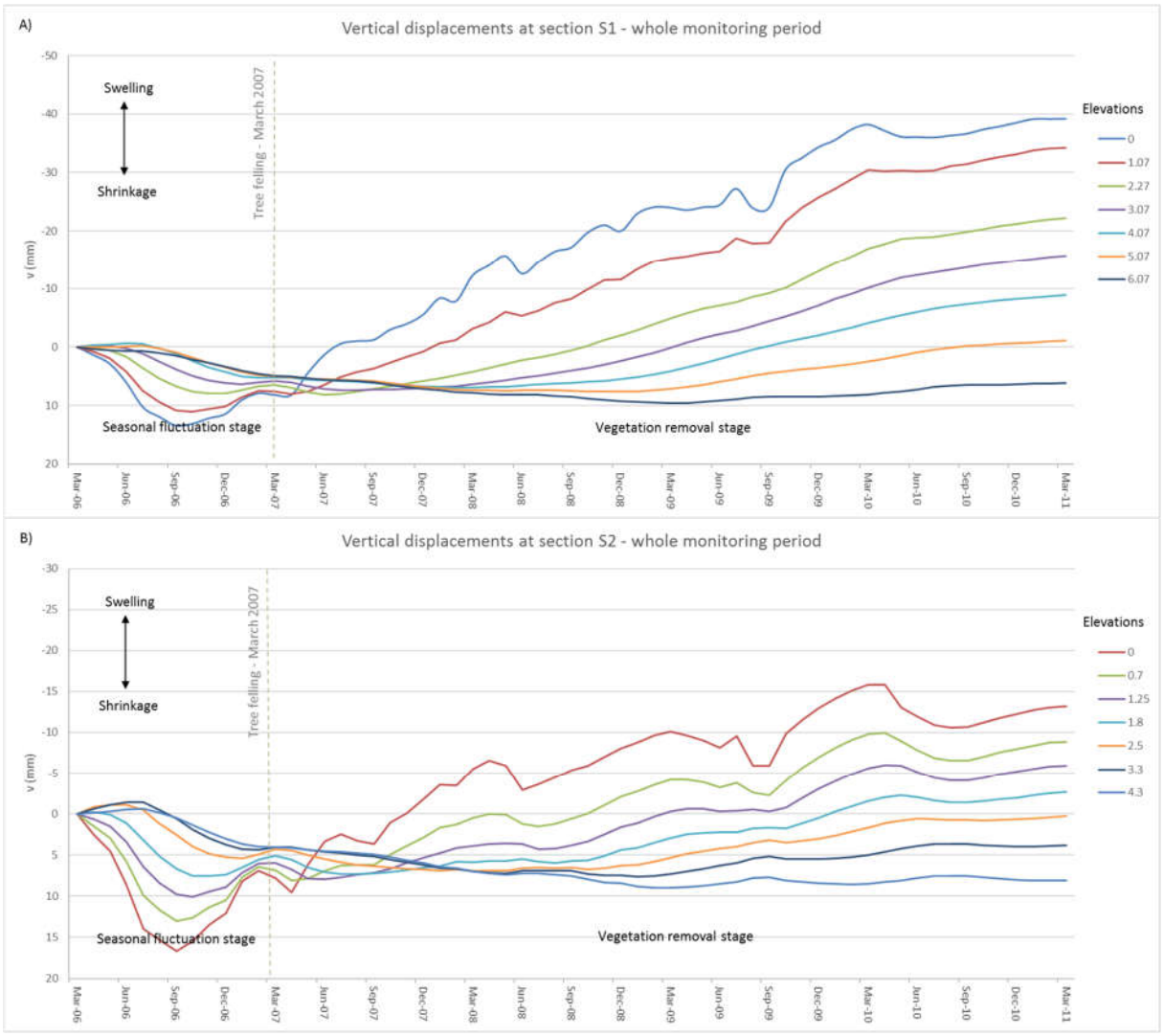

Figure 4.60 Predicted vertical displacements at sections S1 and S2 following vegetation removal for the analysis with Model 81

The evolution of horizontal movements is shown in Figure 4.61. Maximum estimated horizontal displacements at section S1 are around 27 mm and correspond to depths between 2.0 and 3.0 m. The surface horizontal settlements of ash layer at this section are somewhat lower. This can be more clearly seen in Figure 4.63, which illustrates the monthly profiles of predicted horizontal displacements for the entire monitoring period. In section S2 maximum horizontal movements of about 45 mm are obtained, which is some 20 mm less compared to inclinometer recordings.

Variable rates of horizontal movements correlate well potential evapotranspiration and precipitation data. The significant increase in horizontal movement rates during spring periods is connected with higher evapotranspiration rates. In Figure 4.62 estimated potential evapotranspiration, precipitation and net rates for the period April 2009 – March 2010 are presented. As can be seen, sudden change from positive to negative water fluxes, induced by somewhat drier period and concurrent initiation of development stage of vegetation growing cycle, triggers the equally sharp increment of horizontal movements. This is particularly evident in section S2, closer to the embankment toe, where some mature trees have been retained. The subsequent swelling of the tree zone (in the vicinity of the embankment toe), produces movements in the opposite direction. However, their magnitude is very small, and irreversible horizontal movements are steadily accumulating.

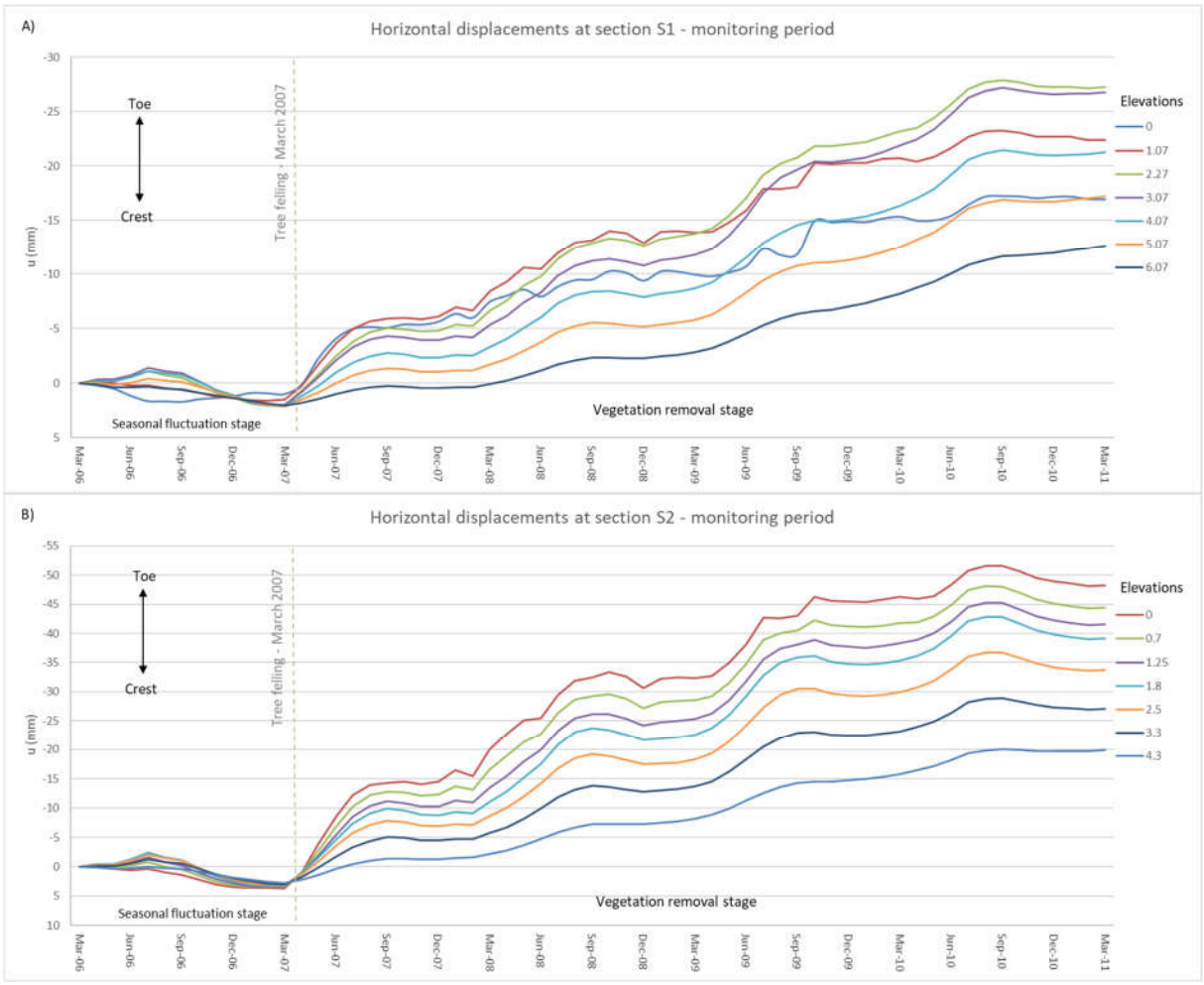

Figure 4.61 Predicted horizontal displacements at sections S1 and S2 following vegetation removal for the analysis with Model 81

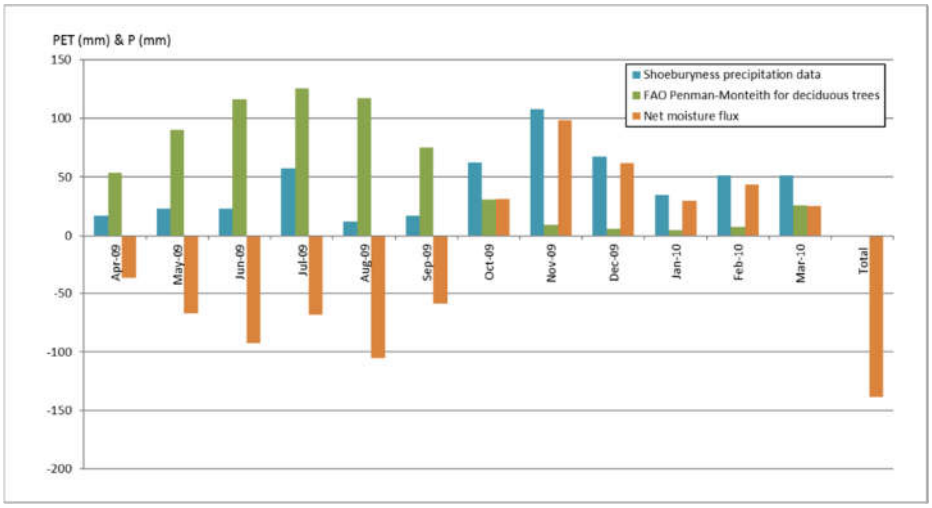

Figure 4.62 Potential evapotranspiration, precipitation and net rates for the year 2009

This finding has some practical implications, in particular with the vegetation management. It seems that leaving the high-water demand trees in the vicinity of the slope toe in low permeability and high

plasticity clay soils, has both beneficial and negative impacts. The generation of persistent deep soil suctions, directly increases the effective confining stress levels, thereby increasing the available shear strength, which in turn contributes positively to overall slope stability. On the other hand, large seasonal pore water pressure variations linked to low permeability soils and saturated conditions, add up to irrecoverable horizontal movements which may bring about the commencement of slope failure.

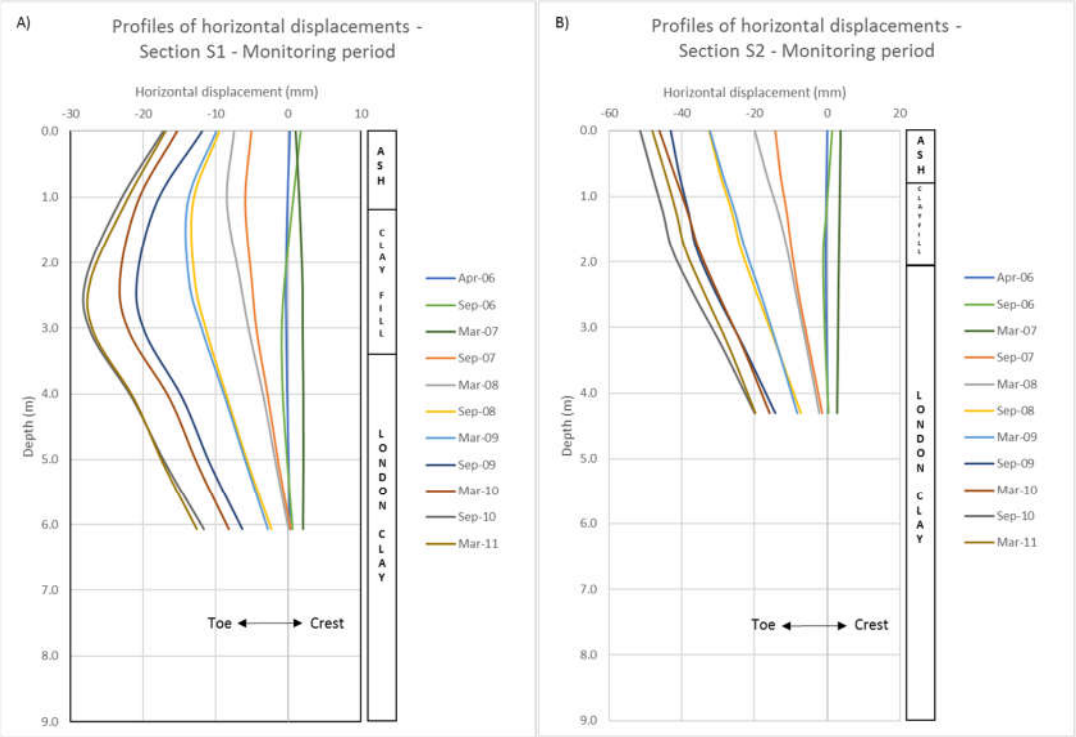

Figure 4.63 Predicted profiles of horizontal displacements following vegetation removal for the analysis with Model 81

4.8.5 Summary and Comparison of the Results

In this section a comparison is made between the results of two main analysis with the field measurements. The key analyses outputs are presented on common plots, thereby allowing more systematic and comprehensive visual inspection. The aim is to gain better understanding of the mechanisms governing the behaviour of embankments subjected to environmental effects, including, inter alia, vegetation and precipitation. In addition, the quality of predictions, in particular from quantitative perspective, as well as suitability of relatively simple unsaturated constitutive model is assessed.

In the Figure 4.64 the comparison between the results of two numerical simulations employing different constitutive models, and field pore water pressure data are presented. Both figures (A & B) illustrate the evolution of pore water pressures for two points corresponding to levels of two piezometers installed within section S1. Selected points are located within the clay fill layer.

It is evident that the results from both analyses shows reasonable agreement with piezometers readings. The results from two numerical analysis differ primarily in the initial conditions achieved through the initialisation stage. As was explained earlier, different permeability model (desaturation model) was adopted for the clay fill in the analysis with ICFEP constitutive Model 81 (modified BBM). Essentially higher permeability of that model has slowed down the drying of the soil and delayed the attainment of higher initial pore suction levels. Another difference between two numerical

analysis, also emerging from the inconsistent hydraulic conductivities, is the instant of time corresponding to the peak of summer suctions during the fluctuation stage. Lower permeability of Model 81 postpones the reach of maximum suctions, with the effect being amplified with depth.

As was previously discussed, the proposed numerical approach fails to reproduce the phenomenon of wetting front propagation. Rather, more uniform pressure changes are predicted, which is generally in accordance with the hydraulic behaviour of homogeneous, uniform fine-grained soils. The distinctive internal structure of dumped clay fills, marked by more permeable matrix that surrounds impermeable clay clods, is most likely reason for rapid saturation observed at a site. Additionally, the rotting and deterioration of the root system, caused by tree felling, could also potentially contribute to creation of preferential flow pathways.

It should be emphasized that the piezometers were not installed in the same borehole, and that is the reason why the deeper one has been wetted first. That finding reveals that the hydraulic properties of the clay fill are highly heterogenous, which significantly complicates the numerical representation of inherently complex physical problem.

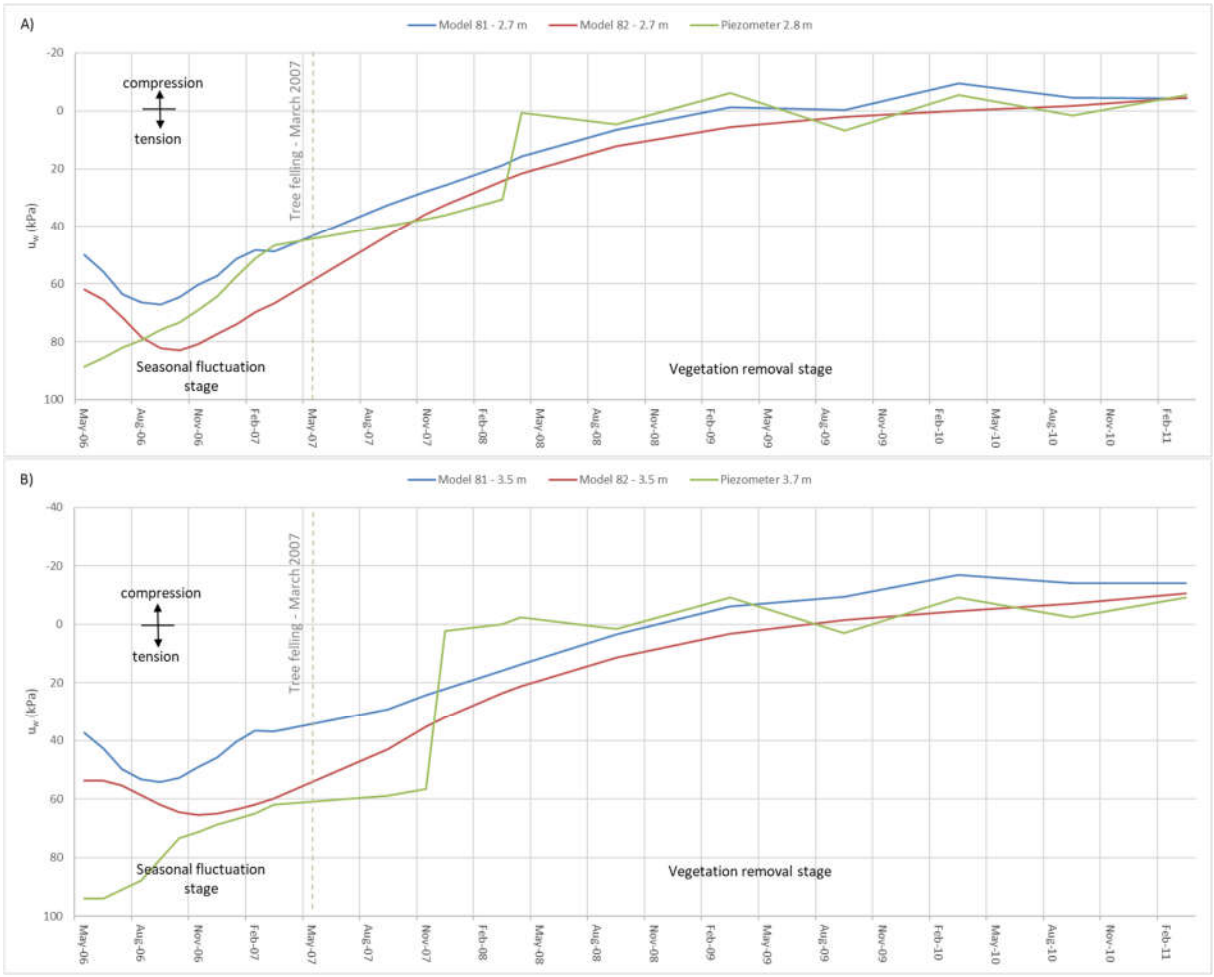

Figure 4.64 Comparison of numerical results and in-situ measurements of pore water pressures for A) piezometer at 2.1m depth of section S1, and B) piezometer at 3.0m depth of section S1

In order to eliminate the effect of differing permeabilities, additional analysis with Model 82 (partially saturated Mohr-Coulomb) has been performed, with the same nonlinear desaturation permeability

function as in the case of Model 81 (modified BBM). The results of numerical simulations and piezometric readings are presented in Figure 4.65.

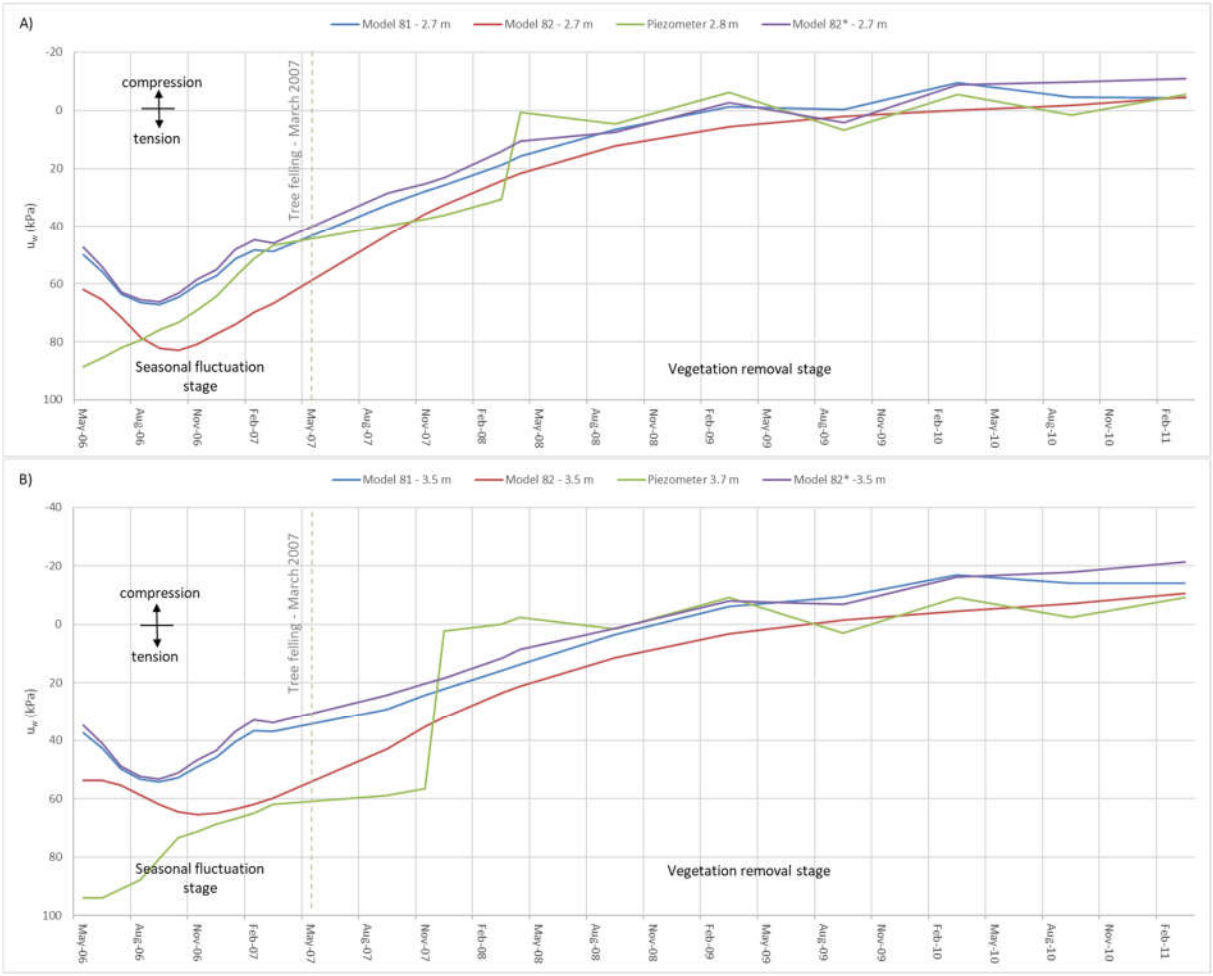

Figure 4.65 Additional comparison of numerical results and in-situ measurements of pore pressures for A) piezometer at 2.1m depth of section S1, and B) piezometer at 3.0m depth of section S1

The results of additional numerical analysis are denoted with * sign, and purple line. The diagrams effectively demonstrate that the hydraulic response of the clay fill embankment to climatic boundary conditions, is practically insensitive to the type of unsaturated mechanical model. That does not mean that the mechanical aspect of behaviour is irrelevant to resulting hydraulic regime. On the contrary, the coupling of flow and deformation has been proved to be of upmost importance in modelling the response of geotechnical earthworks to climate and vegetation impacts (Tsiampousi, Zdravkovic & Potts, 2017). It has been shown in Chapter 2 of this thesis, that pure hydraulic approach, based on disregarding the deformation of soil skeleton, has proved to be inappropriate (Briggs *et al.*, 2016). Despite the observed wetting-drying patterns have been reasonable simulated, the quantitative predictions were in huge discrepancy with piezometric readings, with pore suctions being excessively overestimated (Briggs *et al.*, 2016).

The Figure 4.66 presents the pore water pressure profiles at section S1, obtained from numerical analysis and piezometer measurements. It can be seen that two fundamentally different constitutive models (classical elasto-plastic Mohr-Coulomb and critical state type BBM model) have produced the same hydraulic response. The profiles nearly coincide with each other throughout the full monitoring period.

The predicted profiles show moderate agreement with the measured ones. The reasonable matching is obtained within clay fill, which was already demonstrated in Figures 4.64 and 4.65. On the other hand, the piezometer located deeper in the London Clay records higher suction values compared to numerical simulations. This difference could potentially be reduced if initialisation stage is continued for several more cycles, thereby inducing further drying of the soil domain.

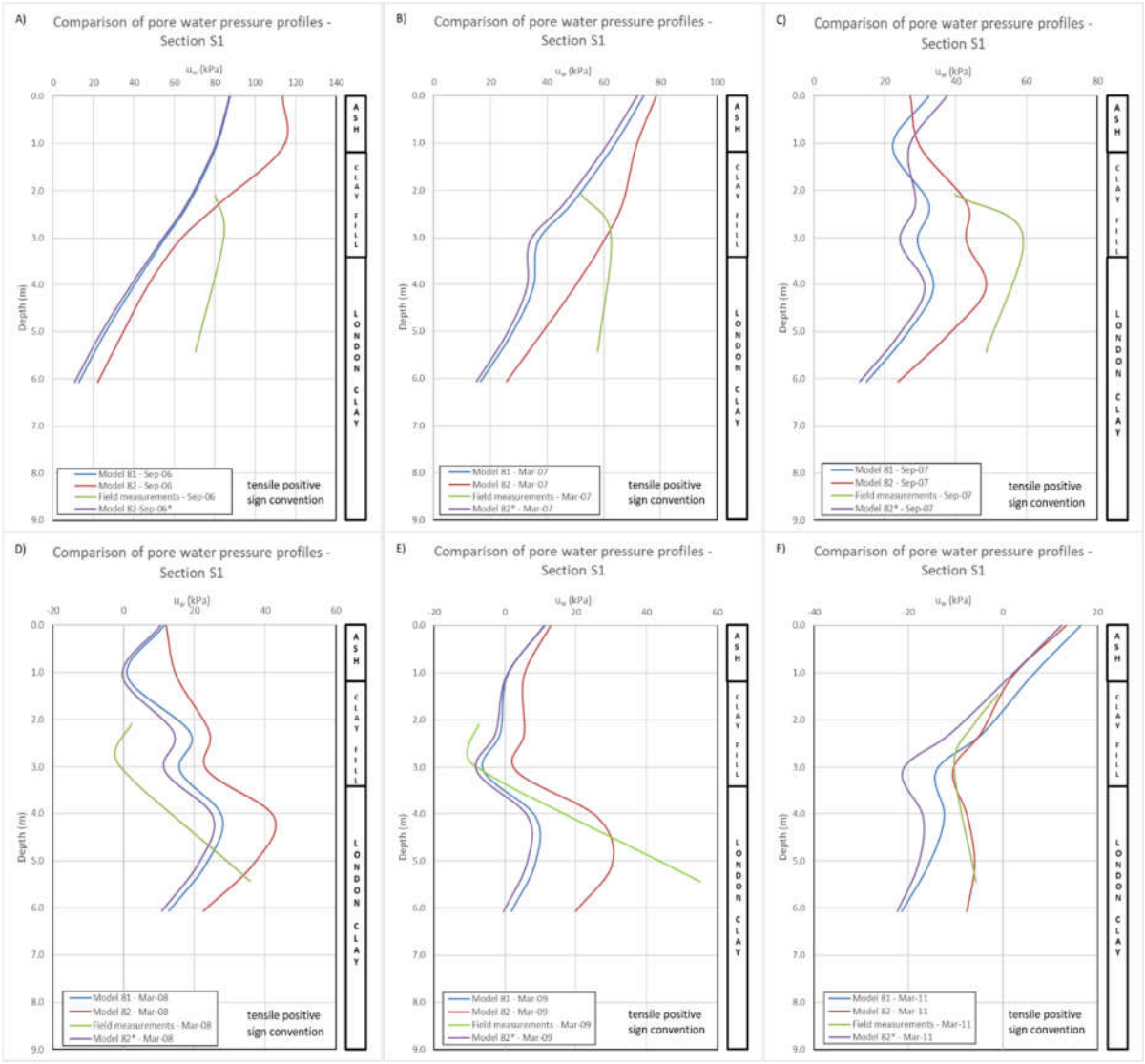

Figure 4.66 Comparison of numerically estimated and on site measured pore water pressure profiles for section S1

The comparison of estimated and recorded evolution of vertical displacements as sections S1 and S2, are illustrated in Figure 4.67_A and 4.67_B, respectively. Two points in section S1, one located on the upper boundary of the clay fill and the other closer to the foundation soil, were chosen for the assessment of two constitutive models with respect to deformational behaviour. It can be seen from Figure 4.67_A, that the numerical models underestimate the magnitudes of vertical movements in section S1, both prior and following vegetation removal. Following vegetation removal two constitutive models with the same permeability functions exhibit essentially the same response. In contrast, prior to the felling of large trees, despite the same magnitudes of seasonal suction variations across the embankment, the partially saturated Mohr-Coulomb behaves more flexibly compared to the modified BBM. This basically means that *H* modulus, governing volumetric strains related to

suction changes, is lower compared to reciprocal of compressibility coefficient κ_s, which represents the equivalent stiffness parameter in critical state type unsaturated models. If the stiffness linked to suction changes of BBM model is expressed in terms of modulus H, instead of κ_s the following relationship between H modulus and suction is obtained (see Figure 4.68). It is obvious that the initial stiffness of the modified BBM model with respect to suction changes is greater than in the case of partially saturated Mohr-Coulomb and that it is increasing further with suctions.

It is interesting to note the differences between the numerical predictions of the two analysis performed with the same mechanical constitutive model (partially saturated Mohr-Coulomb) but with different permeability. It can be seen that during the fluctuation stage, the analysis with more permeable clay fill layer (Model 82*), has yielded greater magnitudes of heave/settlement cycles. This directly arises from higher and more uniform seasonal suction variations over the depth of the clay fill layer. Contrary, following tree removal, the other analysis with lower constant permeability function of the clay fill, has generated larger heave movements. The reason lies in the fact that soil was initially drier (after the initialisation stage), with higher suction levels (see Figure 4.66). Therefore, the subsequent wetting induced by water infiltration (from March 2007) has produced larger loss of pore suctions, and as a consequence greater swelling movement.

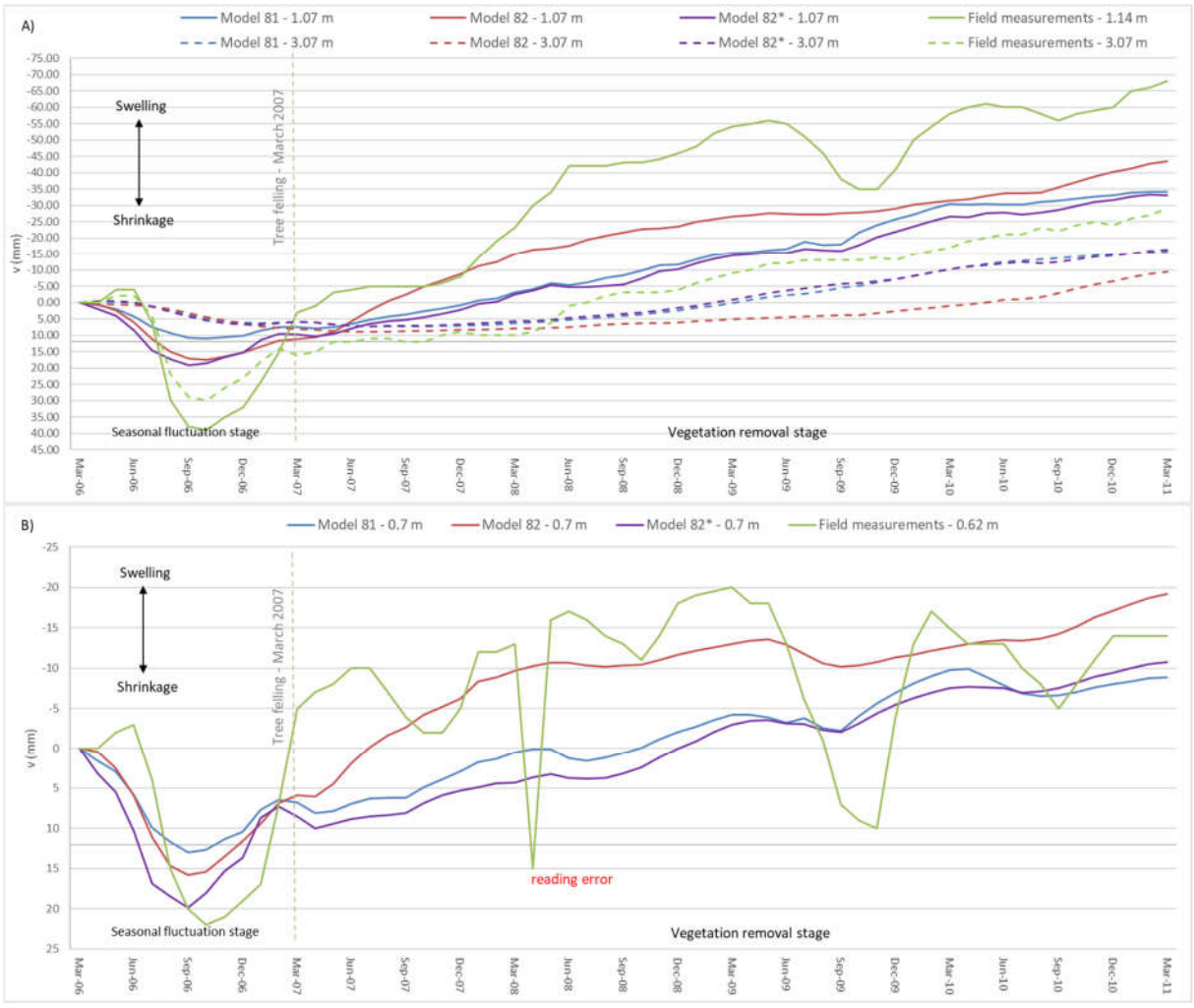

Figure 4.67 Comparison of numerical results and in-situ measurements of vertical displacements

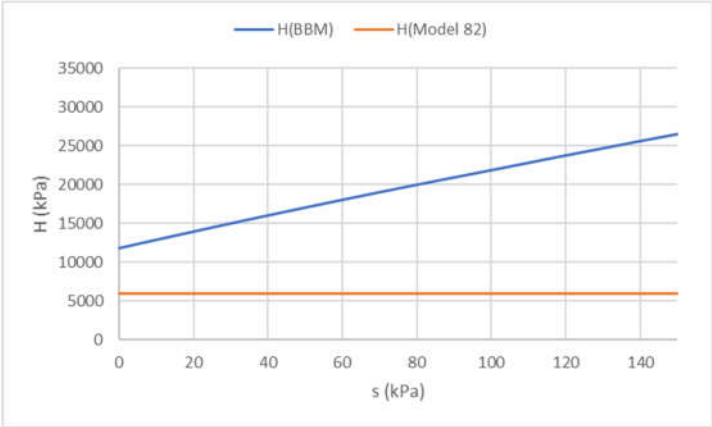

Figure 4.68 Relationship between the stiffness modulus H and suction for the two models

The comparison of numerical simulations and inclinometer loggings of horizontal movements is presented in Figure 4.69. Both qualitatively and quantitatively, predictions of all three analyses very accurately comply with filed observations. The comparative analysis of horizonal movements, verifies previously drawn conclusion that the assumed coefficient of compressibility value κ_s of Model 81, produces stiffer response.

It is also interesting to note that the removal of the high-water demand trees over the embankment slope has modified the swelling mechanism, in particular at the lower part of the slope. While the trees were still present on the slope, the swelling movements during winter months were predominantly vertical, with minor horizontal components. After the tree felling, the proportion of the horizontal component has significantly increased, so that the orientation of the resultant swelling movements has become mainly horizontal. Although the wetting induced by tree felling encompasses much deeper zone of soil relative to seasonal winter wetting, this alteration in swelling behaviour can primarily be attributed to the mature trees retained around the embankment toe. These horizontal movements could initiate or contribute to the progression of slope failure, thereby increasing the overall risk of slope instability.

This finding has an important practical implication to vegetation management, in particular to the extent of tree removal from the railway slopes. However, it should be noted that in this study only high-water demand trees, defined by corresponding evapotranspiration rates and maximum root depts (lower limit assumed (Nyambayo & Potts, 2010), were accounted for. These include, Oak, Poplar, Willow, Hawthorn and other species (NHBC standards, 2007). NHBC guidelines divide the trees according to the water extraction ability into three main groups, namely high, moderate and low-water demand.

The National House Building Council guidance “Building near trees” (NHBC standards, 2007), addresses the problem of tree-induced movements through the zone of influence. It is stated that shrink/swell movements are likely to be expected, within the distance of influence form the tree. The distance of influence is defined in terms of the tree height and the tree species (water demand), acknowledging also the impact of soil volume change potential (see Figure 4.70).

Despite the exact height of the Oak and Ash trees present at the Hawkwell site was not available, field reports describe them as being large and mature. With average height of Oak trees being around 20 m (can grow up to 40-45 m) (Tree Works, n.d.), it means that the zone of influence measures around 25 m, enclosing without doubt both considered sections, S1 and S2. The NHBC guidance, essentially builds confidence in obtained results and stated hypothesis regarding the trees impacts on the overall hydro-mechanical response of the studied embankment. It can also be argued that these

findings validate the proposed numerical approach and in particular the vegetation boundary condition implemented into ICFEP numerical code.

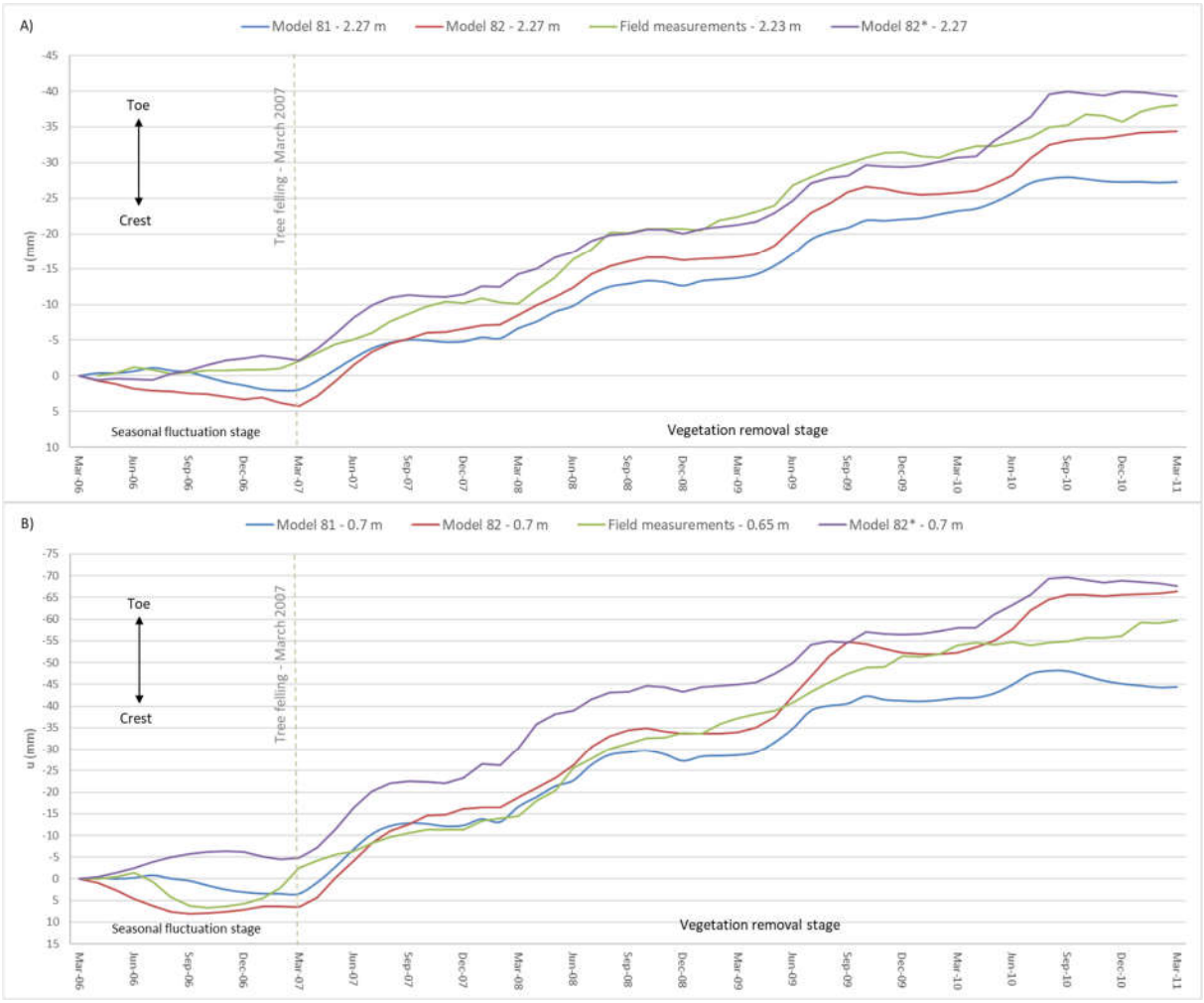

Figure 4.69 Comparison of numerical results and in-situ measurements of horizontal displacements

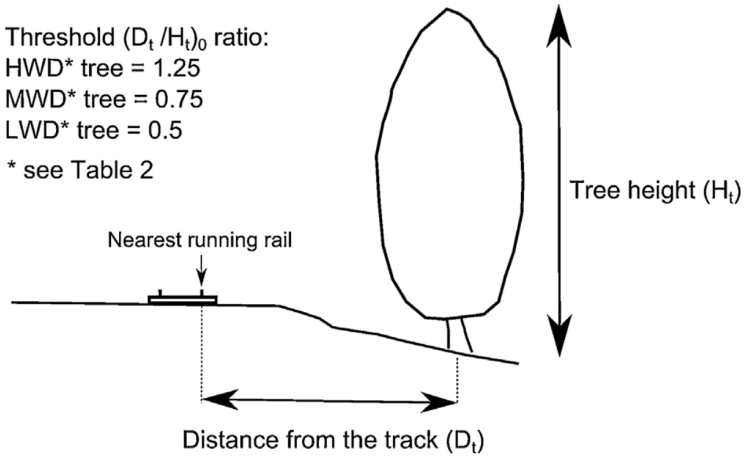

Figure 4.70 Definition of the zone of influence of individual tree, after (NHBC standards, 2007)

Chapter 5: Parametric Analysis

The focus of this chapter is to further investigate the effects of various parameters involved in the soil-vegetation-atmosphere interaction, that were deemed relevant to the performance of Hawkwell embankment. The primary aim is to improve the understanding of the influence of certain pertinent factors on the hydro-mechanical behaviour of unsaturated clay materials subjected to "atmospheric actions". In this regard, another important aspect is the identification of key parameters and their gradation based on the level of sensitivity they have to the relevant outputs (pore suctions and movements).

Parametric analyses are conducted using the same FE mesh and as in the two main analyses presented in previous chapter. Additionally, displacement and general hydraulic boundary conditions were also kept the same.

The presentation of results is organised based on the analysis stage. For the seasonal fluctuation stage, characterised by successive wetting and drying cycles driven by combined effect of vegetation and precipitation, following variables are considered:

- the effect of precipitation
- the effect of evapotranspiration
- the effect of SWR curve (for both mechanical constitutive models)
- the effect of permeability of the clay fill and foundation soil
- the effect of H (for Model 82)
- the effect of compressibility coefficient κ_s (for Model 81)
- the effect of OCR (for Model 81)

For the vegetation clearance phase, characterised by prevailing infiltration and resulting progressive loss of persistent suctions, accompanied by swelling movements, following factors are investigated:

- the effect of root reinforcement
- the effect of extent of tree removal

The discussion of the results is concentrated mainly on the patterns and magnitudes of movements and suction changes.

5.1 Seasonal Fluctuation Stage

5.1.1 Effect of Meteorological Data – Precipitation

For the investigation of the influence of precipitation data two analysis with identical set of input parameters were selected. The analyses differ only in the employed precipitation data. For the analysis RUN_IC the rainfall data from the Shoeburyness weather station, the closest meteorological observational post, have been used. On the other hand, for the analysis RUN_ID the long-term average monthly rainfall measurements from Greenwich were applied. The Table 5.1 shows only a fraction of the entire set of input parameters. Only the most relevant material parameters, specifically for the clay fill material, are provided. It can be seen that some of the parameters, in particular the ones related to stiffness and SWR curve, differ somewhat from the main analysis discussed in Chapter 4.

In the Figure 5.1, the distribution of the precipitations from the Shoeburyness weather station for the five-year period from April 2006 to March 2011, is depicted alongside the long-term average monthly

rainfall data. The presented data suggest that on the yearly basis the precipitation distribution is pretty irregular and stochastic in nature, whereas the long-term averages exhibit quite uniform distribution with small fluctuations over the year.

Table 5.1 Model 82 parameters values and climatic boundary conditions – effect of precipitation

Analysis name	Number of cycles	CLAY FILL (partially saturated-Model 82)												CLIMATIC & VEGETATION boundary conditions			
		Stiffness parameters				*Strenght*			*Permeability*		*SWRC*						
		K [kPa]	G [kPa]	Small strain stiffness	H [kPa]	ϕ [°]	c [kPa]	v [°]	k [m/s]	Variable permeability	s_{air} [kPa]	a	n	m	*S3 [kPa]*	r_{max} *[m]*	*Rainfall data*	*Evapotranspiration data*
RUN_IC	5	3125	1445	no	12500	*22.9*	*5*	0	2.00E-09	no	20	0.033	1.15	0.13	200	2	Shoeburyness 2006-2011	Thornthwait 2006-2011
RUN_ID	5	3125	1445	no	12500	*22.9*	*5*	0	2.00E-09	no	20	0.033	1.15	0.13	200	2	long term average	Thornthwait 2006-2011

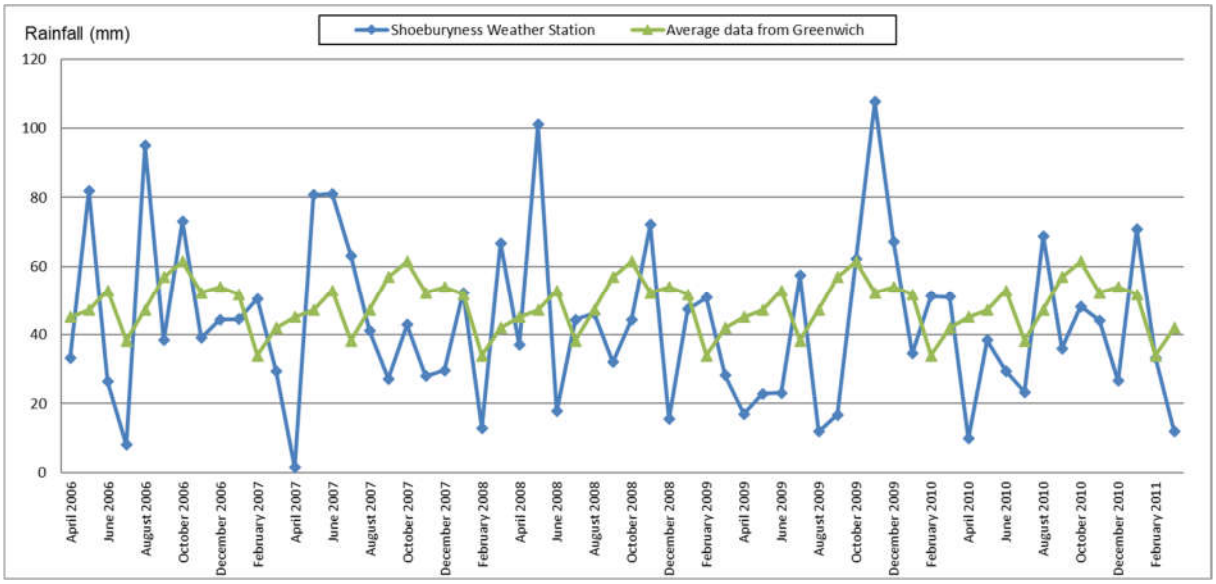

Figure 5.1 Precipitation data from Shoeburyness weather station and monthly long-term averages

The seasonal pore water pressure variations for the section S2, for the five years of combined evapotranspiration and precipitation moisture fluxes are presented in Figure 5.2. In the case of monthly long-term average precipitation data, quite uniform seasonal suction variations are obtained. This obviously results from repeatedly using the same set of monthly rainfall data inputs for all five years. However, the predicted pattern also reveals that the evapotranspiration data are also fairly uniform from year-to-year. Although, numerous meteorological variables are involved in the calculation of potential evapotranspiration rates, yearly growing/developing cycle of deciduous trees has predominant influence on the root water uptake distribution throughout the year.

On the other hand, the yearly distributions of pore water suctions, in the case of short term (real) rainfall data from Shoeburyness, are quite uneven. The magnitudes of seasonal suction variations range from 40 kPa (for Year 2) to 140 kPa (for Year 4), whereas in the case of long-term average rainfalls are very consistent and are of the order of 40-50 kPa.

In order to better understand the causes of such a large predicted difference in seasonal suction variations, the potential evapotranspiration, precipitation and net rates for the Year 4 are shown in Figure 5.3. It can be seen that the spring/summer period was significantly drier (lower precipitation rates) compared to long-term averages, whereas the autumn, in particular November, was wetter with greater amount of rainfall relative to long-term averages. Bearing in mind that evapotranspiration

rates are more or less uniform on a yearly basis, means that the precipitation distribution governs the magnitudes of seasonal pore water pressure variations.

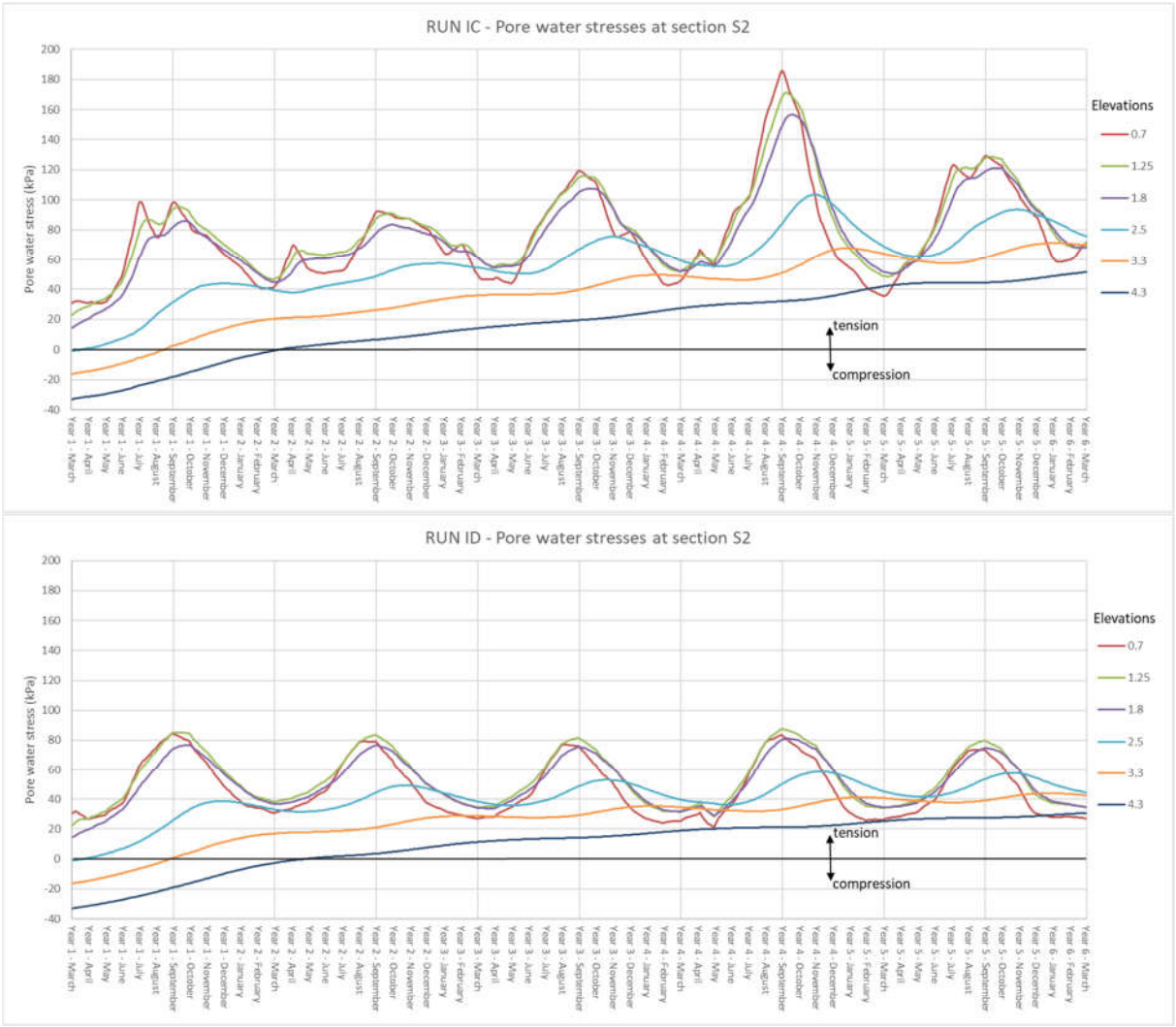

Figure 5.2 Predicted seasonal pore water pressure variations for two different precipitation data sets (top-Shoeburyness WS, bottom-long term average)

The results of Year 4, suggest that most critical conditions arise when the plant growth stages, especially the development and mid-season stage, coincide with lower precipitations, combined with higher rainfall matching with the late-season senescence stage of vegetation. The combination of two markedly different seasons, the extremally dry followed by extremally wet, could potentially be very adverse, as desiccation cracking induced by excessive shrinkage may dramatically increase the overall mass permeability. The higher permeability of surficial zone, would allow rainwater to infiltrate more easily and therefore rapidly rewet the soil.

These findings have an important practical implication suggesting that long-term average monthly precipitations are inadequate and nonconservative for the evaluation of serviceability of infrastructure earthworks. Furthermore, the climate changes could bring about the paradigm shift with respect to perception of present climate patterns. Therefore, further investigations of infrastructure embankment performance with respect to future climatic scenarios are necessary.

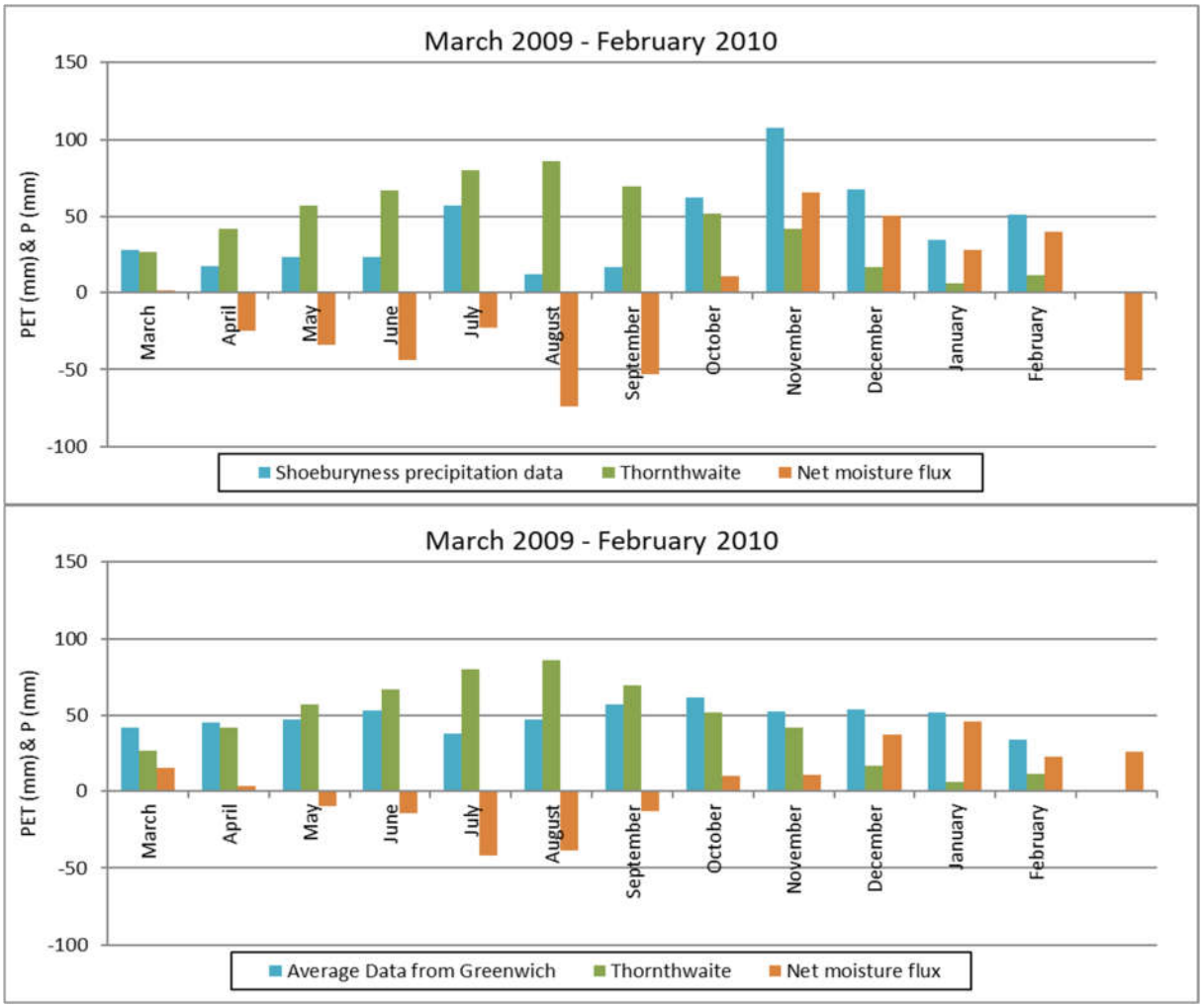

Figure 5.3 Potential evapotranspiration, precipitation and net rates for the Year 4

The Figure 5.4 illustrates the evolution of vertical movements corresponding to the same section, S2, for which the pore water pressure distributions have already been discussed. As can be seen the analysis with Shoeburyness precipitation data set has produced more pronounced shrink/swell cyclic response. The largest settlement-heave movements have been obtained, as expected, for Year 4, consistent with the pore water suction variations.

Comparing the two plots, it is obvious that the overall shrinkage movement after five years of climatic boundary condition application for analysis RUN_IC is some 30-40% greater with respect to results from RUN_ID. This is particularly evident in the root zone and follows from higher desaturation caused by lower total precipitation. The total amount of measured rainfall at Shoeburyness weather station for the period March 2006 – March 2011 equals 2593 mm, whereas the five times total long-term annual equals 2918 mm. This essentially means that the total negative (outward) moisture flux is greater for the analysis RUN_IC.

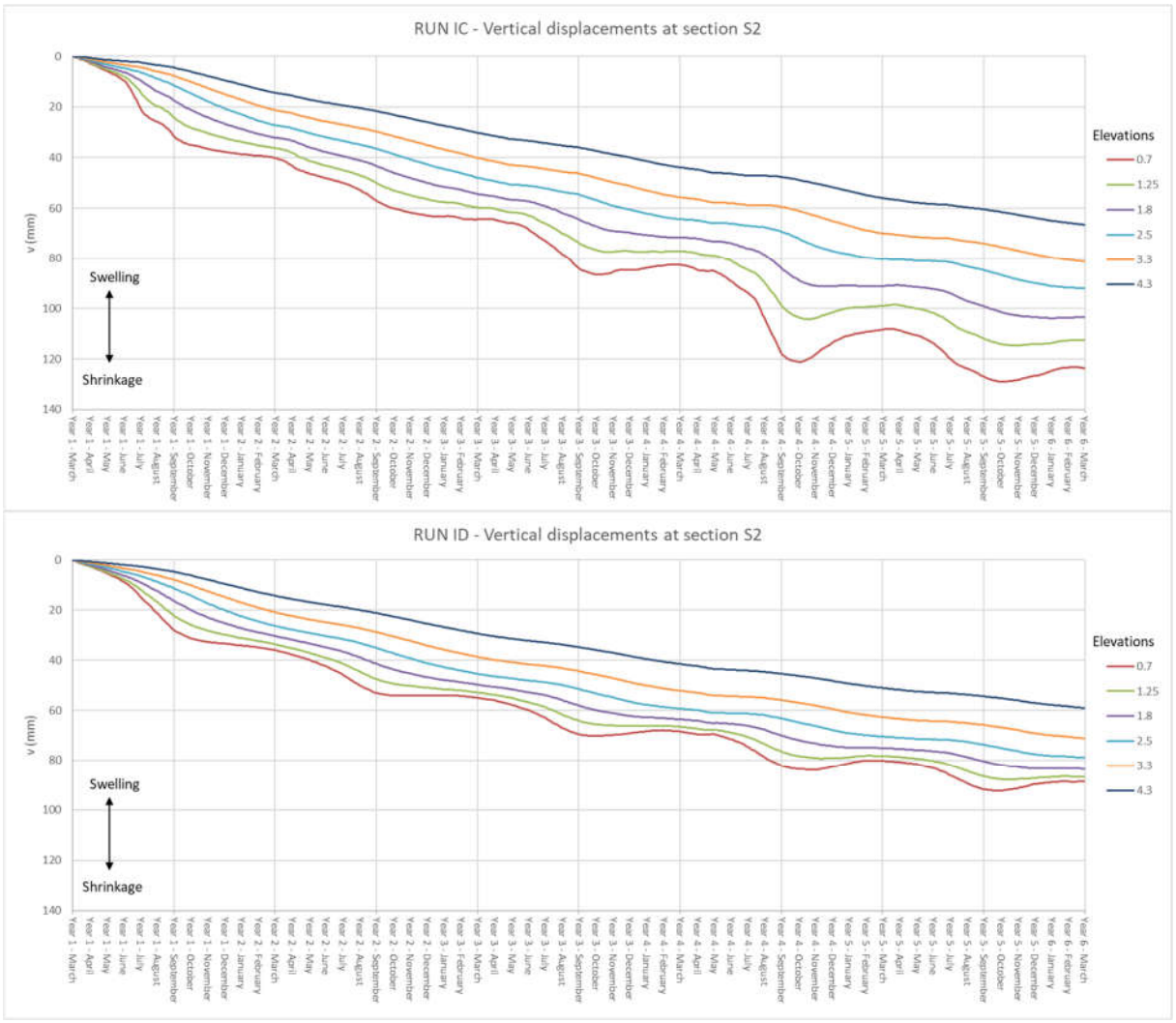

Figure 5.4 Predicted seasonal vertical movement fluctuations for two different precipitation data sets (top-Shoeburyness WS, bottom-long term average)

5.1.2 Effect of Meteorological/Vegetation Data – Evapotranspiration

The effect of evapotranspiration is examined based on comparison of results of two analyses that differ only in utilised evapotranspiration data. First analysis, RUN_IB3 is based on the Mat Office data from 1971 to 1974, for deciduous fruit trees. For the last fifth year the data corresponding to the first year have been repeated. The Meteorological Office routinely computes the values of potential evapotranspiration, for a number of plant species using the Meteorological Office Rainfall and Evaporation Calculation System (MORECS). It should be noted that MORECS is actually based on the version of Penman-Monteith method, which as an input uses several meteorological variables. The second analysis, RUN_IC, is the same analysis discussed in former section regarding the precipitation effects. The potential evapotranspiration data used in this analysis is calculated based on the Thornthwaite empirical method, which as an input uses solely monthly average air temperatures. The part of the input parameters values for two analyses is presented in Table 5.2.

The evapotranspiration rate distributions are illustrated in Figure 5.5. It can be seen that both distributions are quite uniform, which as explained earlier correlates with the plant growth cycle.

Table 5.2 Model 82 parameters values and climatic boundary conditions – effect of evapotranspiration

Analysis name	Number of cycles	CLAY FILL (partially saturated-Model 82)													CLIMATIC & VEGETATION boundary conditions			
		Stiffness parameters				*Strenght*			*Permeability*		*SWRC*							
		K [kPa]	G [kPa]	Small strain stiffness	H [kPa]	ϕ [°]	c [kPa]	v [°]	k [m/s]	Variable permeability	s_{air} [kPa]	a	n	m	*S3 [kPa]*	r_{max} *[m]*	*Rainfall data*	*Evapotranspiration data*
RUN_IB3	5	3125	1445	no	12500	*22.9*	*5*	0	2.00E-09	no	20	0.033	1.15	0.13	200	2	Shoeburyness 2006-2011	Mat office 70'-74' + 70'-71'
RUN_IC	5	3125	1445	no	12500	*22.9*	*5*	0	2.00E-09	no	20	0.033	1.15	0.13	200	2	Shoeburyness 2006-2011	Thornthwait 2006-2011

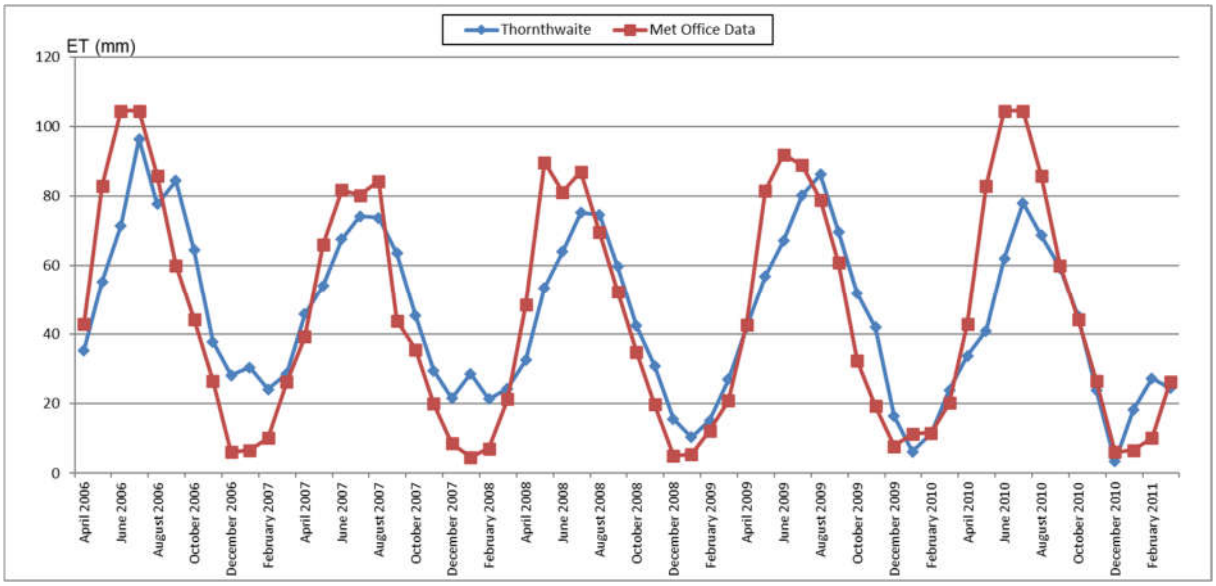

Figure 5.5 Evapotranspiration data estimated from Thornthwaite method and MORECS data for 1971-1974 + 1971

The Figure 5.6 illustrates the pore water pressure variations over the depth of section S1 for five years of combined vegetation-precipitation effects. The overall shape of pore suction variations for two analyses is almost identical, just scaled based on the ratio of total annual potential evapotranspiration rates of two data sets. This finding coincides with the conclusions from the previous section, that the precipitation distribution relative to plant growth stages is the key component of the water flux boundary condition, directly controlling the magnitude of seasonal pore water pressure variations.

The evolution of vertical movements for two analysis is depicted in Figure 5.7. It can be seen that general trends and the total magnitude of heave, induced by persistent drying, are very similar. The main reason lies in the fact that total potential evapotranspiration rates for the two data sets differ by very small amount. Namely, for the Thornthwaite method total potential evapotranspiration equals 2725 mm, whereas for the Met Office equals 2770 mm. It should be noted that for FAO Penman-Monteith semi-empirical method used in the main analyses, presented in the previous Chapter 4, the estimated total potential evapotranspiration for five-year period between March 2006 and March 2011 for deciduous trees equals 3253 mm. Despite FAO Penman-Monteith yearly evapotranspiration rates are about 20% higher compared to the other two sets, they were judged as more appropriate and reliable, because they correspond explicitly to Hawkwell embankment (Shoeburyness WS) and exact monitoring period. Besides, they are more accurate and rigours compared to Thornthwaite method.

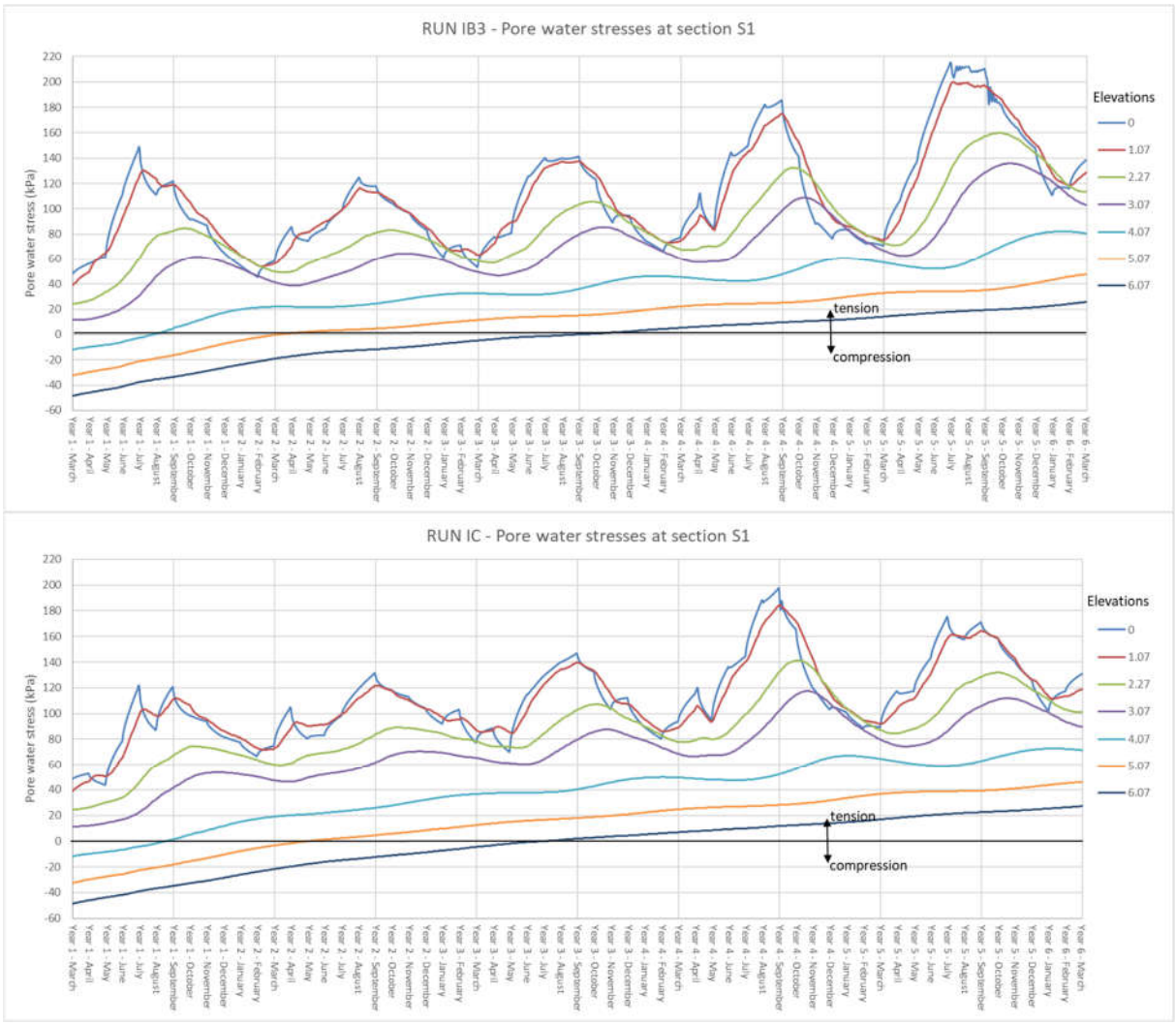

Figure 5.6 Predicted seasonal pore water pressure variations for two different evapotranspiration data sets (top-Mat Office, bottom-Thornthwaite)

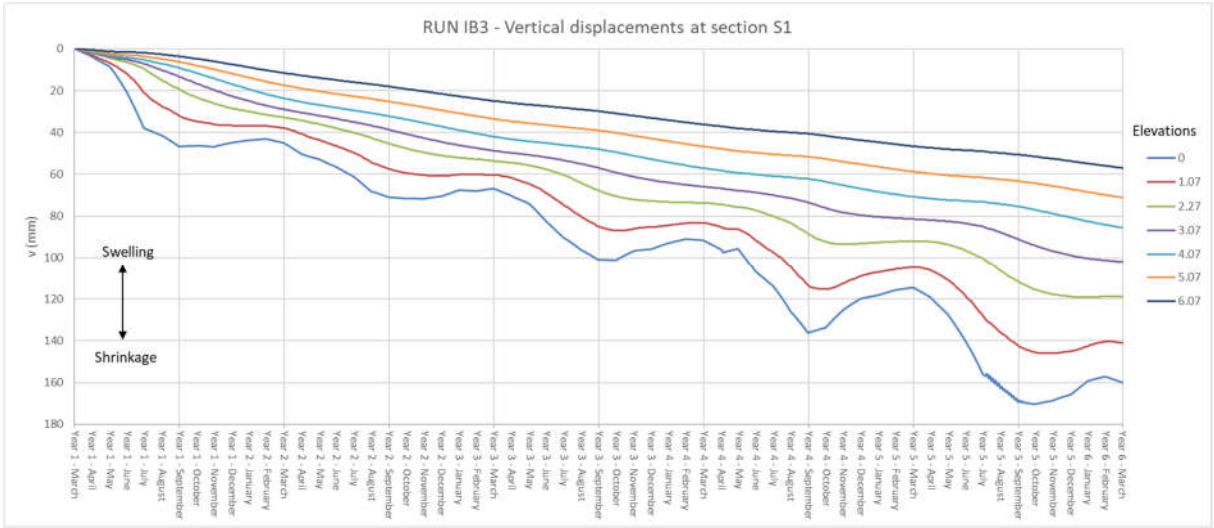

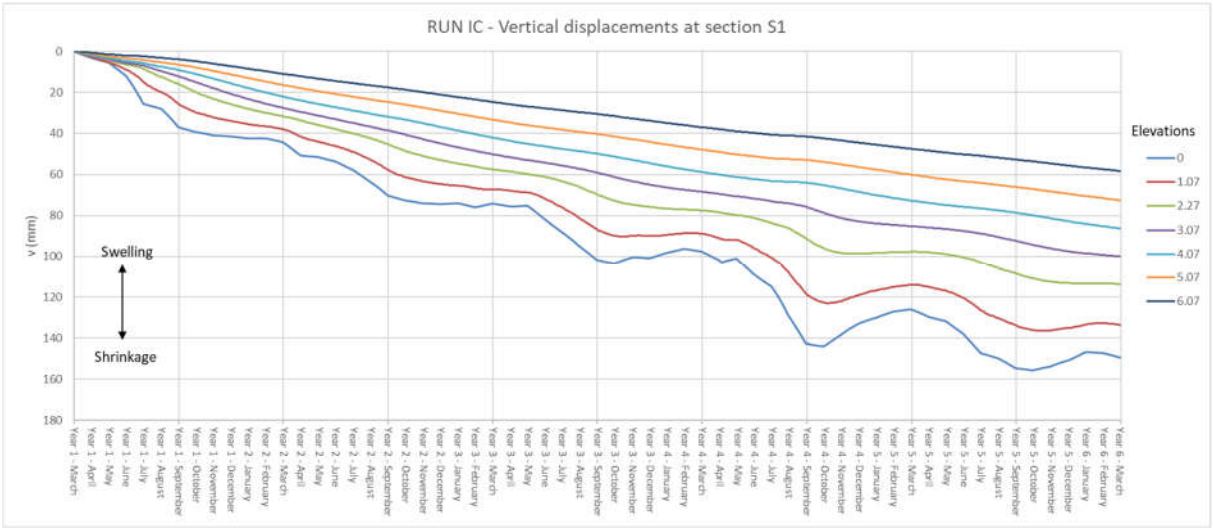

Figure 5.7 Predicted vertical movement fluctuations for two different evapotranspiration data sets (top-Mat Office, bottom-Thornthwaite)

5.1.3 Effect of SWR Curve

The influence of the shape of SWR curve on the predicted hydraulic and mechanical behaviour of clay fill embankment is investigated, and results and conclusions are presented. Four analyses differing only in the form of SWR curves, with all other inputs being equal, have been performed. In order to eliminate the effect of saturation/desaturation switch, the same air-entry suction value has been assumed for all presented analyses. This effectively means that only the gradient of SWR curve appears in the governing coupled flow-deformation equations. The Table 5.3 presents the adopted climatic/vegetation boundary conditions and Model 82 parameter values for the clay fill. It highlights the differences between fitting parameters of the Van Genuchten SWR curves. The obtained SWR curves are plotted in Figure 5.8 together with the curve from the main analysis RUN_IR (Chapter 4). It can be seen that the SWRC for analyses RUN_IR and RUN_IH practically coincide in the predicted and observed interval of suction values. Divergency starts to increase for the suction levels that were of no interest. The other three curves are significantly different, in particular their slopes in the highlighted suction range. The parameters of intermediate curve (RUN_IB3) are analogous to the ones assumed by (Briggs *et al.*, 2013, 2016) for the clay fill, whereas the upper two curves agrees closer to the unweathered natural London Clay.

Table 5.3 Model 82 parameters values and climatic boundary conditions – effect of SWRC

Analysis name	Number of cycles	CLAY FILL (partially saturated-model82)													CLIMATIC & VEGETATION boundary conditions			
		Stiffness parameters				*Strenght parameters*			*Permeability*		*SWRC*				*S3 [kPa]*	r_{max} *[m]*	*Rainfall data*	*Evapotranspiration data*
		K [kPa]	G [kPa]	Small strain stiffness	H [kPa]	φ [°]	c [kPa]	v [°]	k [m/s]	Variable permeability	s_{air} [kPa]	a	n	m				
RUN_IB3	5	3125	1445	no	12500	*22.9*	*5*	0	2.00E-09	no	20	0.033	1.15	0.13	200	2	Shoeburyness 2006-2011	Mat office 70'-74' + 70'-71'
RUN_IF	5	3125	1445	no	12500	*22.9*	*5*	0	2.00E-09	no	20	0.0033	1.15	0.13	200	2	Shoeburyness 2006-2011	Mat office 70'-74' + 70'-71'
RUN_IG	5	3125	1445	no	12500	*22.9*	*5*	0	2.00E-09	no	20	0.033	1.08	0.07	200	2	Shoeburyness 2006-2011	Mat office 70'-74' + 70'-71'
RUN_IH	5	3125	1445	no	12500	*22.9*	*5*	0	2.00E-09	no	20	0.0195	1.7	0.2	200	2	Shoeburyness 2006-2011	Mat office 70'-74' + 70'-71'

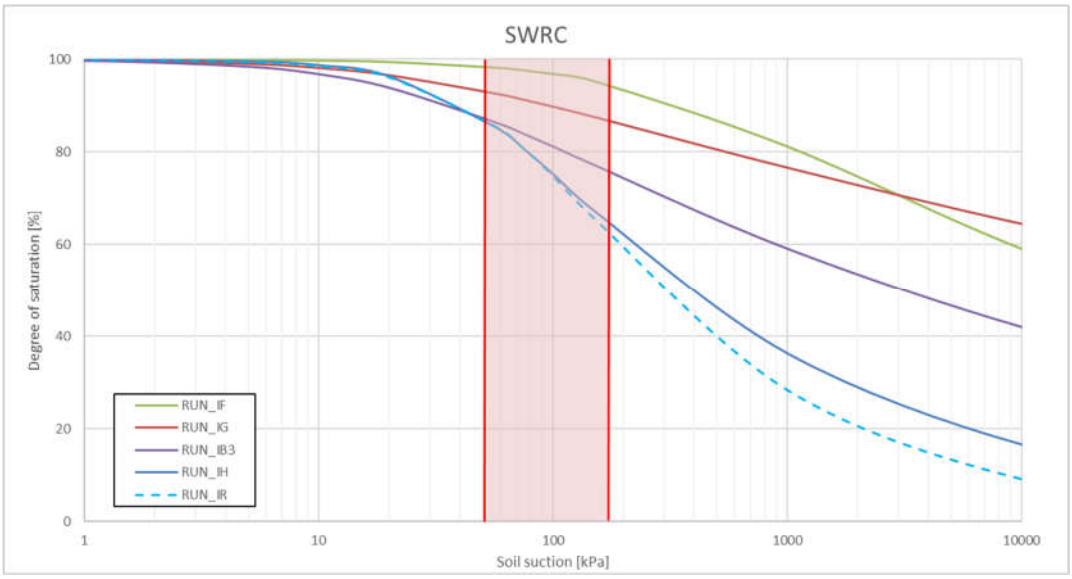

Figure 5.8 Soil water retention curves for the unsaturated clay fill used in parametric analysis

In the Figure 5.9 volumetric water content θ_w and degree of saturation S_r profiles corresponding to the end of summer of year four are illustrated. It can be seen that the flattest SWR curve (RUN_IF) has produced the lowest desaturation. On the contrary, analysis with steepest curve (RUN_IH) has allowed the largest quantity of water to be sucked out by dominant summer evapotranspiration process. This finding suggests that the flatter the SWR curve is, the higher resistance towards water extraction it will provide.

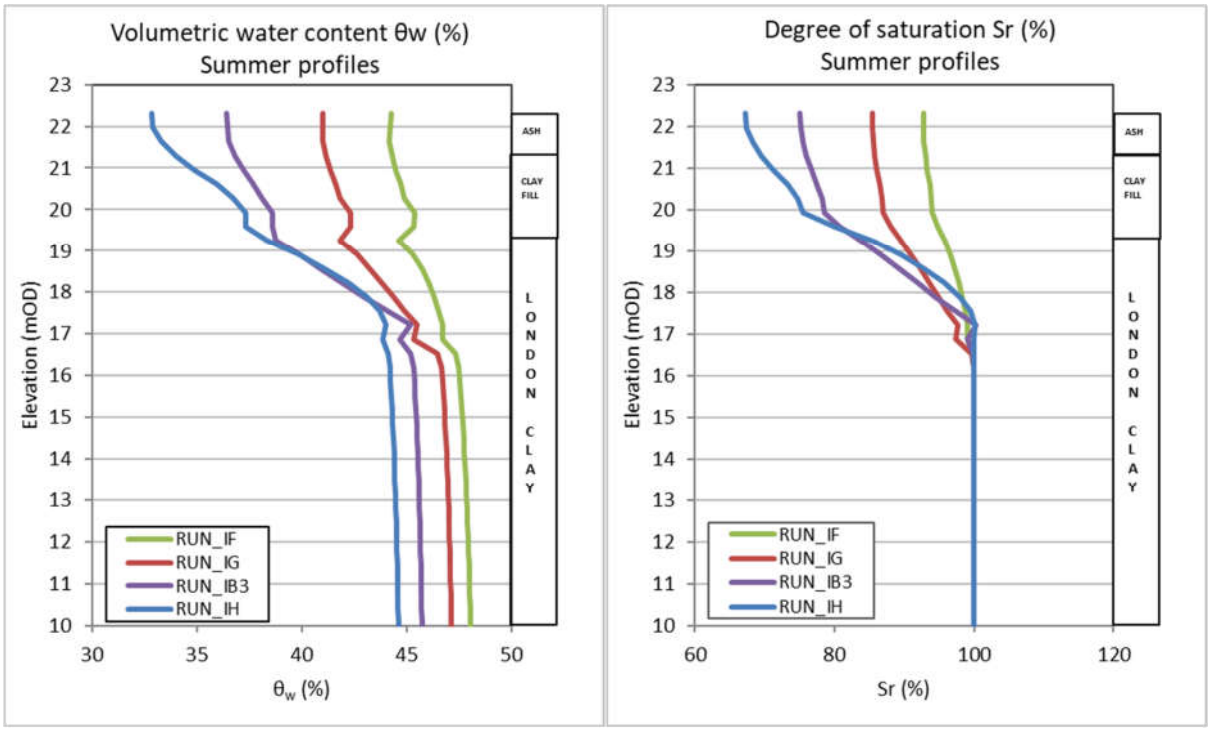

Figure 5.9 Predicted volumetric water content θ_w and degree of saturation S_r summer profiles for different SWR curves corresponding to the fourth year

It should be noted that the shape, in particular the slope and air-entry suction value, of the SWR curve depend mostly on the pore size distribution. This means that for soils containing larger void spaces in higher percentage, SWR curves would be initially steeper and would be moved more to the left. The curve used in main analysis presented in Chapter 4 has not been established through laboratory testing, but calibrated based on the in-situ water content and pore suction measurements. Considering that the dumped clay fills of London Clay origin are highly heterogeneous and possess coarse-grained inclusions, the curve assumed for main analysis is probably the most suitable one. However, the further research in this field should definitely include the planning and execution of systematic and detailed laboratory investigation of hydraulic properties of undisturbed and non-reconstituted clay fills from UK railway infrastructure earthworks.

The Figure 5.10 shows the pore water pressure and corresponding vertical movement variations for the point at depth 1.07 m below the surface of section S1. As can be seen the SWR curve characterised by the most gentle slope (RUN_IF) has exhibited the greatest seasonal pore suction and consequently greatest vertical displacement variations. Compared to analysis RUN_IH, the magnitude of seasonal suction variations has more than doubled. To improve the understanding of the effect of SWR curve on the pore suction predictions the governing FE equations of the coupled unsaturated formulation are analysed. It can be seen that the SWRC enters the governing equations in the lower right sub-matrix (marked by red frame), specifically its right highlighted term. The first term in the expression for ω coefficient, 1/R, represents the gradient of the SWRC at current suction level. It should be noted that the slope of SWRC is always negative.

$$\begin{bmatrix} [K_G] & [L_d] \\ \Omega[L_G]^T & -\beta\Delta t[\Phi_G] - \omega[M_N] \end{bmatrix} \begin{Bmatrix} \{\Delta d\}_{nG} \\ \{\Delta p_f\}_{nG} \end{Bmatrix} = \begin{Bmatrix} \{\Delta R_G\} \\ ([n_G] + Q + [\Phi_G]\{p_f\}_{nG})\Delta t \end{Bmatrix}$$

$$\omega = \left(\frac{1}{R} - \frac{3\Omega}{H}\right)$$

The left term of the lower right sub-matrix controls the effect of permeability through the permeability matrix [Φ_G]. This essentially means that the effects of permeability and SWRC should be analysed together in an integral sense, and not separately. Bearing in mind that the slope of SWRC is negative, combined with the minus sign in front of it, yields the positive sign linked to the second term. This indicates that the SWR curve opposes the influence of permeability. This conclusion could aid in explaining why the saturated analyses with the same permeabilities (not reported in this thesis) have yielded higher maximum suctions (up to 450 kPa), as well as higher seasonal variations ($\Delta \approx 400$ kPa) as response to water flux boundary condition Q, compared to all four analyses presented in this section. If, for instance, very high air-entry suction value has been assumed, that would effectively imply that the gradient of SWRC is zero. Therefore, the second term practically vanishes, which reduces to saturated formulation presented here for convenience.

$$\begin{bmatrix} [K_G] & [L_d] \\ [L_G]^T & -\beta\Delta t[\Phi_G] \end{bmatrix} \begin{Bmatrix} \{\Delta d\}_{nG} \\ \{\Delta p_f\}_{nG} \end{Bmatrix} = \begin{Bmatrix} \{\Delta R_G\} \\ ([n_G] + Q + [\Phi_G]\{p_f\}_{nG})\Delta t \end{Bmatrix}$$

Actually, the cross-coupling sub-matrix [L_G] would still differ slightly, but that will be discussed later in this chapter. It should be recalled that the Ω function is introduced in partially saturated case to define the proportion of the total flow generated by volumetric deformations, that refers to water phase. The remaining part relates to air phase, which is assumed to be free flowing and therefore omitted from the formulation. The Ω function varies linearly in range from 1.0 (fully saturated case) to zero for residual conditions, characterised by discontinuity of water phase. For obtained suction levels the Ω parameter is approximately between 0.9 and 1.0, which essentially implies that this parameter isn't responsible for differences obtained between the coupled saturated (classical Mohr-Coulomb constitutive model used with the same parameters' values) and unsaturated analyses.

However, for more definitive and sound conclusions regarding the differences between saturated and unsaturated analyses predictions, the effect of stiffness of soil skeleton with respect to suction changes (modulus H), should also be investigated to obtain more comprehensive understanding of coupled unsaturated formulation. This point is addressed in more detail in separate section of this chapter.

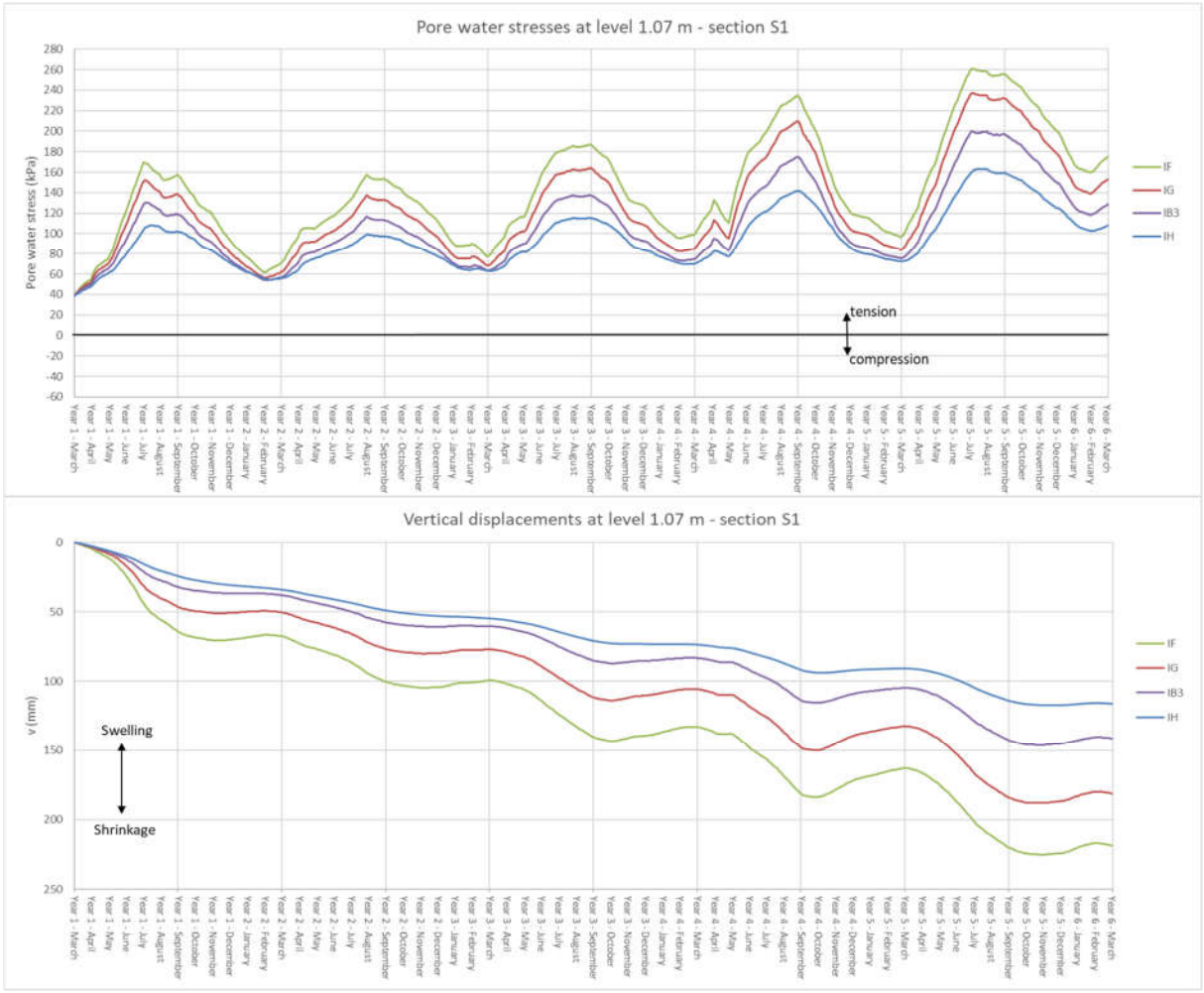

Figure 5.10 Predicted seasonal pore water pressure and vertical displacement variations for point at an elevation of 1.07 m at section S1, for different SWR curves

Additionally, the predictions of pore water pressure and vertical displacement variations for the point at depth 3.07 m, close to the foundation soil boundary is presented in Figure 5.11. As can be seen, the same trend is obtained, but with even more pronounced differences in seasonal suction fluctuations between the conducted analysis.

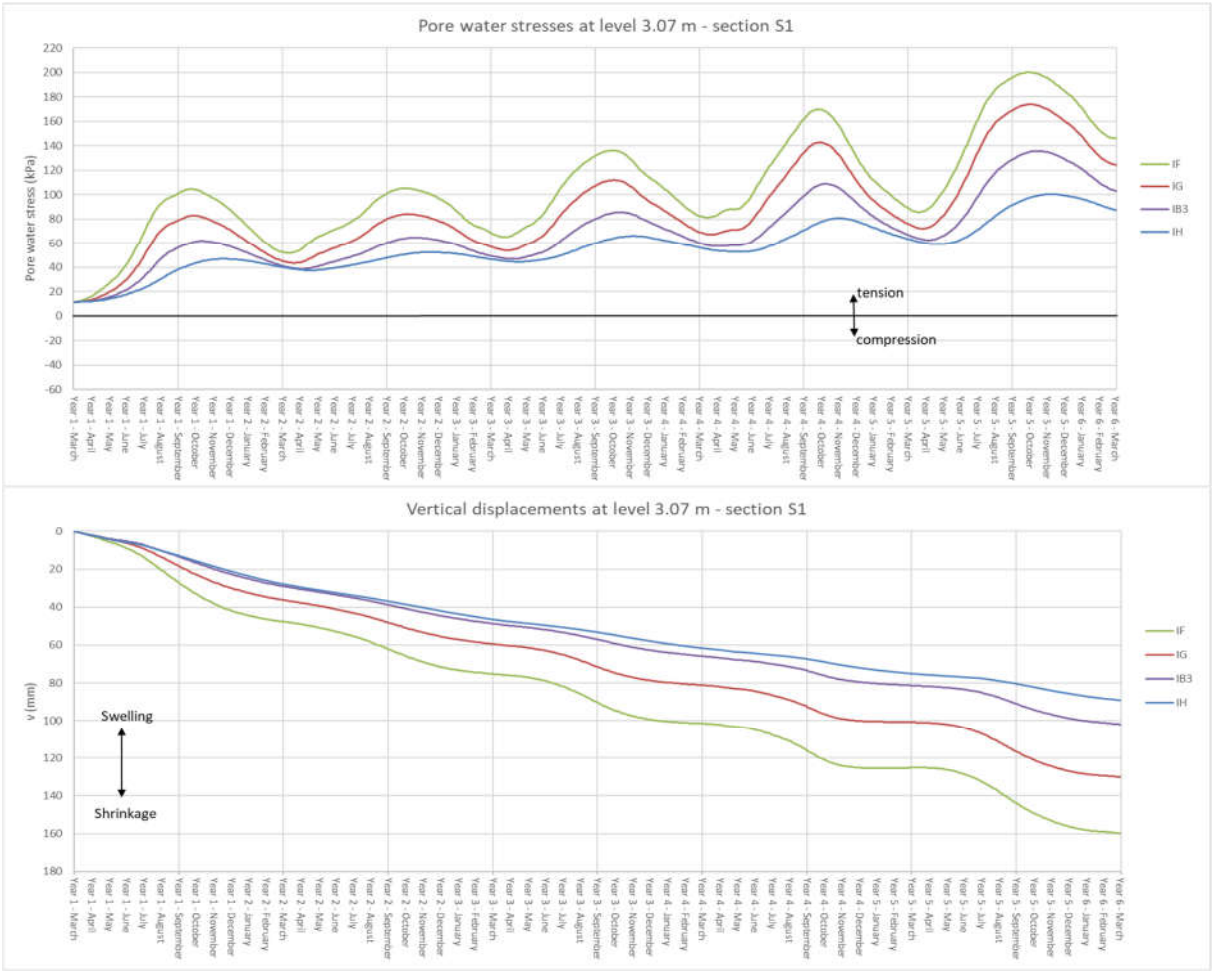

Figure 5.11 Predicted seasonal pore water pressure and vertical displacement variations for point at an elevation of 3.07 m at section S1, for different SWR curves

The influence of SWR curve was also examined in combination with the modified BBM (Model 81) constitutive model. The Table 5.4 presents the material input parameters corresponding to the clay fill. The two investigated curves are plotted in Figure 5.12. It can be seen that the curve from analysis RUN_IB (BBM) is identical to the curve from "main analysis" discussed in previous chapter.

The Figure 5.13 illustrates the seasonal pore water pressure and vertical movement variations for two nodes located along the section S1. It can be seen that the overall effect of the shape of SWR curve does not differ from the first parametric analysis conducted with Model 82, which essentially implies that the type of constitutive model does not alters the already established impact of the SWRC.

Also, it is interesting to note that pore water suction time curves for two analyses match quite well for lower suction ranges, which results from the fact that SWRCs almost coincide to the level of suction of about 60 kPa.

Table 5.4 Model 81 parameters values – effect of SWRC

Analysis name	Number of cycles	CLAY FILL (partially saturated-Model81)																																
		Linear parameters		Small strain stiffness	Plastic potential and yield surface			Hardening&Softening parameters								Initial hardening parameters				Other parameters							Permeability		SWRC			
		K [kPa]	G [kPa]		$\alpha_{g,f}$	$\mu_{g,f}$	$M_{g,f}$	α^c	λ(0)	κ	r	β	κ_{sat}	χ	ω	v_1	OCRS	OCR	k	p_{atm}	SMS	ν	s_{air}	K_{min}	S_{oi}	λ_s	k [m/s]	Variable permeability	s_{air} [kPa]	a	n	m
BBM_IB	5	2000	923	no	0.4	0.9	1	-1.98	0.152	0.02	0.45	0.011	0.07	1	0	2.75	4	10	-1	100	2	0.35	20	2000	1.00E+06	0.3	2.00E-07	desaturation switch	20	0.0125	1.5	0.33
BBM_ID	5	2000	923	no	0.4	0.9	0.89	-1.98	0.152	0.02	0.45	0.011	0.07	1	0	2.75	4	10	-1	100	2	0.35	20	2000	1.00E+06	0.3	2.00E-07	desaturation switch	20	0.033	1.15	0.13

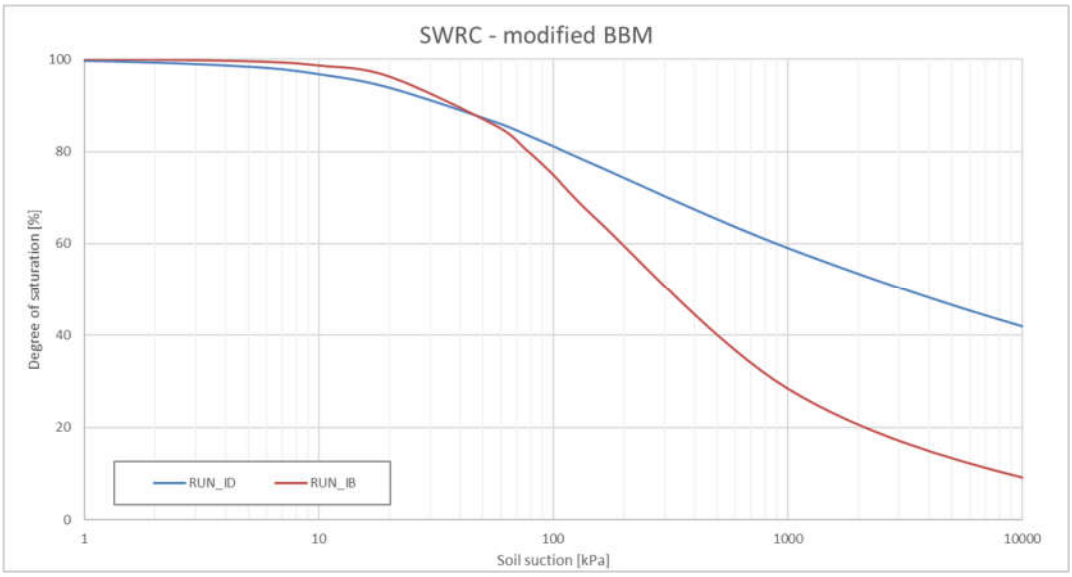

Figure 5.12 Soil water retention curves for the unsaturated clay fill used in parametric analysis corresponding to the Model 81

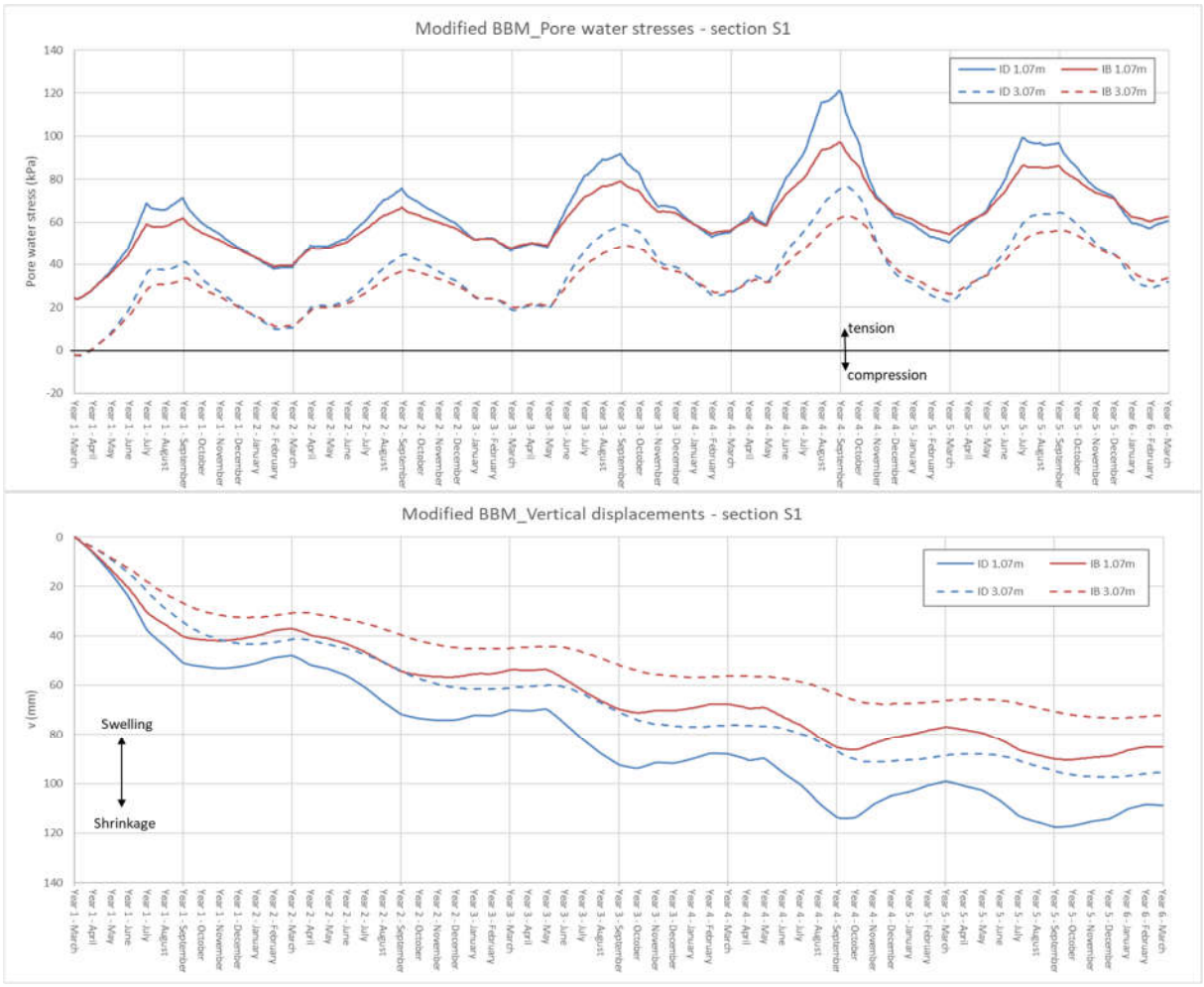

Figure 5.13 Predicted seasonal pore water pressure and vertical displacement variations at section S1 corresponding to modified BBM (Model 81), for two different SWR curves

5.1.4 Effect of Permeability of the Clay Fill and Foundation Soil

The effect of permeability of the unsaturated clay fill was already very extensively discussed in the previous chapter. Recall that the observed differences with respect to both hydraulic and mechanical response were primarily provoked by employed permeability model, rather than by the type of unsaturated constitutive model. In this section the influence of permeability is discussed one more time, with further investigation of governing FE equations of coupled unsaturated problems.

The Table 5.4 presents only the most relevant input parameters, highlighting the differences between the two analyses. The analysis RUN_IR is the "main" analysis comprehensively described in previous Chapter 4, and was based on the constant uniform hydraulic conductivity. The other analysis, RUN_IS/2, was also introduced at the end of Chapter 4 in part that dealt with comparison and summary of the two "main" analyses. It utilizes the nonlinear permeability model, that varies with suction. The permeability value listed in the table below, corresponds to saturated conditions, specifically compressive pore water pressure states. Transition of water stresses from compressive to tensile region induces the steady decrease of permeability until the lower unsaturated limit of $2 \cdot 10^{-9}$ m/s is reached. Detailed explanation of the desaturation permeability function, as well as corresponding graphical representation are provided in Chapter 4.

Table 5.5 Model 82 parameters values and climatic boundary conditions – effect of clay fill permeability

Analysis name	Number of cycles	CLAY FILL (partially saturated-model82)													CLIMATIC & VEGETATION boundary conditions			
		Stiffness parameters				*Strenght*			*Permeability*		*SWRC*				*S3 [kPa]*	r_{max} *[m]*	*Rainfall data*	*Evapotranspiration data*
		K [kPa]	G [kPa]	Small strain stiffness	H [kPa]	φ [°]	c [kPa]	v [°]	k [m/s]	Variable permeability	s_{air} [kPa]	a	n	m				
RUN_IR	5	2000	923	no	6000	*23*	*5*	0	2.00E-09	no	20	0.0125	1.5	0.33	200	2	Shoeburyness 2006-2011	FAO Penman-Monteith 2006-2011
RUN_IS/2	5	2000	923	no	6000	*23*	*5*	0	2.00E-07	desaturation switch	20	0.0125	1.5	0.33	200	2	Shoeburyness 2006-2011	FAO Penman-Monteith 2006-2011

In the Figure 5.14 the seasonal pore water pressure and vertical movement variations at section S1 are presented. The analysis with lower permeability (RUN_IR) have exhibited larger seasonal variations in shallow surface zone (1.07 m), but at the same time significantly lower variations at the deeper elevations closer to the foundation soil (3.07 m). The same trend, but somewhat less pronounced have been observed in section S2, as can be seen in Figure 5.15. The obvious reason arises from the fact that the clay fill layer in section S2 is considerably thinner compared to section S1, thereby markedly reducing the impact of the clay fill permeability on the overall hydraulic response in that zone.

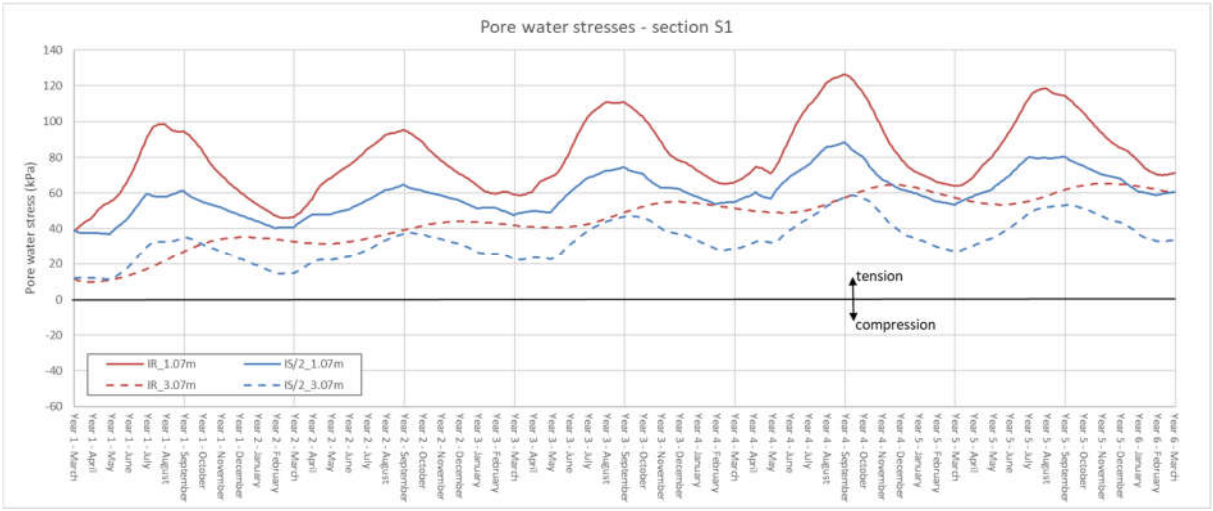

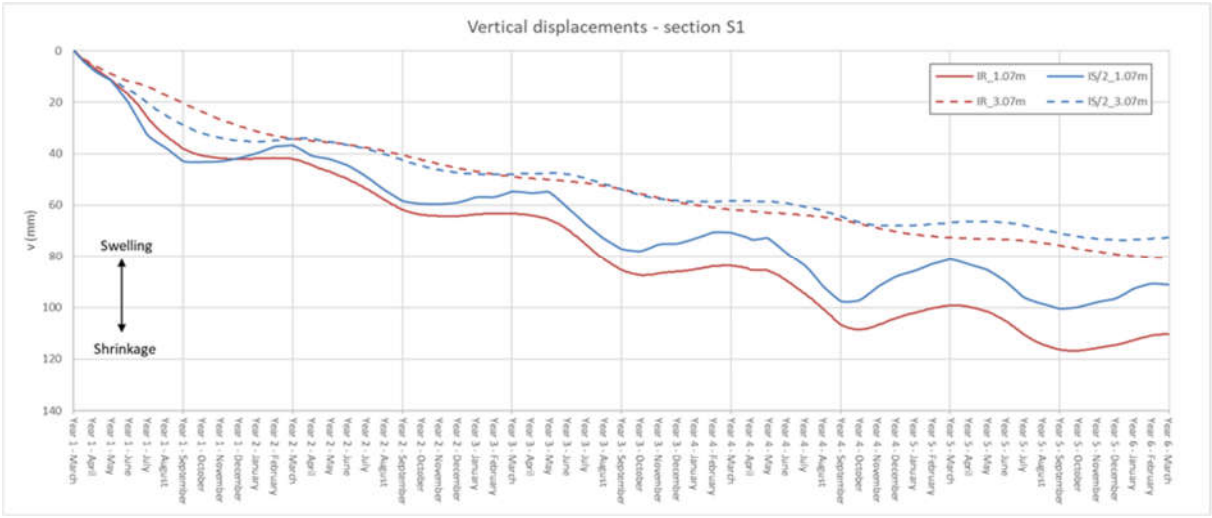

Figure 5.14 Predicted seasonal pore water pressure and vertical displacement variations for two points along the section S1, for different permeabilities

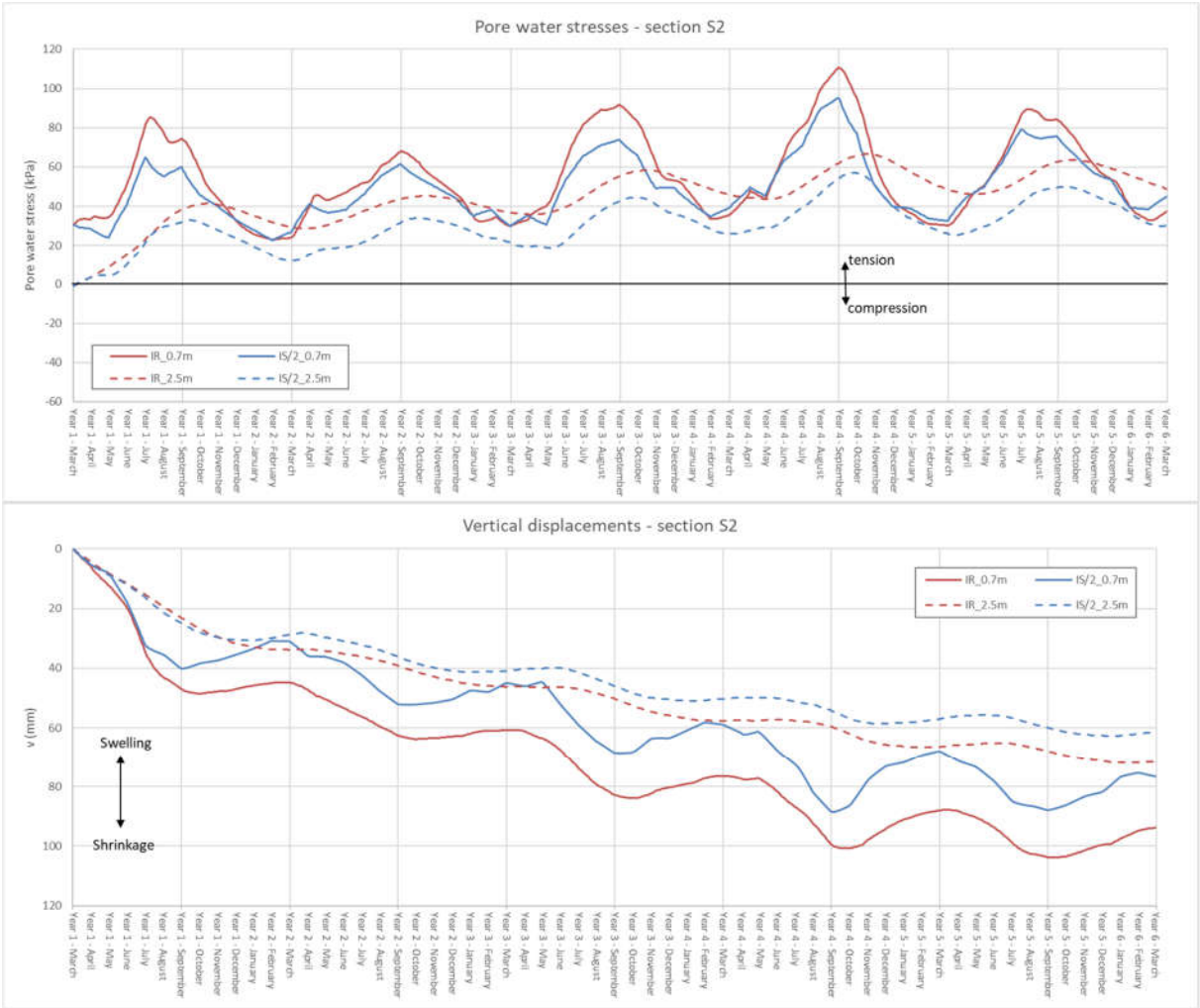

Figure 5.15 Predicted seasonal pore water pressure and vertical displacement variations for two points along the section S2, for different permeabilities

The Figure 5.16, presents the end of summer/winter pore water pressure profiles for an arbitrarily chosen year. It is clear that the higher permeability associated with analysis RUN_IS/2 has produced more uniform seasonal pore suction variations over the entire depth of the clay fill. In contrast, lower permeability has restricted seasonal variations to a surficial slope zone. Considering that the same net water fluxes have been used as a hydraulic (climatic) boundary conditions, it could be argued that integrals of the seasonal pore water suction changes over the depth of influence are practically equal. Simply stated, the areas between the summer/winter profiles for two analysis are most likely identical, which could be visually confirmed. This implies that permeability affects only the distribution of pore suctions over the depth, but does not impact the overall extraction rates, unless high suctions related to lower permeabilities indirectly alters the reduction function α(s).

Regarding the distributions, it can be seen that lower permeability confines seasonal wetting-drying cycles closer to the ground surface (Figure 5.17). In the case of higher permeability, the extent of the zone of influence is increased allowing the hydrological water cycle to affect deeper soil strata.

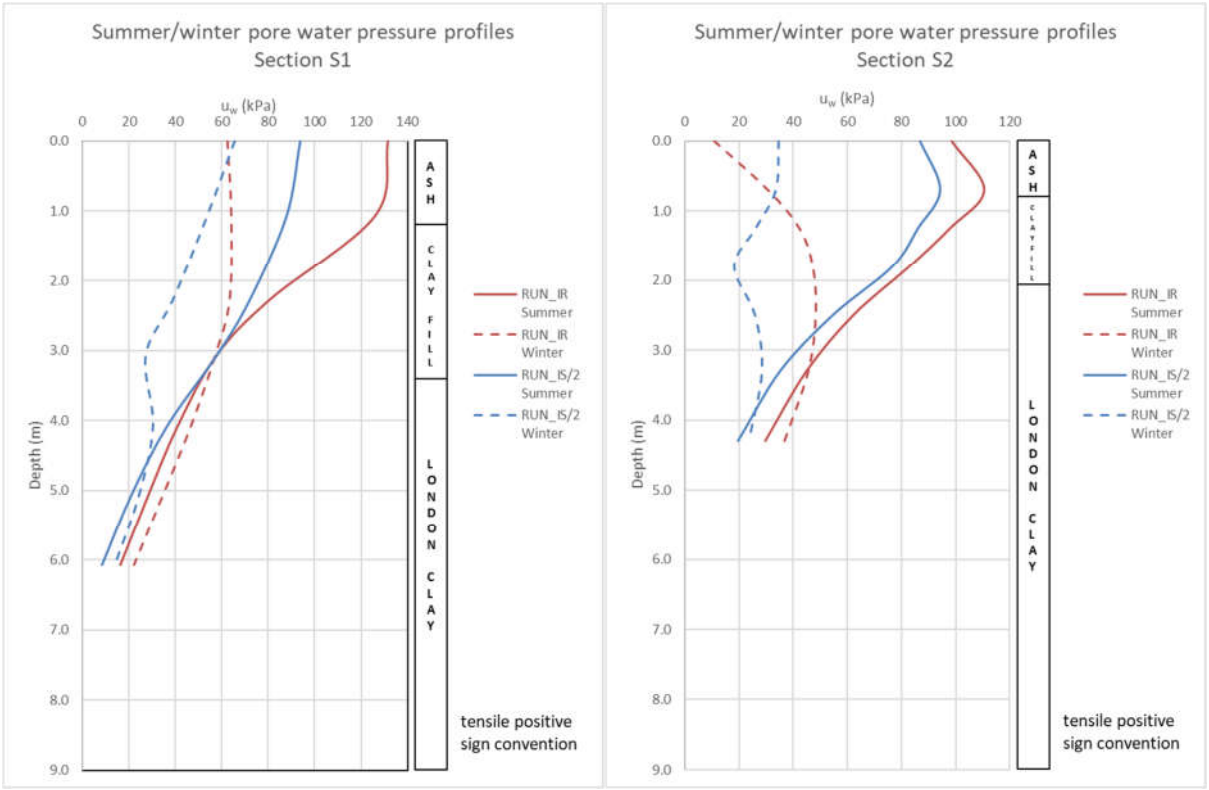

Figure 5.16 Predicted summer/winter pore water pressure profiles for two different permeability models

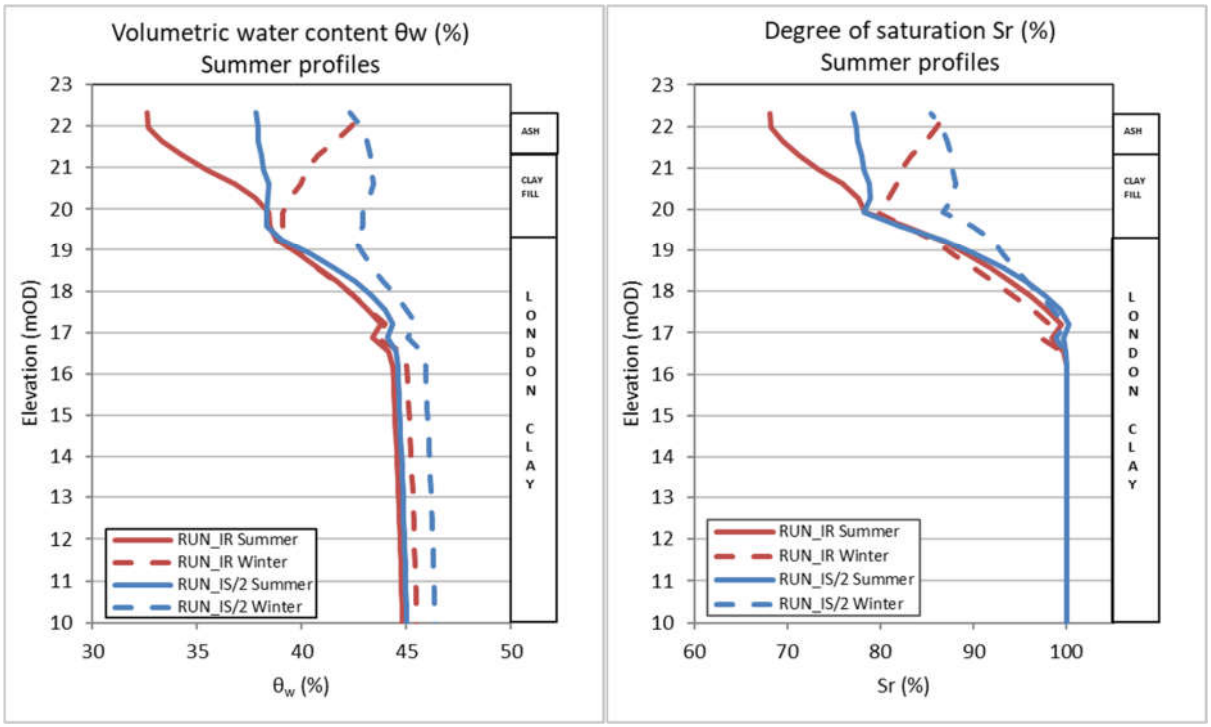

Figure 5.17 Predicted volumetric water content θ_w and degree of saturation S_r summer/winter profiles for two different permeability functions

As was discussed in the previous section the effect of permeability is introduced in the unsaturated/saturated coupled formulation in the bottom right sub-matrix. For the soil-atmosphere interaction problems, the climate/vegetation boundary conditions are defined in terms of water fluxes (flows). In the case of precipitation boundary condition, the prescribed rainfall rates are directly assigned to surface nodes as equivalent nodal flows, unless the maximum soil capacity to accommodate infiltrated water is exceeded. In the case of root water uptake model (RWUM), the flows are estimated for the integration points based on the root depth, pore suction distribution and entered potential evapotranspiration rates together with specified time step. Employing numerical integration over the elements containing integration points encompassed by root zone, an estimate of equivalent nodal flows is obtained. The prescribed flow rates are introduced into the flow vector on the right-hand side of the governing equations, and they will generate changes in pore water pressures, which are the unknowns in this case. Despite the governing equations for unsaturated coupled problems are complex in the sense that every term is directly or indirectly linked to the others, for the sake of simplicity the permeability matrix is isolated (assuming rigid soil skeleton and fully saturated conditions) to better understand its influence. Simply stated, it is clear that low permeability soil (very small k_f value), for some prescribed known flows, will yield higher suction changes compared to high permeabilities.

$$\begin{bmatrix} [K_G] & [L_d] \\ \Omega[L_G]^T & -\beta\Delta t[\Phi_G] - \omega[M_N] \end{bmatrix} \begin{Bmatrix} \{\Delta d\}_{nG} \\ \{\Delta p_f\}_{nG} \end{Bmatrix} = \begin{Bmatrix} \{\Delta R_G\} \\ ([n_G] + Q + [\Phi_G]\{p_f\}_{nG})\Delta t \end{Bmatrix}$$

The analogy could be drawn between the flow and stress-strain behaviour, particularly when flow boundary condition is prescribed. The assigned water flux is equivalent to the prescribed force boundary condition – load vector $\{\Delta R_G\}$. The stiff soil medium, characterized by high values of stiffness matrix coefficients, would induce small changes in displacements vector $\{\Delta d\}_{nG}$. On the other hand, "stiff" porous medium in terms of pure hydraulic behaviour is characterised by low values

of permeability matrix coefficients, and as such would induce large changes in pore water suctions/pressures in response to prescribed equivalent "forces" (flows).

Beside the permeability of the clay fill which has proven to be important parameter, especially with respect to the extent of the zone of seasonal wetting and drying, the permeability of the foundation soil was also investigated. Two analyses, namely RUN_IO with variable permeability model proposed by (Vaughan, 1994), and RUN_IP with constant isotropic permeability, have been compared. The Table 5.6 presents the used input parameters for mentioned analyses.

Table 5.6 Model 82 parameters values and climatic boundary conditions – effect of London Clay permeability

Analysis name	Number of cycles	CLAY FILL (partially saturated-Model82)													CLIMATIC & VEGETATION boundary conditions				part of LONDON CLAY (partially saturated-Model82)					
		Stiffness parameters				*Strenght*			*Permeability*		*SWRC*								*Permeability*		*SWRC*			
		K [kPa]	G [kPa]	Small strain stiffness	H [kPa]	φ [°]	c [kPa]	v [°]	k [m/s]	Variable permeability	s_{air} [kPa]	a	n	m	*S3 [kPa]*	r_{max} *[m]*	*Rainfall data*	*Evapotranspiration data*	k [m/s]	Variable permeability	s_{air} [kPa]	a	n	m
RUN_IO	5	2000	923	no	6000	*23*	*5*	0	2.00E-09	no	20	0.0125	1.5	0.33	200	2	long term average	Thornthwait 2006-2011	5.00E-10	$k=k_0e^{-bp'}$ b=0.003	20	0.0125	1.5	0.33
RUN_IP	5	2000	923	no	6000	*23*	*5*	0	2.00E-09	no	20	0.0125	1.5	0.33	200	2	long term average	Thornthwait 2006-2011	1.25E-09	no	20	0.0125	1.5	0.33

The Figure 5.18 plots the adopted relationship between the permeability and mean effective stress. The predicted pore water pressure variations at section S2 for the two analyses are illustrated in Figure 5.19. It can be seen that, although the section S2 is relatively close to embankment toe and foundation soil, the patterns and magnitudes of seasonal pore water suction variations close to ground surface are essentially unaffected. At deeper levels the lower permeability London Clay (RUN_IO) delays the desaturation, but nearing the end of five-year cycles it catches up the other analysis (RIN_IP) pore water suction distribution.

The corresponding horizontal movements for section S2 are shown in Figure 5.20. It is interesting to note that the reduction of permeability of foundation soil has completely changed the pattern, in particular the direction of horizontal movements. In all previous analyses the steady drying has induced accumulation of shrinkage movements, which despite being dominantly vertical, had small horizontal component oriented inwards.

The analysis with lower permeability has changed the direction of horizontal movements inverting them towards the embankment toe. This is closely linked to higher suction levels generated in foundation soil beyond the embankment, which are depicted in Figure 5.21. The mechanism that governs the obtained response is explained below.

In the case of the analysis with variable permeability model (RUN_IO) low initial permeability has induced large suction changes, which reflected to generation of higher summer suctions. In turn the rise in suctions has directly affected mean effective stress and led to further decrease in permeability, which caused even greater change in suction. The large seasonal suction variations, amplified by permeability fluctuations, attract the lower part of embankment slope towards the vegetated zone beyond the toe of the embankment.

These findings have important practical implications, suggesting that the same tree species rooted in different soils could produce diametrically opposed deformational response. It is therefore important that material, in particular hydraulic and index properties, of the foundation soil encompassed by root zone, be reliably estimated.

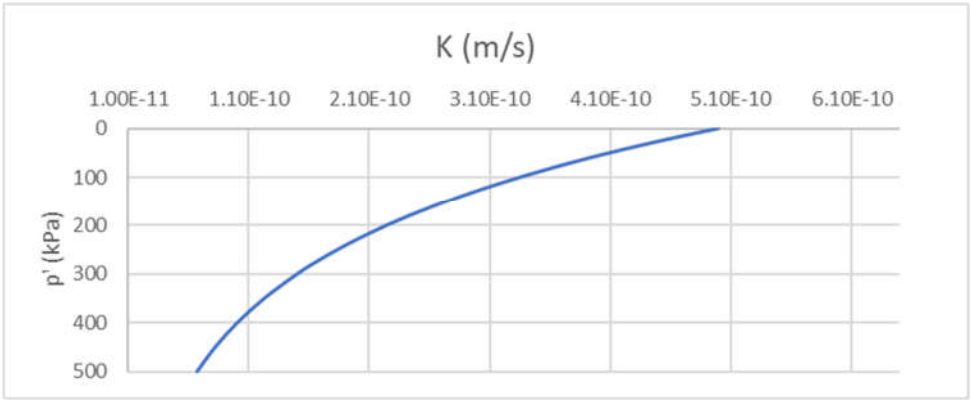

Figure 5.18 Adopted relationship between permeability and mean effective stress

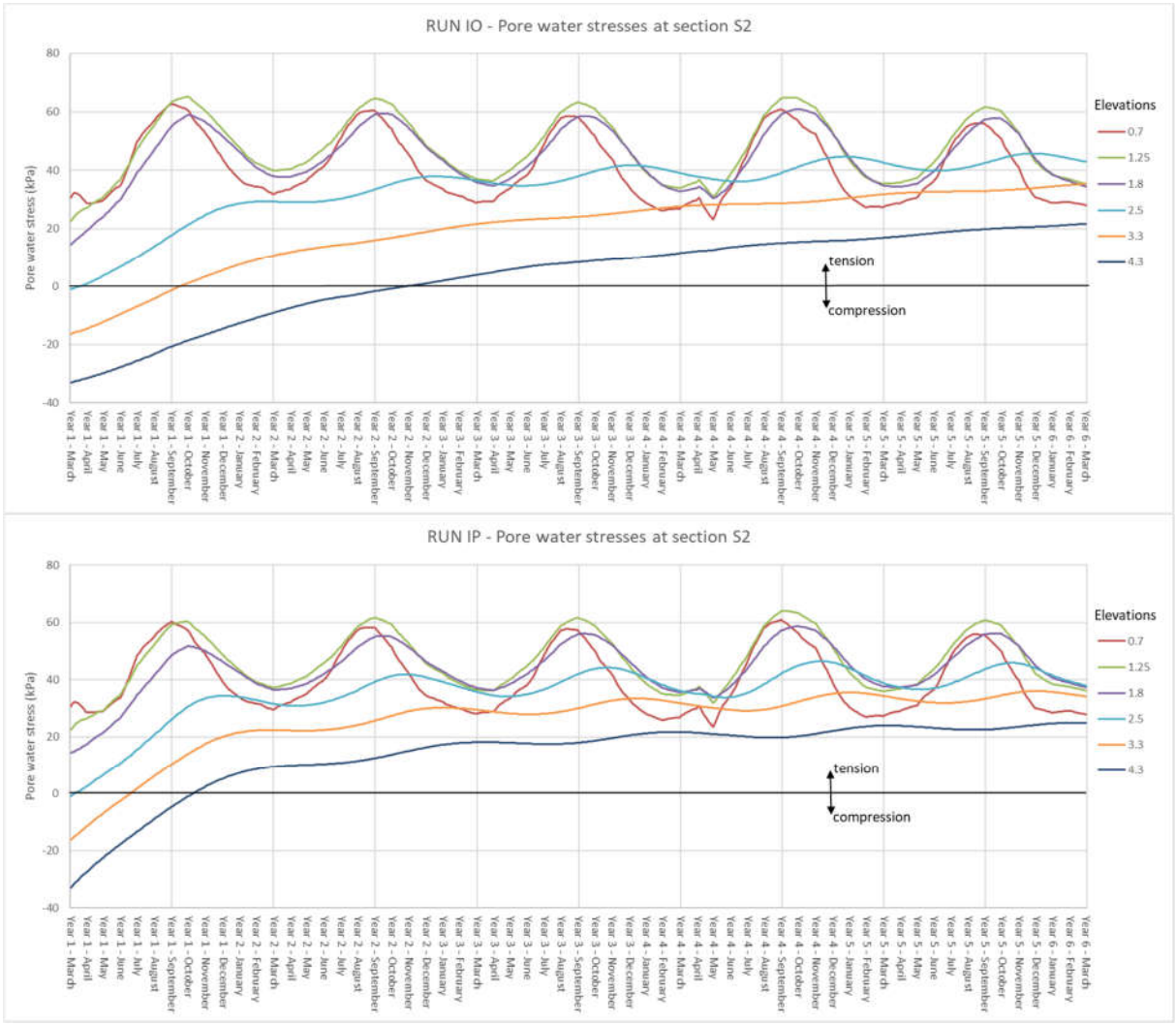

Figure 5.19 Predicted seasonal pore water pressure variations over the depth of section S2, for two different permeability functions of London Clay

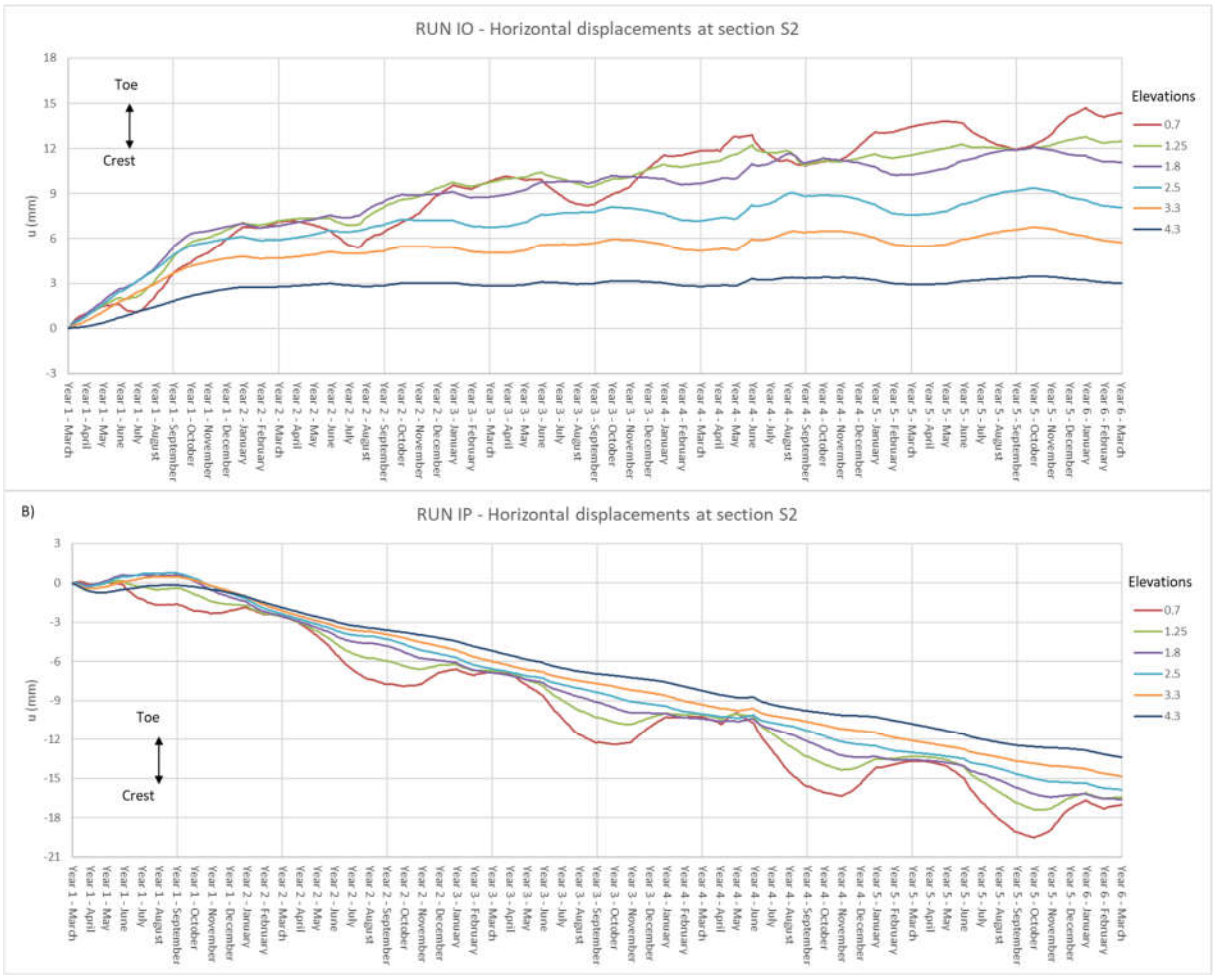

Figure 5.20 Predicted horizontal movements variations over the depth of section S2, for two different permeability functions of London Clay

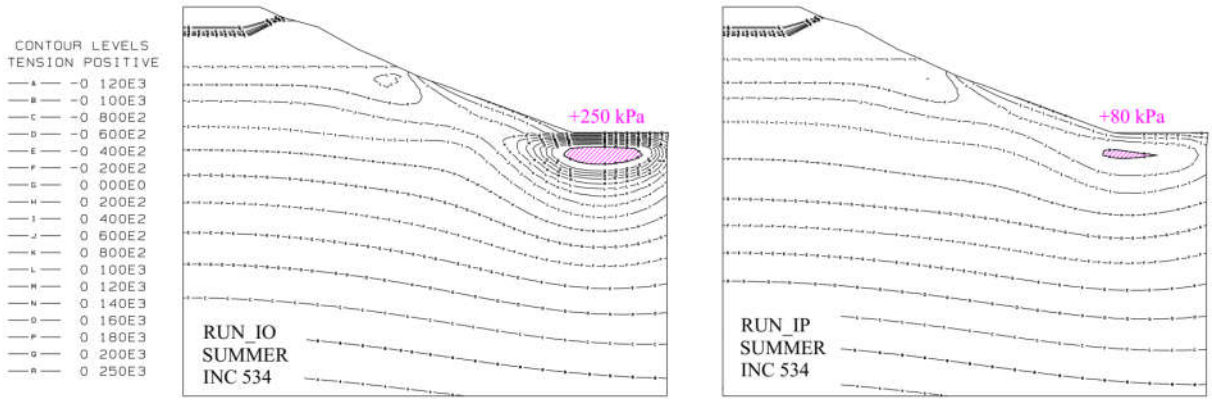

Figure 5.21 Predicted pore water pressure contours for two different foundation soil permeability models

5.1.5 Effect of H Modulus – Model 82

It was demonstrated earlier in this chapter that the unsaturated coupled flow-deformation formulation is very cumbersome and complex. Despite the effects of SWRC and permeability have been proven to be particularly important for the response of unsaturated soils to climatic/vegetation perturbations, it was stated that for more complete understanding, the effects of the soil skeleton stiffness with respect to suction changes should also be investigated. Therefore, in this section two analyses with different *H* moduli have been compared. The set of model parameters corresponding to the clay fill, as well as precipitation/vegetation boundary conditions, are presented in Table 5.7.

Beside the *H* moduli, the two analyses differ also in linear elastic stiffness parameters and SWR curves. However, as was previously explained in section 5.1.3 that the two curves coincide in the range of suctions relevant to current analyses. Also, it is worth recalling that the *H* modulus is actually derived from consistency requirement between saturated and unsaturated elastic constitutive relation of the soil structure $H = \frac{E}{(1-2\nu)}$. However, in the analysis RUN_IH a somewhat greater value (the minimum would be 9375 kPa), was adopted. It should be noted that in reality H modulus gradually increase with suction, beyond the air-entry suction level, but due to the lack of experimental data was assumed constant. Also, the fact that the predicted suction levels for the clay fill finite elements are generally in excess of the prescribed air-entry suction value of 20 kPa, justifies the specification of somewhat higher *H* modulus value.

Table 5.7 Model 82 parameters values and climatic boundary conditions – effect H modulus

Analysis name	Number of cycles	CLAY FILL (partially saturated-Model 82)													CLIMATIC & VEGETATION boundary conditions			
		Stiffness parameters				*Strenght*			*Permeability*		*SWRC*							
		K [kPa]	G [kPa]	Small strain stiffness	H [kPa]	φ [°]	c [kPa]	v [°]	k [m/s]	Variable permeability	s_{air} [kPa]	a	n	m	*S3 [kPa]*	*r_{max} [m]*	*Rainfall data*	*Evapotranspiration data*
RUN_IH	5	3125	1445	no	12500	*22.9*	*5*	0	2.00E-09	no	20	0.0195	1.7	0.2	200	2	Shoeburyness 2006-2011	Mat office 70'-74' + 70'-71'
RUN_IN	5	2000	923	no	6000	*22.9*	*5*	0	2.00E-09	no	20	0.0125	1.5	0.33	200	2	Shoeburyness 2006-2011	Mat office 70'-74' + 70'-71'

The comparison of pore water pressure and vertical movement variations along the clay fill layer in section S1, is presented in Figure 5.22. As was expected, the analysis with lower *H* modulus has generated larger deformations, reflecting in both greater seasonal and total accumulated heave (shrinkage) movements. However, the larger displacements have at the same time been accompanied by lower seasonal suction variations. This conclusion is in contrast to hitherto findings, which had indicated that greater seasonal pore water suction changes are related to consequently larger deformations.

To better understand the causes of opposite impacts of the *H* modulus the governing equations are once again examined, but this time in context of *H* modulus and soil skeleton deformation. The *H* modulus is introduced in the governing equations within the upper right cross-coupling matrix $[L_d]$. In addition, it is also implemented into the ω function, reflecting the effect of net total stresses on the water phase (see Chapter 3). However, the contribution of this term is generally of lesser importance compared to the gradient of the SWR curve and would be omitted from further discussion.

$$\begin{bmatrix} [K_G] & \boxed{[L_d]} \\ \Omega[L_G]^T & -\beta\Delta t[\Phi_G] - \omega[M_N] \end{bmatrix} \begin{Bmatrix} \{\Delta d\}_{nG} \\ \{\Delta p_f\}_{nG} \end{Bmatrix} = \begin{Bmatrix} \{\Delta R_G\} \\ ([n_G] + \boxed{Q} + [\Phi_G]\{p_f\}_{nG})\Delta t \end{Bmatrix}$$

$$\omega = \left(\frac{1}{R} - \boxed{\frac{3\Omega}{H}}\right)$$

As already explained the vegetation and precipitation (infiltration part) boundary conditions affect the flow vector Q on the right-hand side of the governing equations. Despite no load (force) boundary conditions have been applied, the fact the two equations are coupled and are solved simultaneously, implies that prescribing only the flow boundary condition would indirectly affect the upper equation, in particular the displacement vector. The mechanism and in-between steps are explained in more detail below.

The assigned flow directly affects the changes in pore water pressures through the second equation. The changes in pore water pressures via the cross-coupling matrix $[L_d]$ generate the reactions-load vector $\{\Delta R_G\}$, which produces the volumetric deformations of the soil skeleton. In turn, volume changes generate water flow through the lower right cross-coupling matrix $\Omega[L_G]^T$. This indirectly induced flow is crucial in controlling the amount of pore water pressure changes. For example, if negative water flows (evapotranspiration) are prescribed as only boundary condition, they will induce the increase in pore water suction, which will in turn generate shrinkage of the soil structure. Successively, the contraction of the soil skeleton will cause the water and air to be squeezed out from the soil, thereby facilitating the extraction of water driven by evapotranspiration process. Finally, as a result lower changes in suction are generated. This essentially means, that more flexible the soil skeleton is, it would provide less resistance to water extraction/injection, and as a result will produce lower pore water pressure changes.

These findings explicitly question the applicability of pure hydraulic approach, especially in the case of medium to high volume change potential soils. On the other hand, only in the case of very stiff soil structures (rare), the assumption of rigid soil skeleton and pure hydraulic behaviour could be justified. The proof for these statements and hypothesis could be found in the work of (Briggs *et al.*, 2016). In Chapter 2, it was already explained that the authors have employed pure unsaturated hydraulic modelling approach. The results reported by (Briggs *et al.*, 2016) are once again illustrated for convenience in Figure 5.23.

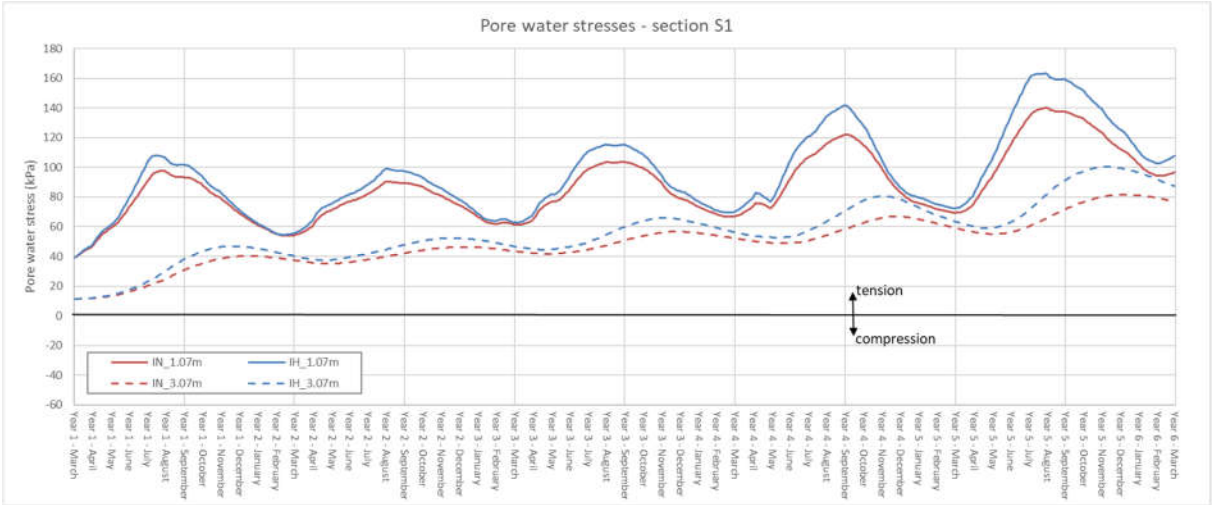

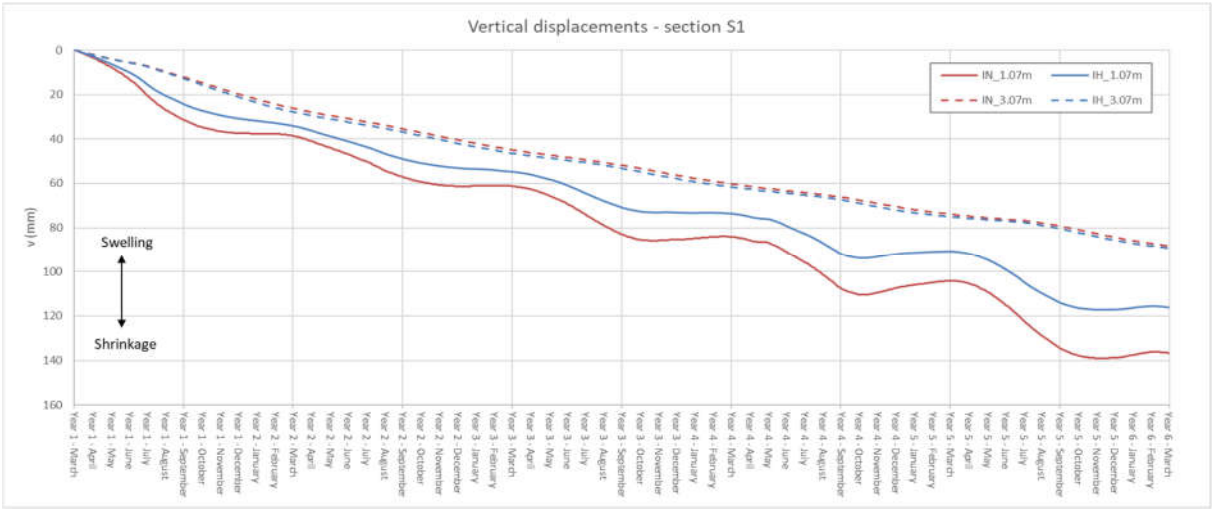

Figure 5.22 Predicted seasonal pore water pressure and vertical displacement variations for two points along the section S1, for different H moduli

It can be seen that the predicted suction seasonal variations at 1.0 m depth are up to 1500 kPa. Also, very high suctions, with variations of 700 kPa and peaks of around 1500 kPa have been obtained at 2.0 m depth. At higher depths the seasonal fluctuations are practically absent. The obtained results are indicative that rigid soil skeleton, implicitly assumed by neglecting the equilibrium equations form the FE formulation, resists the water abstraction governed by evapotranspiration, thereby inducing very high suction levels. It should be noted that the authors have applied the same $\alpha(s)$ reduction function, proposed by (Feddes, Kowalik & Zaradny, 1978), with the same generally recommended s_4 = 1500 kPa, corresponding to the plant wilting point. This implies that the $\alpha(s)$ function, have prevented even greater increase in suction levels by effectively ceasing further evapotranspiration.

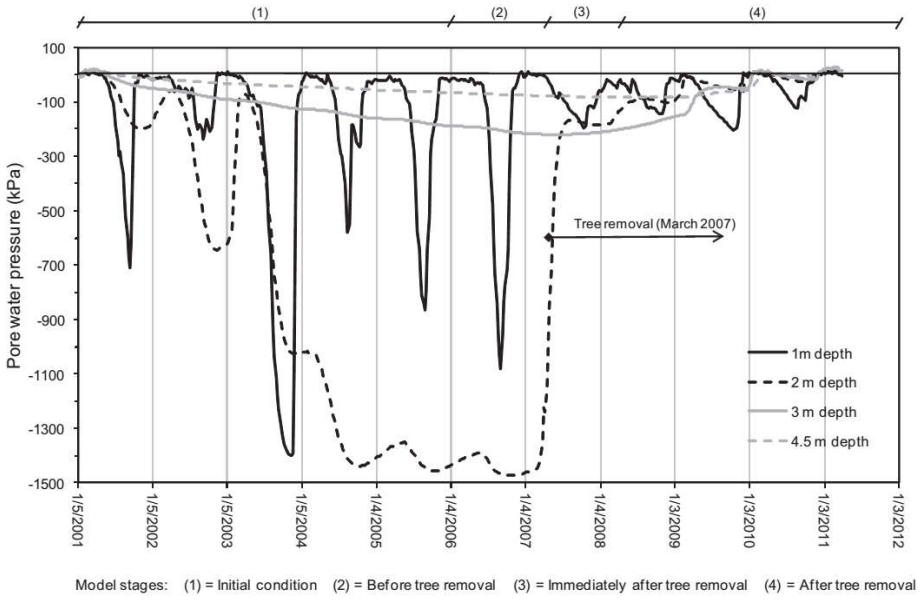

Figure 5.23 Mid-slope pore water pressure variation predicted by the finite element model after (Briggs et al., 2016)

In the Figure 5.24 the end of summer/winter pore water pressure profiles are presented. It can be seen that while the summer profiles differ significantly, the winter profiles practically coincide. Such results verify the previous statements, that soil structure stiffness governs solely the magnitudes of seasonal suction variations, but does not affect the overall desaturation patterns.

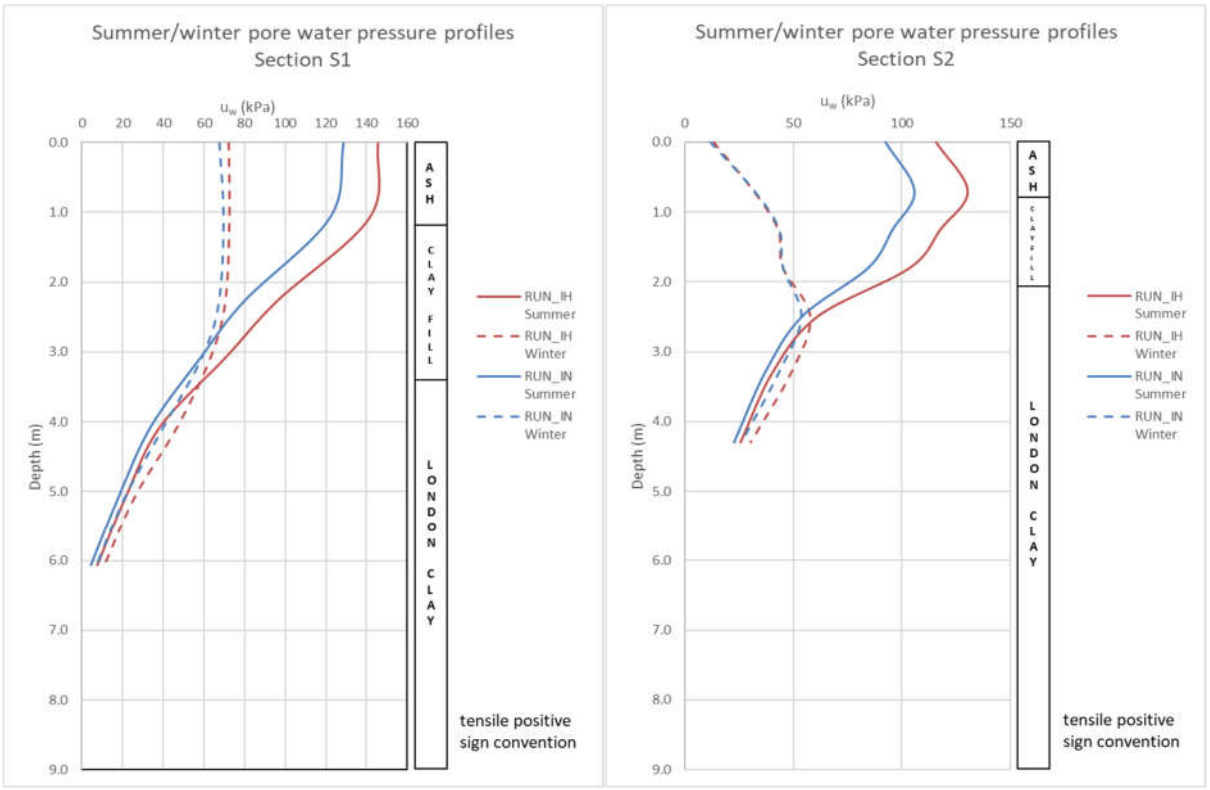

Figure 5.24 Predicted summer/winter pore water pressure profiles for two different H moduli

5.1.6 Effect of Compressibility Coefficient κ_s – Model 81

The influence of coefficient of compressibility κ_s is examined in this section. Considering that κ_s defines the response of soil structure to suction changes, its effect on the clay fill embankment hydro-mechanical response to climatic/vegetation actions is expected to be analogous to the influence of *H* modulus.

The Table 5.8 illustrates the set of material parameters adopted for the modified BBM (Model 81) representing the clay fill. Except the κ_s, which in the analysis RUN_IG was moderately higher compared to reference analysis RUN_IB, all other parameters were mutually equal. The higher compressibility coefficient κ_s value, signifies that the soil is actually more flexible with respect to suction changes.

Table 5.8 Model 81 parameters values – effect of κ_s

Analysis name	Number of cycles	CLAY FILL (partially saturated-Model 81)																																		
		Linear parameters		*Small strain stiffness*	*Plastic potential and yield surface*			*Hardening&Softening parameters*									*Initial hardening parameters*				*Other parameters*									*Permeability*		*SWRC*			
		K [kPa]	G [kPa]		$\alpha_{g,f}$	$\mu_{g,f}$	$M_{g,f}$	α^c	$\lambda(0)$	κ	r	β	κ_{sat}	χ	ω		v_1	OCRS	OCR	k	p_{atm}	SMS	v	s_{air}	K_{min}	S_{oi}	λ_s		k [m/s]	Variable permeability		s_{air} [kPa]	a	n	m
BBM_IB	5	2000	923	no	0.4	0.9	1	-1.98	0.152	0.02	0.45	0.011	0.07	1	0		2.75	4	10	-1	100	2	0.35	20	2000	1.00E+06	0.3		2.00E-07	desaturation switch		20	0.0125	1.5	0.33
BBM_IG	5	2000	923	no	0.4	0.9	0.89	-1.98	0.152	0.02	0.45	0.011	0.1	1	0		2.75	4	10	-1	100	2	0.35	20	2000	1.00E+06	0.3		2.00E-07	desaturation switch		20	0.0125	1.5	0.33

The pore water pressure and vertical movement fluctuations along the depth of the clay fill at section S2 are presented in Figure 5.25. The obtained results indicate that, the more flexible the (higher κ_s) soil structure with respect to changes in water stress is, the smaller seasonal pore suction variations would be. This observation is consistent with the findings from previous section related to the effects of *H* modulus. The differences between the two analysis are not so pronounced as in the case of *H* modulus, primarily due to the fact that the ratio of compressibility coefficients of two runs is 1.43, whereas in the case of *H* moduli, their ratio was 2.08.

In addition, the end of summer/winter pore water pressure profiles corresponding to the fourth year of successive climate/vegetation boundary conditions, are illustrated in Figure 5.26. Similarly to *H* modulus, it can be seen that the compressibility coefficient affects primarily the summer pore water suction profiles, with the winter ones basically matching.

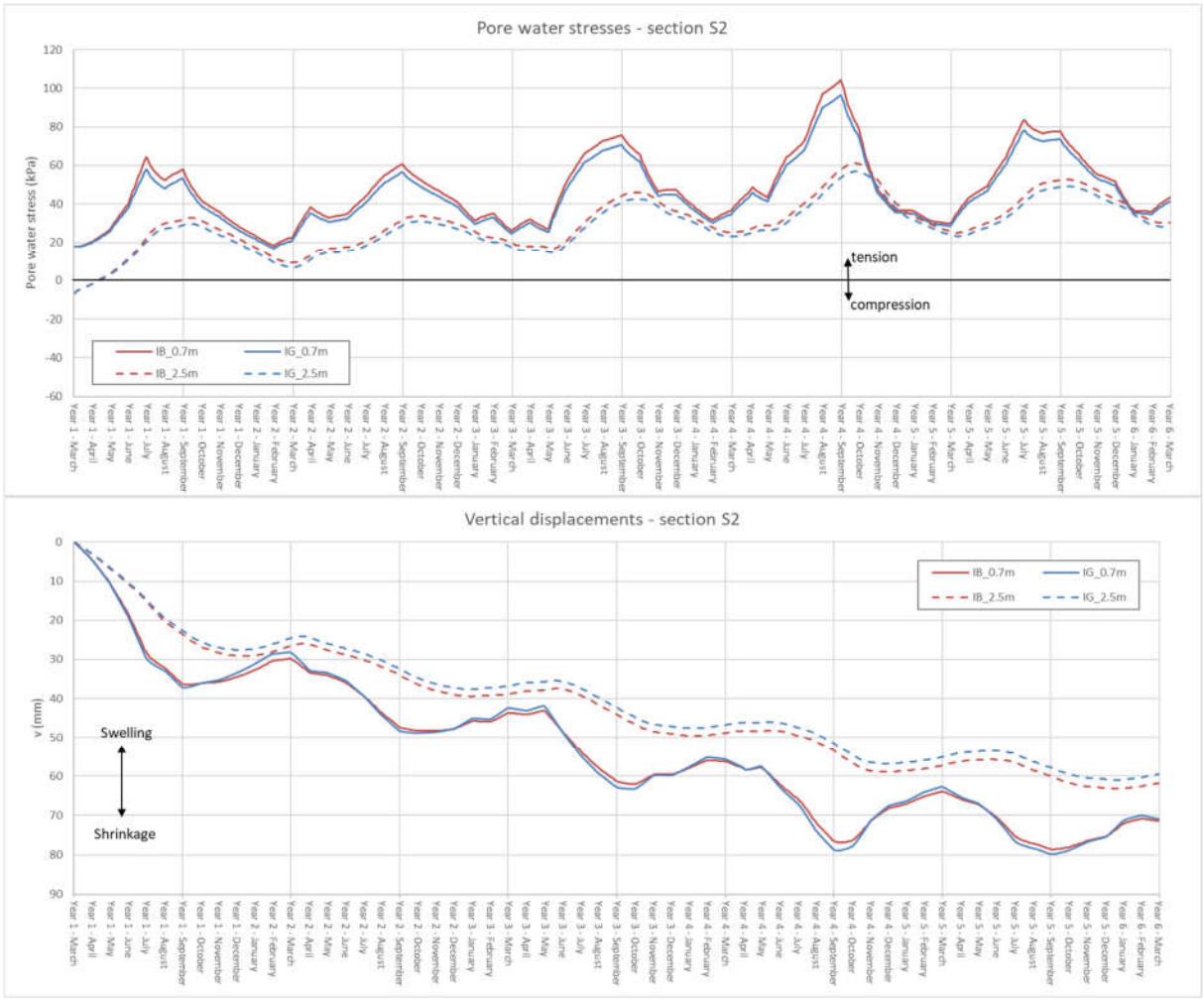

Figure 5.25 Predicted seasonal pore water pressure and vertical displacement variations over the depth of the clay fill at section S2, for different κ_s

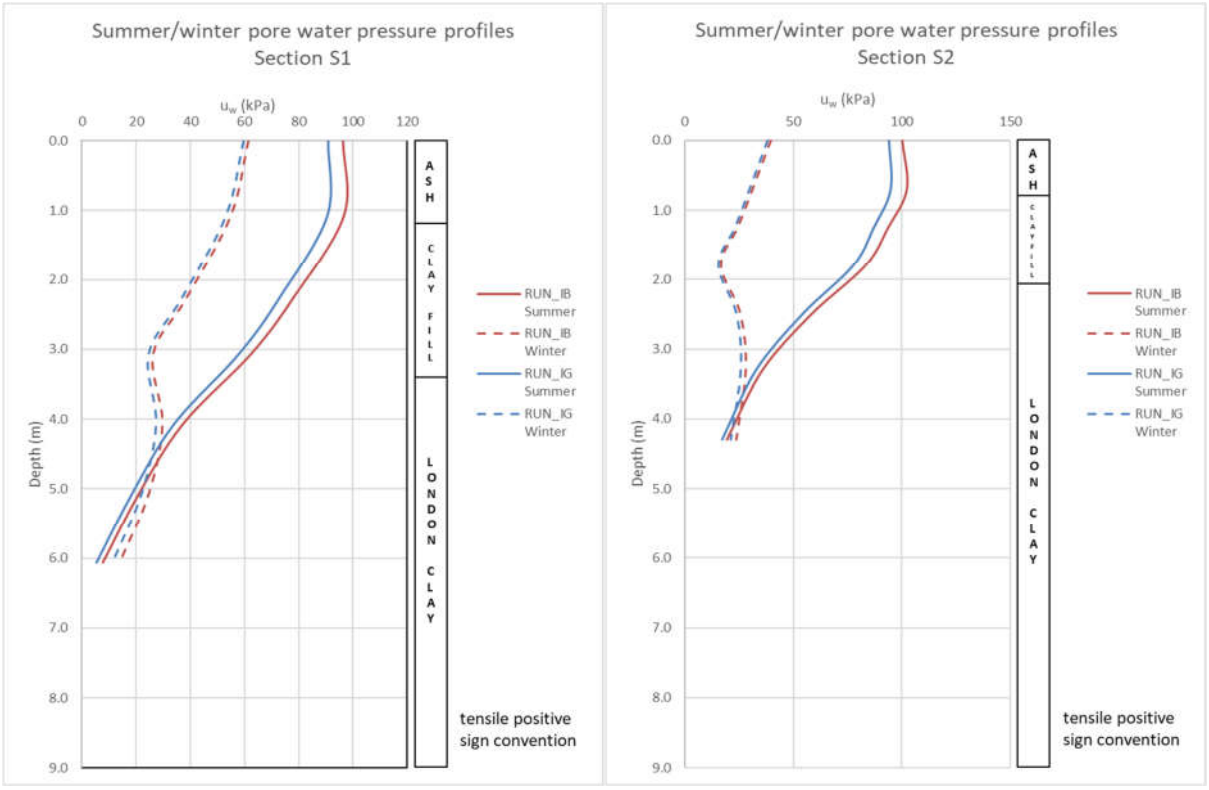

Figure 5.26 Predicted summer/winter pore water pressure profiles for two different compressibility coefficients κ_s

5.1.7 Effect of OCR – Model 81

The influence of the overconsolidation ratio (OCR) value adopted for the clay fill represented by the modified BBM model (Georgiadis, 2003) is studied in this section. The OCR value in combination with initial stresses defines the value of hardening parameter p_0^* - equivalent fully saturated yield stress. In the present study, the initialisation of hardening parameter p_0^* was performed indirectly through the use of the LC curve and initial yield stress p_0, established via OCR and absolute value of the mean total stress.

The Table 5.9 presents the adopted set of material parameters for the clay fill, represented by the modified BBM (Model 81). The OCR value corresponding to the reference analysis (RUN_IB) is equal to 10, whereas for the other analysis (RUN_IF) a value of 5 was assumed.

Table 5.9 Model 81 parameters values – effect of OCR

Analysis name	Number of cycles	CLAY FILL (partially saturated-Model 81)																																	
		Linear parameters		Small strain stiffness	Plastic potential and yield surface			Hardening&Softening parameters									Initial hardening parameters			Other parameters							Permeability		SWRC							
		K [kPa]	G [kPa]		$\alpha_{g,f}$	$\mu_{g,f}$	$M_{g,f}$	α^c	$\lambda(0)$	κ	r	β	κ_{sat}	χ	ω		v_1	OCRS	OCR	k	p_{atm}	SMS	ν	s_{air}	K_{min}	S_{oi}	λ_s	k [m/s]	Variable permeability	s_{air} [kPa]	a	n	m				
BBM_IB	5	2000	923	no	0.4	0.9	1	-1.98	0.152	0.02	0.45	0.011	0.07	1	0		2.75	4	10	-1	100	2	0.35	20	2000	1.00E+06	0.3	2.00E-07	desaturation switch	20	0.0125	1.5	0.33			
BBM_IF	5	2000	923	no	0.4	0.9	0.89	-1.98	0.152	0.02	0.45	0.011	0.07	1	0		2.75	4	5	-1	100	2	0.35	20	2000	1.00E+06	0.3	2.00E-07	desaturation switch	20	0.0125	1.5	0.33			

The Figure 5.27 illustrates the seasonal changes in pore water pressures and vertical displacements over the depth of the clay fill for section S1. As can be seen from the plots, the curves are completely identical, suggesting that the OCR value in examined range 5-10, has no effect on the outcomes. The

obvious reason, despite not being reported, is the position of the stress path relative to the LC yield curve. The insensitivity of the results implies that the stress paths induced by wetting/drying cycles are positioned far to the left from the LC (loading-collapse) curve, deep within the elastic region. It could be stated with certainty that the yield surfaces are not violated, especially considering that drying is the prevailing process. For convenience, the expected (not predicted) stress paths within isotropic stress plane, induced by wetting/drying cycles, are schematically illustrated in Figure 5.28.

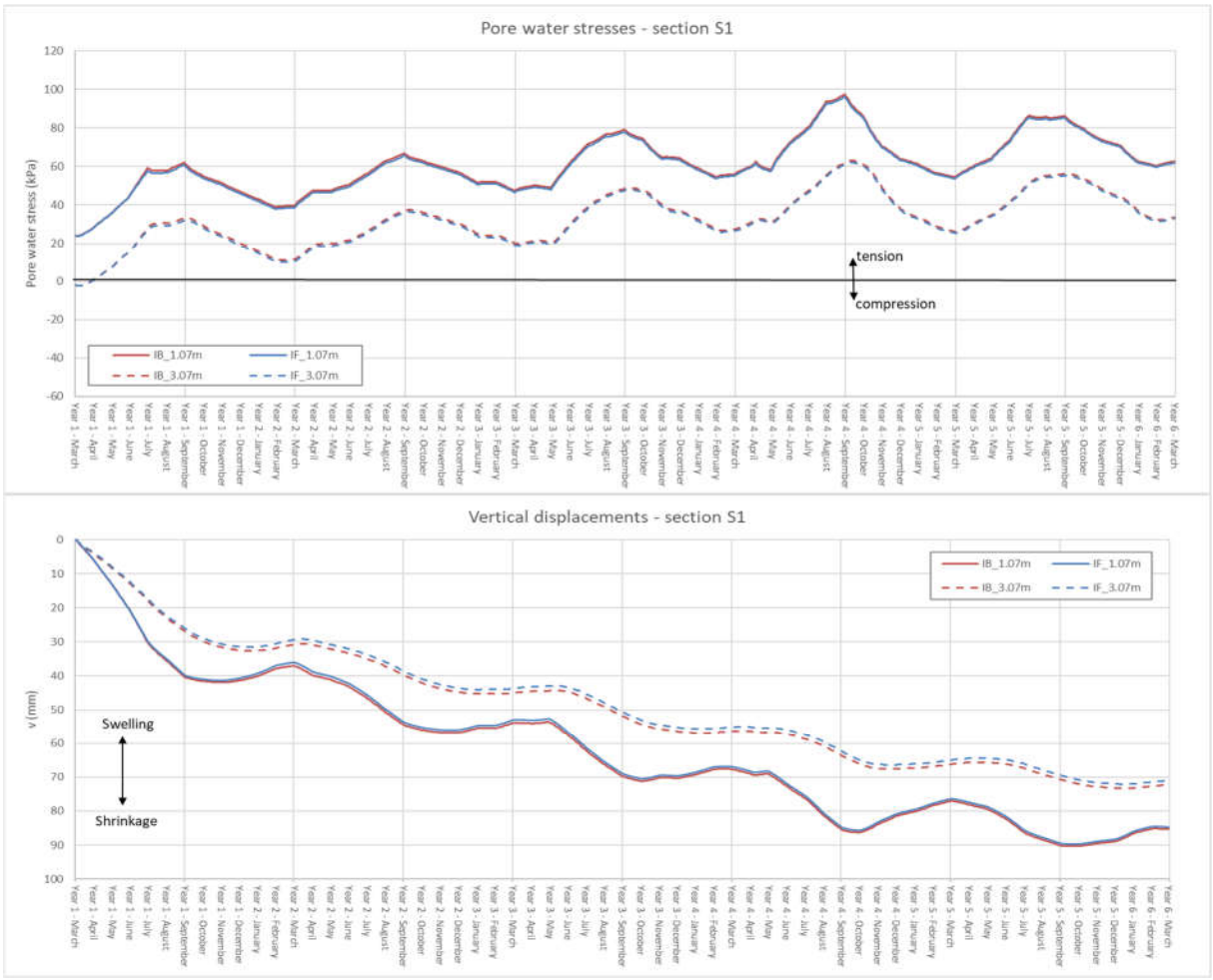

Figure 5.27 Predicted seasonal pore water pressure and vertical displacement variations over the depth of the clay fill at section S1, for two different OCR values

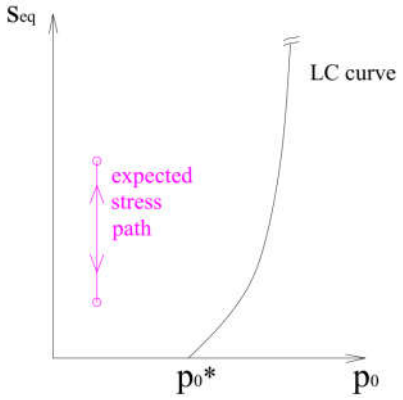

Figure 5.28 Schematic representation of expected stress pats induced by wetting/drying cycles

The Figure 5.29 presents the end of summer/winter pore water pressure profiles obtained from numerical simulations. It can be seen that the profiles are entirely identical over the entire depth of sections S1 and S2, confirming the tested OCR interval has no effect on the numerical predictions.

It would be interesting for some further research to investigate the effect of lower OCR values, especially in the vegetation clearance phase, governed by rapid rewetting of the soil domain.

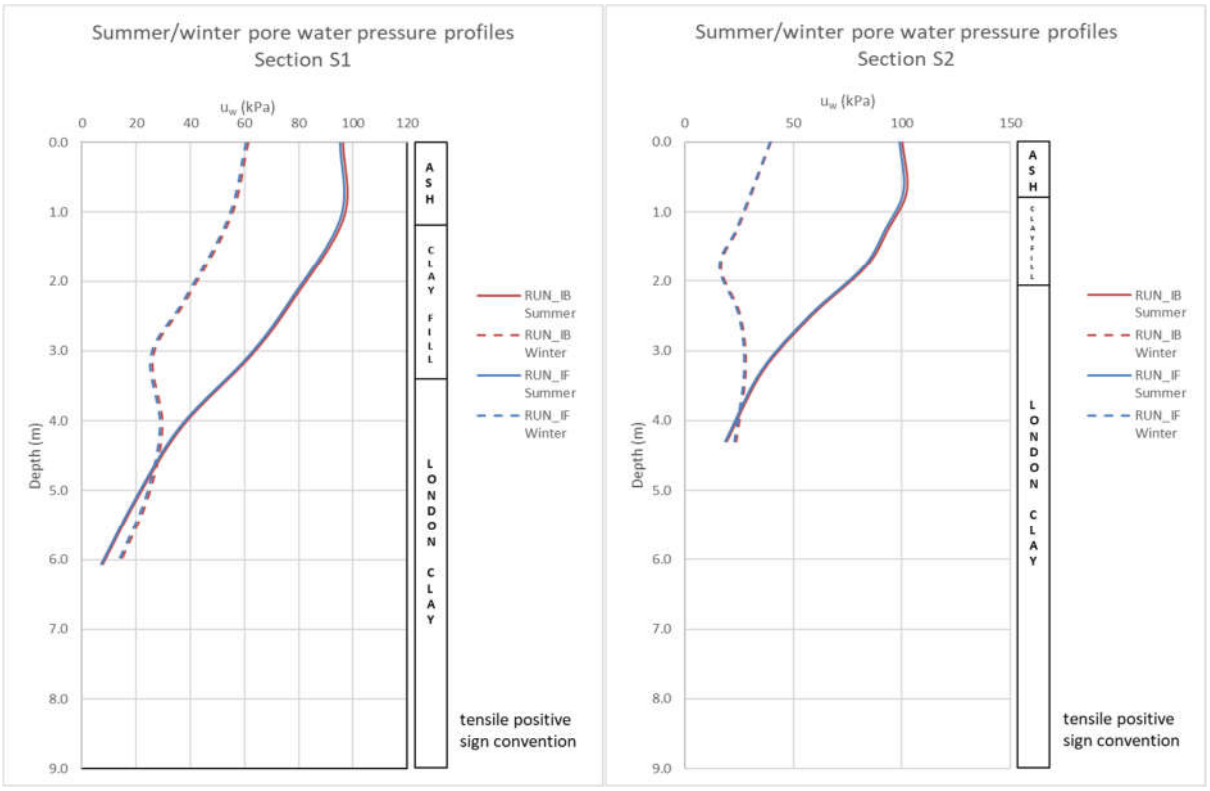

Figure 5.29 Predicted summer/winter pore water pressure profiles for two different OCR values

5.2 Vegetation Clearance Phase

5.2.1 Effect of Root Reinforcement

It was demonstrated in Chapter 4 as part of the main analysis, that vegetation removal has brought about the formation of failure mechanism in the upper part of the slope. The schematic illustration of failure mechanism is given here once again in Figure 5.30, for discussion purposes. It can be seen that the failure is of a shallow type, about 1.0-1.5 m deep, and is located primarily in ash layer, encompassing the small part of the ballast around the embankment crest. The lower margin of the unstable material is located close to midslope, around the section S1. The evolution of horizontal displacements along the depth of section S1, presented in Figure 5.31, has allowed to precisely identify the time instance corresponding to the formation of failure mechanism. It can be seen that around March-April 2008 sharp change in the gradient of the horizontal displacement curve corresponding to ground surface (elevation 0.0) has occurred. This clearly indicates that the rupture surface has been formed and that it includes the surficial zone of ash material within the section S1. Besides, relative ratio of displacement vectors magnitudes and distribution of plastic deviatoric strains, shown in Figure 5.30, confirm that failure has developed.

It is important to note that although the very large displacements have been obtained for a part of the finite element mesh, the convergence of the solution was not compromised, and the execution of program routine has not terminated.

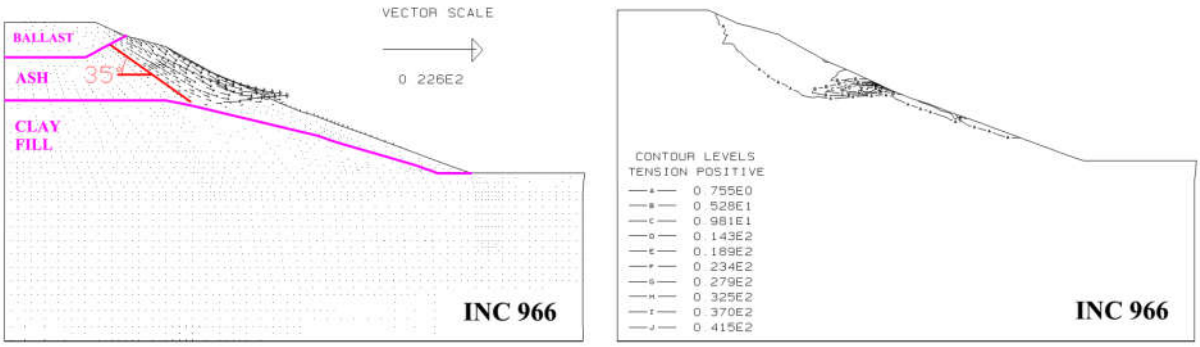

Figure 5.30 Predicted vectors of accumulated displacements and contours of accumulated plastic deviatoric strain

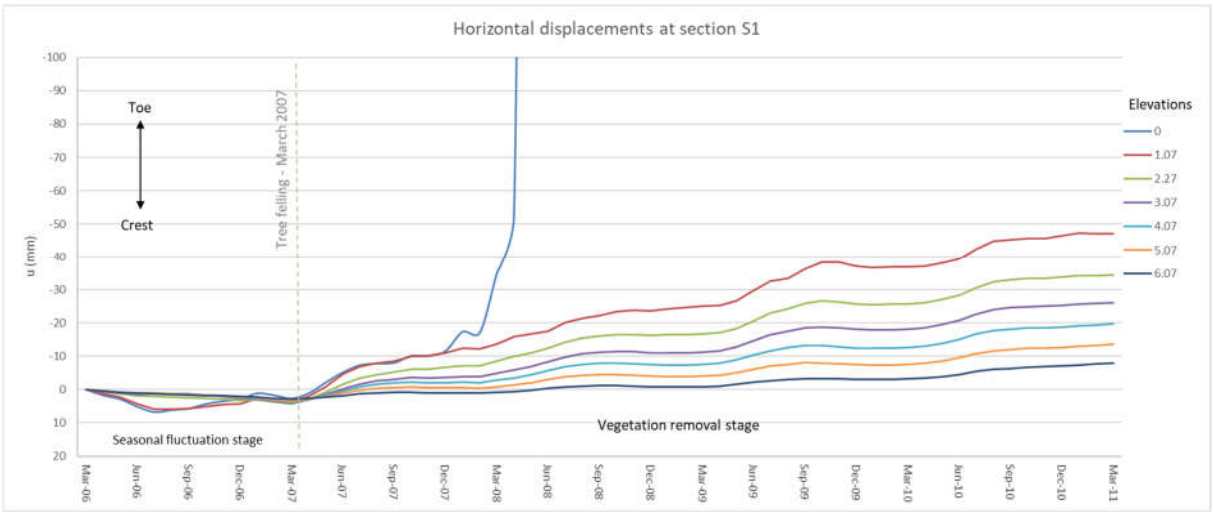

Figure 5.31 Predicted evolution of horizontal movements at section S1, highlighting the initialisation of failure mechanism

In Chapter 4, the possible causes that contributed to the formation of sliding surface have been discussed. They include the ratio of the ash-clay fill permeability, the geometry of the upper part of the slope and rapid infiltration of surface water induced by removal of mature trees.

It was shown in the work of (Briggs *et al.*, 2013) that an order of magnitude lower permeability of the underlying foundation soil compared to overlying embankment material represents the most onerous condition with respect to hydraulic response to the extreme wet winter rainfall. In the main analysis of the present study, the assumed ratio of the ash versus clay fill permeability is 10^4. Such huge difference in permeability is most likely the primary cause of relatively early formation of failure mechanism within the ash layer. The prevailing infiltration of surface rainwater into the embankment slope following tree removal, which led to rapid saturation of ash material and accompanying loss of pore water suctions, is definitely the last straw in chain of events that led to failure. However, a number of factors have attributed to establishment of poor initial conditions. One of important factors to which the instability could obviously be imputed was the very low permeability of the underlying clay fill that prevented drainage of excessive and continuous inflow of surface water. The clay fill upper surface has acted as impermeable boundary and allowed the establishment of hydrostatic

compressive conditions above it, known as perched water. The compressive pore water pressures within the upper ash stratum have reduced effective confining stresses, thereby resulting in the loss of available shear strength and ultimate failure.

The 'coat-hanger' shape of the embankment, with an over-steepened upper slope has further worsened the stability conditions. It was explained in Chapter 2 that the successive cycles of wetting and drying, and corresponding nonmatching swelling-shrinkage movements are the driving force behind the ratcheting-type (irreversible) deformation mechanism, which accumulation lead to a 'coat-hanger' appearance.

In the report by (Mott MacDonald, 2011) more than half of the 95 ULS failures observed in period 2003-2009, located in Network Rail's Southern Territories, were classified as local crest instability and unravelling of over-steepened ash/ballast at the shoulder. Despite the failure was not reported during the monitoring period following tree removal at Hawkwell embankment, the frequent local crest instabilities observed along the UK railway network, suggest that numerical model predictions are plausible representative of reality. However, certain discrepancies between the computer model and physical reality exist (Brinkgreve & Engin, 2013), and in the following the most obvious ones will be discussed.

The probably most evident physical phenomenon related to vegetation, that was not included into proposed numerical model, is the mechanical root reinforcing action. In addition to strength increase through generation of negative, tensile pore water pressures, the plants contribute to weak soil stabilisation through anchoring effect of the roots (Greenwood, Norris & Wint, 2004). The tensile strength of the roots could be very high, in excess of 200 MPa, as shown in Figure 5.32 by (Bischetti *et al.*, 2005). The authors have demonstrated that one of the most important factors influencing the tensile strength of the roots is their diameter. It was shown that the root tensile strength is strongly decreasing with increase in diameter. Same results, but with other plant species have been obtained by (Ji *et al.*, 2012), who also observed great variations between two examined vegetation species. Moreover, it was established that the roots' mechanical properties depend on the biological components, in particular the lignin/cellulose ratio (Zhang, Chen & Jiang, 2014). Another important factor governing the root mechanical reinforcement effect is the Root Area Ratio (RAR), that describes the distribution of the roots within soil medium. RAR is heavily influenced by soil and climate conditions, and generally decreases with depth as a consequence of a lack of nutrients and aeration.

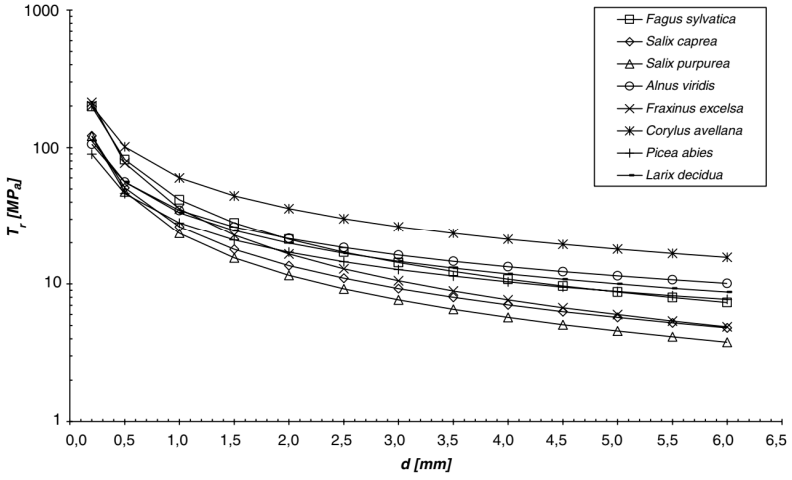

Figure 5.32 Tensile strength versus root diameter for different tree species, after (Bischetti et al.*, 2005)*

The tensile strength and pull-out resistance of roots, together with root architecture and density within the soil mass are fundamental components that govern the plants reinforcement effects on the overall slope stability. The experimental data derived from laboratory direct shear tests have suggested that the presence of roots directly contribute to increase in cohesion intercept, while maintaining the friction angle unchanged (Wu, McKinnell & Swanston, 1979; Ali & Osman, 2008; Askarinejad, 2013). Therefore, the reinforcement effects of roots are commonly accounted for as an additional cohesion in classical Mohr-Coulomb failure criterion. The total cohesion of rooted soil could be expressed as the sum of bare soil effective cohesion intercept *c'* and the additional root-induced cohesion term c_r. The Wu-Waldron Method (Waldron, 1977; Wu, McKinnell & Swanston, 1979) is most widely used approach for the estimation of additional cohesion c_r. For the sake of simplicity, the reduced form of the WWM expression is provided below.

$$c_r = 1.2 \sum_{i=1}^{n} (T_r)_i \cdot (RAR)_i$$

where coefficient of 1.2 combines the effects of soil friction angle and the angle that the roots form with the sliding plane, T_r represents the roots tensile strength and RAR, as explained earlier, represents the cross-sectional area of soil occupied by roots. Several studies based on the in-situ tests have shown that the WWM equation overestimates the root apparent cohesion (Fan & Su, 2008; Wu, 2013). Therefore a reduction function *k'* (0.4-1.0) have been proposed in order to adjust the WWM expression to experimental measurements.

$$c_r = 1.2k' \sum_{i=1}^{n} (T_r)_i \cdot (RAR)_i$$

However, the main limitation in employing WWM approach for assessing the additional cohesion stemming from the root's reinforcement was the lack of site investigation data regarding the root features. In the paper by (O'Brien, 2007) it was suggested that the additional cohesion due to the presence of fine roots can be in the range between 3 and 30 kPa. However, it should be noted that positive effects of root reinforcement are generally limited to surficial soil zone and are closely related to root depth and distribution. The estimated root cohesion values and distributions for different vegetation species are illustrated in Figure 5.33 (De Baets *et al.*, 2008). The authors have conducted a comprehensive study in order to establish the tensile strengths of Mediterranean plant species and their contribution to soil shear strength. Although the investigated vegetation comprises small shrubby plants, herbs and grasses, it can be seen that additional strength imparted by plant roots, can be immense, in particular in very shallow zone permeated by fine roots.

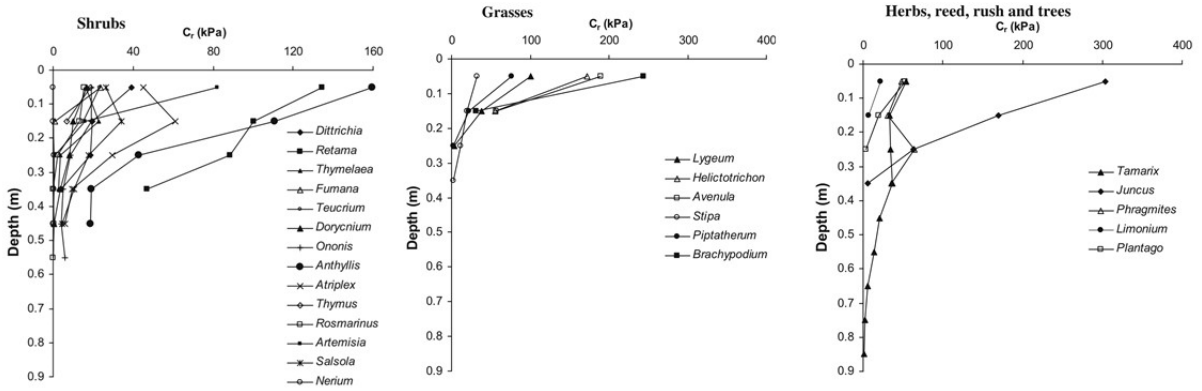

Figure 5.33 Distribution of additional root cohesion with depth, after (De Baets et al.*, 2008)*

In addition to root reinforcing effect, another source of discrepancy between performed numerical simulations and reported observations is possibly the spatial distribution of permeability across the embankment. It is most likely that the constant permeability model together with rather low value assumed for the clay fill within the "main" analysis are inconsistent with the in-situ permeability at the Hawkwell site. The dumped clay fill due to its intrinsic heterogeneity, characterized by higher permeability matrix and inclusions of coarse-grained pockets, represents very complex material from hydrological perspective. Additionally, the presence of roots and their decay, crates small cavities in form of conduits, which act as preferential pathways for the flow of water. It is obvious that constant permeability model is unable to capture realistically the stated physical phenomena.

The predicted shallow failure clearly indicates that the stability of upper slope is marginal and is heavily dependent on the mechanical root effects. Therefore, one of the important aims of the parametric study related to vegetation clearance stage was to identify the minimal additional root cohesion required to prevent the occurrence of failure. To achieve this, a number of additional numerical simulations with different magnitudes of root-induced cohesion c_r which were added to the base effective cohesion intercept of the ash, have been performed. It was deemed appropriate to assign a constant homogeneously distributed, apparent root cohesion across the entire ash layer. This assumption could be justified by the fact that the root biomass of large Oak and Ash trees may spread to 2 m depth, whereby the thickness of ash layer is 0.5 m at the toe and maximum 2.0 m at the upper part of the slope, below the ballast. However, it should be emphasized that most of the roots lie within 0.5 m from the ground and spread up radially 3 to 7 times the diameter of the tree's crown (WebPage-StudiousGuy, n.d.).

Besides, the different combinations of the additional root cohesion and clay fill permeability were also conducted. The goal was to establish how the change (increase) in permeability will affect the occurrence of upper slope instability.

The obtained results have indicated that the minimal additional root cohesion, superposed to the bare effective cohesion of the ash material, necessary to avoid failure is $c_r = 25$ kPa. It implies that a total cohesion intercept value of $c' = 30$ kPa, was sufficient to prevent the formation of failure mechanism throughout the entire simulated period (up until the end of increment 1325). The vectors of sub-accumulated displacements for the last increment of the analysis (increment 1325) are illustrated in Figure 5.34.

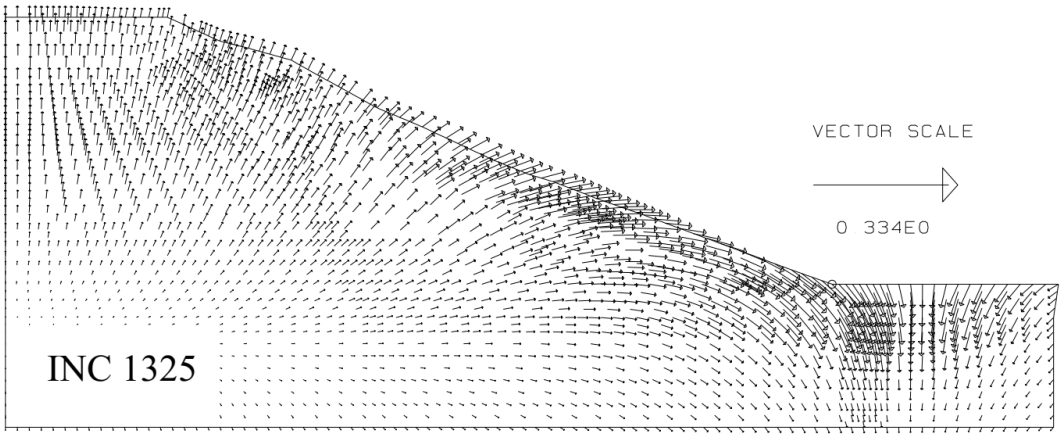

Figure 5.34 Predicted vectors of accumulated displacements, corresponding to the March 2011

The increase in permeability from $2 \cdot 10^{-9}$ m/s to $2 \cdot 10^{-7}$ m/s of the one row of finite elements representing the clay fill material just beneath the ash, enabled the minimal additional root cohesion

to be reduced to c_r = 15 kPa. The assumed permeability increase of uppermost zone of the clay fill, is sensible considering the most likely presence of roots and resulting preferential pathways.

Compared to established mechanical root contributions presented in the literature, the obtained magnitudes of additional root cohesion seem reasonable and indicate that root mechanical effects have great significance on preventing and protecting the slopes against shallow instabilities.

5.2.2 Effect of Extent of Tree Removal

The analyses discussed so far were based on the assumption that the vegetation is removed from the entire slope. In the section 4.7.5 it was stated that the high-water demand trees were retained solely in a narrow zone just beyond the embankment toe, whereas along the slope were replaced by grass cover.

The predicted results have indicated that the trees felling have completely eliminated the seasonal cyclic shrinkage/swelling movements, that were deemed as the main source of railway track serviceability issues. However, the removal of high-water demand trees has also produced several side effects. These include the formation of shallow failure mechanism in the upper part of the slope, discussed extensively in the previous section, and the rapid loss of previously established persistent pore water suctions in both reference sections, S1 and S2. While the local ash instability close to the crest arises from marginal stability of that zone and from disregarding the mechanical root reinforcement contribution, the loss of stabilizing effects related to deep persistent pore water suctions may have more sever implications. Although, the deep-seated failure was not predicted, at least not during the four-year simulated period following tree clearance, the risk of overall embankment failure has definitely increased significantly. The predicted volumetric water content and degree of saturation profiles corresponding to the last increment of the main numerical analysis, suggested that the entire embankment slope has approached the full saturation. Such conditions are considered highly detrimental, because if they are succeeded by extreme wet weather, the compressive pore water pressures could rapidly develop and further jeopardize the embankment stability.

In this section, the influence of the extent of tree removal on the patterns and magnitudes of movements and suction variations, is investigated. In addition, the volumetric water content and degree of saturation profiles corresponding to two different schemes of vegetation removal are also compared.

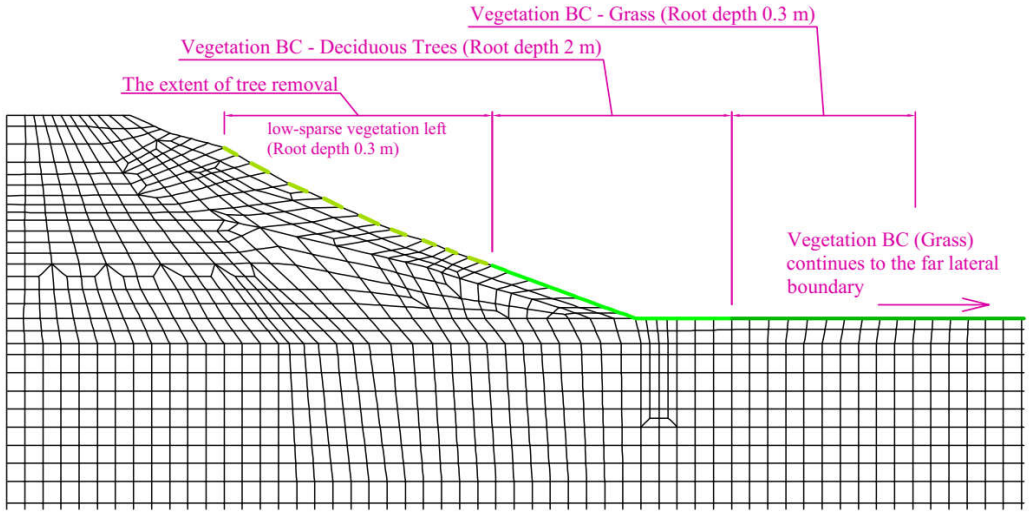

Figure 5.35 The additionally examined vegetation clearance layout

As the reference for comparison, the main analysis performed with Model 82 (partially-saturated Mohr-Coulomb), and enhanced cohesion to account for root reinforcing effects, is used. Also, the permeability of one layer of finite elements corresponding to the clay fill upper boundary has been increased. The vegetation removal layout proposed by (Briggs, Smethurst & Powrie, 2014; Briggs *et al.*, 2016), consisting of cutting the mature trees over the upper 2/3 of the embankment slope, is studied. The extent of vegetation removal zone is illustrated in the Figure 5.35.

The set of material parameters for the ash and the clay fill layers, along with climatic boundary conditions is illustrated in Table 5.10

Table 5.10 Ash and the clay fill parameters values and climatic boundary conditions

Analysis name	Number of cycles	ASH (fully saturated - model16)						CLAY FILL (partially saturated-model82)													CLIMATIC & VEGETATION boundary conditions				
		Stiffness		*Strenght*			*Permeability*	*Stiffness parameters*				*Strenght*			*Permeability*		*SWRC*				*S3 [kPa]*	r_{max} *[m]*	*Rainfall data*	*Evapotranspiration data*	*Extent of tree removal*
		E [kPa]	μ	φ [°]	c [kPa]	v [°]	k [m/s]	K [kPa]	G [kPa]	Small strain stiffness	H [kPa]	φ [°]	c [kPa]	v [°]	k [m/s]	Variable permeability	s_{air} [kPa]	a	n	m					
RUN_VR9C2	4	30000	0.2	35	20	0	4.00E-05	2000	923	no	6000	*23*	*5*	0	2.0E-7 2.0E-9	no	20	0.0125	1.5	0.33	200 50	2 0.3	Shoeburyness 2006-2011	FAO Penman-Monteith 2006-2011	entire
RUN_VR9C3A	4	30000	0.2	35	20	0	4.00E-05	2000	923	no	6000	*23*	*5*	0	2.0E-7 2.0E-9	no	20	0.0125	1.5	0.33	200 50	2 0.3	Shoeburyness 2006-2011	FAO Penman-Monteith 2006-2011	upper 2/3

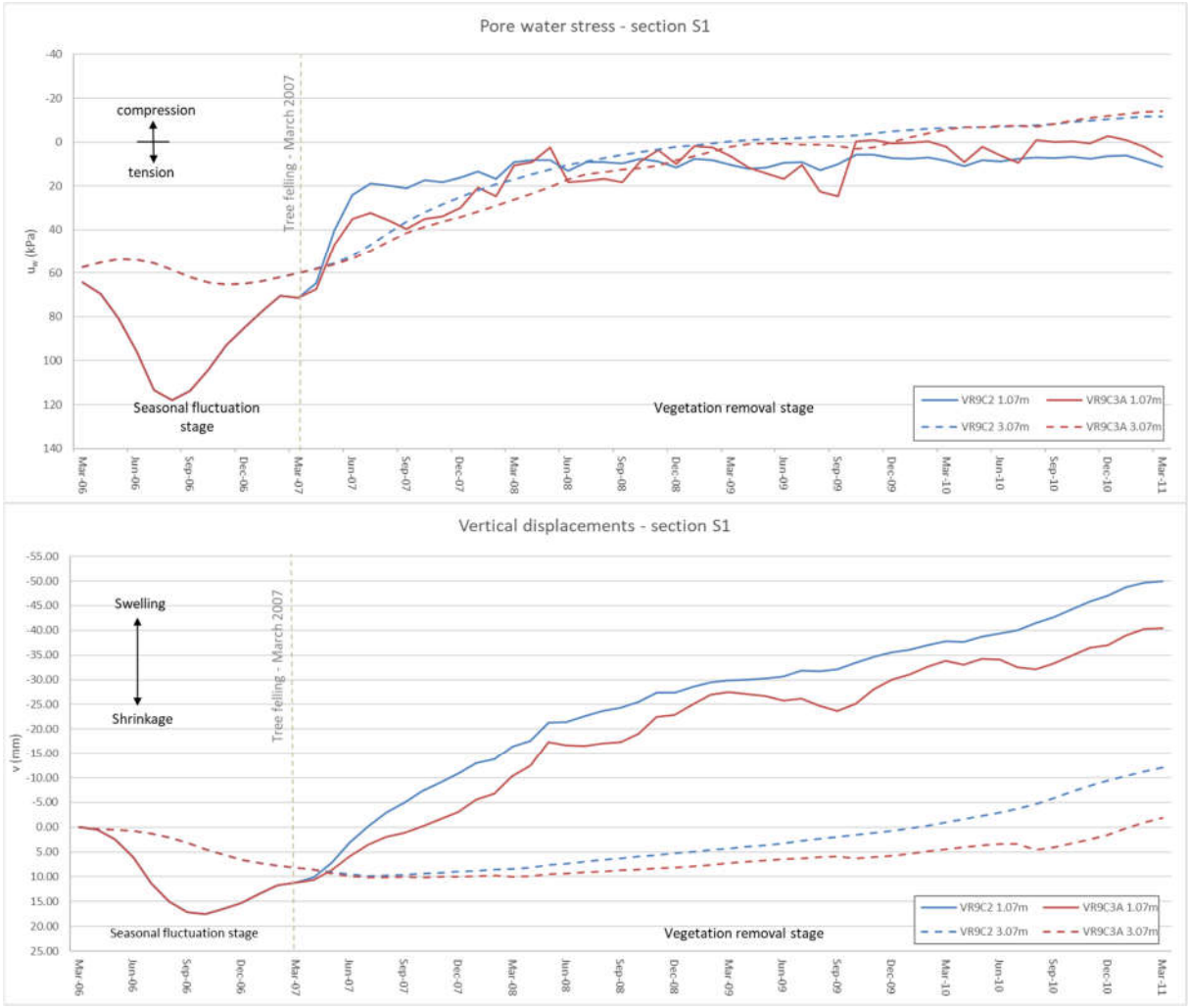

Figure 5.36 Predicted pore water pressure and vertical movement variations for the two different vegetation removal layouts at section S1

The Figure 5.36 plots the pore water pressure and vertical movement evolutions following tree removal along the depth of the clay fill in section S1. It can be seen that the pore water pressure time curves are very similar. On the other hand, the heave movements caused by continuous infiltration of surface water are moderately mitigated by the large trees retained at the lower part of the slope. Most importantly the seasonal cyclic shrinkage/swelling movements are reduced by approximately 3 times, compared to fluctuation stage (prior to tree removal)

In Figure 5.37 the predicted time progress of pore water pressures and vertical movements at section S2 is presented. The section S2 is around 1.5 m away from the point at which the vegetation boundary condition ceases. In the case of partial vegetation removal (red lines), the general trend of steady decrease of pore water suctions accompanied by seasonal fluctuations is observed. It can be seen that the magnitudes of seasonal variations have somewhat reduced, but have significantly shifted towards the zero-pressure line. The main reason behind such pronounced change in hydraulic response, is most likely the lateral flow component from the upper unvegetated parts of the slope and the fact that the clay fill acts as a quasi-impermeable boundary relative to ash, thereby amplifying the later water inflow effects. The magnitudes of seasonal vertical movements are essentially unchanged from the fluctuation stage prior to tree felling. At deeper levels, the trend of ongoing settlements, though at lower rate compared to fluctuation stage, is obtained.

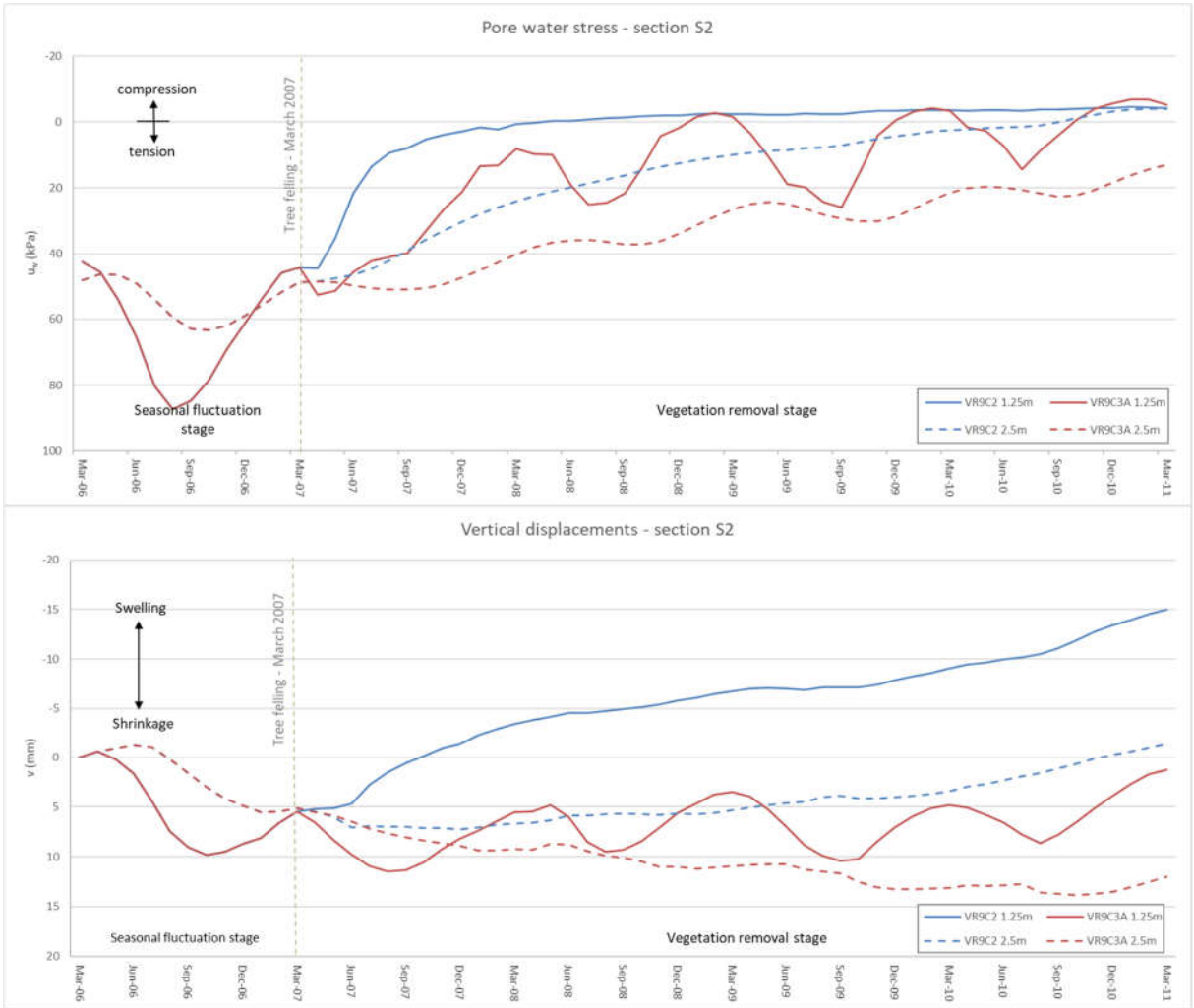

Figure 5.37 Predicted pore water pressure and vertical movement variations for the two different vegetation removal layouts at section S1

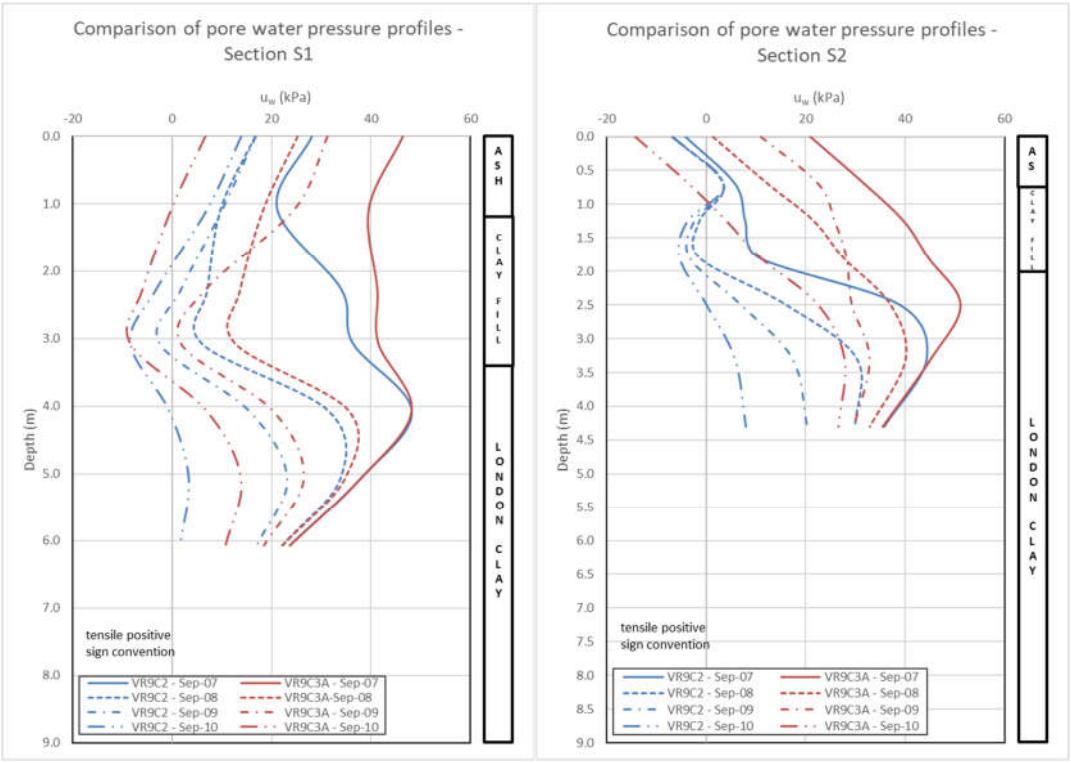

Figure 5.38 Predicted summer pore water pressure profiles following tree removal for two different vegetation removal layouts, at sections S1 and S2

The Figure 5.38 illustrates the evolution of end of summer (September) pore water pressure profiles. It is obvious that retained trees at the lower third of the embankment slope have impeded the saturation process, which is particularly true for the section S2. Although the surface pore water suctions have completely vanished, the deeper ones appear to asymptotically gravitate towards the limiting lower value of around 20 kPa (at section S2).

The effects of the two different tree removal schemes are investigated further through the volumetric water content and degree of saturation profiles corresponding to the last increment of the analyses (March 2011), which are presented in Figure 5.39. It can be seen that, although the degree of saturation values are relatively close to 100 %, quasi-saturated (unsaturated) zone in the case of partial, upper slope tree removal is significantly deeper compared to full vegetation clearance.

The obtained results indicate that vegetation management, in particular the design of tree clearance or modification schemes, represents a highly complex task, primarily due to the diametrically opposing effects the trees produce. High water demand trees adversely affect serviceability, as they represent the driving force behind seasonal wetting-drying cycles and resulting shrink-swell deformation patterns. At the same time mature trees provide stabilizing effects against deep-seated instabilities by generating and maintaining the persistent soil suctions deeper below the seasonally affected surficial zone. Similar to steel fibres in concrete, the roots mechanically reinforce the top soil zone directly affected by seasonal wetting and drying, and therefore make it more resistant to shallow types of instability. All these findings suggest that the balance is very delicate, and that the tree removal should be managed so that positive effects are maximised while concurrently minimizing the detrimental ones.

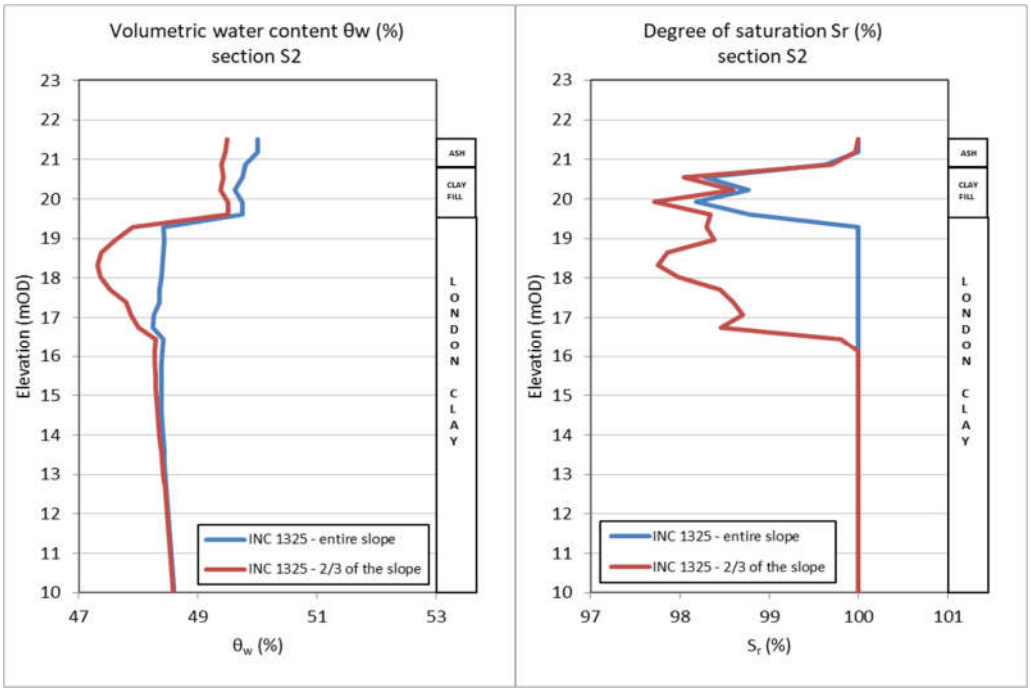

Figure 5.39 Predicted volumetric water content θ_w and degree of saturation S_r profiles for the March 2011, for two different vegetation removal schemes

Chapter 6: Conclusions and Recommendations for Further Research

6.1 Research Implications Related to Numerical Modelling of Clay Fill Embankments Subjected to Atmospheric Actions

Probably the most important contribution of this thesis is the demonstration that the hydraulic response of the clay fill embankment to climatic boundary conditions is practically insensitive to the type of unsaturated mechanical constitutive model. It was proved that the simple unsaturated Mohr-Coulomb model, based essentially on only one additional material parameter compared to saturated version, modulus *H,* can quantitatively reproduce the observed hydro-mechanical behaviour. The additional convenience lies in the fact that the initial *H* modulus value, corresponding to the low suction range, could be directly estimated from the elastic stiffness moduli of the soil skeleton.

The finding that immensely more complex modified BBM model, offers no increase in the accuracy over the simple unsaturated Mohr-Coulomb model for this specific physical problem, represents the significant step forward in the progress of numerical modelling of clay fill embankments subjected to soil-vegetation-atmosphere interaction.

However, as was shown within parametric study, these findings do not mean that the mechanical aspect of behaviour is irrelevant to resulting hydraulic predictions. On the contrary, the coupling of flow and deformation has been proved to be of upmost importance in modelling the response of geotechnical earthworks to climate and vegetation impacts. It was demonstrated that the flexible soil skeleton would provide less resistance to water extraction/injection, and as a result will produce lower pore water pressure changes. These findings explicitly question the applicability of pure hydraulic approach, especially in the case of medium to high volume change potential soils. There are indications that rigid soil skeleton, implicitly assumed in pure hydraulic models, offers high resistance to water abstraction driven by evapotranspiration process, thereby inducing very high suction levels.

Additionally, it was suggested that only one of the required 23 material parameters of modified BBM model effectively influences the deformational response of heavily overconsolidated clay fills subjected to wetting/drying cycles. It is the coefficient of compressibility of soil structure related to suction changes, κ_s. It was shown that the more flexible the (higher κ_s, or lower *H*) soil structure with respect to changes in water stress is, the smaller seasonal pore suction variations would be. Generally, a stiffer response has been predicted compared to field observations, in particular closer to the crest, which most likely stems from excessively high stiffness of ash layer.

With respect to hydraulic soil properties, it was shown that permeability and SWR curve play a crucial role in overall response. It was demonstrated that the SWR curve actually opposes the influence of permeability. This finding has brought into doubt the suitability of saturated coupled flow-deformation approach. It was shown that saturated analysis with the same permeabilities have yielded 3 times higher maximum absolute suctions, and seasonal suction variations, as response to water flux boundary condition Q, compared to unsaturated analysis.

Regarding the permeability of clay fill, it was shown that the lower permeability has confined seasonal wetting-drying cycles closer to the ground surface. On the other hand, the extent of the zone of influence has increased in the case of higher permeability, allowing the hydrological water cycle to affect deeper soil strata.

With respect to climatic boundary conditions, it was shown that the precipitation distribution relative to plant growth stages is the key component of the water flux boundary condition, directly controlling the magnitude of seasonal pore water pressure variations. It was suggested that most critical conditions arise when the plant growth stages, especially the development and mid-season stage,

coincide with lower precipitations, combined with higher rainfall matching with the late-season senescence stage of vegetation. The combination of two markedly different seasons, the extremally dry followed by extremally wet, could potentially be very adverse, as desiccation cracking induced by excessive shrinkage may dramatically increase the overall mass permeability. The higher permeability of surficial zone, would allow rainwater to infiltrate more easily and therefore rapidly rewet the soil. These findings have an important practical implication suggesting that long-term average monthly precipitations are inadequate and nonconservative for the evaluation of serviceability of infrastructure earthworks. Furthermore, the climate changes could bring about the paradigm shift with respect to perception of present climate patterns. Therefore, further investigations of infrastructure embankment performance with respect to future climatic scenarios are necessary.

With respect to stability it was shown that the high ratio of ash over clay fill permeability forms very unfavourable hydraulic conditions. It was suggested that the clay fill upper surface acts as impermeable boundary and allows the establishment of hydrostatic compressive conditions above it, known as perched water. The compressive pore water pressures within the upper ash stratum directly reduce effective confining stresses, thereby resulting in the loss of available shear strength and local upper surface crest failure mechanism. It was demonstrated that to prevent the shallow instabilities occurring in numerical models it is necessary to account for mechanical root reinforcement effects. This is most easily achieved through inclusion of additional root cohesion. It was shown that a value of additional root cohesion up to 30 kPa is plausible representative of reality.

Regarding the initialisation stage, it was suggested that 4-10 years of successive wetting-drying cycles, simulating the previous history of combined vegetation and precipitation effects, should be appropriate. Surely, if field measurements are available it would be easier to calibrate the number of cycles, to achieve the initial in-situ conditions.

Finally, it can be stated that the obtained results in combination with high quality field data, verify the RWUM (root water uptake model) implemented into ICFEP numerical code and concurrently validate the created numerical model (computer model). The proposed model, which consists essentially of combination of numerical tools, methods, models and boundary/initial conditions available in ICFEP, have proved to be plausible representative of reality.

6.2 Research Implications Related to Vegetation Management of Clay Fill Embankments

The predicted results have indicated that the removal of high-water demand trees from the entire slope has completely eliminated the seasonal cyclic shrinkage/swelling movements, that were the main source of railway track serviceability issues. However, the removal of mature trees has also produced several side effects. These include the formation of shallow failure mechanism in the upper part of the slope, and the rapid loss of previously established persistent pore water suctions in both reference sections, S1 and S2. While the local ash instability close to the crest arises from marginal stability of that zone and from disregarding the mechanical root reinforcement contribution, the loss of stabilizing effects related to deep persistent pore water suctions may have more sever implications. Although, the deep-seated failure was not predicted, at least not during the four-year simulated period following tree clearance, the risk of overall embankment failure has definitely increased significantly. The predicted volumetric water content and degree of saturation profiles corresponding to the last increment of the main numerical analysis, suggested that the entire embankment slope has approached the full saturation. Such conditions are considered highly detrimental, because if they are succeeded by extreme wet weather, the compressive pore water pressures could rapidly develop and further jeopardize the embankment stability.

It was also demonstrated that the removal of the high-water demand trees over the embankment slope has modified the swelling mechanism, in particular at the lower part of the slope. While the trees were still present on the slope, the swelling movements during winter months were predominantly vertical, with minor horizontal components. After the tree felling, the proportion of the horizontal component has significantly increased, so that the orientation of the resultant swelling movements has become mainly horizontal. It was shown the alteration in swelling behaviour can primarily be attributed to the mature trees retained around the embankment toe. These horizontal movements could initiate or contribute to the progression of slope failure, thereby increasing the overall risk of slope instability.

In addition, it was shown that the very low permeability of foundation soil beyond the toe, in the zone where the trees have been retained, further exacerbates the conditions with respect to the magnitude and orientation of horizontal movements. This is closely linked to higher suction levels generated in foundation soil beyond the embankment. These findings have important practical implications, suggesting that the same tree species rooted in different soils could produce diametrically opposed deformational response. It is therefore important that material, in particular hydraulic and index properties, of the foundation soil encompassed by root zone, be reliably estimated.

The obtained results indicate that vegetation management, in particular the design of tree clearance schemes, represents a highly complex task, primarily due to the diametrically opposing effects the trees produce. High water demand trees adversely affect serviceability, as they represent the driving force behind seasonal wetting-drying cycles and resulting shrink-swell deformation patterns. At the same time mature trees provide stabilizing effects against deep-seated instabilities by generating and maintaining the persistent soil suctions deeper below the seasonally affected surficial zone. Similar to steel fibres in concrete, the roots mechanically reinforce the top soil zone directly affected by seasonal wetting and drying, and therefore make it more resistant to shallow types of instability. All these findings suggest that the balance is very delicate, and that the tree removal should be managed so that positive effects are maximised while concurrently minimizing the detrimental ones.

6.3 Suggestions for Future Research

The analyses presented within this thesis constitutes only a part of the entire scope of numerical simulations that were performed during a course of this research. Numerous analyses were either automatically terminated due to divergence of the solution and violation of specified tolerances, or have taken excessively long time, and were therefore aborted manually. The obvious reason is the immensely high nonlinearity of governing equations. The analyses that proved to be most unstable were the ones incorporating simultaneously the effects of desiccation and desaturation. Therefore, that aspect should be further investigated, with particular emphasis on identifying the causes of observed numerical instabilities.

Within the scope of the present thesis only the vegetation removal schemes were investigated as a measure to mitigate serviceability issues. As part of the future research an alternative bioengineering measure, consisting of substitution of existing high-water demand trees by more suitable medium to low-demand tree species, with designed planting scheme across the slope, is suggested. The design criteria for optimal planting layout should include the reduction of seasonal cyclic deformations but with the preservation of deeper persistent soil suctions. Also, keeping the lineside vegetation along railway infrastructure, ensures the visual and acoustic barriers for the surrounding residential areas. The numerical modelling of planting should include the simulation of the root growth, through gradual increase of maximum root depth during the plant growing season. Also, the potential evapotranspiration rates should be accordingly adjusted.

Another interesting and important future research direction includes the investigation of effects of the climate change on hydro-mechanical response of clay fill embankments. Considering that future climate scenarios are likely to include increased frequency or intensity of extreme weather events, the increment durations as well as the climatic data periods should be drastically reduced to account for such rapid transient events.

Within present thesis only the non-hysteretic soil water retention behaviour was simulated, due to the lack of reliable SWRC data. The further research in this field should definitely include the planning and execution of systematic and detailed laboratory investigation of hydraulic properties, in particular both drying and wetting SWRC and permeability of undisturbed and non-reconstituted clay fills from UK railway infrastructure earthworks. This would allow the hysteresis effect of SWRC to be readily investigated, because hysteretic SWRC model is already implemented into the ICFEP numerical code (Tsiampousi, 2011). It was demonstrated in Chapter 3 that seasonal wetting-drying cycles trace the secondary paths, which have more gentle slopes compared to primary paths. The more reliable hydraulic properties in combination with more sophisticated retention models would bring the numerical model even closer to physical reality.

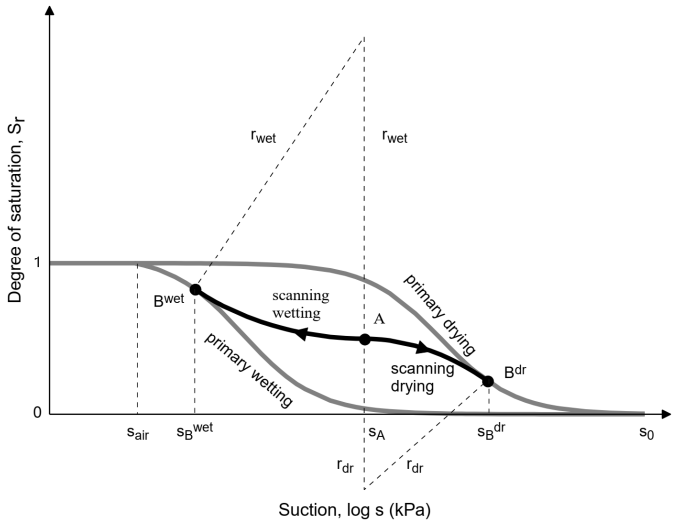

Figure 6.1 Primary and scanning paths of the ICFEP hysteretic-SWRC model, after (Tsiampousi, 2011)

The limitation of one-dimensional RWUM incorporated into ICFEP is the inability to simulate the effects of discrete trees, especially on horizontal movements during the seasonal fluctuation stage. The field observations have shown that the magnitudes and directions of horizontal movements prior to tree felling were closely corelated to the location of nearest tree. Therefore, the further research should include the extension of existing RWUM to three-dimensional spatial conditions. The same linear distribution of root water uptake function could be assumed as well for radial direction.

Although, the effects of mechanical root reinforcement (the additional cohesion term) were used only in relation to ash material, which was simulated as simple saturated elastoplastic Mohr-Coulomb, the extension for the critical state type constitutive models available in ICFEP should be considered in the future. This could be possible achieved by modifying the hardening rules, which describe the evolution of the equivalent fully saturated isotropic yield stress p_0^* in the case of unsaturated modified Barcelona Basic Model implemented in ICFEP (Georgiadis, 2003).

REFERENCES

Ali, F.H. & Osman, N. (2008) Shear strength of a soil containing vegetation roots. *Soils and Foundations*. [Online] 48 (4), 587–596. Available from: doi:10.3208/sandf.48.587.

Allen, R.G., Pereira, L.S., Raes, D., Smith, M., et al. (1998) *Crop evapotranspiration: guidelines for computing crop water requirements*. FAO irrigation and drainage paper. [Online]. Rome, Italy, FAO Irrigation and drainage paper 56. Food and Agriculture Organization. Available from: http://www.fao.org/docrep/X0490E/X0490E00.htm.

Alonso, E.E., Gens, A. & Josa, A. (1990) A constitutive model for partially saturated soils. *Géotechnique*. [Online] 40 (3), 405–430. Available from: doi:10.1680/geot.1991.41.2.273.

Alonso, E.E. & Pinyol, N.M. (2016) Numerical analysis of rapid drawdown: Applications in real cases. *Water Science and Engineering*. [Online] 9 (3), 175–182. Available from: doi:10.1016/j.wse.2016.11.003.

Andrei, A. (2000) Embankment stabilisation works between Rayners Lane and South Harrow Underground stations, Antoine Andrei. *GROUND ENGINEERING*. 33, 24–26.

Arup Geotechnics (2007) *Monitoring of London Clay Embankments: Geotechnical Interpretative Report*.

Askarinejad, A. (2013) *FAILURE MECHANISMS IN UNSATURATED SILTY SAND SLOPES TRIGGERED BY RAINFALL*. PhD Thesis, ETH ZURICH.

De Baets, S., Poesen, J., Reubens, B., Wemans, K., et al. (2008) Root tensile strength and root distribution of typical Mediterranean plant species and their contribution to soil shear strength. *Plant and Soil*. [Online] 305 (1–2), 207–226. Available from: doi:10.1007/s11104-008-9553-0.

Bear, J. (1972) *Dynamics of fluids in porous media*. New York, Dover Publications.

Biddle, G. (1998) *Tree root damage to buildings.* Willowmead Publishing Ltd.

Biot, M.A. (1941) General theory of three dimensional consolidation. *Journal of Applied Physics*. [Online] 12 (2), 155–164. Available from: doi:10.1063/1.1712886.

Bischetti, G.B., Chiaradia, E.A., Simonato, T., Speziali, B., et al. (2005) Root strength and root area ratio of forest species in lombardy (Northern Italy). *Plant and Soil*. [Online] 278 (1–2), 11–22. Available from: doi:10.1007/s11104-005-0605-4.

Bishop, A.W. & Blight, G.E. (1963) *Some Aspects of Effective Stress in Saturated and Partly Saturated Soils*.

Blight, G.E. (1997) Interactions between the atmosphere and the Earth. *Géotechnique*. [Online] 47 (4), 713–767. Available from: doi:10.1680/geot.1997.47.4.713.

Blight, G.E. (2003) The vadose zone soil-water balance and transpiration rates of vegetation. *Géotechnique*. [Online] 53 (1), 55–64. Available from: doi:10.1680/geot.2003.53.1.55.

Bowen, I.S. (1926) The ratio of heat losses by conduction and by evaporation from any water surface. *Physical Review*. [Online] 27 (6), 779–787. Available from: doi:10.1103/PhysRev.27.779.

Briaud, J.-L. (2013) *Geotechnical Engineering: Unsaturated and Saturated Soils | Wiley*. Wiley Professional Development (P&T).

Briggs, K., Smethurst, J. & Powrie, W. (2014) Modelling the influence of tree removal on embankment slope hydrology. In: *Landslide Science for a Safer Geoenvironment: Vol.1- The International Programme on Landslides (IPL)*. [Online]. 2014 2-6 June 2014, Beijing, Springer. pp. 241–246. Available from: doi:10.1007/978-3-319-04999-1_32.

Briggs, K.M., Smethurst, J. a., Powrie, W. & O'Brien, A.S. (2013) Wet winter pore pressures in railway embankments. *Proceedings of the ICE - Geotechnical Engineering*. [Online] 166 (5), 451–465. Available from: doi:10.1680/geng.11.00106.

Briggs, K.M., Smethurst, J.A., Powrie, W. & Brien, A.S.O. (2016) The influence of tree root water uptake on the long term hydrology of a clay fill railway embankment. *Transportation Geotechnics*. [Online] 9, 31–48. Available from: doi:10.1016/j.trgeo.2016.06.001.

Brinkgreve, R.B.J. & Engin, E. (2013) Validation of geotechnical finite element analysis. *18th International Conference on Soil Mechanics and Geotechnical Engineering: Challenges and Innovations in Geotechnics, ICSMGE 2013*. 1, 677–682.

Chalmers, T. (2013) *Effect of seasonal changes in pore water pressures on the behaviour of railway embankments in the UK*. MSc thesis, Imperial College London.

Chandler, R. (2000) Clay sediments in depositional basins : the Geotechnical Cycle. *The Quarterly Journal of Engineering Geology and Hydrology*. 33 (1), 7–39.

Croney, D. (1977) *The design and performance of road pavements*. [Online]. Available from: https://trid.trb.org/view/367894.

Croney, D. (1952) The movement and distribution of water in soils. *Geotechnique*. [Online] 3 (1), 1–16. Available from: doi:10.1680/geot.1952.3.1.1.

Croney, D. & Coleman, J.D. (1954) Soil structure in relation to soil suction (pF). *Journal of Soil Science*. [Online] 5 (1), 75–84. Available from: doi:10.1111/j.1365-2389.1954.tb02177.x.

D'Onza, F., Wheeler, S.J., Gallipoli, D., Barrera Bucio, M., et al. (2015) Benchmarking selection of parameter values for the Barcelona basic model. *Engineering Geology*. [Online] 196, 99–118. Available from: doi:10.1016/j.enggeo.2015.06.022.

Dakshanamurthy, V., Fredlund, D.G. & Rahardjo, H. (1984) Coupled Three-dimensional Consolidation Theory of Unsaturated Porous Media | Fifth International Conference on Expansive Soils 1984: Preprints of Papers. In: *Fifth International Conference on Expansive Soils*. 21 May 1984 Adelaide. pp. 99–103.

Davies, O. (2011) *Numerical analysis of the effect of climate change on slope stability*. PhD Thesis. Newcastle University.

Davies, O., Rouainia, M., Glendinning, S., Cash, M., et al. (2014) Investigation of a pore pressure driven slope failure using a coupled hydro-mechanical model. *Engineering Geology*. [Online] 178, 70–81. Available from: doi:10.1016/j.enggeo.2014.05.012.

Duong, T. V., Trinh, V.N., Cui, Y.J., Tang, A.M., et al. (2013) Development of a large-scale infiltration column for studying the hydraulic conductivity of unsaturated fouled ballast. *Geotechnical Testing Journal*. [Online] 36 (1). Available from: doi:10.1520/GTJ20120099.

Elia, G., Cotecchia, F., Pedone, G., Vaunat, J., et al. (2017) Numerical modelling of slope–vegetation–atmosphere interaction: an overview. *Quarterly Journal of Engineering Geology and Hydrogeology*. [Online] 50 (3), 249–270. Available from: doi:10.1144/qjegh2016-079.

Fan, C.C. & Su, C.F. (2008) Role of roots in the shear strength of root-reinforced soils with high moisture content. *Ecological Engineering*. [Online] 33 (2), 157–166. Available from: doi:10.1016/j.ecoleng.2008.02.013.

Fatahi, B., Khabbaz, H. & Indraratna, B. (2014) Modelling of unsaturated ground behaviour influenced by vegetation transpiration. *Geomechanics and Geoengineering*. [Online] 9 (3), 187–207. Available from: doi:10.1080/17486025.2014.880520.

Fatahi, B., Khabbaz, H. & Indraratna, B. (2009) Parametric studies on bioengineering effects of tree root-based suction on ground behaviour. *Ecological Engineering*. [Online] 35 (10), 1415–1426. Available from: doi:10.1016/j.ecoleng.2009.05.014.

Feddes, R.A., Bresler, E. & Neuman, S.P. (1974) Field test of a modified numerical model for water uptake by root systems. *Water Resources Research*. [Online] 10 (6), 1199–1206. Available from: doi:10.1029/WR010i006p01199.

Feddes, R.A., Hoff, H., Bruen, M., Dawson, T., et al. (2001) Modeling root water uptake in hydrological and climate models. *Bulletin of the American Meteorological Society*. (82), 2797–2809.

Feddes, R.A., Kowalik, P.J. & Zaradny, H. (1978) *Simulation of field water use and crop yield.* New York, Halsted Press, John Wiley & Sons.

Feddes, R.A. & Raats, P.A.C. (2004) Parameterizing the soil - water - plant root system. In: *Unsaturated-zone modeling; Progress, challenges and applications*. [Online]. Dordrecht, Kluwer Academic Publishers. pp. 95–141. Available from: https://library.wur.nl/WebQuery/wurpubs/333516.

Fredlund, D. (1998) Bringing Unsaturated Soil Mechanics into Engineering Practice. In: *Second International Conference on Unsaturated Soil*. [Online]. 1998 Beijing China. p. Available from: https://www.researchgate.net/publication/348336699_Bringing_Unsaturated_Soil_Mechanics_into_Engineering_Practice.

Fredlund, D. (1978) The shear strength of unsaturated soils. *Canadian Geotechnical Journal*. [Online] 321, 313–321. Available from: http://www.nrcresearchpress.com/doi/abs/10.1139/t78-029.

Fredlund, D.G. (2000) The 1999 R.M. Hardy Lecture: The implementation of unsaturated soil mechanics into geotechnical engineering. *Canadian Geotechnical Journal*. [Online] 37 (5), 963–986. Available from: doi:10.1139/t00-026.

Fredlund, D.G. & Morgenstern, N.R. (1976) Constitutive relations for volume change in unsaturated soils. *Canadian Geotechnical Journal*. [Online] 13 (3), 261–276. Available from: doi:10.1139/t76-029.

Fredlund, D.G. & Morgenstern, N.R. (1977) Stress State Variables for Saturated and Unsaturated Soils. *Journal of Geotechnical Division*. [Online]. 103 (GT5) pp.447–466. Available from: doi:doi:10.1061/40802(189)202.

Fredlund, D.G., Morgenstern, N.R. & Widger, R.A. (1978) The shear strength of unsaturated soils.

Canadian Geotechnical Journal. [Online] 15 (3), 313–321. Available from: doi:10.1139/t78-029 [Accessed: 6 April 2021].

Fredlund, D.G. & Rahardjo, H. (1993) Soil Mechanics for Unsaturated Soils. *Stress The International Journal on the Biology of Stress*. [Online] 517. Available from: doi:10.1016/0267-7261(93)90011-F.

Freeze, R.A. & Cherry, J.A. (1979) *Groundwater - R. Allan Freeze, John A. Cherry - Google Книге*. [Online]. Prentice-Hall. Available from: https://books.google.rs/books/about/Groundwater.html?id=8P7kFowKnGUC&redir_esc=y.

Gardner, W.R. (1964) Relation of Root Distribution to Water Uptake and Availability 1. *Agronomy Journal*. [Online] 56 (1), 41–45. Available from: doi:10.2134/agronj1964.00021962005600010013x.

Garg, A., Leung, A.K. & Ng, C.W.W. (2015) Comparisons of soil suction induced by evapotranspiration and transpiration of S. Heptaphylla. *Canadian Geotechnical Journal*. [Online] 52 (12), 2149–2155. Available from: doi:10.1139/cgj-2014-0425.

Gash, J.H.C. (1979) An analytical model of rainfall interception by forests. *Quarterly Journal of the Royal Meteorological Society*. [Online] 105 (443), 43–55. Available from: doi:10.1002/qj.49710544304.

Van Genuchten, M.T. (1980) A Closed-form Equation for Predicting the Hydraulic Conductivity of Unsaturated Soils. *Soil Science Society of America Journal*. [Online]. 44 (5) p.892. Available from: doi:10.2136/sssaj1980.03615995004400050002x.

Georgiadis, K. (2003) *Development, implementation and application of partially saturated soil models in finite element analysis*. PhD Thesis. Imperial College, University of London, UK.

Georgiadis, K., Potts, D.M. & Zdravkovic, L. (2005) Three-Dimensional Constitutive Model for Partially and Fully Saturated Soils. *International Journal of Geomechanics*. [Online] 5 (3), 244–255. Available from: doi:10.1061/(ASCE)1532-3641(2005)5:3(244).

Geotechnical Observations (2013) *07 - 011 Magnolia Road Southend - Raw Data*.

Gerwitz, A. & Page, E.R. (1974) An Empirical Mathematical Model to Describe Plant Root Systems. *The Journal of Applied Ecology*. [Online] 11 (2), 773. Available from: doi:10.2307/2402227.

Glendinning, S., Loveridge, F., Starr-Keddle, R.E., Bransby, M.F., et al. (2009) Role of vegetation in sustainability of infrastructure slopes. In: *Proceedings of the Institution of Civil Engineers - Engineering Sustainability*. [Online]. 25 June 2009 Thomas Telford Ltd. pp. 101–110. Available from: doi:10.1680/ensu.2009.162.2.101 [Accessed: 15 March 2021].

Grammatikopoulou, A., Zdravkovic, L. & Potts, D.M. (2008) The influence of previous stress history and stress path direction on the surface settlement trough induced by tunnelling. *Geotechnique*. [Online] 58 (4), 269–281. Available from: doi:10.1680/geot.2008.58.4.269.

Greenwood, J.R., Norris, J.E. & Wint, J. (2004) Assessing the contribution of vegetation to slope stability. *Proceedings of the ICE - Geotechnical Engineering*. [Online] 157 (4), 199–207. Available from: doi:10.1680/geng.2004.157.4.199.

Herkelrath, W.N., Miller, E.E. & Gardner, W.R. (1977) Water Uptake By Plants: II. The Root Contact Model. *Soil Science Society of America Journal*. [Online] 41 (6), 1039–1043. Available from:

doi:10.2136/sssaj1977.03615995004100060004x.

Hight, D.W., Gasparre, A., Nishimura, S., Minh, N.A., et al. (2007) Characteristics of the London Clay from the terminal 5 site at heathrow airport. *Geotechnique*. [Online] 57 (1), 3–18. Available from: doi:10.1680/geot.2007.57.1.3.

Hight, D.W., McMillan, F., Powell, J.J.M., Jardine, R.J., et al. (2003) Some characteristics of London clay. *Characterisation and engineering properties of natural soils*. 2 (JANUARY 2003), 851–907.

Hillel, D. (1982) *Introduction to Soil Physics*. [Online]. Academic Press, San Diego. Available from: doi:10.1016/C2009-0-03052-9.

Hillel, D., Talpaz, H. & Van Keulen, H. (1976) A macroscopic model of water uptake by a non-uniform root system and of water and salt movement in the soil profile. *Soil Science*. [Online] 121, 242–255. Available from: https://journals.lww.com/soilsci/Abstract/1976/04000/A_MACROSCOPIC_SCALE_MODEL_OF_WATER_UPTAKE_BY_A.9.aspx.

Hoogland, J.C., Feddes, R.A. & Belmans, C. (1981) ROOT WATER UPTAKE MODEL DEPENDING ON SOIL WATER PRESSURE HEAD AND MAXIMUM EXTRACTION RATE. *Acta Horticulturae*. [Online] (119), 123–136. Available from: doi:10.17660/actahortic.1981.119.11.

Hough, M.N. & Jones, R.J.A. (1997) The United Kingdom Meteorological Office rainfall and evaporation calculation system: MORECS version 2.0-an overview. *Hydrology and Earth System Sciences*. [Online] 1 (2), 227–239. Available from: doi:10.5194/hess-1-227-1997.

Jardine, R.J., Burland, J.B., Fourie, a. B. & Potts, D.M. (1986) Studies of the influence of non-linear stress–strain characteristics in soil–structure interaction. *Géotechnique*. [Online] 36 (3), 377–396. Available from: doi:10.1680/geot.1986.36.3.377.

Ji, J., Kokutse, N., Genet, M., Fourcaud, T., et al. (2012) Effect of spatial variation of tree root characteristics on slope stability. A case study on Black Locust (Robinia pseudoacacia) and Arborvitae (Platycladus orientalis) stands on the Loess Plateau, China. *Catena*. [Online] 92, 139–154. Available from: doi:10.1016/j.catena.2011.12.008.

Kovacevic, N., Hight, D.W. & Potts, D.M. (2007) Predicting the stand-up time of temporary London Clay slopes at Terminal 5, Heathrow Airport. *Géotechnique*. [Online] 57 (1), 63–74. Available from: doi:10.1680/geot.2007.57.1.63.

Kovacevic, N., Hight, D.W. & Potts, D.M. (2004) Temporary slope stability in London Clay - back analyses of two case histories. *Advances in Geotechnical Engineering: The Skempton Conference*. 5, 842–855.

Kovacevic, N., Potts, D.. & Vaughan, P.. (2001) Progressive failure in clay embankments due to seasonal climate changes - Search results - Pascal and Francis Bibliographic Databases. In: *International Conference on soil mechanics and geotechnical engineering*. 2001 Istanbul, A A. Balkema, Lisse. pp. 2127–2130.

Lagioia, R., Puzrin, A.M. & Potts, D.M. (1996) A new versatile expression for yield and plastic potential surfaces. *Computers and Geotechnics*. [Online] 19 (3), 171–191. Available from: doi:10.1016/0266-352X(96)00005-5.

Laloui, L. (2013) *Mechanics of Unsaturated Geomaterials*. [Online]. John Wiley and Sons. Available from: doi:10.1002/9781118616871.

Lees, A. (2013) Seasonal slope movements in an old clay fill embankment dam. *Canadian Geotechnical Journal*. [Online] 50 (5), 503–520. Available from: doi:10.1139/cgj-2012-0356.

Leung, A.K., Garg, A. & Ng, C.W.W. (2015) Effects of plant roots on soil-water retention and induced suction in vegetated soil. *Engineering Geology*. [Online] 193, 183–197. Available from: doi:10.1016/j.enggeo.2015.04.017.

Linsley, R.K., Kohler, M.A. & Paulhus, J.L.H. (1982) *Hydrology for engineers /*. McGraw-Hill.

Loveridge, F.A., Spink, T.W., O'Brien, A.S., Briggs, K.M., et al. (2010) The impact of climate and climate change on infrastructure slopes, with particular reference to southern England. *Quarterly Journal of Engineering Geology and Hydrogeology*. [Online] 43 (4), 461–472. Available from: doi:10.1144/1470-9236/09-050.

Maas, E. & Hoffman, G.J. (1977) Crop Salt Tolerance–Current Assessment. *Journal of the Irrigation and Drainage Division*. 103 (2), 115–134.

McKenney, M.S. & Rosenberg, N.J. (1993) Sensitivity of some potential evapotranspiration estimation methods to climate change. *Agricultural and Forest Meteorology*. [Online] 64 (1–2), 81–110. Available from: doi:10.1016/0168-1923(93)90095-Y.

Melgarejo, L.M.C. (2004) *Laboratory and numerical investigations of soil-water retention curves*. PhD thesis, Imperial College London.

Molz, F.J. & Remson, I. (1970) Extraction Term Models of Soil Moisture Use by Transpiring Plants. *Water Resources Research*. [Online] 6 (5), 1346–1356. Available from: doi:10.1029/WR006i005p01346.

Monroy, R. (2005) *THE INFLUENCE OF LOAD AND SUCTION CHANGES ON THE VOLUMETRIC BEHAVIOUR OF COMPACTED LONDON CLAY by*. (November), 545.

Mott MacDonald (2011) *RSSB 1386 (Revised) The effects of railway traffic on embankment stability Final Report*. [Online]. Available from: www.mottmac.com.

NHBC standards (2007) National house building council standards, Chapter 4.2, Building near trees. In: *NHBC Standards 2006. Part 4 - Foundations.* NHBC. p.

Novák, V. (1987) Estimation of soil-water extraction patterns by roots. *Agricultural Water Management*. [Online] 12 (4), 271–278. Available from: doi:10.1016/0378-3774(87)90002-3.

Novák, V. (2012) *Evapotranspiration in the soil-plant-atmosphere system*. [Online]. Springer Netherlands. Available from: doi:10.1007/978-94-007-3840-9.

Nyambayo, V.P. (2004) *Numerical analysis of evapotranspiration and its influence on embankments*. PhD Thesis. Imperial College, University of London, UK.

Nyambayo, V.P. & Potts, D.M. (2010) Numerical simulation of evapotranspiration using a root water uptake model. *Computers and Geotechnics*. [Online] 37 (1–2), 175–186. Available from: doi:10.1016/j.compgeo.2009.08.008.

Nyambayo, V.P., Potts, D.M. & Addenbrooke, T.I. (2004) The influence of permeability on the

stability of embankments experiencing seasonal cyclic pore water pressure changes. *Advances in Geotechnical Engineering: The Skempton Conference - Proceedings of a Three Day Conference on Advances in Geotechnical Engineering, organised by the Institution of Civil Engineers*. 898–910.

O. C. Zienkiewicz, A. H. C. Chan, M. Pastor, B. A. Schrefler, et al. (1999) *Computational Geomechanics with Special Reference to Earthquake Engineering, , , Chichester, 1999, No. of pages: 398, ISBN 0-471-98285-7, Price £105*. Wiley.

O'Brien, A. (2007) Rehabilitation of urban railway embankments: investigation, analysis and stabilisation. In: A. Cuéllar, V., Dapena, E., Alonso, E., Echave, J.M., Gens, A., De Justo, J.L., Oteo, C., Rodríguez-Ortiz, J.M., Sagaseta, C., Sola, P., Soriano (ed.). *Proceedings of the 14th International Conference (SMGE)*. [Online]. September 2007 IOS Press. pp. 125–143. Available from: http://www.iospress.nl/book/proceedings-of-the-14th-european-conference-on-soil-mechanics-and-geotechnical-engineering/.

O'Brien, A. (2013) The assessment of old railway embankments - Time for a change? *Partial Saturation in Compacted Soils: Geotechnique Symposium in Print 2011*. [Online] 19–32. Available from: doi:10.1680/GEOT2013.57753.0002.

O'Brien, A.S., Ellis, E.A. & Russell, D. (2004) Old Railway Embankment Clay Fill - Laboratory Experiments, Numerical Modelling and Field Behaviour. *Advances in Geotechnical Engineering: The Skempton Conference*. [Online] 911–921. Available from: doi:10.1680/aigev2.32644.0020.

Ordnance Survey (2013) *Blackwater Estuary, Maldon, Burnham-on-Crouch, Southend-on-sea. 1:25,000. Explorer Sheet 176.* [Online]. Available from: digimap.edina.ac.uk.

P. A. C. Raats (1976) Analytical Solutions of a Simplified Flow Equation. *Transactions of the ASAE*. [Online] 19 (4), 0683–0689. Available from: doi:10.13031/2013.36096.

Papastathis, V. (2014) *Numerical Analysis of the Soil-Plant- Atmosphere System Interaction*. MSc thesis, Imperial College London.

Penman, H.L. (1946) WEATHER AND CROPS. *Weather*. [Online] 1 (6), 169–171. Available from: doi:10.1002/j.1477-8696.1946.tb00074.x.

Potts, D.M. & Zdravković, L. (1999) *Finite Element Analysis in Geotechnical Engineering: Volume One - Theory*. [Online]. Thomas Telford Ltd. Available from: doi:10.1680/feaiget.27534.

Potts, D.M. & Zdravković, L. (2001) *Finite Element Analysis in Geotechnical Engineering: Volume two - Application*. [Online]. Thomas Telford Publishing. Available from: doi:10.1680/feaigea.27831.

Prasad, R. (1988) A linear root water uptake model. *Journal of Hydrology*. [Online] 99 (3–4), 297–306. Available from: doi:10.1016/0022-1694(88)90055-8.

Rahardjo, H., Satyanaga, A. & Leong, E.C. (2012) Unsaturated soil mechanics for slope stabilization. *Geotechnical Engineering Journal of the SEAGS & AGSSEA*.43 (1).

Rees, S.W. & Ali, N. (2006) Seasonal water uptake near trees: A numerical and experimental study. *Geomechanics and Geoengineering*. [Online] 1 (2), 129–138. Available from: doi:10.1080/17486020600823855.

Richards, L.A. (1931) Capillary conduction of liquids through porous mediums. *Journal of Applied Physics*. [Online] 1 (5), 318–333. Available from: doi:10.1063/1.1745010.

Ridley, A.M., Dineen, K., Burland, J.B. & Vaughan, P.R. (2003) Soil matrix suction: some examples of its measurement and application in geotechnical engineering. *Géotechnique*. [Online] 53 (2), 241–253. Available from: doi:10.1680/geot.2003.53.2.241 [Accessed: 23 March 2021].

Rouainia, M., Davies, O., O'Brien, T. & Glendinning, S. (2009) Numerical modelling of climate effects on slope stability. *Proceedings of the Institution of Civil Engineers - Engineering Sustainability*. [Online] 162 (2), 81–89. Available from: doi:10.1680/ensu.2009.162.2.81.

Rushton, K.R. (2003) *Groundwater Hydrology*. John Wiley & Sons, Ltd.

Russell, D., Ellis, E., O'Brien, A. & Mcginnity, B. (2000) Role of vegetation in the stability and servicibility of railway embankments. In: M.C. Forde (ed.). *Proceedings of the international conference, railway engineering*. [Online]. July 2000 London, UK, ENGINEERING TECHNICS PRESS. p. Available from: https://trid.trb.org/view/768665 [Accessed: 17 March 2021].

Rutqvist, J., Wu, Y.S., Tsang, C.F. & Bodvarsson, G. (2002) A modeling approach for analysis of coupled multiphase fluid flow, heat transfer, and deformation in fractured porous rock. *International Journal of Rock Mechanics and Mining Sciences*. [Online] 39 (4), 429–442. Available from: doi:10.1016/S1365-1609(02)00022-9.

Rutter, A.J., Kershaw, K.A., Robins, P.C. & Morton, A.J. (1971) A predictive model of rainfall interception in forests, 1. Derivation of the model from observations in a plantation of Corsican pine. *Agricultural Meteorology*. [Online] 9 (C), 367–384. Available from: doi:10.1016/0002-1571(71)90034-3.

Rutter, A.J. & Morton, A.J. (1977) A Predictive Model of Rainfall Interception in Forests. III. Sensitivity of The Model to Stand Parameters and Meteorological Variables. *The Journal of Applied Ecology*. [Online] 14 (2), 567. Available from: doi:10.2307/2402568.

Sanders, L.L. (1998) *Manual of field hydrogeology*. Prentice Hall.

Scott, J.M., Loveridge, F. & O'Brien, A.S. (2007) Influence of climate and vegetation on railway embankments. In: *Geotechnical Engineering in Urban Environments: Proceedings of the 14th European Conference on Soil Mechanics and Geotechnical Engineering*. [Online]. 2007 Mill Press. pp. 659–664. Available from: https://eprints.soton.ac.uk/349489/1/isocsco.pdf.

Skaggs, T.H., van Genuchten, M.T., Shouse, P.J. & Poss, J.A. (2006) Macroscopic approaches to root water uptake as a function of water and salinity stress. *Agricultural Water Management*. [Online] 86 (1–2), 140–149. Available from: doi:10.1016/j.agwat.2006.06.005.

Skempton, A.W. (1996) Embankments and Cuttings on the early Railways. *Construction History*. Vol. 11, 33–49.

Smethurst, J., Clarke, D. & Powrie, W. (2012) Factors controlling the seasonal variation in soil water content and pore water pressures within a lightly vegetated clay slope. *Géotechnique*. [Online] 62 (5), 429–446. Available from: doi:10.1680/geot.10.P.097.

Smethurst, J.A., Briggs, K.M., Powrie, W., Ridley, A., et al. (2015) Mechanical and hydrological impacts of tree removal on a clay fill railway embankment. *Géotechnique*. [Online] 65 (11), 869–882. Available from: doi:10.1680/jgeot.14.P.010 [Accessed: 15 March 2021].

Smith, P.G., Potts, D.M. & Addenbrooke, T.I. (2008) A precipitation boundary condition for finite element analysis. *Unsaturated Soils: Advances in Geo-Engineering - Proceedings of the 1st European Conference on Unsaturated Soils, E-UNSAT 2008*. [Online] (1998), 773–778. Available from: doi:10.1201/9780203884430.ch105.

Smith, P.G.C. (2003) *Numerical Analysis Of Infiltration Into Partially Saturated Soil Slopes*. PhD thesis, Imperial College London.

Southampton, U. of (2009) *Rain data 18mar09*.

Sun, D. mei, Li, X. min, Feng, P. & Zang, Y. ge (2016a) Stability analysis of unsaturated soil slope during rainfall infiltration using coupled liquid-gas-solid three-phase model. *Water Science and Engineering*. [Online] 9 (3), 183–194. Available from: doi:10.1016/j.wse.2016.06.008.

Sun, D. mei, Li, X. min, Feng, P. & Zang, Y. ge (2016b) Stability analysis of unsaturated soil slope during rainfall infiltration using coupled liquid-gas-solid three-phase model. *Water Science and Engineering*. [Online] 9 (3), 183–194. Available from: doi:10.1016/j.wse.2016.06.008.

Thornthwaite, C.W. (1948) An Approach toward a Rational Classification of Climate. *Geographical Review*. [Online] 38 (1), 94. Available from: doi:10.2307/210739.

Toll, D.G. (1995) A conceptual model for the drying and wetting of soil. In: *PROCEEDINGS OF THE FIRST INTERNATIONAL CONFERENCE ON UNSATURATED SOILS/UNSAT '95/PARIS/FRANCE/6-8 SEPTEMBER 1995. VOLUME 2*. Unsaturated soils. 1995 Paris, A A Blakema. pp. 805–810.

Tratch, D.J., Wilson, G.W. & Fredlund, D.G. (1995) An Inroduction to Analytical Modelling of Plant.pdf. In: *Proceedings of the 48th Canadian Geotechnical Conference*. 1995 pp. 771–780.

Tree Works (n.d.) *Oak Tree – Tree Works*. [Online]. Available from: http://treeworksguernsey.co.uk/tree-identification/oak/.

Tsiampousi, A. (2011) *Numerical Analysis of Slopes in Unsaturated Soils*. Imperial College London.

Tsiampousi, A., Vitsios, I., Zdravković, L. & Potts, D.M. (2014) Effect of previous stress history and vegetation on the coefficient of earth pressure at-rest, K0, in London clay. In: *Numerical Methods in Geotechnical Engineering - Proceedings of the 8th European Conference on Numerical Methods in Geotechnical Engineering, NUMGE 2014*. [Online]. 2014 Taylor and Francis - Balkema. pp. 209–214. Available from: doi:10.1201/b17017-39.

Tsiampousi, A., Zdravkovic, L. & Potts, D.M. (2017) Numerical study of the effect of soil–atmosphere interaction on the stability and serviceability of cut slopes in London clay. *Canadian Geotechnical Journal*. [Online] 54 (3), 405–418. Available from: doi:10.1139/cgj-2016-0319.

Tsiampousi, A., Zdravković, L. & Potts, D.M. (2013) A new Hvorslev surface for critical state type unsaturated and saturated constitutive models. *Computers and Geotechnics*. [Online] 48, 156–166. Available from: doi:10.1016/j.compgeo.2012.09.010.

Vaughan, P.R. (1994) Assumption, prediction and reality in geotechnical engineering. *Géotechnique*. [Online] 44 (4), 573–609. Available from: doi:10.1680/geot.1994.44.4.573.

Vaughan, P.R., Kovacevic, N. & Potts, D.M. (2004) Then and now: some comments on the design and analysis of slopes and embankments. In: *Skempton Conference*. 2004 p.

Waldron, L.J. (1977) The Shear Resistance of Root-Permeated Homogeneous and Stratified Soil. *Soil Science Society of America Journal*. [Online] 41 (5), 843–849. Available from: doi:10.2136/sssaj1977.03615995004100050005x.

WebPage-StudiousGuy (n.d.) *Oak Tree Root System – StudiousGuy*. [Online]. Available from: https://studiousguy.com/oak-tree-root-system/.

Wheeler, S.J., Sharma, R.S. & Buisson, M.S.R. (2003) Coupling of hydraulic hysteresis and stress–strain behaviour in unsaturated soils. *Géotechnique*. [Online] 53 (1), 41–54. Available from: doi:10.1680/geot.2003.53.1.41.

Wheeler, S.J. & Sivakumar, V. (1995) An elasto-plastic critical state framework for unsaturated soil. *Géotechnique*. [Online] 45 (1), 35–53. Available from: doi:10.1680/geot.1995.45.1.35.

Wilson, G. (1990) *Soil evaporative fluxes for geotechnical engineering problems*. Phd Thesis, University of Saskatchewan, Saskatoon.

Wong, T.T., Fredlund, D.G. & Krahn, J. (1998) A numerical study of coupled consolidation in unsaturated soils. *Can. Geotech. J.* [Online] 35 (1953), 926–937. Available from: doi:10.1139/cgj-35-6-926.

Wu, T.H. (2013) Root reinforcement of soil: Review of analytical models, test results, and applications to design. *Canadian Geotechnical Journal*. [Online] 50 (3), 259–274. Available from: doi:10.1139/cgj-2012-0160.

Wu, T.H., McKinnell, W.P. & Swanston, D.N. (1979) STRENGTH OF TREE ROOTS AND LANDSLIDES ON PRICE OF WALES ISLAND, ALASKA. *Can Geotech J*. [Online] 16 (1), 19–33. Available from: doi:10.1139/t79-003.

Xu, C.Y. & Singh, V.P. (2002) Cross comparison of empirical equations for calculating potential evapotranspiration with data from Switzerland. *Water Resources Management*. [Online] 16 (3), 197–219. Available from: doi:10.1023/A:1020282515975.

Zhang, C.B., Chen, L.H. & Jiang, J. (2014) Why fine tree roots are stronger than thicker roots: The role of cellulose and lignin in relation to slope stability. *Geomorphology*. [Online] 206, 196–202. Available from: doi:10.1016/j.geomorph.2013.09.024.

Appendix A - Calculation of reference evapotranspiration

Atmospheric pressure, P

$$P = 101.3\left(\frac{293 - 0.0065z}{293}\right)^{5.26}$$

Psychrometric constant, γ

$$\gamma = \frac{c_p P}{\varepsilon\lambda} = 0.665 \times 10^{-3} P$$

z elevation above the sea level (m),
c_p specific heat at constant pressure, $1.013*10^{-3}$ MJ/kg°C,
ε ratio between the molecular weight of water vapour and dry air, 0.622,
λ latent heat of vaporisation, 2.45 MJ/kg

Mean daily air temperature, T_{mean}

$$T_{mean} = \frac{T_{max} + T_{min}}{2}$$

Gradient of the relationship between saturation vapour pressure and temperature, Δ

$$\Delta = \frac{4098\left[0.6108exp\left(\frac{17.27T_{mean}}{T_{mean} + 237.2}\right)\right]}{(T_{mean} + 237.3)^2}$$

Saturation water vapour pressure, $u_{v,sat}$

$$u_{v,sat} = \frac{u_{v,sat}^{max} + u_{v,sat}^{min}}{2}$$

Saturation water vapour pressure at the daily maximum and minimum temperatures, $u_{v,sat}^{max}$, $u_{v,sat}^{min}$

$$u_{v,sat}^{max} = 0.6108exp\left(\frac{17.27T^{max}}{T^{max} + 237.3}\right)$$

$$u_{v,sat}^{min} = 0.6108exp\left(\frac{17.27T^{min}}{T^{min} + 237.3}\right)$$

Actual water vapour pressure. u_α

$$u_a = 0.6108exp\left(\frac{17.27T_{dew}}{T_{dew} + 237.3}\right)$$

T_{dew} dewpoint temperature – temperature at which air becomes saturated with water vapour $T_{dew} \approx T_{min}$

Net radiation parameter, R_n

$$R_n = R_{ns} - R_{nl}$$

R_{ns} net shortwave radiation,
R_{nl} net longwave radiation

$$R_{ns} = (1 - a)R_s$$

R_s net solar radiation (MJ/m^{2}day)

$$R_s = \left(0.25 + 0.5\frac{n}{N}\right) R_a$$

or,

$$R_s = k_{Ra}\sqrt{(T_{max} - T_{min})} \times R_a$$

R_a extra-terrestrial radiation (MJ/m^{2}day),
k_{Ra} adjustment coefficient (0.16 – 0.19)

$$R_a = \frac{24(60)}{\pi} \times G_{sc} \times d_r \times [\omega_s \times \sin\varphi \times \sin\delta + \cos\varphi \times \cos\delta \times \sin\omega_s]$$

G_{sc} solar constant equal to 0.082 MJ/m^{2}min,
d_r inverse relative distance between Earth and Sun,
ω_s sunset hour angle (rad),
φ latitude (rad),
δ solar declination (rad)

$$d_r = 1 + 0.033\cos\left(\frac{2\pi}{365} \times J\right)$$

$$\delta = 0.409\sin\left(\frac{2\pi}{365} \times J - 1.39\right)$$

$$\omega_s = \arccos[-\tan\varphi \times \tan\delta]$$

J corresponds to the number of the days in a calendar year, 1 – 365

Net longwave radiation, R_{nl}

$$R_{nl} = \sigma \times \left[\frac{T_{max,K}^4 + T_{min,K}^4}{2}\right] \times \left(0.34 - 0.14\sqrt{u_a}\right)\left(1.35\frac{R_s}{R_{so}} - 0.35\right)$$

σ Stefan-Boltzmann constant equal to 4.903*10^9 MJ/K^{4}m^{2}day,
R_{so} clear sky solar radiation (MJ/m^{2}day)

$$R_{so} = (0.75 + 2 \times 10^{-5}z) \times R_a$$

Soil heat flux, G

$$G_{month,i} = 0.07\left(T_{month,i+1} - T_{month,i-1}\right)$$

$T_{month,i+1}$ mean air temperatures of the next month,
$T_{month,i-1}$ mean air temperatures of the previous month

Mean wind velocity at a standard hight of 2.0 m, v_2

$$\vartheta_2 = \vartheta_z \frac{4.87}{ln(67.8z - 5.42)}$$

v_z mean wind velocity at a different height, z
If wind velocity for site under consideration is not known, a value of v_2=2 m/s can be used, which is the average wind speed measured by 2000 weather stations around the world.

Appendix B - Model 81 (BBM modification)

Yield (YS) and plastic potential (PP) surfaces

$$\left.\begin{matrix} F_1 \\ G_1 \end{matrix}\right\} = \frac{p + f(s_{eq})}{p_0 + f(s_{eq})} - \frac{\left(1 + \frac{\eta}{K_2}\right)^{\frac{K_2}{\beta_f}}}{\left(1 + \frac{\eta}{K_1}\right)^{\frac{K_1}{\beta_f}}} = 0$$

$$K_{1,2} = \frac{\mu_i(1-\alpha_i)}{2(1-\mu_i)} \times \left(1 \pm \sqrt{1 - \frac{4\alpha_i(1-\mu_i)}{\mu_i(1-\alpha_i)^2}}\right)$$

$$\beta_f = (1-\mu_i) \times (K_1 - K_2)$$

$$\eta = \sqrt{J_{2\eta} \Big/ J_{2\eta i}}$$

$$J_{2\eta} = \left(\frac{J}{p + f(s_{eq})}\right)^2$$

$$\frac{2}{\sqrt{27}} C_i \sin(3\theta) \times \left(\sqrt{J_{2\eta i}}\right)^3 + (C_i - 3) \times \left(\sqrt{J_{2\eta i}}\right)^2 - (C_i - 9) = 0$$

$$C_i = \frac{9 - M_i^2}{\frac{2M_i^3}{27} - \frac{M_i^2}{3} + 1}$$

$$M_i = \frac{6 \sin \varphi_{cs}}{3 - \sin \varphi_{cs}}$$

Option 1

$$f(s_{eq}) = k \times s_{eq}$$

Option 2

$$f(s_{eq}) = S_r \times s_{eq}$$

Apparent cohesion, J_{ci}

$$J_{ci} = \sqrt{J_{2\eta i}} \times f(s_{eq})$$

Unsaturated isotropic compression line

$$\vartheta_1(s_{eq}) = \vartheta_1 - k_s \times ln \frac{s_{eq} + p_{atm}}{p_{atm}} - \left(\lambda(0) - \lambda(s_{eq})\right) ln\, p^c$$

Initial specific volume

$$\vartheta = \vartheta_1(s_{eq}) - \lambda(s_{eq}) ln\, p_0 + k\, ln \frac{p_0}{p}$$

Critical state line (CSL)

Mean equivalent stress at critical state point, p_{cs}

$$p_{cs} = \left(p + f(s_{eq})\right) \cdot \frac{\left(1 + \frac{\sqrt{J_{2\eta g}} \Big/ \sqrt{J_{2\eta f}}}{K_{2f}}\right)^{\frac{K_{2f}}{\beta_f}}}{\left(1 + \frac{\sqrt{J_{2\eta g}} \Big/ \sqrt{J_{2\eta f}}}{K_{1f}}\right)^{\frac{K_{1f}}{\beta_f}}} - f(s_{eq})$$

Deviatoric stress at critical state point, J_{cs}

$$J_{cs} = \sqrt{J_{2\eta g}} \cdot \left(p_{cs} + f(s_{eq})\right)$$

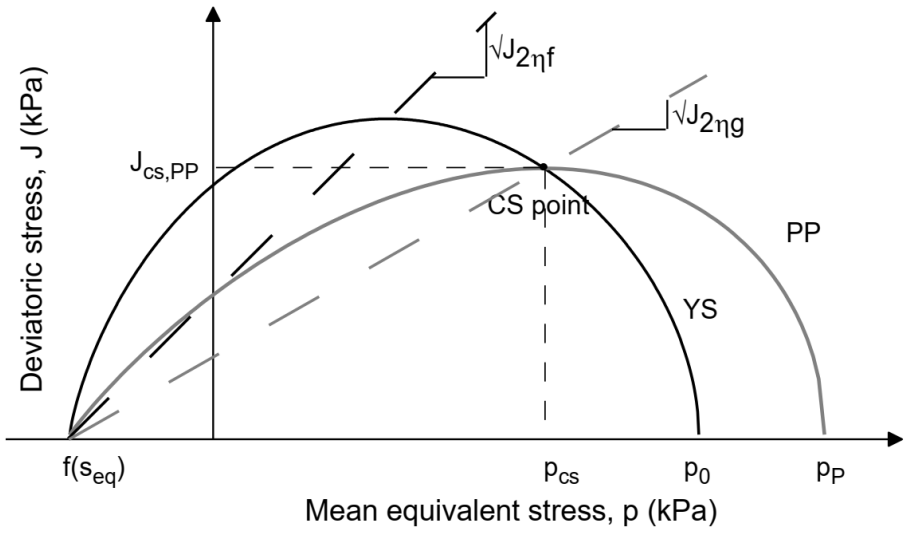

Biography

Veljko Pujević is a teaching assistant at the Department of Geotechnical engineering at the Faculty of Civil Engineering - University of Belgrade from 2012.

Veljko Pujević was born on January 17, 1985 in Belgrade where he finished primary and secondary school. He has obtained the Master Degree in Civil Engineering at the Faculty of Civil Engineering - University of Belgrade, Structural Department in 2011. Shortly after MSc graduation, he enrolled in PhD studies at the same Faculty.

Since January 2012, he has been employed at the Faculty of Civil Engineering, University of Belgrade, as a teaching assistant for the scientific field of Geotechnical engineering. Since his election as teaching assistant, he supervised numerous B.Sc. and M.Sc. theses.

The domain of scientific work of Veljko Pujević is related to the numerical analysis of soil-structure and soil-vegetation-climate interaction problems. His PhD thesis is done in collaboration with Imperial College, London (Department of Civil and Environmental Engineering). Another important field of his scientific work encompasses the investigation of soil stabilization using industrial by-products, specifically non self-cementing fly ash.

He is the author and co-author in the number of publications: 3 papers in international journals from the SCI list, over 20 papers published in refereed national and international conference proceedings and 1 national technical solution M82.

Veljko Pujevic is a member in the following scientific and professional organizations: Serbian Association of Soil Mechanics and Geotechnical Engineering, International Association for Soil Mechanics and Geotechnical Engineering (ISSMGE) and Technical Committee for Standardisation U182 – Geotechnical engineering.

Изјава о ауторству

Име и презиме аутора Вељко Б. Пујевић

Број индекса 914/2011

Изјављујем

да је докторска дисертација под насловом

Нумеричко моделирање утицаја вегетације и атмосфере на понашање насипа грађевинске инфраструктуре

- резултат сопственог истраживачког рада;
- да дисертација у целини ни у деловима није била предложена за стицање друге дипломе према студијским програмима других високошколских установа;
- да су резултати коректно наведени и
- да нисам кршио/ла ауторска права и користио/ла интелектуалну својину других лица.

Потпис аутора

У Београду, јун 2021.

_____

Изјава о истоветности штампане и електронске верзије докторског рада

Име и презиме аутора:	Вељко Б. Пујевић
Број индекса:	914/2011
Студијски програм:	Грађевинарство
Наслов рада:	**Нумеричко моделирање утицаја вегетације и атмосфере на понашање насипа грађевинске инфраструктуре**
Ментор:	др Мирјана Вукићевић, редовни професор, Универзитет у Београду, Грађевински факултет

Изјављујем да је штампана верзија мог докторског рада истоветна електронској верзији коју сам предао/ла ради похрањена у **Дигиталном репозиторијуму Универзитета у Београду.**

Дозвољавам да се објаве моји лични подаци везани за добијање академског назива доктора наука, као што су име и презиме, година и место рођења и датум одбране рада.

Ови лични подаци могу се објавити на мрежним страницама дигиталне библиотеке, у електронском каталогу и у публикацијама Универзитета у Београду.

Потпис аутора

У Београду, јун 2021.

_____

Изјава о коришћењу

Овлашћујем Универзитетску библиотеку „Светозар Марковић“ да у Дигитални репозиторијум Универзитета у Београду унесе моју докторску дисертацију под насловом:

Нумеричко моделирање утицаја вегетације и атмосфере на понашање насипа грађевинске инфраструктуре

која је моје ауторско дело.

Дисертацију са свим прилозима предао/ла сам у електронском формату погодном за трајно архивирање.

Моју докторску дисертацију похрањену у Дигиталном репозиторијуму Универзитета у Београду и доступну у отвореном приступу могу да користе сви који поштују одредбе садржане у одабраном типу лиценце Креативне заједнице (Creative Commons) за коју сам се одлучио/ла.

1. Ауторство (CC BY)

2. Ауторство – некомерцијално (CC BY-NC)

3. Ауторство – некомерцијално – без прерада (CC BY-NC-ND)

4. Ауторство – некомерцијално – делити под истим условима (CC BY-NC-SA)

5. Ауторство – без прерада (CC BY-ND)

6. Ауторство – делити под истим условима (CC BY-SA)

(Молимо да заокружите само једну од шест понуђених лиценци.
Кратак опис лиценци је саставни део ове изјаве).

Потпис аутора

У Београду, јун 2021.

_____

1. **Ауторство**. Дозвољавате умножавање, дистрибуцију и јавно саопштавање дела, и прераде, ако се наведе име аутора на начин одређен од стране аутора или даваоца лиценце, чак и у комерцијалне сврхе. Ово је најслободнија од свих лиценци.

2. **Ауторство – некомерцијално**. Дозвољавате умножавање, дистрибуцију и јавно саопштавање дела, и прераде, ако се наведе име аутора на начин одређен од стране аутора или даваоца лиценце. Ова лиценца не дозвољава комерцијалну употребу дела.

3. **Ауторство – некомерцијално – без прерада**. Дозвољавате умножавање, дистрибуцију и јавно саопштавање дела, без промена, преобликовања или употребе дела у свом делу, ако се наведе име аутора на начин одређен од стране аутора или даваоца лиценце. Ова лиценца не дозвољава комерцијалну употребу дела. У односу на све остале лиценце, овом лиценцом се ограничава највећи обим права коришћења дела.

4. **Ауторство – некомерцијално – делити под истим условима**. Дозвољавате умножавање, дистрибуцију и јавно саопштавање дела, и прераде, ако се наведе име аутора на начин одређен од стране аутора или даваоца лиценце и ако се прерада дистрибуира под истом или сличном лиценцом. Ова лиценца не дозвољава комерцијалну употребу дела и прерада.

5. **Ауторство – без прерада**. Дозвољавате умножавање, дистрибуцију и јавно саопштавање дела, без промена, преобликовања или употребе дела у свом делу, ако се наведе име аутора на начин одређен од стране аутора или даваоца лиценце. Ова лиценца дозвољава комерцијалну употребу дела.

6. **Ауторство – делити под истим условима**. Дозвољавате умножавање, дистрибуцију и јавно саопштавање дела, и прераде, ако се наведе име аутора на начин одређен од стране аутора или даваоца лиценце и ако се прерада дистрибуира под истом или сличном лиценцом. Ова лиценца дозвољава комерцијалну употребу дела и прерада. Слична је софтверским лиценцама, односно лиценцама отвореног кода.